NUMERICAL MODELING WITH A MOVING COORDINATE SYSTEM: APPLICATION TO FLOW THROUGH POROUS MEDIA

by

Ole Krogh Jensen

A dissertation submitted in partial fulfillment
of the requirements for the degree of

DOCTOR OF PHILOSOPHY

University of Washington

1980

Approved by _____
(Chairperson of Supervisory Committee)

Department _____
(Departmental Faculty Sponsoring Candidate)

Date _____

University of Washington

Abstract

NUMERICAL MODELING WITH A MOVING COORDINATE SYSTEM: APPLICATION TO FLOW THROUGH POROUS MEDIA

By

Ole Krogh Jensen

Chairperson of Supervisory Committee: Professor Bruce A. Finlayson
Department of Chemical Engineering

A new numerical technique for solving convective diffusive equations is developed. Convective diffusive equations arise from mass conservation relations in flow through porous media. When convection dominates diffusion the equations are very difficult to solve numerically, because inaccurate oscillating solutions can result. Simulation of enhanced oil recovery processes requires solution of several coupled convective diffusive equations and they can not be adequately solved because of these numerical difficulties.

An analysis and comparison of numerical methods are performed. Criteria are given for the spatial mesh size (Δx) to eliminate the oscillations for weighted residual methods.

The new solution technique minimizes the oscillations. The differential equations are transformed into a moving coordinate system with a time-dependent velocity, which eliminates the influence of the convective term, but makes the boundary location change in time. Both linear and nonlinear, one- and two-dimensional equations are solved with physically realistic parameters. Methods for deter-

mining the moving coordinate system velocity and changing the location of the boundary conditions are described. Orthogonal collocation on finite elements, finite difference and the Galerkin finite element method are applied. Several integration schemes including variable timestep schemes are used. Comparison of the accuracy and the solution cost to exact solutions and schemes with a fixed coordinate system are made. The feasibility of solving coupled nonlinear elliptic-parabolic problems is discussed. A new solution technique for solving elliptic equations in both a fixed and a moving coordinate system is developed.

The moving coordinate system is applicable to both one- and two-dimensional problems at a cost savings of a factor 20-50 for physical realistic parameters.

In presenting this dissertation in partial fulfillment of the requirements for the doctoral degree at the University of Washington, I agree that the Library shall makes its copies freely available for inspection. I further agree that extensive copying of this dissertation is allowable only for scholarly purposes. Requests for copying or reproduction of this dissertation may be referred to University Microfilms, 300 North Zeeb Road, Ann Arbor, Michigan 48106, to whom the author has granted "the right to reproduce and sell (a) copies of the manuscript in microform and/or (b) printed copies of the manuscript made from microform."

Signature _____

Date _____

TABLE OF CONTENTS

TABLE OF CONTENTS (Continued)

TABLE OF CONTENTS (Continued)

TABLE OF CONTENTS (Continued)

TABLE OF CONTENTS (Continued)

LIST OF FIGURES

LIST OF FIGURES (Continued)

LIST OF FIGURES (Continued)

LIST OF TABLES

LIST OF TABLES (Continued)

NOTATION

$a_1, a_2, a_3 \ldots a_i$	constants
A, B	constants
A1, B1	Constants for description of S, k_r
ACCX, ACCY	accumulated velocity (distance travelled)
$b_1, b_2, b_3 \ldots b_i$	constants
BP0	boundary pressure
BP1	initial pressure
c	dimensionless concentration
C°	continuity between elements
C^1	continuity in slope between elements
Co	Courant number $\frac{Pe\Delta t}{\Delta x}$
CPU	Central Processing Unit
D	molecular diffusion coefficient
E	error
$f_1, f_2 \ldots f_n$	functions
g	acceleration of gravity
h	spatial increment
h(x,y)	height of formation
i,j,I,J,k	index space discretization
$\underline{\underline{J}}$	Jacobian
$\underline{j}$	diffusive flux
k, k_r	(relative) permeability
$\underline{\underline{K}}$	dispersion/diffusion tensor

$K_{\xi\rho}$	components of $\underline{\underline{K}}$
K_1, K_2	constants
L	length of domain
LB	stability constant
$\underline{\underline{M}}$	difference equation matrix (chap II)
$\underline{\underline{M}}$	mass matrix (Chapter V/VI)
Mo	mobility ratio
n	index
NCOL	number of interior collocation points
NE	number of element
N_I, N_J	shape (trial) functions
NP	number of collocation points plus two
NT	total number of nodes
p, p_c	(capillary) pressure
Pe, Pe_x, Pe_y	Peclet number (in x/y direction)
PV	pore volumes injected (PV = $t \cdot 2(Pe \cdot \pi/4)$)
q, q_1	flux
q_w	volumetric flux
r	radius
r_w	well radius
r_i	reactions (adsorption)
RSU	resource units
s	iteration number

S, S_r	(residual) saturation
t, τ, η	(dimensionless) time
u	dimensionless length within elements
$\underline{u}$	velocity
u_x , u_y	components of $\underline{u}$
x, y, ξ, ρ	(dimensionless) spatial length
x_g, y_g	Gaussian quadrature points
Z	depth of formation
w_i	weight fractions
w_6	quadrature weights

Greek symbols

α	Crank-Nicholson parameter
α_L, α_T	mixing length
α_i, β_i	constants
δ	variation
ε	time constant
λ_i	eigenvalue
λ, λ_x, λ_y	frontal velocity
λ_m	maximum eigenvalue
ρ	density
ρ_i	mass density
ρ_r	rock density (capacity)
ρ^*	density at surface conditions

μ	viscosity
$\emptyset$	porosity
$\emptyset$	similarity variable (section 4.2)
Φ	potential (section 5.2)
ψ	(difference equation) function
θ	adsorbed amount

ACKNOWLEDGMENTS

The author extends his gratitude to Prof. B.A. Finlayson for his helpful advice and guidance throughout the course of this work.

In addition, thanks are due to fellow students and other faculty members for making the stay in Seattle learningful and enjoyable both culturally as well as socially.

The work was financially supported by the American Chemical Society and the Department of Chemical Engineering at the University of Washington. Additional funds were also given by Egmont H. Pedersen's Fund and Kjøbenhavns Handelsbanks Rejselegat (both from Denmark).

Thanks to my neglected bride Susanne for her understanding and encouragements during this endeavor.

Chapter I

INTRODUCTION

Existing oil deposits are being depleted at a fast rate and with current consumption all known oil fields will have been extracted within the next 50-100 years. Research on enhanced oil recovery techniques strives to increase the efficiency of the oil production process, thereby leaving less oil in the ground.

When a new oil reservoir has been found, the production is initiated by letting oil flow under its own pressure to the surface. This production period is often termed primary recovery, and more than 50% of the original oil deposit is left underground, when production stops.

Enhanced recovery techniques [Haynes et al., 1976] seek to extract the remaining 50% of the oil. Different methods have been developed depending on the properties of the oil and the reservoir.

Waterflooding, often called secondary recovery, injects saline water and pushes the oil from one well to the next [Buckley and Leverett, 1952]. This process has been used since the 1930's and can extract 10-30% more of the original deposit.

A number of tertiary oil recovery processes have evolved and are broadly categorized into thermal, carbon dioxide (CO_2) miscible and chemical flooding [Haynes, 1976]. Currently only the thermal processes are commercially applied. CO_2 and chemical flooding are researched in laboratory and field tests.

Thermal recovery [Stegemeier, 1977] and in situ combustion are applied for very viscous crude oils. Heat is added to the reservoir to reduce oil viscosity or to vaporize the oil. In both cases, the oil is made more mobile so that it is more effectively displaced.

Carbon dioxide is capable of miscibly displacing low viscosity oils, thus permitting recovery of most of the oil from the reservoir rock that is contacted. High pressure and temperature are necessary. The miscibility overcomes the capillary forces which otherwise retain oil in pores of the rock. This idea is also used in miscible displacement with alcohols, developed in the 1950's. The soluble fluid is injected to dissolve the trapped oil [Haberman, 1960].

Chemical flooding techniques include surfactant, polymer, and alkaline flooding [Foster, 1973; Haynes, 1976]. In surfactant flooding a small amount (slug) of surfactant material in saline water is injected followed by a polymer solution. The surfactant bank lowers the interfacial tension between the injected fluid and the reservoir oil to almost zero. The capillary forces are thereby minimized, improving the displacement efficiency. The polymer solution is injected for stability considerations. In alkaline flooding the surfactants are formed in situ by injection of reactants such as sodium hydroxide, sodium silicate and sodium carbonate in water. The wettability can be altered by the alkaline chemicals too. The polymer flooding technique is an augmented water-flood. High molecular weight polymers are added to the injection water to increase the mobility contrast between the in-place and injected fluids and better sweep efficiency is obtained.

Analysis of oil reservoir processes by numerical solution of appropriate mathematical models has become an important engineering tool for evaluating and analyzing enhanced oil recovery techniques. The physical phenomena must be accurately described in the mathematical model. For all the processes mentioned above convective transport (forced by the injection) has been found to dominate the dispersive transport. Adsorption and ion exchange of chemicals to the rock surface, phasebehavior of the water, oil and chemicals are important too. The interactions between the trapped oil and injection fluids occur over a relative small region compared to the distance between wells.

An oil reservoir is a three-dimensional structure. Numerical simulation of the processes is most often done in one plane (two dimensions) and the reservoir properties are then averaged over the third dimension. The solutions represent therefore also an average with respect to this plane. Sweep efficiencies and recovery predictions etc. for future years can then be determined. The finite difference method has traditionally been applied to solve the equations [Peaceman, 1978]. The differential equations are approximated at a number of points (grid blocks) giving a set of algebraic equations which are solved on a computer. With convective dominating transport an extensive number of grid blocks is necessary to obtain accurate solutions [Price et al., 1966]. For all the mathematical models to enhanced oil recovery techniques, the number of grid blocks prohibits reasonable solutions thus only one-dimensional models have been used. The weighted residual

methods [Finlayson, 1972] have been considered for reducing the computation time but have only been found competitive for only simple problems (Settari, 1976).

Examples of convective dominating transport can be found in other engineering problems also. Simulation of moisture transport in dessicated soils is important for analyzing the migration of radioactive nuclea buried underground [Finlayson, 1976]. Problems concerning coal gasification [Bailey, 1960], fluid mechanics [Roache, 1972] and reactor design [Eigenburger, 1976] are other examples. An extensive number of gridblocks is necessary for accurate simulation of these processes, too. Because they are one-dimensional problems, solution can thus be obtained but at some cost.

This study was undertaken to develop efficient numerical techniques to solve these problems. An alternative solution method named Moving Coordinate System is proposed to overcome the difficulties. The method is tested on relatively simple mathematical models of the processes. Comparison to experimental data is not done.

Part I of this work reviews, analyzes and compares existing numerical methods for solving convective dominated equations. Special consideration is given to the finite element methods.

In Part II the concept of a moving coordinate system is introduced for one-dimensional problems. Two examples are solved using this method and comparisons are made to conventional solutions methods.

The application of a moving coordinate system to two-dimensional problems is addressed in Part III. A miscible displacement model is

used as a representative model where the velocity field is either known analytically or calculated numerically. This problem can be made very difficult to solve numerically depending on the physical parameters. The results are compared to other methods in accuracy and computation time.

For simulating enhanced oil recovery processes adequately cost savings by a factor of one order of magnitude are necessary. The goal for this study was to accomplish at least this reduction with the moving coordinate system.

PART I

NUMERICAL METHODS FOR PARABOLIC BOUNDARY VALUE PROBLEMS

The state-of-the-art of numerical methods applied to parabolic differential equations is reviewed. An analysis of weighted residual methods provides criteria for obtaining accurate numerical methods. A comparison of numerical methods is made.

Chapter II

NUMERICAL METHODS: DESCRIPTION AND INVESTIGATION

2.1 Introduction

The physical situations discussed in Chapter I can be modelled by second order coupled partial differential equations (PDE). Second order PDE's are grouped into either of parabolic, hyperbolic or elliptic type [Carrier and Pearson, 1976] . The models of interest here are of parabolic type. The linear equation

$$\frac{\partial c}{\partial t} + Pe \frac{\partial c}{\partial x} = \frac{\partial^2 c}{\partial x^2} \tag{2.1}$$

has one spatial (x) and one time (t) variable and is a second order parabolic PDE. The two-dimensional form

$$\frac{\partial c}{\partial t} + Pe_x \frac{\partial c}{\partial x} + Pe_y \frac{\partial c}{\partial y} = \frac{\partial^2 c}{\partial x^2} + \frac{\partial^2 c}{\partial y^2} \tag{2.2}$$

is of parabolic type too, if each space variable (x,y) is examined separately.

The numerical difficulties mentioned in Chapter I arise with the first derivative being significantly larger than the second derivatives (Pe, Pe_x, $Pe_y > 10^3$). In the limiting case Pe, Pe_x, $Pe_y \rightarrow \infty$, Eqs. (2.1) and (2.2) become

$$\frac{\partial c}{\partial (Pe \cdot t)} + \frac{\partial c}{\partial x} = 0$$

$$\frac{\partial c}{\partial (Pe \cdot t)} + \frac{\partial c}{\partial x} + \frac{\partial c}{\partial y} = 0 \qquad (2.3)$$

which are hyperbolic. Typical analytical solutions to (2.1) and (2.2) are shown in Fig. 2.1. For parabolic problems a smooth solution arises whereas the hyperbolic type problem develops a discontinuity (shock). The numerical difficulties result in either an oscillatory behavior or a smoothing of the front. This problem is often referred to in the literature as the sharp front problem or a solution of parabolic equations with hyperbolic character.

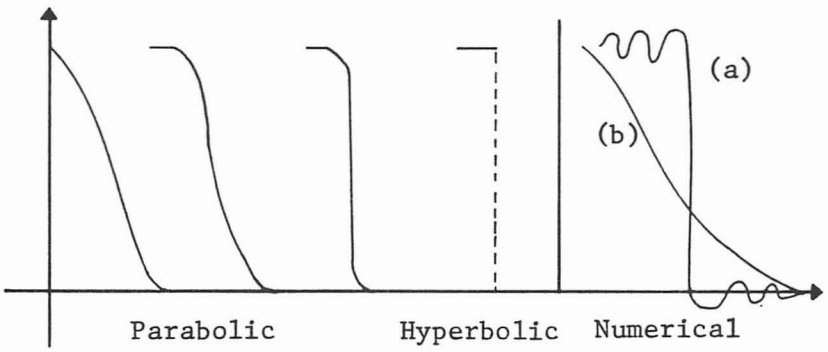

Figure 2.1

Typical Analytical and Numerical Solutions

An indication of the importance of solving parabolic type models in the engineering field is the very large amount of literature existing on the subject. A complete description of all the analytical and numerical methods is not given here. Instead an overview of "the state-of-the-art" will be made with emphasis on the most practical and promising methods.

A parabolic equation can be solved by a variety of methods and often more than one method (or procedure) is necessary for a solution. The initial procedure can be an analytical transformation of the original equation into another form, which then is more easily solved. For example a Laplace- or Fourier-transformation to some problems gives a form from which the solution can be obtained through algebraic manipulation. Other examples of transformations are similarity, method of characteristic and coordinate transformations. After this initial procedure, which might not be used, either an analytical technique (e.g. separation of variables) or a numerical method (e.g. method of lines) is used to obtain a solution. We can schematically divide the whole solution procedure into two parts: an initial part consisting of an analytical transformation (sometimes not used) and a second part which can be either an analytical or numerical method. This is illustrated in Fig. 2.2, by following the arrows to give the various combinations. In the bottom of the figure is shown another possibility where analytical solutions are incorporated into the numerical procedure. This approach is frequently taken for solving nonlinear elliptic equations to avoid approximating singularities (see

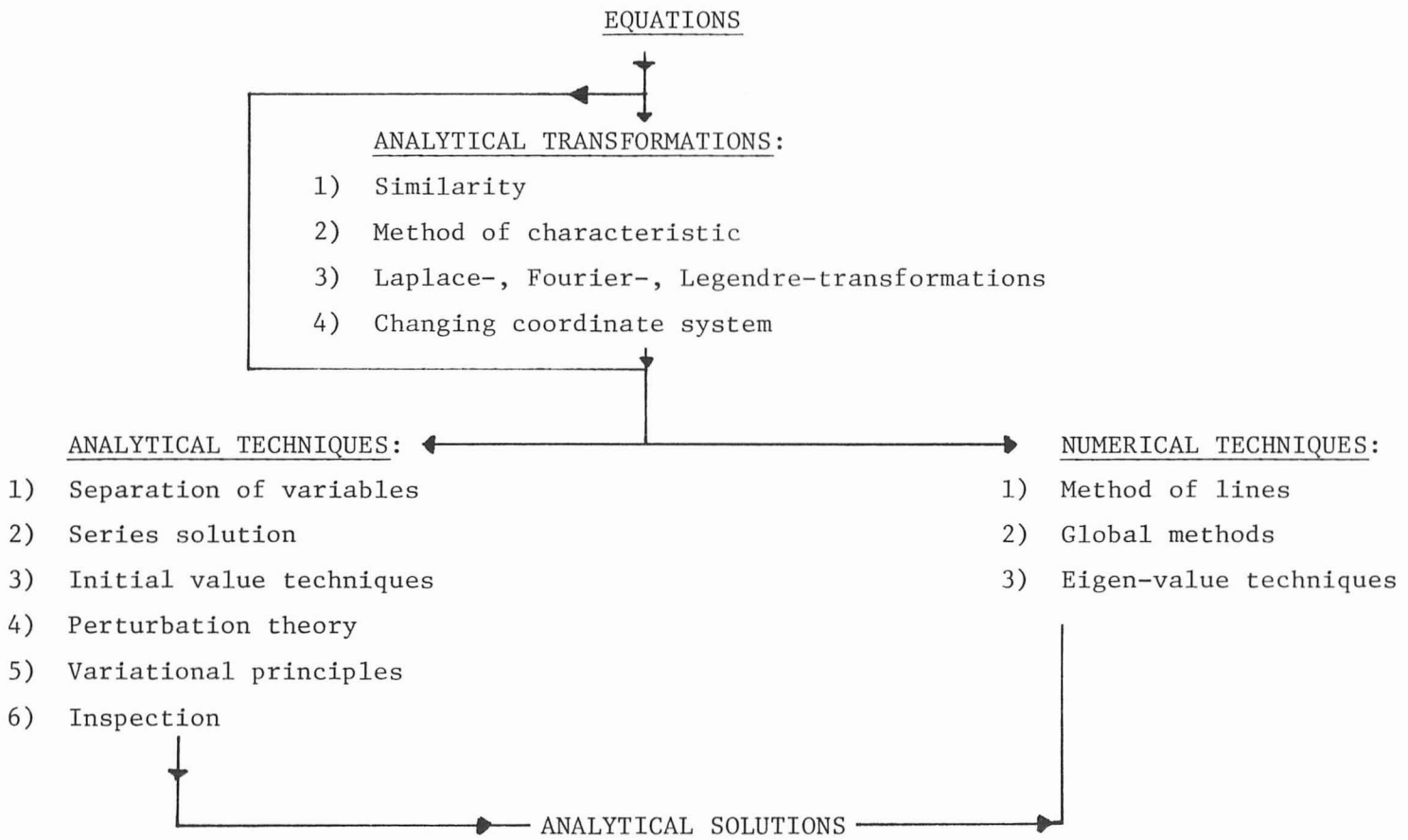

Figure 2.2

Solution Procedures for Parabolic Differential Equations

below). For parabolic problems a similar approach could be taken incorporating an analytical behavior but has not been seen in the literature. The most common transformations and solution techniques are listed.

The transformations and analytical techniques are traditionally (and historically) separated from the numerical methods. Jenson and Jeffrey (1963), Carslaw and Jaeger (1959), and Carrier and Pearson (1969) describe transformations and analytical techniques in detail and give solutions to many linear and some nonlinear problems.

For nonlinear and multidimensional problems, numerical methods are introduced. The method of lines [Finlayson, 1979] is most widely used. The solution is approximated separately in time and space, i.e., to the Eq. (2.2) we have

$$\tilde{c}_i(n\Delta t) \simeq f_1(x_i)\ f_2(y_i)\ f_3(n\Delta t)$$

and each function f_1, f_2, and f_3 is solved for pointwise (finite difference) or piecewise (polynomial expansion). In global methods the variables are combined

$$\tilde{c}_i(n\Delta t) \simeq f(x_i, y_i, n\Delta t)$$

and f determined point- or piecewise as above. Regardless of which methodology is used to get a numerical solution, the finite difference technique [Peaceman, 1978] and the method of weighted residuals [Finlayson, 1972] form the basic theory, from which any numerical approach proceeds.

The numerical methods are usually applied directly to an equation even though a proper transformation could simplify the solution technique considerably. Combination of analytical transformations and numerical methods can give solutions to problems that otherwise were very expensive (or impossible) to solve computationally. Some examples are given.

Laplace- and Fourier-transformations are very useful techniques for many linear problems. For nonlinear problems such as encountered in process control theories, the transformation back to the real time domain is done numerically [Brigham, 1974] (a linearization is done initially). More complex situations can then be analyzed.

Similarity transformations are normally only applied to linear problems. For nonlinear problems a similarity transformation can change a problem to a form much more easily solved numerically. In Chapter IV (Section 4.2) a highly nonlinear diffusion equation is transformed into a form which is easily solved using standard methods. Without the transformation, the cost of solving it would be much higher.

The moving coordinate system discussed in Parts II and III is another example of applying a transformation before using a conventional numerical scheme, thereby forming a computationally efficient yet simple scheme.

Incorporating analytical solutions into the numerical procedure (see Fig. 2.2) is a relative new idea which has found application for nonlinear elliptic problems. Singularities are often known analy-

tically from a corresponding linear problem and can therefore be used as a first approximation. For calculating pressures near oil wells this idea has been extensively applied [Chappelear and Williamson, 1979]. In Chapter VI an alternative method for incorporating singularity behavior is introduced.

Summarizing, the solution procedures for parabolic differential equations are traditionally separated into analytical techniques for mostly linear problems and numerical methods for nonlinear and multidimensional problems. Powerful techniques can be made by combining analytical tools and numerical methods. In this study several combinations are introduced, resulting in computationally efficient methods.

The finite difference method and weighted residual method constitute the basic principles for numerical techniques. In Section 2.2 these methods are described. A review and an analysis of the method of lines are given in Section 2.3 to determine under which circumstances accurate solutions are obtained. The most widely used methods are compared in accuracy and cost.

2.2 Description

Finite difference and weighted residual methods are reviewed.

2.2-1 Finite Difference Methods

Finite difference has been used since Newton for interpolating and extrapolation of data. With the introduction of computers a large variety of problems can be solved with the same principles.

To solve differential equations, the derivative is approximated pointwise by linearization. For example can the first and second derivative be approximated by

$$y = f(x) \qquad a < x < b$$

$$f'(x_n) = \frac{y_{n+1} - y_{n-1}}{2\Delta x} + \Delta x^2/6\ f^{III}(x_n) + \ldots$$

$$f''(x_n) = \frac{y_{n+1} - 2y_n + y_{n-1}}{\Delta x^2} + \Delta x^2/2\ f^{IV}(x_n) + \ldots \tag{2.4}$$

where $x_n = n\Delta x$, $n = 0,1,\ldots N$, $\Delta x = \frac{b-a}{N}$. The formulas 2.4 are called central difference approximation (CDA) and widely used because of their simplicity. When applied to convective diffusive equations, the solutions tend to oscillate as illustrated in Fig. 2.1a. Backward (or upstream) difference formulation [Peaceman and Rachford, 1962; Spalding, 1970] tends to smooth the front (Fig. 2.1b) instead of oscillate. Higher order spatial discretizations were made by Saitoh (1977); Chien (1977) and Chan (1978) combine backward and central difference approximation for reducing the artificial dispersion. Other special formulations are reviewed in Sections 2.3, 3.1, 4.1 and 5.1.

2.2-2 Weighted Residual Methods

In contrast to the finite difference formulation which approximates pointwise, the weighted residual method uses a piecewise polynomial approximation. Finlayson (1972) reviewed the application of the method of weighted residuals (MWR) to transport phenomena.

By introducing a polynomial approximation in an equation, a residual is formed. Different methods exist that differ in how the residual is minimized. In the collocation method [Villadsen and Michelsen, 1978] the residual is minimized at certain points within the domain. The Galerkin methods average the error over the whole domain [Smith, 1973]. The finite element method [Zienkiewicz, 1971] is a Galerkin method too and widely used because of its ability to approximate irregular boundaries.

2.3 Investigation of Methods

2.3-1 Review

The numerical methods described in 2.2 have been examined in numerous studies. It is important to know under which circumstances accurate solutions are obtained. Different approaches have been considered in the literature each giving some information about the numerical schemes. Equation (2.1) with the boundary conditions

$$\left.\begin{array}{ll} c = 1 & x = 0 \\ \dfrac{\partial c}{\partial x} = 0 & x = 1 \end{array}\right\} \quad t > 0 \qquad (2.5)$$

$$c = 0 \qquad x > 0 \qquad t = 0$$

has been used as a model equation. Also the steady state equation

$$Pe \frac{\partial c}{\partial x} = \frac{\partial^2 c}{\partial x^2} \qquad (2.6)$$

with the boundary conditions

$$c = 1 \qquad x = 0$$

$$c = 0 \qquad x = 1$$

has been studied.

Price et al. (1966) were the first to recognize that the difficulties are due mainly to the spatial discretization. They proved that a finite difference solution with a central difference approximation to Eq. (2.1) for both first and second derivatives will not oscillate provided

$$Pe\ \Delta x < 2 \quad . \tag{2.7}$$

This result was obtained by examining the oscillation matrices associated with the transient problem and is a sufficient condition for the matrices to have real, negative eigenvalues. For $Pe\Delta x > 2$ the eigenvalues are complex and the solution will oscillate. Some weighted residual methods are analyzed in Section 2.3-3 to determine when complex eigenvalues arise. Similar criteria as (2.1) are obtained.

Christie et al. (1976, 1978) analyzed the steady state equation (2.6) in a manner described in detail in Section 2.3-2. They solved the discretized equations and showed that a Galerkin finite element method will not oscillate if Eq. (2.7) is satisfied. A scheme was presented for using weighting functions which provide an additional dispersion term

$$\beta \frac{Pe\Delta x}{2} \frac{\partial^2 c}{\partial x^2} \quad .$$

While the oscillations are eliminated the solution exhibits more dispersion than desired. For quadratic trial functions, they showed that oscillations do not occur at the elements' corner nodes, and that the solution at the midside nodes oscillates unless

$$Pe\Delta x < 4 \quad .$$

This result is examined further in Section 2.3-2. Other weighted residual methods are analyzed in Section2.3-2 too. The results are summarized in Jensen and Finlayson (1979).

Oscillations will be introduced into the transient solution if the temporal integration is not appropriate. Price et al. (1966) showed that an explicit, Euler scheme will not oscillate provided

$$\Delta t \leqslant 1/\lambda_m$$

where λ_m is the maximum eigenvalue of the matrix resulting from the discretized equations. An implicit, backward Euler temporal integration method does not oscillate at all, whereas a Crank-Nicholson method (equal weighting at the old and new times) does not oscillate when

$$\Delta t \leqslant 2/\lambda_m$$

Similar guidelines are provided by Smith et al. (1976) for other temporal integration schemes. The criterion for oscillations is summarized by applying the temporal integration method to the equation

$$\frac{dy}{dt} = - Pey$$

The resulting expression for $y_{n+1}/y_n = \psi(Pe\Delta t)$ is examined as a function of $Pe\Delta t$. If $\psi < 0$ for large $Pe\Delta t$ then the scheme oscillates unless $Pe\Delta t$ is kept small enough. Further discussion of the stability criteria for integration-formula can be found in Lapidus and Seinfeld (1971) and Smith (1976).

Chaudhari (1971) analyzed finite difference methods with Taylor series expansion, when the first derivative is approximated by a backward difference

$$\frac{dc}{dx} = \frac{c_i - c_{i-1}}{\Delta x}$$

and the second derivative by a central difference, artificial dispersion is introduced. The equation solved is then

$$\frac{\partial c_i}{\partial t} + Pe \left.\frac{\partial c}{\partial x}\right|_i = \left(1 + \frac{Pe\Delta x}{2}\right) \left.\frac{\partial^2 c}{\partial x^2}\right|_i$$

A combination of central difference and backward scheme has been made [Chien, 1977; Chan, 1978] to reduce the artificial dispersion. Saitoh (1977) made higher order finite difference approximations to reduce the oscillations. Todd (1971) introduced a two point upstream method to lower the artificial dispersion.

Lantz (1971) combined the spatial and temporal truncation errors with Taylor series expansion in Eq. (2.1) by using $\Delta x = Pe\Delta t$ in an explicit formulation using backward differences for the convective derivative. Van Genuchten (1976) and Laumbach (1975) have both made equivalent combinations (using higher order temporal integrations) to

improve the accuracy of the calculations. As yet these manipulations have not been extended to nonlinear problems, although Lantz (1971) achieves some success in special nonlinear problems.

A Fourier series analysis provides information on how well numerical schemes progress a sinus wave in terms of phase delay and amplication of wave length. A single component of the Fourier series is compared to the same component in the exact solution of discretized equation. Stone and Brian (1963), Ziewieniuch (1978) examined finite difference methods in order to construct especially suited schemes. Gray and Pinder (1976), Gresho et al. (1976) and Runchal (1977) analyzed weighted residual methods and made comparisons to finite difference methods. The general conclusion is that weighted residual methods are better.

When the convection-diffusion equation is dominated by convection, the solution exhibits hyperbolic character. Analogy between the parabolic equation (2.1) and the hyperbolic equation (2.3) suggests that stability criteria for the hyperbolic equation can be used in computations of (2.1) when Pe is large. Courant and Hilbert (1962) found that an explicit difference scheme is stable if the Courant number

$$Co = \frac{Pe\Delta t}{\Delta x} < 1 \quad . \tag{2.8}$$

Peacemann (1978) found for no convection that for explicit finite difference formulation the criterion

$$\frac{\Delta t}{\Delta x^2} < 1/2 \qquad (2.9)$$

must be satisfied in order to get no oscillations.

Summarizing the criteria, the three coefficients

$$(Pe \neq 0) \qquad Pe\Delta x < a \qquad (2.7)$$

$$(Pe = \infty) \qquad \frac{Pe\Delta t}{\Delta x} < 1 \qquad (2.8)$$

$$(Pe = 0) \qquad \frac{\Delta t}{\Delta x^2} < 1/2 \qquad (2.9)$$

indicate when accurate solutions can be obtained. By combining (2.7) and (2.8)

$$\frac{Pe\Delta t}{\Delta x}(\Delta x) < 1 \cdot (\Delta x) \rightarrow (Pe\Delta x)\frac{\Delta t}{\Delta x^2} < 1$$

and as

$$\frac{\Delta t}{\Delta x^2} < \frac{1}{Pe\Delta x} = \frac{1}{2}$$

(2.9) is obtained. This combination is only valid for explicit finite difference schemes, but suggests that all criteria are important for solution of convection diffusion equations. Roache (1972) concludes similarly based on an analysis of artificial dispersion in finite difference methods.

2.3-2 Spatial Oscillation Limits—Steady State Equation

Criteria for accurate solutions can be obtained for the numerical methods to the model equation (2.6)

$$Pe \frac{dc}{dx} - \frac{d^2c}{dx^2} = 0 \tag{2.10}$$

which is the steady state equation of (2.1). The theoretical solution of (2.10) is

$$c = \frac{e^{Pe} - e^{Pex}}{e^{Pe} - 1} \quad . \tag{2.11}$$

The solution (2.12) satisfies

$$\frac{dc}{dx} < 0 \quad \text{for all } x \in [0,1] \tag{2.12}$$

so c is monotone over the whole interval zero to one. We must therefore also require that the numerical solution obeys (2.12), otherwise oscillations are introduced.

In the following an analysis is given of a weighted residual method to examine when (2.12) is satisfied. Within an element the dependent variable is approximated by a polynomial (of degree NP)

$$c_i(x) = \sum_{j=0}^{NP} a_j^* x^j \quad , \quad x\varepsilon[i\Delta x, (i+1)\Delta x] \quad . \tag{2.13}$$

and by defining

$$u = \frac{x - i\Delta x}{\Delta x}$$

Equation (2.14) becomes

$$c_i(u) = \sum_{j=1}^{NP} a_j u^i \quad , \; u\varepsilon[0.1] \tag{2.14}$$

The criterion for no oscillations is then defined by analogy to the analytical solution (2.11) and (2.12). A monotone numerical solution (no oscillations) is obtained, if the derivative

$$\frac{d}{du}\left(c_i(u)\right) = \sum_{j=1}^{NP} a_j \cdot j \cdot u^{j-1} < 0 \quad \text{for all } u\varepsilon[0.1] \tag{2.15}$$

at all points is negative.

The analysis of monotonicity is illustrated with the Galerkin equation using qaudratic trial functions. The interval zero to one is divided into NE elements $x_i = i\Delta x$, i = 0,1,2,...,NE and the midside nodes are denoted by i + 1/2, i = 0,...,NE-1. The value of c is given by an index corresponding to the nodal numbering. The Galerkin equations are

$$\left(1 + \frac{Pe\Delta x}{2}\right)c_{i-1} + (-8 - 2\,Pe\Delta x)c_{i-1/2} + 14c_i + (-8 + 2\,Pe\Delta x)c_{i+1/2} + \left(1 - \frac{Pe\Delta x}{2}\right)c_{i+1} = 0 \tag{2.16}$$

at the corner nodes (i = 2,...,N-1) and

$$(4 + Pe\Delta x)c_i - 8c_{i+1/2} + (4 - Pe\Delta x)c_{i+1} = 0 \tag{2.17}$$

at the midside nodes (i = 0,1,...,N-1). In matrix notation the set of Eqs. (2.16) and (2.17) for various i become

$$\underline{\underline{M}} \cdot \underline{c} = b \tag{2.18}$$

where

$\underline{\underline{M}}$: coefficient matrix

$\underline{c}$: solution at nodal points

$\underline{b}$: boundary conditions at nodal points

The structure of $\underline{\underline{M}}$ is

$$\begin{pmatrix} 1 & 0 & 0 & & & & & & & \\ x & x & x & & & & & & & \\ x & x & x & x & x & & & & & \\ & & x & x & x & & & & & \\ & & x & x & x & x & x & & & \\ & & & & x & x & x & & & \\ & & & & & & x & x & x & x & x \\ & & & & & & & & 0 & 0 & 1 \end{pmatrix} \cdot \begin{pmatrix} c_o \\ c_{1/2} \\ c_1 \\ c_{1+1/2} \\ \\ \\ \\ \\ \\ \end{pmatrix} = \begin{pmatrix} 1 \\ 0 \\ 0 \\ 0 \\ \\ \\ \\ \\ \\ 0 \end{pmatrix}$$

Figure 2.3

Structure of Matrix $\underline{\underline{M}}$

The solution $\underline{c}$ is obtained analytically rather than inverting $\underline{\underline{M}}$. Using the equations at node i-1/2, i, i+1/2 (box in Fig. 2.3) the variables $c_{i-1/2}$ and $c_{i+1/2}$ can be eliminated, and we obtain

$$[1 + Pe\Delta x/2 + Pe^2\Delta x^2/12]c_{i-1} - [2 + Pe^2\Delta x^2/6]c_i + [1 - Pe\Delta x/2 + Pe^2\Delta x^2/12]c_{i+1} = 0 \qquad (2.19)$$

Equation (2.19) has the analytical solution

$$c_i = A + B\,\psi^i \tag{2.20}$$

where

$$\psi = \frac{1 + Pe\Delta x/2 + Pe^2\Delta x^2/12}{1 - Pe\Delta x/2 + Pe^2\Delta x^2/12} \tag{2.21}$$

and A, B are determined from the boundary conditions. The solution at the midside node is determined by substituting (2.20) into (2.14), the expression becomes

$$c_{i+1/2} = A + B\,\psi^i\,\frac{1 - Pe^2\Delta x^2/24}{1 - Pe\Delta x/2 + Pe^2\Delta x^2/12} \tag{2.22}$$

We can now determine the constants a_j in (2.13) so the solution can be evaluated at any point. For a quadratic trial function we have

$$c_j(u) = a_o + a_1\,u + a_2\,u^2 \tag{2.23}$$

with the conditions

$$c(o) = c_i, \quad c(1/2) = c_{i+1/2}, \quad c(1) = c_{i+1} \quad .$$

The constants a_j are now

$$\begin{aligned} a_o &= c_i \\ a_1 &= -3c_i + 4c_{i+1/2} - c_{i+1} \\ a_2 &= 2c_i - 4c_{i+1/2} + 2c_{i+1} \quad . \end{aligned} \tag{2.24}$$

The criterion (2.15)

$$\frac{dc}{du} = a_1 + 2a_2\, u < 0 \qquad \text{for } u\varepsilon[0,1] \tag{2.25}$$

can now be examined. Substituting (2.20) and (2.22) into (2.24), we have

$$\frac{dc}{du} = A \cdot [u - u_1], \quad u\varepsilon[0,1] \tag{2.26}$$

where

$$u_1 = \frac{1}{2} - \frac{1}{Pe\Delta x}$$

and

$$A = \frac{\psi^N}{\psi^{N-1}} > 0 \quad .$$

Examining (2.26) for u between zero and one, the slope within an element is positive if u is greater than u_1 so the solution will oscillate. This occurs when

$$Pe\Delta x > 2$$

so to have a negative slope at any point within the element and therefor no oscillations, we must have

$$Pe\Delta x < 2 \quad . \tag{2.27}$$

If the monotonicity requirement is used only at the nodal values (c_i, $c_{i+1/2}$, c_{i+1}) the limit is $Pe\Delta x < 4$ as reported by Christie et al. (1976).

This analysis has been made for other weighted residual methods. The results are given in Table 2.1 with "the critical grid Peclet

Table 2.1

Oscillation Limits for Weighted Residual Methods

Scheme	Criterion 2.15	Criterion Only Nodal Values Monotone	Criterion For Transient Problem	Order Of Method (SS)
Finite Difference*				
— Central Diff	2	2	2	$O(h^2)$
— Forward	1	1		$O(h)$
— Upstream	∞	∞	∞	$O(h)$
Galerkin-Legendre				
— Linear, upstream**	$\frac{2}{1-\alpha}$	$\frac{2}{1-\alpha}$		$O(h)$, $\alpha = 0\ 1$ (h^2)
— Quadratic	2	4		$O(h^3)$
— Quadratic, upstream	2	∞		$O(h)$
— Cubic	4.6444	4.6444		$O(h^4)$
OCFE-Legendre				
— Quadratic	2	2	2.12	$O(h^3)$***
— Cubic	$\sqrt{12}$ = 3.46410	4.3912	4.0	$O(h^4)$***
— Quartic	4.6444	4.6444	4.7	$O(h^5)$***
OCFE-Hermitic				
— Cubic	$\sqrt{12}$	∞		$O(h^4)$***
— Quartic	4.6444	4.6444		$O(h^5)$***
Moments				
— Cubic	$\sqrt{12}$	∞		$O(h^4)$

* Price et al. (1966)

** Huyakorn et al. (1976)

*** Order at coll. point

number" (or oscillation limit) $Pe\Delta x$. The detailed analysis is given in Appendix B.

All weighted residual methods in Table 2.3 give oscillating (non-monotone) solutions depending on the factor $Pe\Delta x$, the higher order methods can use larger Δx for the same Peclet number. The apparent limit (only looking at nodal values) is in general higher than the true limit and can achieve an infinite value. This latter situation is shown in Fig. 2.4 for OCFE-Hermite with cubic trial functions. Using $Pe\Delta x = 10$, $Pe = 100$ it is seen that the nodal values are all decreasing and the slope at the corner nodes increasingly negative, but in between large oscillations occur. This suggests that when using Hermite-cubic polynomials the solution must be examined over the whole element otherwise large oscillations might not be seen.

The criteria obtained here can be used to estimate the number of elements needed in all elliptic type problems

$$\frac{\partial}{\partial x}\left(f_1 \frac{\partial c}{\partial x}\right) + \frac{\partial}{\partial y}\left(f_2 \frac{\partial c}{\partial y}\right) + f_3 \frac{\partial c}{\partial x} + f_4 \frac{\partial c}{\partial y} = f(x,y,c)$$

Particularly the criteria could be used to estimate the number of elements needed in a boundary layer type problem arising in e.g., fluid mechanic, mass transfer and thermal boundary layer analysis. It is well known that for the model problem 2.6 an irregular grid with small elements near $x = 1$ (the boundary layer) and few elements towards $x = 0$ an accurate solution can be obtained. It is therefore not necessary to discretize the whole domain (zero to one) with the

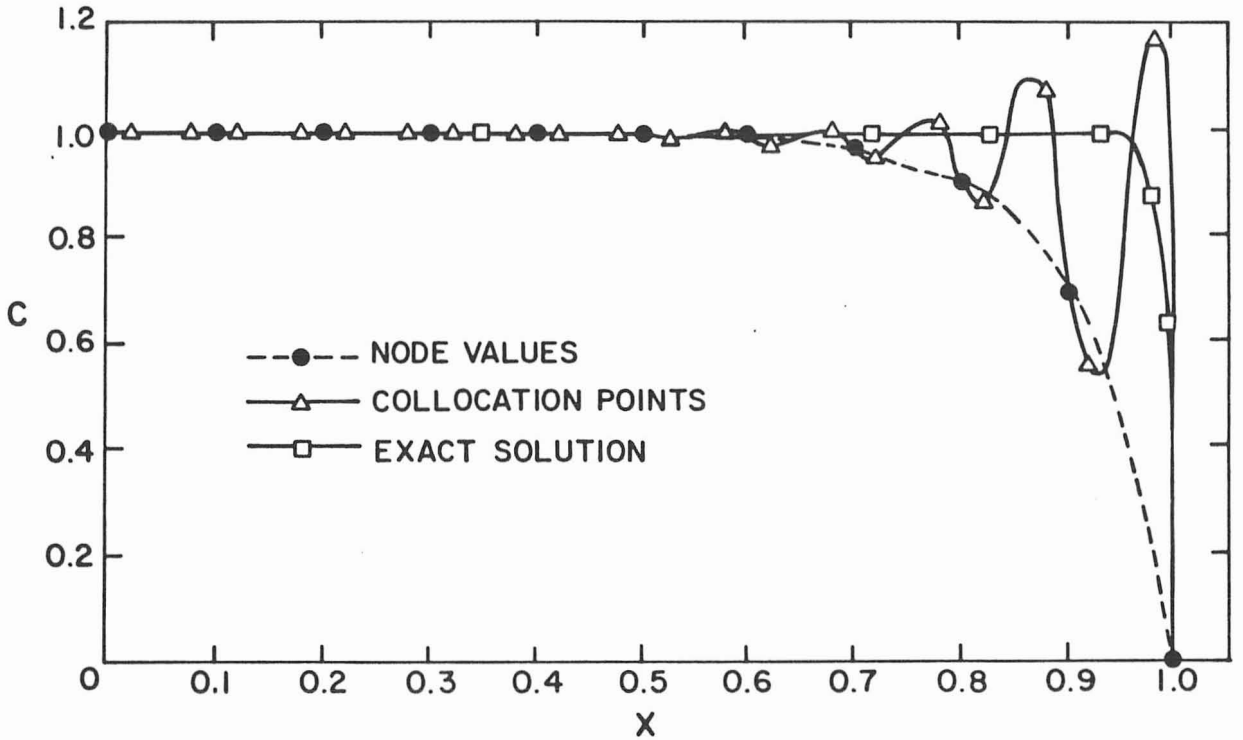

Figure 2.4

Solution to the Steady State Convective-Diffusive Equation,
OCFE-Hermite Pe = 100, $Pe\Delta x = 10$

criteria in Table 2.1. The boundary layer at x = 1 is of thickness 1/Pe, which is easily seen by changing the length scale in Eq. (2.2) [Gresho et al., 1979] to x/ε (ε being a small number). Within the length 1/Pe the criteria in Table 2.1 are used and elsewhere only a few elements are needed.

2.3-3 Eigenvalue Analysis

The analysis of the steady state equation resulted in criteria to determine the number of elements needed to insure accurate numerical solutions of boundary value problems. A parallel analysis of the parabolic type problems (2.1) is an examination of the eigenvalues arising from the discretization. If complex eigenvalues exist, oscillations will occur. Starting with (2.1)

$$\frac{dc}{dt} + Pe\,\frac{dc}{dx} = \frac{d^2c}{dx^2}$$

and using any discretization method we obtain a set of equations

$$\underline{\underline{M}}^{*}\,\frac{d\underline{c}}{dt} = [\underline{\underline{B}} - Pe\cdot\underline{\underline{A}}]\underline{c} = \underline{\underline{M}}\cdot\underline{c}, \quad \underline{c} = c_o \text{ at } t = 0 \tag{2.28}$$

Diagonalizing the matrix $\underline{\underline{M}}^{*-1}\cdot\underline{\underline{M}}$ to $\underline{\underline{T}}\cdot\underline{\underline{\Lambda}}\cdot T^{-1}$, the formal solution to (2.1) is

$$\underline{c} = \underline{c}_o\cdot\underline{\underline{T}}\cdot\exp(\underline{\underline{\Lambda}}\cdot t)\cdot\underline{\underline{T}}^{-1} \tag{2.29}$$

The eigenvalues are then λ_i. The exponential terms in (2.29)

$$a_i\, e^{-\lambda_i t}, \quad \lambda_i > 0$$

will be monotonic increasing or decreasing if Λ_i is real. If λ_i is complex

$$e^{\lambda_i t} = e^{\gamma_i t}\left(\sin(\beta_i t) \pm i\cos(\beta_i t)\right), \quad \lambda_i = \gamma_i \pm i\alpha_i \tag{2.30}$$

the real part is no longer monotonic because of the trigonometric functions.

Price et al. (1966) found theoretically that with a central difference formulation and $Pe\Delta x < 2$ the eigenvalues were all real, but for $Pe\Delta x > 2$ complex eigenvalues arise. Some weighted residual methods are examined to see whether similar results can be obtained.

The exact eigenvalues for the transient problem (2.1) have been calculated in Appendix A. When the boundary condition at $x = 1$ is $c = 0$, the eigenvalues are

$$\lambda_i = Pe^2/4 + n^2\pi^2, \quad n = 0,1,\ldots,\infty$$

If $\frac{dc}{ox} = 0$, the eigenvalues are

$$\lambda_i = Pe^2/4 + f_i^2$$

where λ_i is determined from the transcendental equation

$$\text{tg } f_i = -\frac{2}{Pe} f_i, \text{ for Pe large } f_i \simeq n\pi$$

The eigenvalues of $\underline{\underline{M}}$ (2.28) were calculated using a numerical approach, Housholders method [Wilkinson, 1965]. OCFE with Lagrange polynomials was used to compute $\underline{\underline{M}}$ and $Pe\Delta x$ gradually changed.

The matrix $\underline{\underline{M}}$ is the same as for the steady state problem (see Appendix B) but the continuity equations must be eliminated. The factor $Pe\Delta x$ was gradually changed for the following cases.

I : $Pe\Delta x < 5$ with $10 < Pe < 50$

observation of shift between real and complex eigenvalues

II : $Pe\Delta x < 2$ with $10 < Pe < 20$

convergence of eigenvalues to those predicted theoretically

III : $Pe\Delta x > 50$ with $Pe = 877.9$ or $Pe = 87790$.

In Case I the object was to see whether a shift from real to complex eigenvalues occurred for OCFE. Table 2.2 summarizes the results. For example, NCOL = 1, Pe = 50, 24 elements give no complex eigenvalues, 23 gives complex eigenvalues so that the limit must be between 24 and 23. Thus the critical $Pe\Delta x$ lies between 50/24 = 2.08 and 50/23 = 2.17. For very low values of Pe only a coarse mesh is needed but the limit is poorly determined. For higher values of Pe the limit seems to converge. The limit is poorly determined for two or more interior collocation points, but as these calculations are expensive, further investigations were omitted.

A series of calculations (Case II) were performed to test if the calculated eigenvalues converged to the theoretical predicted. A comparison of the first six eigenvalues is shown in Table 2.3, and convergence is observed.

For case III, the $Pe\Delta x$ is very large (10^2 - 10^3) so only complex eigenvalues were found. For one and two interior collocation points

Table 2.2

Criteria by Eigenvalue Analysis

OCFE	Pe = 10		Pe = 20		Pe = 50		Steady State Oscillation
	NE*	PeΔx	NE*	PeΔx	NE*	PeΔx	(Table 2.1)
NCOL = 1	4	2.92 ± 0.41	8	2.68 ± 0.17	24	2.12 ± 0.04	2
NCOL = 2	3	4.17 ± 0.83	5	4.5 ± 0.5	13	4.01 ± 0.16	3.46
NCOL = 3	2	7.5 ± 2.5	5	4.5 ± 0.5	11	4.77 ± 0.23	4.644
NCOL = 4	2	7.5 ± 2.5	4	5.83 ± 0.83			
NCOL = 5	2	7.5 ± 2.5	3	8.33 ± 1.66			

* Number of elements for which no oscillations were obtained.

For NE* - 1 complex eigenvalues were found

Table 2.3

Exact and Calculated Eigenvalues, Pe = 20

NE	λ_1	λ_2	λ_3	λ_4	λ_5	λ_6
3	108	96 ± i.61	153 ± i.12	324		
4	135 ± i.21	192	220 ± i.24	313 ± i.96	576.	
5	112.5	154.9	195.3	218.2	300.0	424.4
6	110.5	145.4	194.2	248.0	298.4	432.0
7	110.1	142.3	192.0	254.5	325.9	399.2
8	110.94	141.05	190.7	256.5	335.9	427.0
Theoretical	109.869	139.47	188.83	257.91	366.48	455.31

it was found that the minimum and maximum real part always were

$$\text{NCOL} = 1 \begin{cases} \lambda_{min} = 2.7/\Delta x^2 \\ \lambda_{min} = 8/\Delta x^2 \end{cases}$$

$$\text{NCOL} = 2 \begin{cases} \lambda_{min} = 12/\Delta x^2 \\ \lambda_{min} = 36/\Delta x^2 \end{cases} \qquad (2.31)$$

This behavior is also observed for $Pe\Delta x$ low. The imaginary part of the eigenvalues was found to be directly proportional to Pe. In Fig. 2.5 are shown eigenvalues for the two kinds of boundary condition and various number of elements and interior collocation points.

2.3-4 Comparison of Methods

The two analyses described in Section 2.3-2 and 2.3-3 provide criteria for nonoscillating solutions for the steady state and transient equation. For the finite difference method the two criteria are identical and for OCFE they are nearly the same as seen in Table 2.1. Due to the close correspondence we henceforth use the result from the analysis of the steady state equation as the criterion in both steady state and transient equations.

A comparison of the methods for the steady state and transient equation is made based on the criteria in Table 2.1, the interpolation error and the multiplication cost for solving the equations. We first describe how the data for the comparison is calculated.

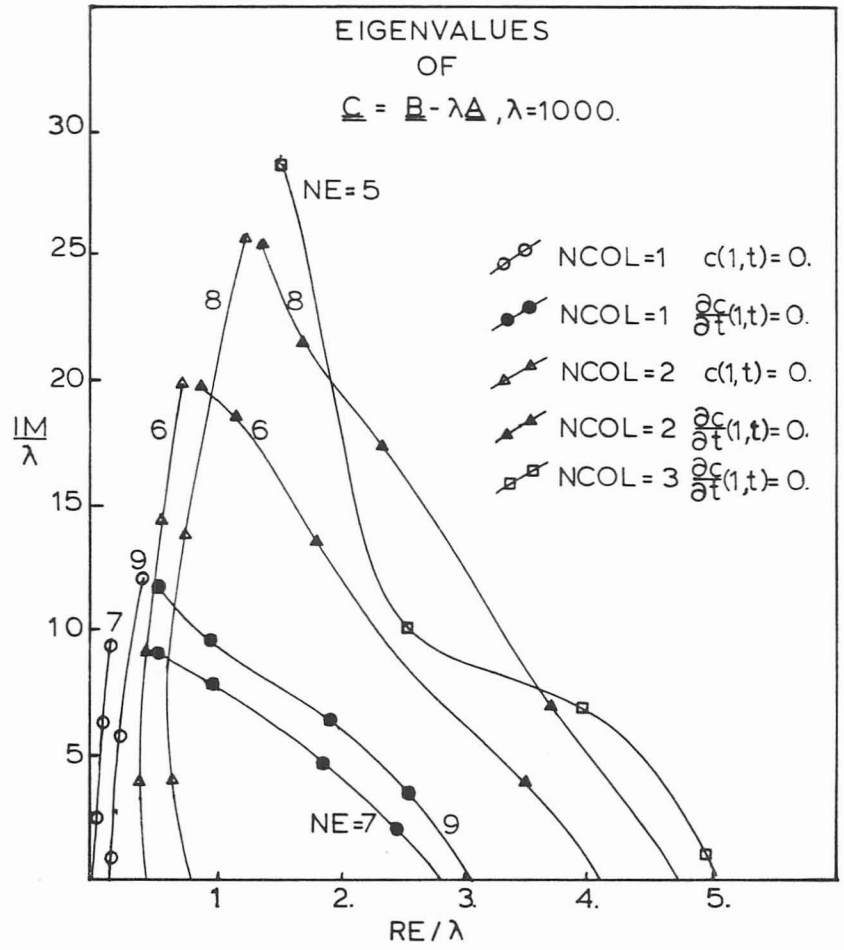

Figure 2.5

Eigenvalues, Pe = 10^3, (λ = Pe)

The multiplication time is the main cost for solving algebraic equations, and the estimate is based on a Gaussian elimination technique taking into account the sparse structure of the matrices (shown in Appendix B for different methods). Necessary multiplications to do the LU-decomposition and solving for one right hand side (RHS) are shown in Table 2.4.

Based on Table 2.1 the number of elements necessary for no oscillations is given in Table 2.4.

Interpolating the exact solution to the steady state equation with a finite difference of finite element method gives an interpolation error. Estimates of this interpolation error for Lagrange and Hermite polynomials are provided by Prenter (1975). For Lagrange interpolation of degree n (n = 0; linear, n = 1; quadratic ,...) the estimate is

$$||c - p|| < \frac{||c^{(n+1)}||\ \Delta x^{n+1}}{4(n+1)} < \varepsilon$$

where p(x) is the interpolation polynomial and the norm is defined as the mean square

$$||c^{(n)}|| = \left\{ \int_0^1 \left[c^{(n)} \right]^2 dx \right\}^{1/2} .$$

For Hermite interpolation and cubic polynomials the estimate is

$$||c - p|| \leqslant \frac{||c^{(4)}||\ \Delta x^4}{4 \cdot 12^4} \leqslant \varepsilon$$

Table 2.4

Multiplication Work for Inversion of Matrix and Criteria for Discretization Methods

Scheme	No. of Multiplications for LU-Decomposition	No. of Multiplications for Solving One RHS	Number of Elements for Monotonicity (Table 2.1)	LB in 2.38
FD				
— Central Difference	2NE	3 NE + 1	0.5 Pe	4
Galerkin-C°				
— linear	2 NE	3 NE + 1	0.5 Pe	12
— quadratic	8 NE	8 NE + 1	0.5 Pe	60
— cubic	20 NE	15 NE + 1	0.215 Pe	--
OCFE-Legendre				
— quadratic	8 NE	8 NE + 1	0.5 Pe	8
— cubic	20 NE	15 NE + 1	0.289 Pe	36
— quartic	40 NE	24 NE + 1	0.215 Pe	98
OCFE-Hermite				
— cubic	7 NE	8 NE + 1	0.289 Pe	36
— quartic	17 NE	15 NE + 1	0.215 Pe	98
Moments				
— cubic	7 NE	8 NE + 1	0.289 Pe	--

The analytical solution to the steady state equation is given in Section 2.3-2 and the m'th derivative is

$$\frac{dc^m}{dx^m} = \frac{-1}{e^{Pe} - 1} Pe^m \, e^{Pex} \tag{2.35}$$

Equation (2.35) is also the m'th derivative of the transient equation for $t >> 1/Pe$. The mean square interpolation error is then for Pe large following Finlayson (1979)

$$\text{Lagrange} \quad : \quad \varepsilon_n = \frac{Pe^{n+1/2} \, \Delta x^{n+1}}{4\sqrt{2} \, (n + 1)} \tag{2.36}$$

$$\text{Hermite} \quad : \quad \varepsilon_3 = \frac{Pe^{3+1/2} \, \Delta x^4}{4 \quad 12^4} \tag{2.37}$$

To estimate the total multiplication cost for solving the transient equation, we need the total number of timesteps necessary to integrate to a certain time. The number of timesteps will be different depending on which discretization method and integration formula is used. With an implicit integration formula, there is not any stability limits and we can therefore not estimate the differences in the number of timesteps without doing numerical calculations. For an explicit Euler integration formula Peaceman (1978) and Finlayson (1979) give stability criterion for the diffusion equation (Pe = 0) as

$$\frac{\Delta t}{\Delta x^2} \leqslant \frac{1}{LB} \quad \text{or} \quad \Delta t \cdot \lambda_{max} \leqslant 2, \quad \lambda_{max} = \frac{LB}{\Delta x^2} \tag{2.38}$$

where LB depends on the spatial discretization method. As discussed in Section 2.3-1 the stability criterion (2.38) is applicable for a nonzero Pe number if used together with the oscillation criteria given in Table 2.1. We can therefore estimate the number of time-steps for each spatial discretization method using (2.38) with Table 2.1. The value of LB is listed in Table 2.4 and taken from Peaceman (1978) and Finlayson (1979).

The work to solve the steady state equation is defined as the total multiplication cost for obtaining a solution and calculated by multiplying the number of elements by the cost to do one LU decomposition and one solution of the right hand side (Table 2.4). For the transient equation the work is defined either per timestep or for a total integration to a time 1/Pe (close to steady state). In the first case, we estimate the work by the number of elements needed (Table 2.1) and the cost to solve one right hand side (as the problem is linear the coefficient matrix needs only to be LU decomposed once). For integrating to 1/Pe the work is calculated by the cost to evaluate n RHS where n is the total number of timesteps needed (found by using Table 2.1 and formula (2.38)).

We first compare the methods for the steady state equation. In Table 2.5 is listed in column 1 the work required by using the discretization given in Table 2.1 (criterion for oscillations) and in column 2 the interpolation error with this discretization is given. The low order methods require less work than the higher order methods to get a monotone solution but has a higher interpolation error. For a fixed

Table 2.5

Comparison of Methods, Steady State Equation

	Work = W	Interpolation Error = E:		
	Oscillation Limit ($W \times Pe^{-1}$)	At Oscillation Limit	For Work = 1/10 Pe $E \times \sqrt{Pe}$	For Work = 100 Pe $E \times \sqrt{Pe}$
FD				
— Central Difference	2.5	0.35	8.8	8.8×10^{-3}
Galerkin-C°				
— linear	2.5	0.35	8.8	8.8×10^{-3}
— quadratic	8.0	0.35	2.3×10^{3}	2.3×10^{-3}
— cubic	7.5	5.93	2.5×10^{6}	2.5×10^{-3}
OCFE-Legendre				
— quadratic	4.0	----	---	---
— cubic	10.1	0.0017	1.8×10^{5}	1.8×10^{-7}
— quartic	13.8	---	---	---
OCFE-Hermite				
— cubic	4.3	0.0017	6×10^{3}	6.1×10^{-9}
— quartic	6.9	----	---	---
Moments				
— cubic	4.3	0.0017	6×10^{3}	6.1×10^{-9}

work of Pe/10 and 100 • Pe the interpolation error is given in columns 3 and 4. The low order methods are preferable for inaccurate solutions and higher order methods are preferable for very accurate solutions.

The results discussed above are applicable for solving the transient equation only at very large times ($t \to 1/Pe$). For implicit integration the work per timestep is given in Table 2.6 column 1 and the total work for explicit integrating to 1/Pe in column 4 where the discretization necessary for monotone solution is used. The maximum timestep for explicit integration is listed in column 2 and compares indeed well with the smallest timestep used in implicit integration. Table 3.1 lists the timesteps for a Crank-Nicholson scheme (implicit) used for the transient equation with OCFE and Legendre cubic polynomials. Minor oscillations are observed at $\Delta t = 2.5 \times 10^{-6}$ (Pe = 877.9). The stability criterion (Table 2.4) is $\Delta t = 2.5 \times 10^{-6}$ for this Peclet number. For the work estimates given in Table 2.6 we can therefore expect a solution with some temporal truncation error. Comparing the methods in Table 2.6 the finite difference method is preferable and next best is OCFE-Hermite cubic polynomials. In general the lower order methods are preferable in cost to the higher order methods as was observed for the steady state equation when the monotonicity criterion is used but they have a higher interpolation error. If more work is used than required to get a monotone solution then higher order methods are preferable in cost as better accuracy is obtained.

Table 2.6

Comparison of Methods, Transient Equation

Scheme	Implicit Work W Per Timestep ($W \cdot Pe^{-1}$)	Explicit		
		Maximum Timestep (Δt) ($\Delta t \cdot Pe^{2}$)	Number of Timesteps N To Time 1/Pe ($N \cdot Pe^{-1}$)	Work W to Integrate to 1/Pe ($W \cdot Pe^{-2}$)
FD				
— central difference	1.5	2.0*	0.5	0.75*
Galerkin-C°				
— linear	1.5	0.67	1.5	2.25
— quadratic	4	0.13	7.5	3.0
— cubic	3.2	----	---	---
OCFE-Legendre				
— quadratic	4	1.	1.	4
— cubic	4.3	0.67	1.5	6.4
— quartic	5.2	0.44	2.3	12.0
OCFE-Hermite				
— cubic	2.3	0.67	1.5	3.5
— quartic	3.2	0.44	2.3	7.4
Moments				
— cubic	2.3	----	---	---

*For example the maximum timestep is $\Delta t = 2 \times Pe^{-2}$, and the number of multiplications required is $W = 0.75\ Pe^{2}$.

The multiplication cost to solve a transient problem increases with the square of the Peclet number. For the steady state equation the work only increases linearly. The interpolation error decreases more rapidly for higher order than for lower order methods.

2.4 Summary and Conclusions

Numerical methods to solve parabolic differential equations have been reviewed and analyzed.

Using the steady state convective diffusive equation as a model equation, weighted residual methods were analyzed. Criteria for non-oscillating monotone solutions were determined. For $Pe\Delta x < A$ a monotone solution is obtained, where Δx is the spatial increment and A varies from two to five (Table 2.1).

For the corresponding transient equation an eigenvalue analysis of orthogonal collocation on finite elements (OCFE) showed when complex eigenvalues (oscillations) arise. For $Pe\Delta x < A$ (A between two and five depending on the order of OCFE) real negative eigenvalues are obtained. The criteria are nearly the same as those found for the steady state equation.

Comparing the numerical methods based on the criteria to eliminate oscillations, the interpolation error and solution cost, the higher order methods such as OCFE-Hermite are preferable if a very accurate solution is desired and lower order methods such as finite difference are preferable if oscillations can be allowed.

For Peclet numbers very large (typically 10^3 - 10^6) we need the spatial increment Δx very small so the solution will be very expensive to obtain. As an example solving a 2D-parabolic equation with a Peclet number of 10^5 with a central finite difference formulation requires $(5 \times 10^4)^2 = 2.5 \times 10^9$ or 2.5 billion nodes to avoid oscillations. With "an acceptable level" of oscillations [$Pe\Delta x < 6$, Settari et al., 1976] we should use 280 million nodes. If we can allow artificial dispersion of smoothing of the front, much larger Δx can be taken. If dispersion cannot be allowed, this type of problem cannot be solved within a reasonable computation time. It is thus a necessity to find new ways to overcome this problem.

PART II

MOVING COORDINATE SYSTEM — ONE DIMENSION

The application of a moving coordinate system to one-dimensional problems is discussed. Chapter III introduces the method and applies it to a simple mathematical model. Chapter IV considers a nonlinear diffusion equation.

Chapter III

CONVECTION DIFFUSION EQUATION

The basic idea of applying a moving coordinate system to a sharp front problem is to reduce the number of elements needed and still achieve an accurate solution. The transformation to a moving coordinate system is discussed and illustrated on the linear convective diffusive equation. The scheme is particularly simple in this case as the frontal velocity is constant. One-dimensional mathematical models of enhanced recovery techniques can be solved using the moving coordinate system.

3.1 Alternative Solution Methods

A great variety of solution methods have been applied to convective-diffusive equations. Most of the conventional methods have been discussed in Chapter II. Here the more specialized techniques are reviewed.

Numerical methods with special consideration to convective diffusive problem are most often an extension or an "optimization" of the conventional formulation. Two point upstream methods [Todd and Chase, 1972; Wheatley, 1979], flux corrected finite difference methods [McDonald and Zalesak, 1979], quick step methods [Leonard, 1979], damping factors [Stone and Brian, 1963], combining spatial and time formulation [Laumbach, 1975] are all examples of such a reformulation. All of these methods can fairly easily be applied to multidimensional problems with irregular geometries. The number of elements/nodes will still be very large, as discussed in Chapter II.

The method of characteristics (MC) applied to parabolic differential equations has been examined by Garder et al. (1963), Rachford (1965), Pinder and Cooper (1971), and Varoglu and Finn (1978). In Garder et al.'s, Rachford's and Pinder and Cooper's approach the differential equations are solved on a fixed grid and with a set of moving points. The velocity of these points are determined by the characteristics. Diffusion is modelled by a marker-and-cell technique, which limits the accuracy. The number of elements is reduced considerably by this technique. Errors smaller than 2% were not achieved and extensive bookkeeping is necessary in two dimensions. In Varoglu and Finn's approach spatial-temporal elements and the method of characteristics are incorporated by orienting the sides of elements at subsequent time levels in a particular direction. A new mesh is generated for each timestep. This method has not been applied to non-

linear problems where the characteristics (velocity) are not known apriori.

The mixed Euler and Lagragian technique [Downing and Morrison, 1976] is very similar to Garder's and Pinder's approach in that two coordinate systems are necessary, one moving with the velocity of the fluid and one stationary. The diffusion of the front is treated in the moving coordinate system and convection in the stationary system. This method has the same disadvantages as the method of characteristic.

For one-dimensional problems the method of characteristic and the mixed Euler/Lagragian technique give major reductions in the computation time.

For purely hyperbolic problems, Concus and Proskurowski (1979), Albright et al. (1979) have developed a random sampling technique which shows promise for this type of problem, improving the efficiency considerably. The technique has not been extended to parabolic equations and the accuracy in the frontal region is limited because the solution is approximated in a discontinuous manner, so many elements might be needed also for this method.

Variable interpolation of self-adaptive mesh spacing has been examined by Russell and Christiansen (1978), Carey and Finlayson (1975), Douglas et al. (1979), and Price et al. (1968). Carey and Finlayson and Russell and Christiansen applied OCFE boundary value problems and minimized the residuals evenly over the whole domain by proper location of the elements. For parabolic and hyperbolic problems Price et al. and Douglas et al. add points before the

front when it advances and remove those behind the front after it passes. This technique greatly improves the efficiency. For two-dimensional problems the mesh is changed in the same manner so that complicated geometries and distorted fronts can be considered [Chase, 1979]. Extensive bookkeeping is necessary and the solution must be interpolated near the frontal position where the solution is not well determined. For approximating multiple fronts in the same grid the advantage of adaptive mesh becomes less evident.

The moving coordinate system [Jensen and Finlayson, 1979] tries to avoid the problems of interpolation in the frontal region and extensive bookkeeping by fixing the coordinate system in the front. Multiple fronts and irregular geometries are more difficult to handle with this technique. The potential for this technique is considered in this study.

The literature review reveals that for numerical solution of two-dimensional problems with large Peclet numbers the only option now is to use a conventional method with a highly optimized formulation [Young, 1978; Settari et al., 1976]. A potential for savings exists though with the method of characteristic, random choice method, adaptive mesh strategies and the moving coordinate system. In this study we show the potential for the moving coordinate system, which incorporates many of the advantages of the other possible techniques.

3.2 Moving Coordinate System

The moving coordinate system is based on the observation that

only near the sharp change in the solution (front) are small elements needed and elsewhere only a few large elements are necessary. The moving coordinate system (abbreviated MCS) involves a transformation of the differential equation from one coordinate system fixed in time to a coordinate system which moves with the velocity of the front. Starting from a general parabolic equation

$$\frac{\partial c}{\partial t} + g(c,x,t)\frac{\partial c}{\partial x} = \frac{\partial}{\partial x}\left(d(c,x,t)\frac{\partial c}{\partial x}\right) \quad , \tag{3.1}$$

and

$$\left.\begin{aligned} a_1 c + a_2 \frac{\partial c}{\partial x} = a_3 \quad &\text{at} \quad x = 0 \\ b_1 c + b_2 \frac{\partial c}{\partial x} = b_3 \quad &\text{at} \quad x = 1 \end{aligned}\right\} \quad t > 0$$

$$c = 0 \qquad x > 0 \qquad t = 0$$

the following transformation is performed

$$\xi = x - \int_0^t \lambda(t')dt' \qquad \eta = t \tag{3.2}$$

$\lambda(t)$ is the velocity of the front, so the integral in (3.2) represents the distance the front has travelled. This velocity can be specified by the user or determined numerically from the solution, as shown below. We now have

$$\frac{\partial c}{\partial t} = \frac{\partial c}{\partial \xi}\frac{\partial \xi}{\partial t} + \frac{\partial c}{\partial \eta}\frac{\partial \eta}{\partial t} = -\lambda(\eta)\frac{\partial c}{\partial \xi} + \frac{\partial c}{\partial \eta}$$

$$\frac{\partial c}{\partial x} = \frac{\partial c}{\partial \xi}\frac{\partial \xi}{\partial x} + \frac{\partial c}{\partial \eta}\frac{\partial \eta}{\partial x} = \frac{\partial c}{\partial \xi} \qquad (3.3)$$

$$\frac{\partial^2 c}{\partial x^2} = \frac{\partial^2 c}{\partial \xi^2}$$

and (3.1) can be rewritten as

$$\frac{\partial c}{\partial \eta} + [(g,\xi,\eta) - \lambda(\eta)]\frac{\partial c}{\partial \xi} = \frac{\partial}{\partial \xi}\left[d(c,\xi,\eta)\frac{\partial c}{\partial \xi}\right] \qquad (3.4)$$

The boundary conditions must also be transformed. We have

$$\left.\begin{aligned} a_1 c + a_2\frac{\partial c}{\partial \xi} = a_3 \qquad & \text{at } \xi = -\int_o^\eta \lambda(\eta')d\eta' \\ b_1 c + b_2\frac{\partial c}{\partial \xi} = b_3 \qquad & \text{at } \xi = 1 - \int_o^\eta \lambda(\eta')d\eta' \end{aligned}\right\} \eta > 0 \qquad (3.5)$$

$$c = 0 \qquad \text{at} \qquad \xi > 0 \qquad \eta = 0$$

The location of the boundary now changes with time. The revised problem, Eqs. (3.4) and (3.5) are exact and merely another version of Eq. (3.1).

The improvement in MCS comes from an optimum location of nodes. Since the front remains fixed in the moving coordinate system, small elements or more grid points can be concentrated there (where they are needed to eliminate oscillations) but larger elements or fewer grid points can be used elsewhere (where they are not needed). It is the use of large elements away from the front that gives rise to the

economy. In a fixed coordinate system the front eventually appears everywhere, so that small elements are needed throughout the domain, leading to excessive computation cost. The key to economy is to pick the right frontal velocity, $\lambda(\eta)$, and use a proper distribution of elements. The difference between calculating in a fixed or moving coordinate system is illustrated in Figure 3.1.

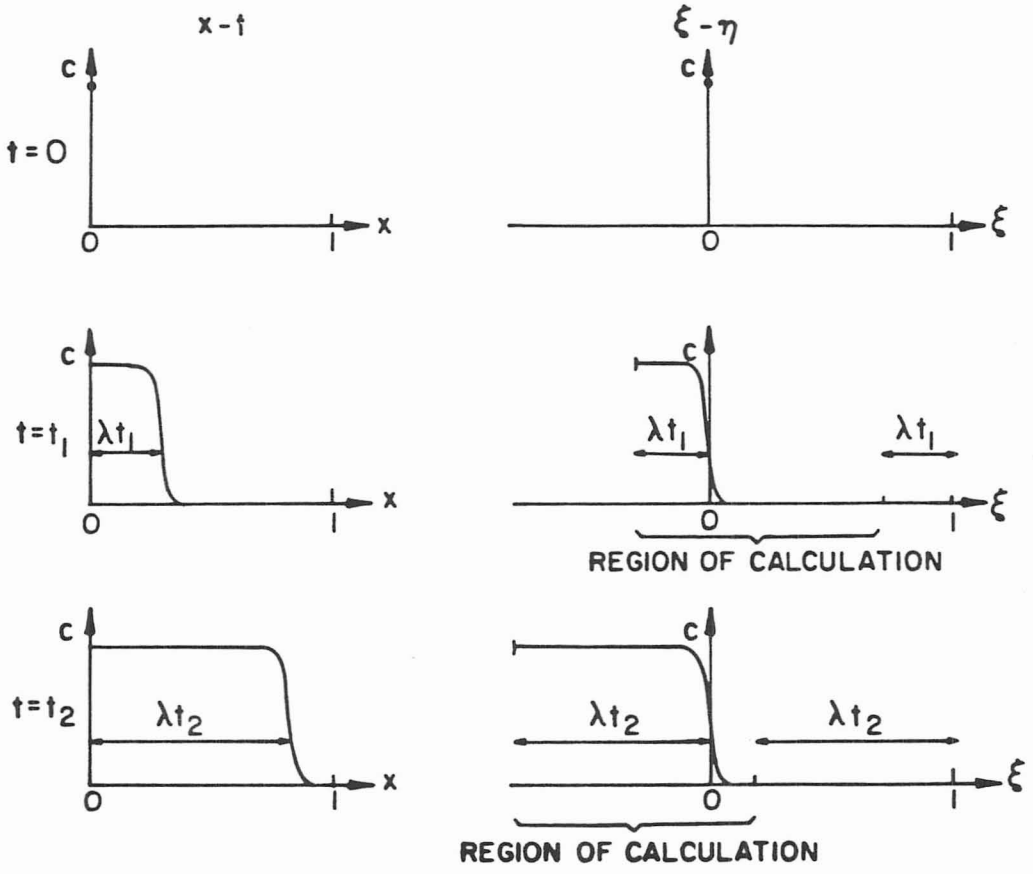

Figure 3.1

Fixed Versus Moving Coordinate System

Considering the linear equation

$$\frac{\partial c}{\partial t} + Pe \frac{\partial c}{\partial x} = \frac{\partial^2 c}{\partial x^2}$$

$$\left.\begin{array}{ll} c = 1 & x = 0 \\ \dfrac{\partial c}{\partial x} = 0 & x = 1 \end{array}\right\} \quad t > 0 \qquad (3.6)$$

$$c = 0 \qquad x > 0 \qquad t = 0$$

The front moves with a constant velocity Pe ($\lambda(t) = Pe$), so we get simply the diffusion equation

$$\frac{\partial c}{\partial \eta} = \frac{\partial^2 c}{\partial \xi^2} \qquad (3.7)$$

and the boundary conditions are then

$$\left.\begin{array}{lll} c = 1 & \text{at} & \xi = -Pe\eta \\ c = 0 & \text{at} & \xi = 1 - Pe\eta \end{array}\right\} \quad \eta > 0 \qquad (3.8)$$

$$c = 0 \qquad \xi > 0 \qquad \eta > 0$$

With the MCS a LU decomposition must be performed every time the boundary node changes, whereas in a fixed coordinate system only one LU decomposition is done per problem. This disadvantage of MCS is unimportant for nonlinear problems and less important for temporal integration methods with a variable step size.

For a nonlinear problem the frontal velocity is not known a priori and we must measure it by either following a specific con-

centration level or the largest gradient. This later choice is illustrated in Chapter IV.

The boundary conditions can be applied in two ways. If the solution at the boundary is known to have a zero gradient (or nearly so) we can just apply the boundary condition at the closest node. The location of the boundary in the numerical calculations then proceed in jumps during the integration. If the solution at the boundary has a nonzero gradient, then the above procedure would introduce significant error. In that case we move the location of the last element so that there is always a node at the actual boundary location.

The distribution of nodes is closely related to the broadening of the initial profile throughout the integration. An estimate of the diffusion length can be found from the solution of the diffusion equation in an infinite medium with an initial step change. The solution is, Carslaw and Jaeger (1959)

$$c = \text{erfc}\ (x/\sqrt{4 \cdot t})$$

For a change in c of 99% (c = 0.01) we get

$$\frac{x}{\sqrt{4 \cdot t}} \simeq 1.8$$

so that the diffusion length is

$$L = 3.6\ \sqrt{t} \quad . \tag{3.9}$$

Since max t = 1/Pe, the maximum L will be

$$L \simeq 3.6/\sqrt{Pe} \tag{3.10}$$

Equation (3.10) can therefore be used to estimate the element location. Sufficiently small elements must be included in a region of length L about the front if the accuracy is not to be degraded. For a nonlinear problem the Peclet number must be estimated in order to obtain the diffusion length.

If we compare the MCS to the technique of moving small elements with the front [Price et al., 1968], the MCS method involves less bookkeeping, and the interpolation and adjustment of the solution occurs at the boundary, where the solution is well behaved, rather than at the front, where it is not. The MCS is closely related to the method of characteristics. If there were no second order terms the method would be a method of characteristics. With second order terms, though, the method of characteristics is not valid. We model the dispersion caused by the second order terms by solving the second order equation (which, in the moving coordinate system, represents diffusion about the front). In contrast Garder et al. (1964) use a marker-and-cell technique to model the dispersion. Finally, any method of spatial discretization can be used.

Equation (3.6) can be solved analytically; the solution is given in Appendix A. The eigenvalues are

$$\lambda_i = Pe^2/4 + n^2\pi^2, \quad n = 0,1,\ldots, \infty$$

It is of interest to examine if the eigenvalues are affected by the coordinate transformation. Starting with (3.7) and assuming

$$c(\xi,\eta) = F(\xi)G(\eta)$$

we find that the solution must be in the form

$$c(\xi,\eta) = \sum A_i e^{-\lambda i^2 \eta} \left(\sin(\lambda_i \xi) + B\cos(\lambda_i \xi)\right)$$

and the eigenvalues are determined from

$$\sin \lambda_i(-Pe\eta) + B\cos \lambda_i(-Pe\eta)$$

$$\sin \lambda_i(1-Pe\eta) + B\cos \lambda_i(1-Pe\eta) = 0$$

or

$$\text{tg}\left(\lambda_i(-Pe\eta)\right) = \text{tg}\left(\lambda_i(1-Pe\eta)\right) \qquad (3.11)$$

and finally

$$\lambda_i = n\pi$$

By the application of moving coordinate system we have decreased the smallest eigenvalue by $Pe^2/4$ and larger timesteps should be possible.

3.3 Numerical Scheme

We can apply any numerical method to solve Eqs. (3.7) and (3.8). As we are only interested in $\eta < 1/Pe$ the discretization only covers [-1, 1]. We choose to apply OCFE, giving a set of ordinary differential equations and algebraic equations. We use the notation j=1,...,NT to identify the j-th node at different ξ. Within each element the notation J=1,...,NP denotes the local numbering systems within the element, which has NP nodes. In the k-th element j=(NP-1)(k-1)+J, since the NP-th node of the (k-1)-th element is the same as the 1-st node of the k-th element. We let $C_I^{(k)}$ be the concentration of the I-th node in the k-th element.

$$\text{Interior collocation } \frac{dc_j}{d\eta} = \frac{1}{\Delta\xi_k^{\,2}} \sum_{I=1}^{NP} B_{JI} c_I(k)$$

(3.12)

$$\text{Continuity } \frac{1}{\Delta\xi k} \sum_{I=1}^{NP} A_{NP,I} c_I(k) = \frac{1}{\Delta\xi_{k+1}} \sum_{I=1}^{NP} A_{I,I} c_I(k+1)$$

Using a Crank-Nicholson time discretization gives

$$\frac{c_j^{\,n+1} - c_j^{\,n}}{\Delta\eta} = \frac{1}{2\Delta\xi_k^{\,2}} \sum_{I=1}^{NP} B_{JI}\left[c_I^{\,(k),n+1} + c_I^{\,(k),n}\right]$$

where $c_j^{\,n} = c_j(\eta=n\Delta\eta)$. The set of equations can be written as

$$\underline{C}\ \underline{c}^{n+1} = \underline{D}\ \underline{c}^{n} \tag{3.13}$$

A similar set of equations could be developed using finite difference or Galerkin finite element methods.

The boundary conditions are applied by modifying the matrices $\underline{C}$, $\underline{D}$ and $\underline{c}^n$. For points to the left of the location of the boundary, $j < IL$, $\xi_j < -Pe\eta$, we replace $\underline{C}$ and $\underline{D}$ by the identity matrix $\underline{I}$ and $\underline{c}^n$ by 1. Similarly for right boundary points we do the same thing if $j > IR$, $\xi_j > 1 - Pe\eta$.

The modified matrices are

$$C^*_{ji} = \begin{cases} I_{ji} & \text{for } j < IL \text{ or } \xi_j < -Pe\eta \\ C_{ji} & \text{for } IL < j < IR \\ I_{ji} & \text{for } j > IR \text{ or } \xi_j > 1-Pe\eta \end{cases}$$

with a similar definition for D_{ij},

$$\underline{c}^{*n} = \begin{cases} 1 & j < IL \\ \underline{c}^{n} & IL < j < IR \\ o & j > IR \end{cases}$$

The structure of C* and D* is shown in Figure 3.2 and the problem is now stated as

$$\underline{\underline{C}}^{*}\ \underline{c}^{*n+1} = \underline{\underline{D}}^{*}\ \underline{c}^{*n}$$

$\underline{\underline{C}}^{*}$ is decomposed using a LU decomposition appropriate to its structure and $\underline{c}^{*n+1}$ is calculated. Since the location of the boundary changes in time, the LU decomposition must be performed every time the boundary location, -Peη or 1-Peη passes another collocation point.

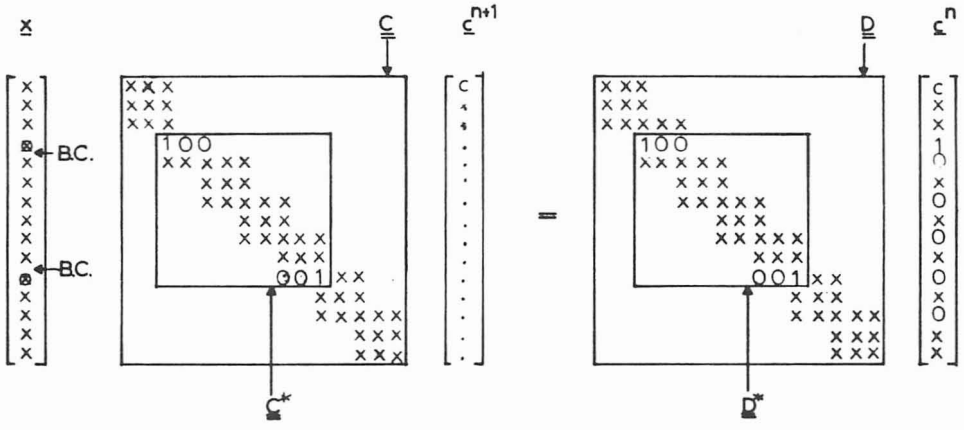

Figure 3.2

Numerical Procedure MCS

3.4 Results

The advantage of using MCS for problems with dominating convection is illustrated by comparisons using the same spatial

discretization (here collocation) with both moving coordinate system and a fixed coordinate system. The convection-diffusion equation is solved with Pe = 877.9 and 87790.0, with results given in Table 3.1.

Figure 3.3 compares a conventional scheme to the MCS-scheme using 4 elements. The scheme with a fixed coordinate system oscillates whereas the MCS solution does not. To eliminate the oscillations in the fixed coordinate scheme require 20 elements, and an increase of computer time by a factor of 5 (compare entries 1 and 8 in Table 3.1). Conversely, for non-oscillating solutions, MCS uses only 20% of the computation time needed with a fixed coordinate system.

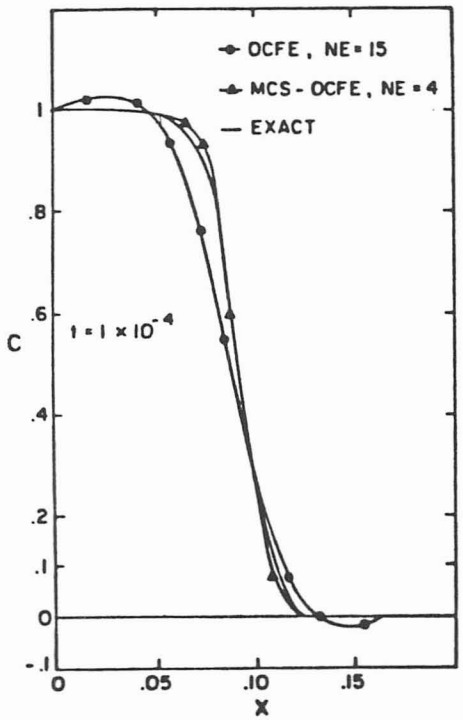

Figure 3.3

Comparison of Standard OCFE Versus Moving Coordinate System.
Pe = 877.9, NE = 4, NCOL = 2, $t = 2.5 \times 10^{-6}$.
Element nodes at ξ = -1, -0.05, 0, 0.05, and 1.

Table 3.1

Comparison of MCS with Conventional Scheme (both using OCFE)

	Entry	Scheme	NE	NCOL	$\Delta t \times 10^6$	CPU*	Error at Pe•t = 0.088	Error at Pe•t = 0.444	Maximum Oscillations at Pe•t = 0.444
Pe = 877.9	1	MCS	4	2	2.5	3.3	0.03	0.04	---
	2	---	6	2	2.5	5.1	0.033	0.005	---
	3	---	6	2	10	1.0	0.04	0.01	---
	4	---	8	2	2.5	6.7	0.008	0.008	---
	5	---	14	2	1.25	15.1	0.004	0.001	---
	6	OCFE	5	2	2	3.2	$\approx$0.1	$\approx$0.1	0.1
	7	---	15	2	2.5	8.1	0.11	0.05	0.04
	8	---	20	3	2.5	17.0	0.03	0.004	0.0022
					$\Delta t \times 10^8$		α		
Pe = 87790	9	MCS	12	2	5	4.5	0.5	0.02	0.005
	10	---	14	2	2.5	8.1	0.5	0.01	0.004
	11	---	16	2	1.25	17.0	0.5	0.004	---
	12	OCFE	50	3	1	70.5	0.0	0.003	0.004
	13	---	50	3	0.5	152.0	0.5	$\approx$0.1	$\approx$0.1
	14	---	50	5	1	140.0	0.0	0.003	---

*CPU on CDC 6400

Another comparison is made in Figure 3.4 with a Gaussian initial distribution and Pe = 10^6. Both schemes use the same number of elements and the same timestep. Severe oscillations appear in the conventional scheme whereas MCS gives none. The moving coordinate system works best for large Pe and oscillations are not introduced provided the initial conditions can be fit without oscillations. As time proceeds the profiles become less steep due to the dispersion indicated by Eq. (3.10), and oscillations are less likely.

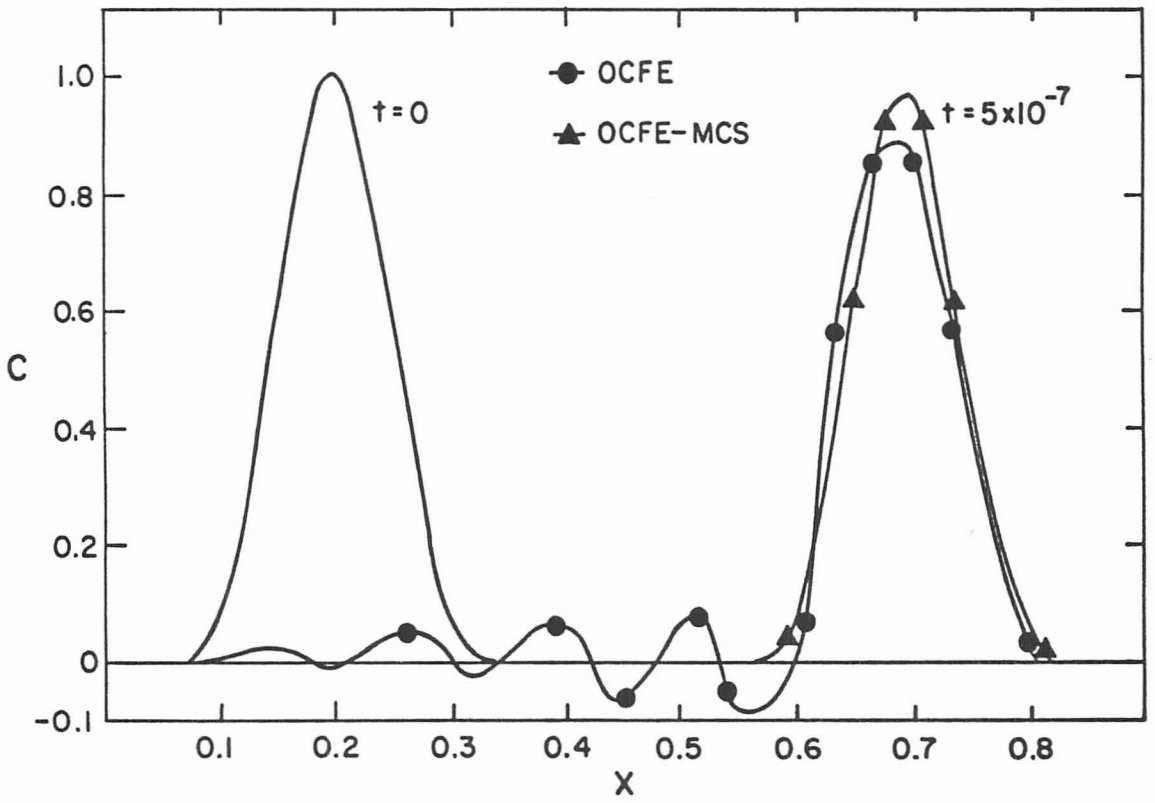

Figure 3.4

Comparison of Standard OCFE Versus Moving Coordinate System. Gaussian initial distribution Pe = 10^6, NE = 13, NCOL = 2, $\Delta t = 2.5 \times 10^{-9}$.

MCS is compared to the method of variable interpolation, Price et al. (1968), in Figure 3.5. The measure of accuracy is given by the maximum deviation from the exact solution

$$E(t) = \underset{i}{\text{Max}}\{|c(x_i,t) - c_{exact}(x_i,t)|\}$$

Both cases have negligible error caused by the time integration. The error decreases with time for the same number of elements and the MCS is more accurate at small times (when the front is steepest). In contrast to the method of charactersitic by Garder et al. (1964), which showed a minimum error of about 2%, the MCS will converge for increasing number of elements and with smaller timesteps, giving errors of 0.1% for the case shown in Figure 3.5.

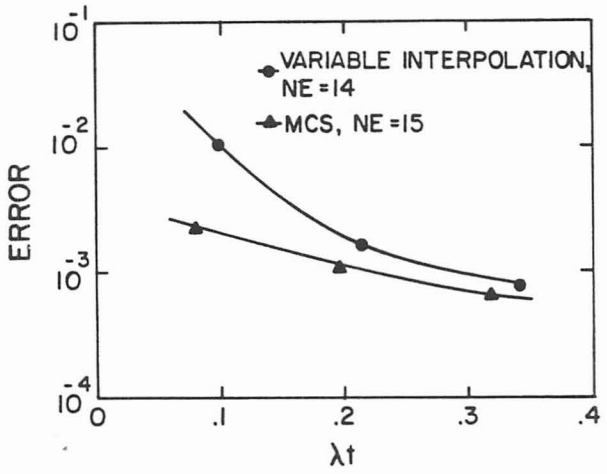

Figure 3.5

Comparison of Moving Coordinate System
Versus Variable Interpolation

The elements are not all the same size in MCS-OCFE. When small elements are used near the front the solution will be good at small times (when all changes occur near the front). At larger times, changes also occur further away from the front so that elements are needed there, too. Thus schemes which have slightly bigger elements may be preferred at later times. Figure 3.6 illustrates the error as a function of time for solutions obtained using different grids.

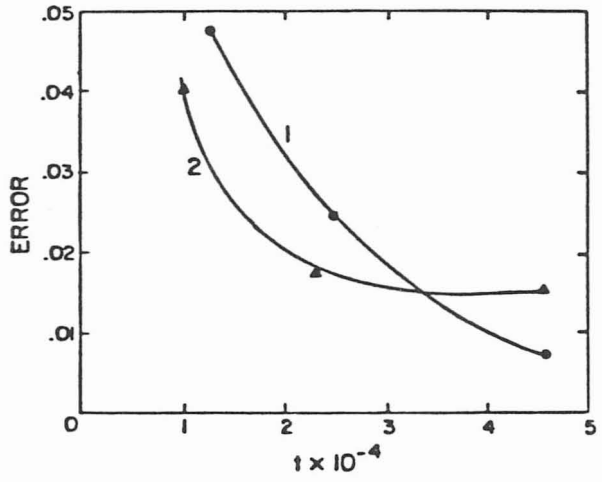

Error as function of time. Effect of mesh location.
Pe = 877.9, NE = 5, $\Delta t = 2.5 \times 10^{-6}$.
Curve 1 element nodes at ξ = -1, -0.2, -0.05, 0.05, 0.2, 1
2 element nodes at ξ = -1, -0.12, -0.04, 0.04, 0.12, 1

Figure 3.6

Error as Function of Time, Effect of Mesh Location

In Table 3.1 are shown results, errors, computation time, number of elements and Δt for Pe = 877.9 and 87790. It is clear that MCS

is superior to the conventional schemes. By having the same number of elements (entries 5 and 7 for 15 elements) the error is decreased by a factor 20-40, but the computation time is only two times longer. For the same computation time (entries 1 and 6 for $\sim$3 seconds) the conventional scheme is unreliable (10%) while MCS gives fairly accurate results (3%). For the same computation time (entries 5 and 8 for 16 seconds) the error is decreased by a factor of 4-8 and MCS gives no oscillations while the conventional scheme does.

For Pe = 87790, the MCS is even better. Table 3.1 shows results for both MCS and conventional OCFE. Comparing entries 13 and 10 the standard OCFE gives excessive oscillation, but MCS gives only 1% error and used only 5% of the computer time.

3.5 Conclusions

The moving coordinate system is very effective in improving the efficiency of numerical solutions to the convective-diffusion equation. The solutions do not suffer from severe oscillations or from excessive numerical dispersion, yet are economical to calculate. Further improvement could be made if a variable time step algorithm is incorporated. Since the front is nearly stationary in time with only slight broadening, and the eigenvalues are decreased by the transformation, larger timesteps are possible with MCS than with a fixed coordinate system. The computation time is reduced by a factor of 20-40 in some cases.

Chapter IV

NONLINEAR DIFFUSION FLOW THROUGH POROUS MEDIA

Chapter III applied the moving coordinate system to a linear one-dimensional equation where the frontal velocity was known. Here we extend the technique to a nonlinear problem where the frontal velocity is not known a priori and must be solved for as part of the problem. An eigenvalue analysis gains insight into the effect of discretization on the difficulty of solving the problem.

4.1 Introduction

Another problem whose numerical solution oscillates arises in moisture transport in desiccated soil. A simplified model for the transport was made by Finlayson (1976). The one-dimensional mass balance for a single liquid phase flowing through a porous media is

$$\frac{\partial}{\partial t}(\phi\rho S) = -\frac{\partial}{\partial y}(\rho q) \tag{4.1}$$

where ϕ is the porosity, ρ is the liquid density, S is saturation (liquid volume/non-solid volume), and q is the volumetric flux. Time is t, distance y, and gravity is neglected. The neglect of gravity allows a similarity solution (see Section 4.2), makes oscillations more evident, and does not appreciably affect the difficulty of the problem. Darcy's law is assumed

$$\rho q = -\frac{\rho k}{\mu}\frac{\partial p'}{\partial y}$$

where μ is the liquid viscosity and p' is the liquid pressure. The equations are non-dimensionalized to give

$$-\frac{dS}{dp_c}\frac{dp}{\partial t} = \frac{\partial}{\partial x}\left[k_r \frac{\partial p}{\partial x}\right] \quad . \tag{4.2}$$

where k_r is the relative permeability, k/k_o, and

$$p = p'/(\rho g L), \quad t = \tau k_o \rho g/(\mu L \phi), \quad x = y/L$$

Both k_r and S depend on the capillary pressure, which is the air pressure (taken as zero) minus the water pressure

$$p_c = -p \tag{4.3}$$

The variations of S and k_r with p_c are taken as

$$\frac{S-S_r}{1-S_R} + \frac{1}{1 + (p_c\, L/A1)^{\alpha}} \qquad k_r = \frac{1}{1 + (p_c\, L/B1)^{\beta}} \tag{4.4}$$

For a typical soil we use

$$S_r = 0.32,\ L = 100\ \text{cm},\ A1 = 231\ \text{cm},\ B1 = 146\ \text{cm},$$
$$\alpha = 3.65,\ \beta = 6.65$$

The boundary conditions are

$$\left.\begin{aligned} p &= BP0 \quad \text{for} \quad x = 0 \\ \frac{\partial p}{\partial x} &= 0 \quad \text{for} \quad x = 1 \end{aligned}\right\} \quad t > 0$$
$$p = BP1 \quad \text{for} \quad x > 0 \quad t = 0 \tag{4.5}$$

Finlayson and Nelson (1977) describe the mathematical difficulties which are associated with solving this equation. The drier the

soil is (decreasing BP1), and the more water imposed at x = 0 (BP0 = 0, soil saturated), the more difficult the problem is to solve. The parameters chosen above are for a gravelly coarse soil. A fine soil will give similar results without so severe a choice of BP1. A similarity solution is derived to give the exact solution for small times. An eigenvalue analysis further quantifies the numerical difficulties in this problem. The numerical techniques used for solving the nonlinear equation in both fixed and moving coordinate systems are described, and comparisons are made between them.

4.2 Similarity Transformation

To give error estimates an exact solution is needed. A similarity transformation can be made.

Equation (4.2) is

$$f(p)\,\frac{\partial p}{\partial t} = \frac{\partial}{\partial x}\left(g(p)\,\frac{\partial p}{\partial x}\right)$$

Having

$$p = f(\phi), \qquad \phi = x/\sqrt{t}$$

$$\frac{\partial p}{\partial t} = \frac{\partial p}{\partial \phi}\,\frac{\partial \phi}{\partial t} = -\frac{1}{2}\,\frac{x}{t\sqrt{t}}\,\frac{\partial p}{\partial \phi}$$

$$\frac{\partial p}{\partial x} = \frac{\partial p}{\partial \phi}\,\frac{\partial \phi}{\partial x} = \frac{1}{\sqrt{t}}\,\frac{\partial p}{\partial \phi}$$

$$\frac{\partial^2 p}{\partial x^2} = \frac{\partial}{\partial x}\left(\frac{1}{\sqrt{t}}\,\frac{\partial p}{\partial \phi}\right) = \frac{1}{t}\,\frac{\partial^2 p}{\partial \phi^2}$$

gives

$$0 = \frac{1}{2}\,\phi\, f(p)\,\frac{\partial p}{\partial \phi} + \frac{\partial}{\partial \phi}\left[g(p)\,\frac{\partial p}{\partial \phi}\right] \tag{4.6}$$

The boundary conditions change to

$$\left.\begin{array}{lll} p = BP1 & x > 0 & t = 0 \\ p = BP1 & x = 1 & t > 0 \end{array}\right\} \quad \phi \to \infty$$
$$p = BP0 \qquad x = 0 \qquad t > 0 \quad \to \phi = 0 \tag{4.7}$$

so that a similarity solution can be found only for semi-infinite domains or for finite domains at small times.

No analytical solution of (4.6) could be found; instead a numerical solution of (4.6) is calculated. Setting a time derivative on the left side

$$\frac{\partial p}{\partial \tau} = \frac{1}{2}\,\phi\, f(p)\,\frac{\partial p}{\partial \phi} + \frac{\partial}{\partial \phi}\left[g(p)\,\frac{\partial p}{\partial \phi}\right] \tag{4.8}$$

$$\begin{array}{lll} p = h(\phi) & \tau = 0 & \phi > 0 \\ p = BP0 & \tau > 0 & \phi = 0 \\ p = BP1 & \tau > 0 & \phi = \phi_{max} \end{array} \tag{4.9}$$

where ϕ_{max} is set to a high number $\phi_{max} = 6$. Integrating (4.8) with (4.9) as the boundary condition gives the steady state solution of (4.8), when $\tau \to \infty$.

We discretize (4.8) using non-equal spacing with central difference formulation as outlined in Section 4.5. The integration is performed using the GEARB package [Hindemarch, 1976] as it permits variable stepsize.

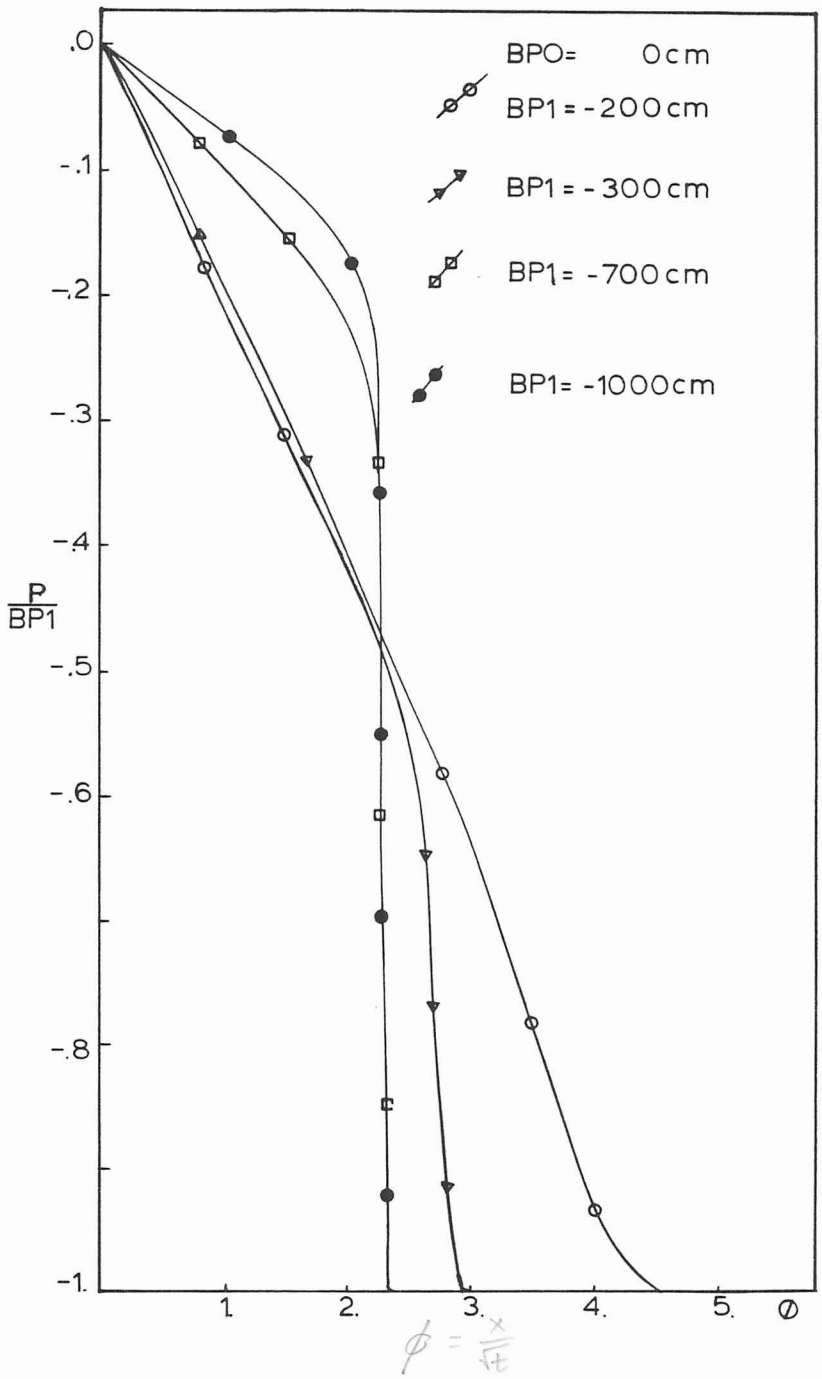

Figure 4.1

Nonlinear Diffusion Equation, Similarity Solution

An initial profile is guessed. For steep profiles a good guess helps to minimize the computation time. The integration is continued until the pressure at any node changes less than $\sim$0.5% of BP1. Integration to τ = 10 was found sufficient. Results were obtained for BP0 = 0 cm and varying BP1 as -200, -300, -700 and -1000 cm.

The result is shown in Figure 4.1. For BP1 = -200, -300 cm the results could be compared with accurate calculations as performed in Section 4.4. The agreement was good results within 0.5% error. For BP1 = -1000 cm the convergence was considerably slower. At a fixed time 0.01 the four solutions are compared in Figure 4.2.

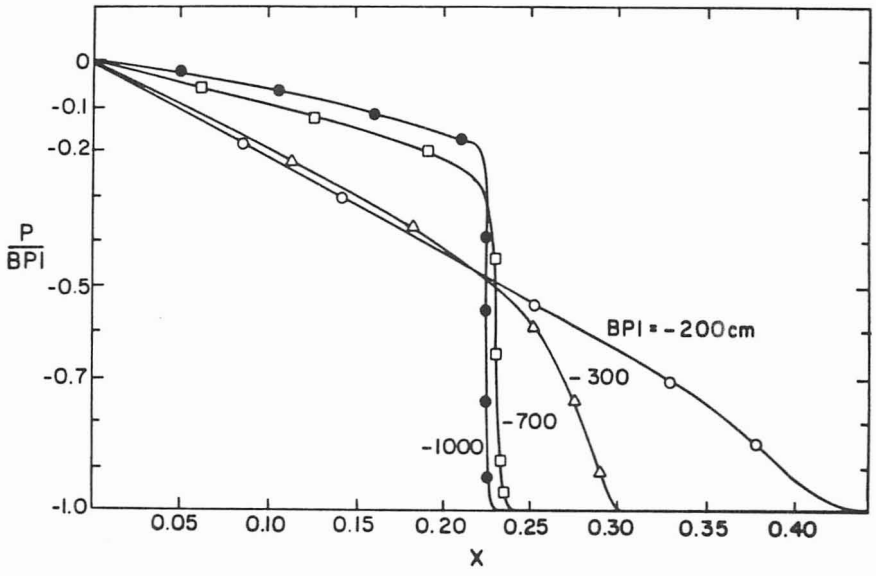

Figure 4.2

Similarity Solution at t = 0.01

4.3 Eigenvalue Analysis

Finlayson (1976) investigated the effect of the initial dryness of the soil. The obtained results are summarized in Table 4.1.

Table 4.1

Eigenvalues of Nonlinear Problems at t = 0.015, different initial dryness

BP0 (cm)	BP1 (cm)	$\max\|\lambda_i\|$	$\min\|\lambda_i\|$	SR
0	-200	1.23(6)	0.248	4.9(6)
-50	-200	1.30(3)	0.220	5.6(3)
5	-300	1.53(8)	0.144	1.1(9)
-50	-300	1.22(3)	0.0315	3.9(4)
0	-500	7.47(3)	0.00529	1.4(7)

For decreasing initial dryness (BP1) of the soil the stiffness ratio

$$SR = \frac{\max|\lambda_i|}{\min|\lambda_i|}$$

increases, and thereby the problem becomes more and more stiff (smaller timesteps required). Also for increasing BP0 (amount of waterflow) the problem becomes stiffer. Here we look at the effect of various discretizations. Discretizing equation (4.2) using orthogonal collocation on finite elements gives a set of nonlinear ordinary differential equations.

$$\sum_i C_{ji}(p) \frac{dp_i}{dt} = \sum_i D_{ji}(p) \cdot p_i \qquad (4.10)$$

The Jacobian for (4.10) can be expressed as

$$\underline{J} = \frac{\partial}{\partial p_R} \left(\underline{C}^{-1} * \underline{D} \right) \tag{4.11}$$

and the eigenvalues of $\underline{J}$ can be found given a solution p and discretization at a certain time.

The results obtained at t = 0.005 and t = 0.015 for BP1 = -300 cm and BP0 = 5 cm are given in Table 4.2 for various discretizations. At t = 0.015 the front is between x = 0.20 and x = 0.30. For uniform discretization the problem becomes stiffer as time proceeds, since the stiffness ratio SR becomes larger. If the system of equations is linear and uncoupled, the absolute value of the reciprocal of the eigenvalue is a time constant. For example

$$\varepsilon \frac{dy}{dt} = -y$$

has an eigenvalue of $-1/\varepsilon$ and a time constant of ε. If ε is small the eigenvalue is large. If we view the eigenvalues of Eq. (4.10) as the reciprocal of the time constants for the nodes in the system, then for a small time constant the eigenvalue becomes large. The time constant at a nodes is then $(-dS/dp_c)_i$. Since the boundary pressure is +5 cm for $p \to 0$ the value of $-dS/dp_c$ approaches zero, giving rise to small time constants and large eigenvalues. As time proceeds more and more nodes are in this situation, and the largest eigenvalue increases. The lowest eigenvalue is associated with nodes at other p where $-dS/dp_c$ takes reasonable values, and it remains constant

Table 4.2

Eigenvalues of Nonlinear Problem, BP1 = -300 cm, BP0 = 5 cm

Time	Discretization	Max. (EV)	Min. (EV)	SR = $\frac{\text{max. (EV)}}{\text{min. (EV)}}$
0.005	uniform NE=20	$6.9 \cdot 10^{7}$	0.16	$4.3 \cdot 10^{8}$
0.015	uniform NE=20	$4.9 \cdot 10^{10}$	0.23	$2.2 \cdot 10^{11}$
	non-uniform NE=10, #1	$4.9 \cdot 10^{10}$	0.23	$2.2 \cdot 10^{11}$
	NE=8 , #2	$3 \cdot 10^{7}$	0.21	$1.4 \cdot 10^{8}$
	NE=7 , #3	$5 \cdot 10^{5}$	0.22	$2.2 \cdot 10^{6}$
	NE=4 , #4	$5 \cdot 10^{5}$	0.22	$2.2 \cdot 10^{6}$

#1	disc:	0.	0.05	0.1	0.15	0.2	0.225	0.25	0.275	0.3	0.65	1.
#2	disc:	0.		0.1		0.2	0.225	0.25	0.275	0.3	0.65	1.
#3	disc:	0.				0.2	0.225	0.25	0.275	0.3	0.65	1.
#4	disc:	0.				0.2		0.25		0.3		1.

since there are always nodes having p between BP0 and BP1. Thus the stiffness ratio increases with time.

For the non-uniform discretizations we take the numerical solution at the appropriate t(0.005 or 0.015) obtained using a uniform grid $\Delta x = 0.05$. This solution is interpolated onto a new, non-uniform grid, and the eigenvalues of the Jacobian, Eq. (4.10), are calculated. In discretization no. 1 we place two additional elements between x = 0.2, and 0.3, and remove elements beyond x = 0.3 (where p = BP1 is a constant); the eigenvalues are unaffected. If elements are removed near x = 0, discretization no. 2, the maximum eigenvalue is reduced. Discretization no. 3 removes just one more of these elements and the stiffness ratio is reduced two orders of magnitude.

The change in discretization from 1 to 3 where nodes near x = 0 are removed gives rise to a reduction of five orders of magnitude in the stiffness ratio. In discretization no. 4 elements in the front are removed, but the stiffness ratio does not change.

In a moving coordinate system, we can concentrate nodes around the front and have few nodes elsewhere. Then the maximum absolute value of the eigenvalue will be lower and larger timesteps should then be possible.

4.4 Solution Methods — Fixed Coordinate System

The standard finite difference technique to solve Eq. (4.2) uses a central difference approximation.

$$-\frac{dS}{dp_c}\bigg|_i \frac{dp_i}{dt} = \frac{1}{\Delta x}\left(k_{i+1/2}\frac{p_{i+1} - p_i}{\Delta x} - k_{i-1/2}\frac{p_i - p_{i-1}}{\Delta x}\right) \tag{4.12}$$

The permeabilities at the half nodes can be evaluated in different ways [Finlayson and Nelson, 1977]:

1) Average Permeabilities

$$k_{i+1/2} = \frac{k_i + k_{i+1}}{2} \quad , \quad O(h^2)$$

2) Upstream Permeabilities

if $|p_{i+1} - p_{i-1}| < \varepsilon \rightarrow$ average permeability

if $p_{i-1} > p_{i+1} \rightarrow k_{i+1/2} = k_i$

if $p_{i-1} < p_{i+1} \rightarrow k_{i-1/2} = k_{i+1}$

This approach is widely used as it increases the stability, but it is less accurate, with errors O(h).

3) Average Pressure

$$k_{i+1/2} \text{ evaluated at } p = \frac{p_i + i_{i+1}}{2} \quad , \quad O(h)$$

Here we use the average permeability as it has the highest order accuracy. A modified Crank-Nicholson method was used to integrate the equations in the form

$$\sum_i C_{ji}(p) \frac{dp_i}{dt} = \sum_i D_{ji}(p) p_i \quad .$$

If we let $p_i^n = p_i$ $(t = n\Delta t)$ we used

$$\sum_i C_{ji}(p^n) \frac{p_i^{n+1} - p_i^n}{\Delta t} = \sum_i D_{ji}(p^n)\left[(1-\alpha)p_i^n + \alpha p_i^{n+1}\right] \qquad (4.13)$$

All function evaluations are explicit and no iterations are performed, in contrast to a regular Crank-Nicholson method.

4.5 Solution Method — Moving Coordinate System

A moving coordinate system is applied to Eq. (4.2) as described in Chapter III, and the transformation gives

$$-\frac{dS}{dp_c}\frac{\partial p}{\partial \eta} = -\lambda(\eta)\,\frac{1}{2}\frac{dS}{dp_c}\cdot\frac{\partial p}{\partial \xi} + \frac{\partial}{\partial \xi}\left[k_r \frac{\partial p}{\partial \xi}\right] \quad , \qquad (4.14)$$

the boundary conditions become

$$\left.\begin{aligned} p &= BP0 \quad \text{at} \quad \xi = -\int_0^\eta \lambda(t')dt' \\ \frac{dp}{d\xi} &= 0 \quad \text{at} \quad \xi = 1 - \int_0^\eta \lambda(t')dt' \end{aligned}\right\} \eta > 0$$

$$p = BP1 \quad \text{for} \quad \xi > 0 \quad \text{and} \quad \eta = 0 \qquad (4.15)$$

Small elements or grid spacings must be used near the front, which remains fixed at $\xi = 0$ in the moving coordinate system. For an efficient calculation we must use a graded mesh, with small elements near the front and larger ones elsewhere. Equation (4.14) is discretized in a finite difference method by letting ξ_i be the location of the i-th node, p_i the pressure at the i-th node, and $h_i = \xi_{i+1} - \xi_i$. The derivative is taken as

$$\frac{\partial}{\partial \xi}\left(k_r \frac{\partial p}{\partial \xi}\right)\Big|_i = \frac{2}{h_i + h_{i-1}}\left(k_r^{i+1/2}\,(p_{i+1} - p_i)/h_i - k_r^{i-1/2}\,(p_i - p_{i-1})/h_{i-1}\right) \qquad (4.16)$$

$$\frac{\partial p}{\partial \xi}\Big|_i = \frac{p_{i+1} - p_{i-1}}{h_i + h_{i-1}}$$

Blöttner (1974) shows these formulas are correct to $O(h_i^2)$ provided the mesh is graded such that

$$\xi_{i+1} - 2\xi_i + \xi_{i-1} = O(h_i^2)$$

A forward difference can also be used for the first derivative since $dS/dp_c < 0$.

$$\frac{\partial p}{\partial \xi}\Big|_i = (p_{i+1} - p_i)/h_i \quad .$$

This formula is correct to $O(h_i)$. For time integration the modified Crank-Nicholson was used as described by Eq. (4.13).

To determine the velocity of the front, the largest gradient at any time is calculated. When the position at which this occurs has moved from one node to another, the coordinate system is moved the same distance so as to keep the largest gradient fixed at the origin. From the discrete values of the velocity an integrated velocity can be calculated with the trapezoid rule.

It was found important to set the boundary conditions exactly by changing the prefixed node location rather than simply using the nearest points as in the linear case. Thus the end elements are adjusted so that a node exists at the ξ given in Eq. (4.15). Suppose

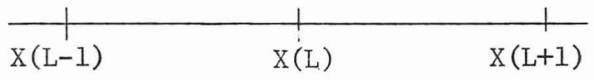

is the preset node location. At any time the accumulated velocity (4.15) is computed to give the location of the right boundary. The distances DIFQ/DIFS to the nearest two points are measured

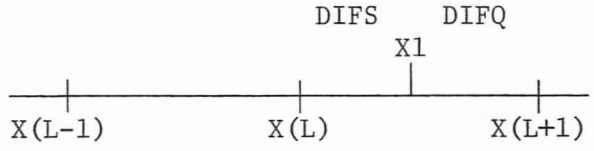

and the mesh location is changed as follows: if

1) DIFS < DIFQ X(L) is changed to X1

2) DIFS > DIFQ X(L+1) is changed to X1

4.6 Results and Discussions

The two methods are compared in two cases:

I) BP0 = 5 cm BP1 = -300 cm

II) BP0 = 5 cm BP1 = -1000 cm

Case I:

The similarity solution for this case is shown in Figure 4.3.

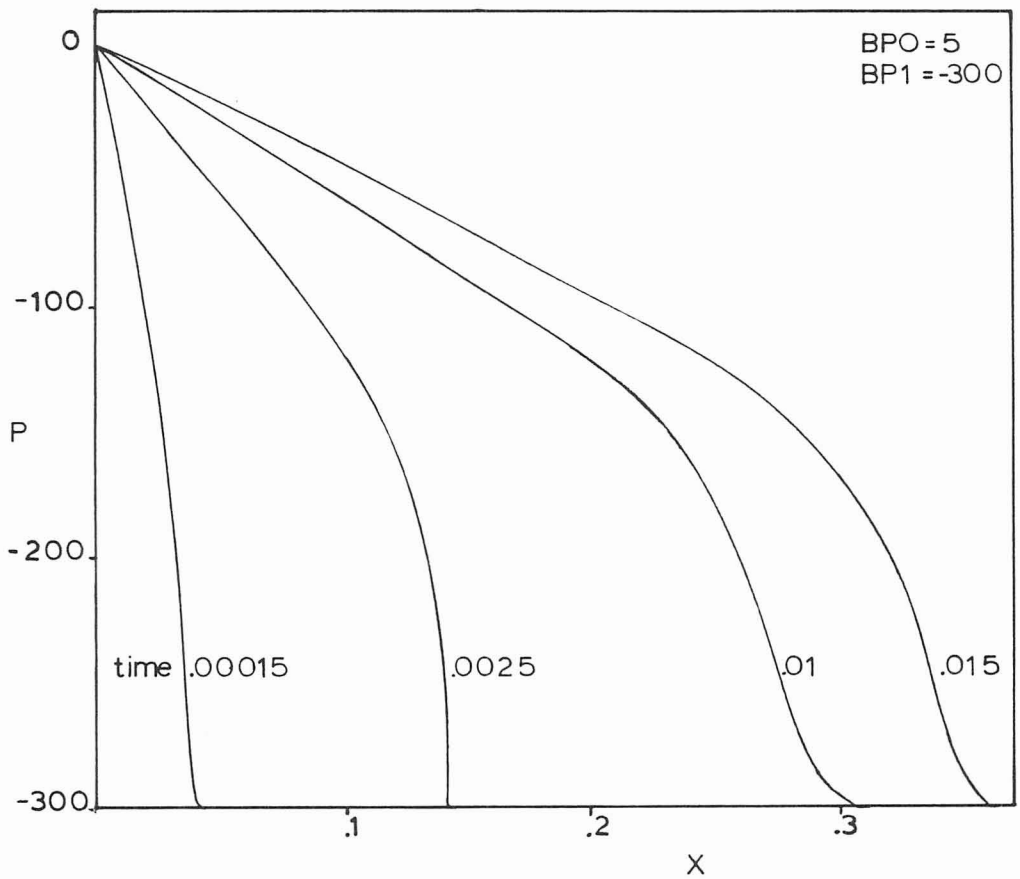

Figure 4.3

Exact Solution, Nonlinear Diffusion, Similarity Solution, BP1 = -300 cm

For Case I the front is not too steep and the efficiency of the two methods is almost the same (see Table 4.3). The error is defined as the maximum deviation from the similarity solution at any node in the domain. The regular finite difference scheme with 21 nodes (run 1) gives a 6% error but to get a more accurate solution many more

Table 4.3

Comparison of MCS With Conventional Scheme (Both Using FD) for Nonlinear Flow Through Porous Media
BP0 = 5 cm, BP1 = -300 cm

Run	Scheme	NE	α	$\Delta t \times 10^{-5}$	$\Delta t/\Delta x^2$ min	Error	CPU*
1	FD-CDA	21	0.5	20	0.08	6%	2 secs
2	FD-CDA	21	0.5	10	0.04	4%	4 secs
3	FD-CDA	81	1.0	5	0.32	1%	28 secs
4	FD-CDA	81	0.5	10	0.64	>15%	16 secs
5	MCS-CDA	23	1.0	20	2	6%	2 secs
6	MCS-CDA	33	0.5	5	2	3%	14 secs
7	MCS-CDA	45	0.5	5	8	0.5%	18 secs
8	MCS-CDA	45	1.0	5	8	2%	18 secs

*CPU on CDC 6400

CDA: Central Difference Approximation

nodes are needed (81 for run 3) and this also requires a smaller timestep. For the moving coordinate system (MCS) fewer nodes (run 7) achieve the same error.

Numerical solution of the diffusion equation will be unstable if

$$\Delta t/\Delta x^2 > 1/2 \tag{4.18}$$

for a central difference approximation and explicit integration scheme [Peaceman, 1978]. In Table 4.3 entry 4 violates Eq. (4.18) and the solutions have oscillations (error > 15%). The modified Crank-Nicholson is not implicit because we do not iterate.

The exact frontal velocity is obtained by the similarity transformation. The velocity is defined in Section 4.5 as the speed of the largest gradient of p. The ϕ corresponding to this point can be determined from Figure 4.1. For BP1 = -300 cm it is

$$\phi_f \left(\frac{\partial p}{\partial \phi} \min \right) = x_{\text{frontal position}} / \sqrt{t} = 2.75$$

and as the velocity is defined as

$$\lambda(t) = \frac{dx_{\text{frontal position}}}{dt}$$

we have

$$\int_0^t \lambda(t)dt = \phi_f \cdot \sqrt{t} = 2.75 \sqrt{t} \qquad (4.17)$$

The frontal velocity is then

$$\lambda(t) = 1.4/\sqrt{t} \qquad (4.18)$$

The numerically determined values of the accumulated velocity are compared with (4.17) in Table 4.4 and illustrated in Figure 4.4. The algorithm is able to determine the frontal velocity accurately.

As the solution develops a sharp front the problem is similar to a convective diffusive equation. Rewriting Eq. (4.2) to

$$\frac{\partial p}{\partial t} = f_1(p,x) \frac{\partial p}{\partial x} + f_2(p,x) \frac{\partial^2 p}{\partial x^2}$$

where

Table 4.4

Nonlinear Diffusion, Frontal Velocity and Accumulated Velocity (Run 7)

Time (x 100)	$\int_0^t \lambda(t)dt$	ϕ_f(num) (4.17)	$\lambda(t)$ (4.18)	f (p,x) (4.20)
0.00015	0.0313	2.55	228	620
0.00045	0.563	2.65	132	380
0.00095	0.813	2.63	89	413
0.00195	0.1187	2.68	62	225
0.00295	0.150	2.76	50	100
0.00500	0.1975	2.79	39	50
0.0075	0.2375	2.75	32	55
0.0100	0.2775	2.78	27	35
0.0150	0.3350	2.73	22	22

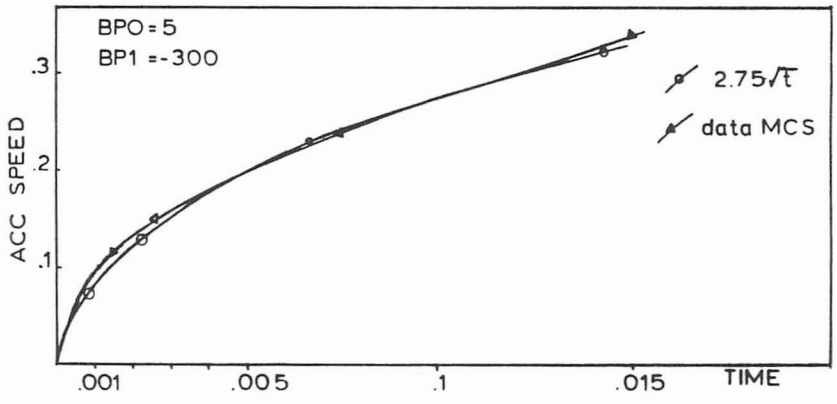

Figure 4.4

Accumulated Speed as Function of Time

$$f_1(p,x) = \frac{dk_r}{dx} \left(-\frac{dS}{dp_c}\right)$$

$$f_2(p,x) = k_r \left(-\frac{dS}{dp_c}\right) \qquad (4.20)$$

$f_1(p,x)$ is a measure of the velocity. This coefficient was calculated numerically at the origin and given in Table 4.4 too. There is a strong relation between f and the calculated velocity (4.18).

No distinct advantage of using MCS is found for Case I. For the same computation time, the same accuracy can be obtained. It has although been demonstrated:

1) MCS solutions give the similarity solution and the frontal velocity is adequately determined.
2) MCS achieves the same accuracy for about half the number of nodes and fewer timesteps.

Case II:

For Case II a very steep front is developed as shown in Figure 4.5. Only implicit integration was used, $\alpha = 1$ in (4.13). Figure 4.6 shows results using both schemes and here the advantages of MCS become significant. The error is defined as percent misplacement of front (at p = BP1/2). With the regular finite difference scheme and 120 nodes (run 1) the velocity of the front is too high and taking smaller timesteps did not affect the solution. Run 2 with 600 nodes is closer to the exact solution, and if the timestep is decreased as in run 3 the profile moves towards the similarity solution.

In contrast MCS with only 62 nodes (run 4) and a higher timestep gives almost the correct solution. A similar solution was achieved using both fewer nodes and higher timesteps (run 5) but then smoothing occurs. By taking higher timesteps the front is placed incorrectly

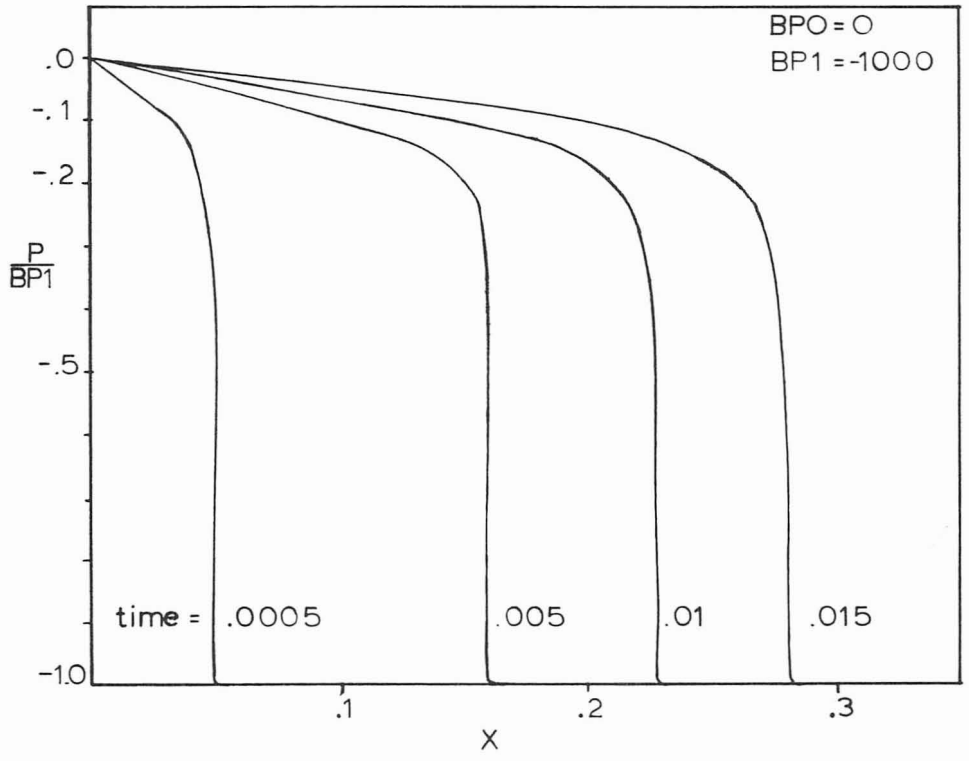

Figure 4.5

Nonlinear Diffusion, BP1 = -1000 cm

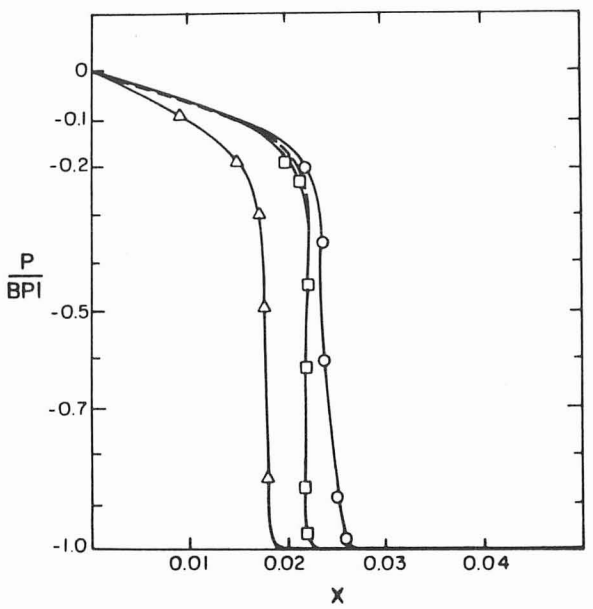

(a)

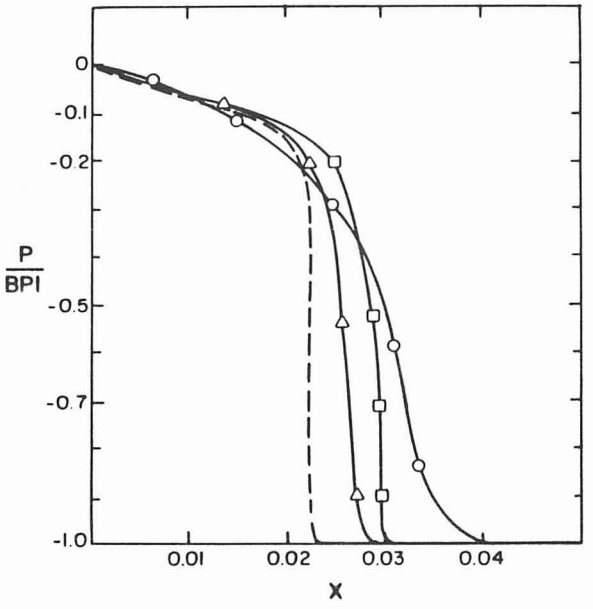

(b)

Figure 4.6

Comparison, Standard Versus Moving FD; Nonlinear Flow Through Porous Media at $t = 1 \times 10^{-4}$. Symbols defined in Table 4.5.

(run 6). The forward difference compared to the central difference approximation for the first derivative was found to place the front more correctly but at the cost of some smoothing, and the forward difference is therefore preferred.

An example of the distribution of nodes for runs 4 to 6 is shown in Table 4.6. By taking fewer nodes before the front higher time-steps can be taken but some smoothing occurs. This result is comparable with the results from the eigenvalue analysis. By decreasing the number of nodes in a region where the node values (pressure) do not change much, the eigenvalues from there will be small and we can take larger timesteps.

Table 4.5

Comparison of MCS With Conventional Scheme (Both Using FD) for Nonlinear Flow Through Porous Media. BPO = 5 cm, BPL = -1000 cm

Symbol in Figure 4.6		Entry	Scheme	NE	$\Delta t \times 10^{+7}$	$\Delta t/\Delta x^2$	Error	CPU*
a	o	1	CDA	120	2.5	0.004	33%	60 secs
a	□	2	CDA	600	2.	0.072	26%	402
a	△	3	CDA	600	1.	0.036	12%	804
b	□	4	MCS-FW	62	1.25/2.5	8000	∿ 0%	57
b	o	5	MCS-FW	62	2.5	8000	3%	36
b	△	6	MCS-FW	42	2.5	2500	22%	24

*CPU on CDC 6400

CDA: Central Difference Approximation

FW: CDA for second derivative, forward difference form for first derivative

Table 4.6

Distribution of Nodes for Run 4 to 6 (MCS)

Node	Run 4,5	Run 6
	No. of grid points between	
-1.		
	1	1
-0.5		
	2	2
-0.1		
	4	2
-0.02		
	6	3
-0.001		
	5	5
-0.0001		
	10	5
0.		
	10	5
0.00005		
	10	7
0.0001		
	10	5
0.01		
	2	2
0.02		
	4	2
0.1		
	2	2
1.0		

The gain in efficiency achieved by using MCS is highest for the very steep front. If we compare run 3 and run 6, we use about 15 times fewer nodes and timesteps about 3 times greater to achieve nearly the same accuracy. MCS is thus about 40 times faster than the same method on a fixed grid. Optimal use of MCS was not accomplished for this nonlinear case. In the two-dimensional calculations

it was found that rather than obtaining the velocities as discrete values, much larger timesteps could be taken if continuous velocities are used (for every timestep), see 5.3-5. Also a variable timestep scheme will reduce the number of timestep.

4.7 Conclusions

The moving coordinate system is applicable to nonlinear equations with unknown frontal velocity.

An eigenvalue analysis shows that a proper node location can reduce the stiffness ratio by five orders of magnitude by changing from a uniform grid to an irregular grid where the nodes are concentrated near the frontal position and few elsewhere. In places where the solution does not change much (near $x = 0$, where the soil is nearly saturated), the nodes give rise to large eigenvalues.

Applying the moving coordinate system achieves a large gain in efficiency when the initial soil is very dry. Comparison to a conventional scheme and an exact solution obtained by similarity transformation shows cost savings of a factor of 40 for comparable accuracy. The frontal velocity is determined by the location of the largest gradient of the solution. The boundary node location must be changed during the integration to specify the boundary conditions exactly.

PART III

MOVING COORDINATE SYSTEM—TWO DIMENSIONS

In Part III of this study the application of a moving coordinate system as a numerical technique to two-dimensional sharp front problems is described. If substantial reduction in the computation time can be achieved, this technique would be applicable for solving models of enhanced oil recovery processes. In Chapter V the convective diffusion equation is solved with a known velocity field and in Chapter VI the velocity field is solved for as part of the problem.

Chapter V

CONVECTIVE DIFFUSIVE EQUATION

5.1 Introduction

The numerical solution of two-dimensional convective diffusive type equations is of prime importance for predictions and analysis of energy related research. In this chapter the application of the moving coordinate system to a simple mathematical model is developed and tested. The model contains all the numerical difficulties arising in models of enhanced oil recovery, yet is simple enough to be tractable. The moving coordinate system worked well for this problem in one dimension. Here we test the technique in two dimensions.

The numerical methods are reviewed in Chapter II and here we review key differences arising for two-dimensional problems. Peaceman and Rachford (1962) developed a finite difference technique with an overshooting scheme to eliminate the oscillations. Later studies by Yanosik and Macracken (1976), Wheatley (1979) have improved the original formulation with a nine rather than five point formulation. Different Galerkin based finite element methods have been evaluated—Settari et al. (1976), Young (1977, 1978), Huyakorn et al. (1976, 1978, 1979), Todd (1979)—and have been shown competitive with the finite difference methods (only proved for a linear problem). The above papers solved the models with Hermite-cubic, C^{o}-cubic and upstream weighted linear elements. Orthogonal collocation on finite elements was considered by Pinder and Frind (1979) and Masliyah and Kumar (1979). For sharp front problems none of the above methods have been shown feasible as an extensive number of elements are needed (Chapter II) for accurate solutions.

The variable interpolation technique has been applied to two-dimensional problems by Chase (1979). It was applied with a Galerkin finite element method and Hermite cubic elements. For comparable accuracy it was found three times more expensive than a conventional finite difference technique. Interpolation and extensive bookkeeping makes the method intractable.

Time split schemes can be applied with any conventional discretization method. The main cost of doing two-dimensional problem is the solution of algebraic equation usually done by a direct elimination

(Gaussian) technique. In time split schemes the equations are iterated to convergence. Baker (1978) and Young (1978) report a gain in efficiency of a factor 5-20 compared to direct schemes.

Application of MSC to two-dimensional problems has been considered by Thomas and Martinez (1976). They transformed the equations into the MCS and the grid was kept fixed and a point source moved in the mesh. A large finite element representation is used to render the effect of boundary conditions (infinite domain). The frontal position was not fixed in space in the moving coordinate system. Computational efficiency is not achieved in this manner.

It is the object in this chapter to compare MCS with the most efficient conventional numerical methods, including schemes using a timesplit procedure.

Only parabolic type problems are examined here

$$\underset{\text{(accumulation)}}{\frac{\partial c}{\partial t}} + \underset{\text{(convection)}}{\underline{u} \cdot \nabla c} = \underset{\text{(dispersion/diffusion)}}{\nabla \cdot (\underline{\underline{K}} \cdot \nabla c)}$$

and the difficulty of obtaining a solution is measured by the ratio of the injection rate to the dispersion. Most energy related processes give one or several equations of the form shown above. Component balances (polymers, surfactants, oil) and heat balances are evolutionary (accumulation) and both convection and dispersion are important. In most cases the velocity field is unknown because of nonlinearities and an elliptic equation must be solved separately. Here we solve the linear problem where $\underline{u}$ is independent of the compo-

nent concentration or temperature. For predicting the recovery from an oil field two cases are important: flow in the vicinity of the wells (radial symmetry) and flow in the whole oil field represented by a five spot well pattern.

The wells are usually placed in a pattern as shown in Fig. 5.1 with alternating rows of producing and injecting wells. Some oil fields might have over a thousand wells arranged in this manner. A five spot pattern is then referred to the area, which represents the whole field, if all reservoirs were homogeneous. Because of symmetry only the triangle shown in Fig. 5.1 needs to be considered in a numerical approximation. Different forms of dispersion tensor $\underline{\underline{K}}$ arises depending on the velocity of the fluids. Two cases are con-

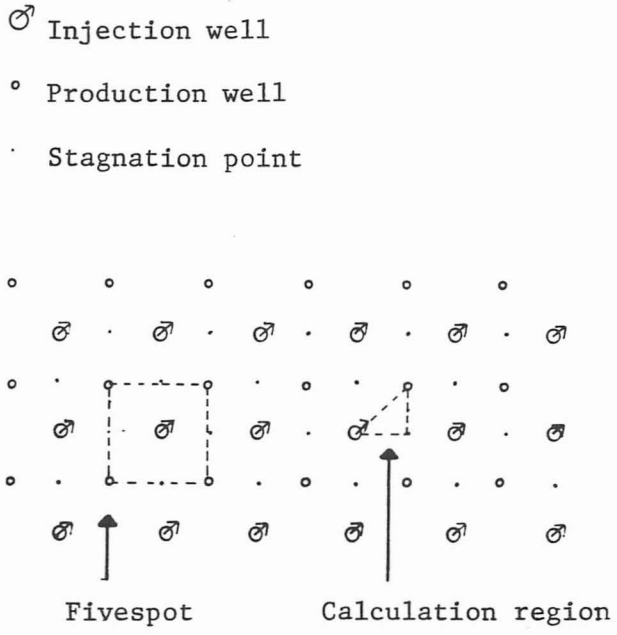

Figure 5.1

Well Pattern

sidered: a constant dispersion dyadic $\underline{\underline{K}}$ and a dispersion dyadic proportional to the velocity (Section 6.1-3). For the two flow fields and dispersion tensors, solutions are obtained for different Peclet numbers.

In Section 5.2 the mathematical models are discussed in detail. The numerical scheme for the moving coordinate system is described in 5.3 and a procedure for finding the frontal velocity is given. Examples of both large and small dispersion levels are calculated with the models (Section 5.4) and mass balances are made to examine the accuracy. Comparisons in both accuracy and computational efficiency are made to conventional schemes.

5.2 Mathematical Model

In Chapter VI Section 6.2 the mathematical model for the miscible displacement process is discussed. Here we apply a number of additional assumptions. The flow field as given by (6.1) is here assumed incompressible and with no gravity effects. Equation (6.1) simplifies to

$$\nabla \cdot \vec{u} = 0 \quad \text{or} \quad \frac{kh}{\mu} \nabla \cdot (\nabla p) = 0 \tag{5.1}$$

By this additional constraint the pressure is independent of the concentration, so (5.1) can be solved separately. Equation (5.1) is Laplace's equation and if we define the potential

$$\vec{u} = \nabla \Phi$$

Equation (5.1) becomes

$$\nabla^2\Phi = 0 \quad . \tag{5.2}$$

Le Blanc and Claude (197o) give the analytical solution to (5.2) for any number of wells.

$$\Phi(x,y) = \Phi + \frac{K_1}{2\pi r_w} \sum_{i=1}^{NWELL} q_i' \ln\left[(x-x_i)^2 + (y-y_i)^2\right] \tag{5.3}$$

where x_i, y_i is the location of the i'th well, and r_w the radius of the wells. Equation (5.3) is obtained by complex variables. The velocity components can now be obtained by differentiating Eq. (5.3)

$$u_x^* = \sum_{i=1}^{NWELLS} q_i^* \frac{(x-x_i)}{(x-x_i)^2 + (y-y_i)^2}$$

$$u_y^* = \sum_{i=1}^{NWELLS} q_i^* \frac{(y-y_i)}{(x-x_i)^2 + (y-y_i)^2} \tag{5.4}$$

The flow field from a single well and from a five spot pattern can be considered using (5.4). For the five spot flow many wells must be taken into account to insure the boundary condition

$$\underline{u} \cdot \vec{n} = 0 \quad \text{(no flow across boundary)}.$$

is specified correctly. The velocity at the symmetry point between injecting and producing wells, called stagnation point is zero (shown in Fig. 5.1 too). The concentration of oil at this point should therefore remain constant during the displacement process. Sixty-one (61) wells placed symmetrically around the triangle (Fig. 5.1) were

found adequately to model the five spot and obtain the correct boundary conditions. The pressure and flow field is shown in Figs. 5.2 and 5.3. The velocity at the stagnation point is here less than 10^{-3}.

The component balance (5.19) is here assumed to have no absorption or

$$\phi \frac{\partial c}{\partial \tau} + \vec{u} \cdot \nabla c = \nabla \cdot (\underline{\underline{K}} \nabla c) \tag{5.5}$$

The dispersion tensor depends in general on the velocity of fluid and the molecular diffusion (Section 6.1-3). Two extremes are considered here: either a constant dispersion dyadic or a dispersion dyadic proportional to the velocity so

$$\begin{aligned} \underline{\underline{K}}^* &= \begin{pmatrix} D & 0 \\ 0 & D \end{pmatrix} && |u| < 10^{-5} \text{ cm/sec} \\ \underline{\underline{K}}^* &= \alpha \sqrt{u_x^2 + u_y^2} \begin{pmatrix} 1 & 0 \\ 0 & 1 \end{pmatrix} && |u| > 5 \times 10^{-4} \text{ cm/sec} \end{aligned} \tag{5.6}$$

where α is the mixing length (6.22). The flow rates for which these extremes are valid are listed too (Scheidegger, 1970).

The component balance in nondimensional form is then

$$\frac{\partial c}{\partial t} + u_x \frac{\partial c}{\partial x} + u_y \frac{\partial c}{\partial y} = \frac{\partial}{\partial x}\left[K \frac{\partial c}{\partial x}\right] + \frac{\partial}{\partial y}\left[K \frac{\partial c}{\partial y}\right] \tag{5.7}$$

where the dispersion is either of the forms

$$K = 1 \quad \text{or} \quad K = \alpha \sqrt{(u_{x1})^2 + (u_{y1})^2} \quad .$$

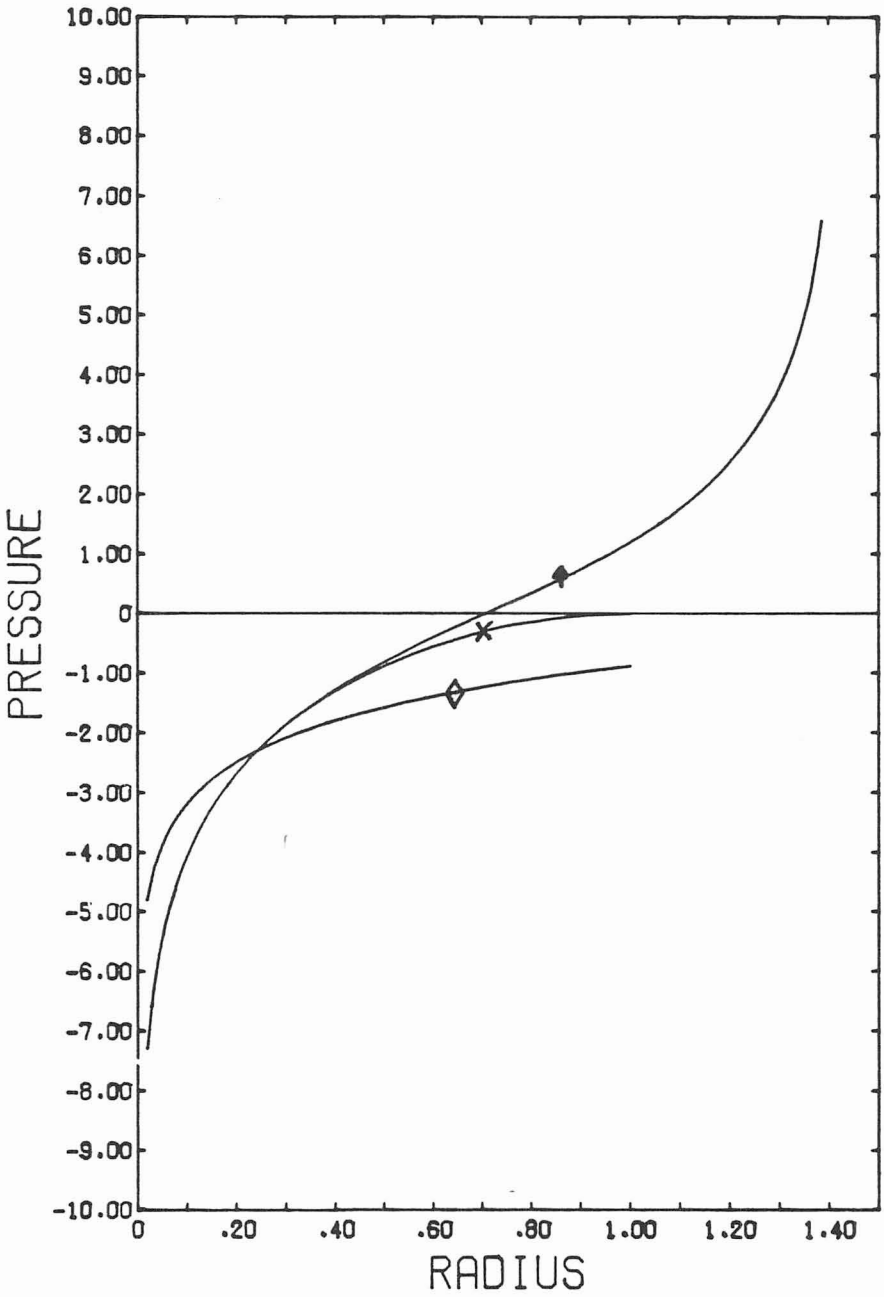

Figure 5.2

Pressure, Analytical Solution for One Well and Five Spot Well Pattern (×: five spot y = 0; ♦: five spot diagonal, ◇ one well)

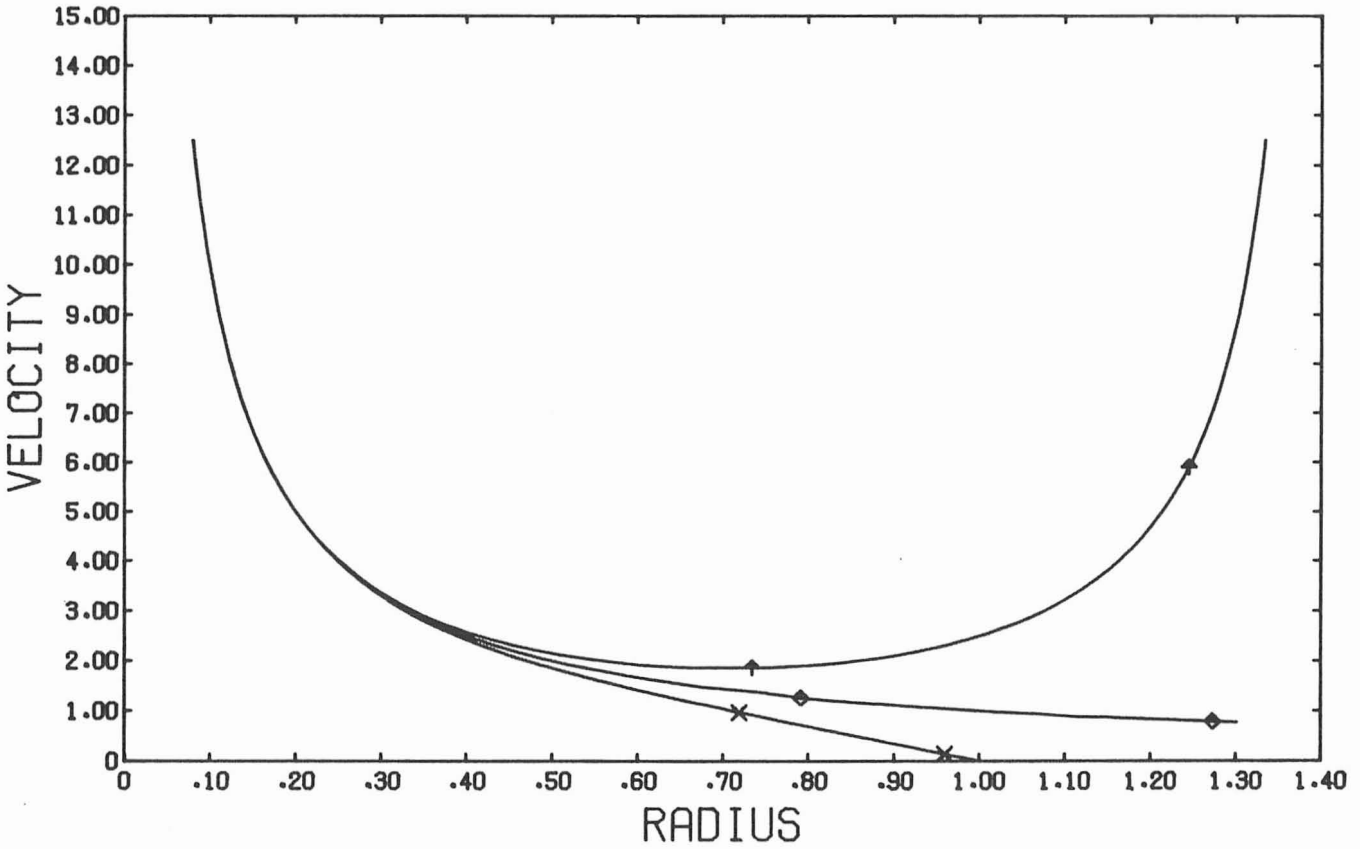

Figure 5.3

Velocity Components, One Well and Five Spot, Exact Solution
(x; five spot y = 0; ♠ ; fivespot x = y; ◇ , one well)

The velocity components are calculated with

$$u_x = Pe \cdot u_{x1} \quad \text{and} \quad u_{x1} = \sum_{i=1}^{NWELLS} q_i \frac{(x-x_i)}{(x-x_i)^2 + (y-y_i)^2}$$

$$u_y = Pe \cdot u_{y1} \quad \text{and} \quad u_{y1} = \sum_{i=1}^{NWELLS} q_i \frac{(y-y_i)}{(x-x_i)^2 + (y-y_1)^2} \tag{5.8}$$

where for five spot flow

injection well : $q_i = 1$

producing well : $q_i = -1$

as injection and production rates are the same. The Peclet numbers become

$$Pe_1 = \frac{\langle u \rangle}{D_M} \cdot L \qquad Pe_1 = L/\alpha \tag{5.9}$$

depending on the dispersion tensor (see 6.3-4 also).

Solutions to (5.7) are obtained using the two different forms of the dispersion tensor (5.6). Because of symmetry it is only necessary to solve (5.7) over part of the domain shown in Fig. 5.1. The triangle is the smallest area which preserves the properties of a five spot flow pattern, and is used in all cases described in this study. Different boundary conditions arise whether a continuous displacement or a slug is injected into the reservoir. These are shown in Fig. 5.4. $\frac{\partial c}{\partial n} = 0$ was used on S_2 for radial flow as the solution was only computed at short distance.

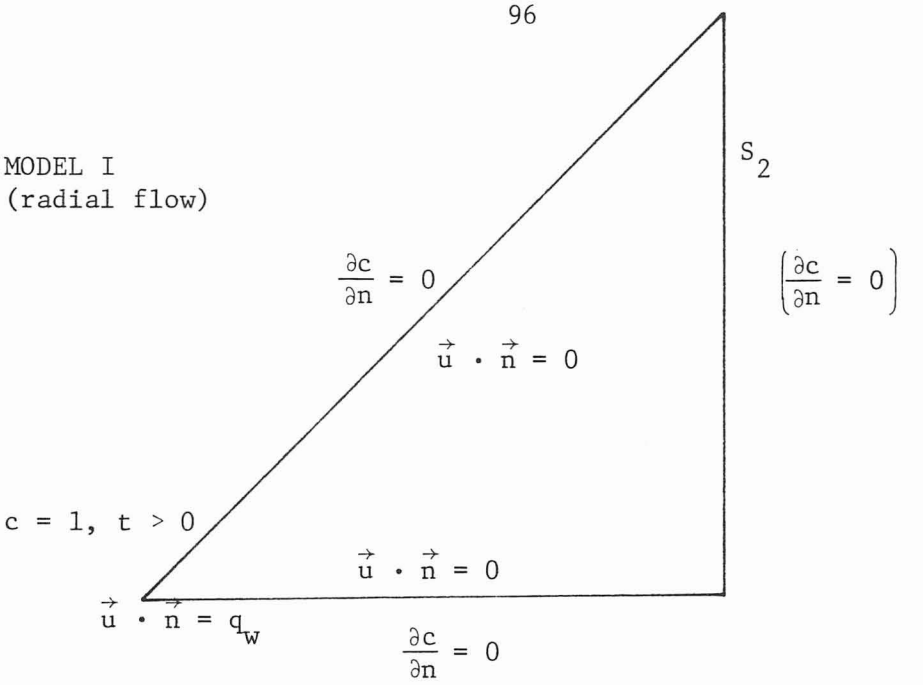

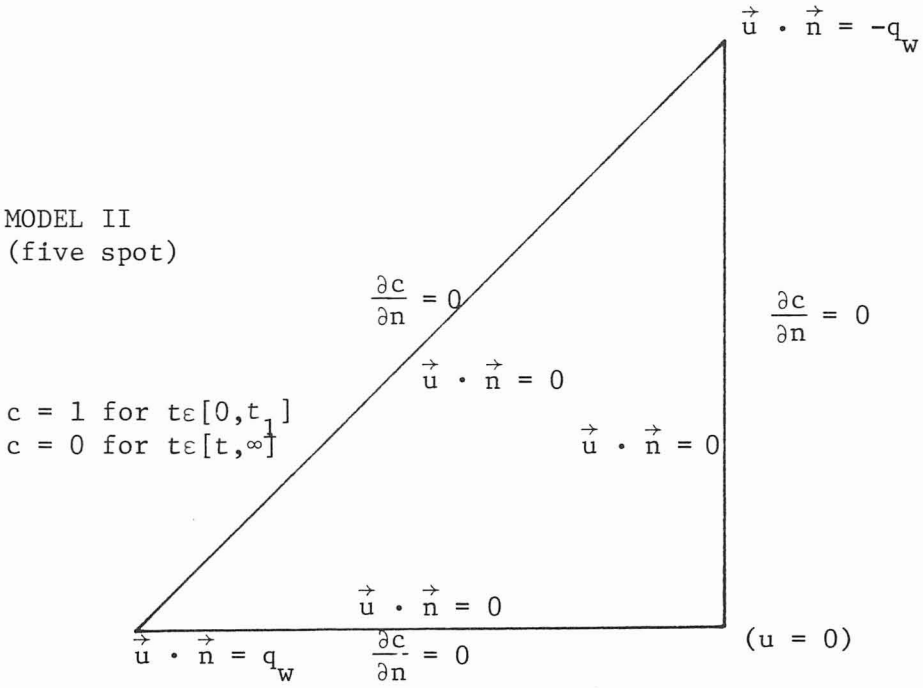

Figure 5.4

Boundary Conditions for Model I and II
(Initial Condition: $c = 0$ in Ω_o)

Summarizing, solutions to Eq. (5.7) with two types of boundary conditions, flow fields and dispersion tensor are considered. The models are referred to by three indices.

The first roman letter indicates the flow field

I : Flow from single well

II : Five spot pattern flow

and the second letter M or D stands for

M : Molecular diffusion

D : Dispersion proportional to $|\vec{u}|$

and the third number 1 or 2 is

1 : Step change (continuous displacement)

2 : Slug injection

These six possibilities present the most common situations encountered in flow through porous media. The Peclet number defined in (5.9) indicates how much the convection (injection rate) dominates the dispersion. Model IM-1 has an analytical solution, which is given in Appendix A.

5.3 Solution Method

This section is divided into several parts, each describing one aspect of the solution method. The utilization of the moving coordinate system constitutes the central part of the whole scheme and is discussed first. The theoretical development and numerical algorithm are described to give an overview of the numerical method. Section 5.3-2 and 5.3-3 treat the spatial discretization technique

and 5.3-4 treats the temporal integration scheme. In 5.3-5 and 5.3-6 specific algorithms necessary to utilize MCS are discussed. Section 5.3-7 describes how a mass balance for a reservoir is performed mathematically and why this is important.

In Appendix C the input instructions to the computer code which performs the tasks described in 5.3 are given.

5.3-1 Moving Coordinate System

For very high Peclet numbers the solution to any of the models given in (5.2) develops very steep profiles in only a small part of the domain. In Fig. 5.5 is shown a slug solution in a three-dimensional prospective. The solution looks very similar to a shock wave or front, and it is seen that the elements away from the wave only approximates a plane in this region.

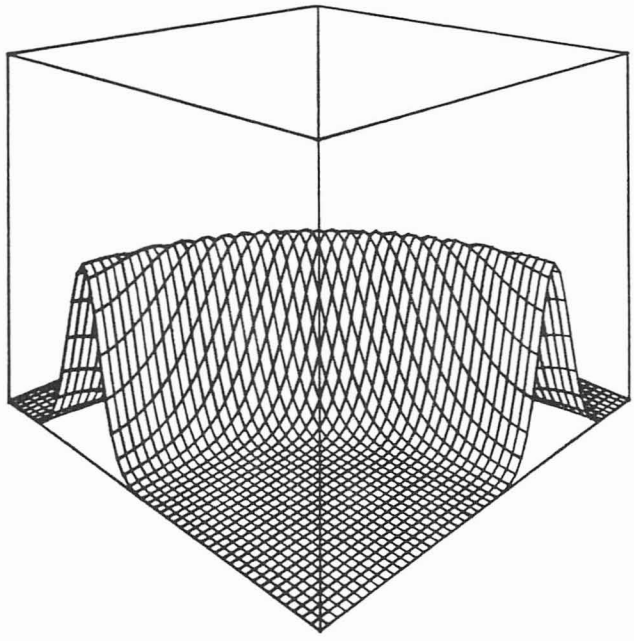

Figure 5.5

Three-Dimensional Prospective of Slug

The MCS can make the front(slug) stationary in time and space. In one dimension this occurs at a point, but in two dimensions it is along a line. The theoretical development and computational aspects are discussed in the following.

Transforming the differential equation into a moving coordinate system is done by

$$\xi = x - \int_o^t \lambda_x(t')dt'$$

$$\rho = y - \int_o^t \lambda_y(t')dt' \qquad (5.10)$$

$$\eta = t$$

The derivatives transform into

$$\frac{\partial c}{\partial t} = \frac{\partial c}{\partial \eta}\frac{\partial \eta}{\partial t} + \frac{\partial c}{\partial \xi}\frac{\partial \xi}{\partial t} + \frac{\partial c}{\partial \rho}\frac{\partial \rho}{\partial t}$$

$$= \frac{\partial c}{\partial \eta} + \frac{\partial c}{\partial \xi}\left[-\lambda_x(t)\right] + \frac{\partial c}{\partial \rho}\left[-\lambda_y(t)\right]$$

$$\frac{\partial c}{\partial x} = \frac{\partial c}{\partial \eta}\frac{\partial \eta}{\partial x} + \frac{\partial c}{\partial \xi}\frac{\partial \xi}{\partial x} + \frac{\partial c}{\partial \rho}\frac{\partial \rho}{\partial x} = \frac{\partial c}{\partial \xi}$$

$$\frac{\partial c}{\partial y} = \frac{\partial c}{\partial \eta}\frac{\partial \eta}{\partial y} + \frac{\partial c}{\partial \xi}\frac{\partial \xi}{\partial y} + \frac{\partial c}{\partial \rho}\frac{\partial \rho}{\partial y} = \frac{\partial c}{\partial \rho}$$

$$\frac{\partial^2 c}{\partial x^2} = \frac{\partial^2 c}{\partial \xi^2}, \qquad \frac{\partial c^2}{\partial y^2} = \frac{\partial^2 c}{\partial \rho^2}$$

Substituting these into (5.9) gives

$$\frac{\partial c}{\partial \eta} + \left(u_x - \lambda_x(t)\right) \frac{\partial c}{\partial \xi} + \left(u_y - \lambda_y(t)\right) \frac{\partial c}{\partial \rho} = K\left[\frac{\partial^2 c}{\partial \rho^2} + \frac{\partial^2 c}{\partial \xi^2}\right] \tag{5.11}$$

and the location of the boundary condition is then changed to (referring to Fig. 5.4)

$$c = 0 \quad \text{at } \xi,\rho \in \Omega_\Delta \qquad\qquad \eta = 0$$

$$n \cdot \underline{\underline{K}} \cdot \nabla c = 0 \text{ at } \rho = -\int_o^t \lambda_y(t')dt'' \qquad (S_3)$$

$$\text{at } \xi + \int_o^t \lambda_x(t')dt = \rho + \int_o^t \lambda_y(t')dt' \quad (S_1) \qquad \eta > 0$$

$$\text{at } \xi = -\int_o^t \lambda_x(t')dt' \qquad (S_2)$$

(5.12)

and the well locations are now a function of η. The injection well is located at

$$\xi = -\int_o^t \lambda_x(t')dt'$$

$$\rho = -\int_o^t \lambda_y(t')dt'$$

but the concentration specification as a function of time, remains unchanged. The location of producing well changes similarly.

The domain for which (5.11) now must be solved is changed to an infinite domain by Eq. (5.10). Here we seek to choose the velocity

of MCS so that the front (slug) remains within a well-defined area. With a proper definition of velocity (5.3-5), the calculation region for reservoir problems is shown as the trapezoid in Fig. 5.6. We use

$$\xi_{min} = \rho_{min} = -1 \quad .$$

which corresponds to a hyperbolic shock wave being moved from the injection well to the producing well.

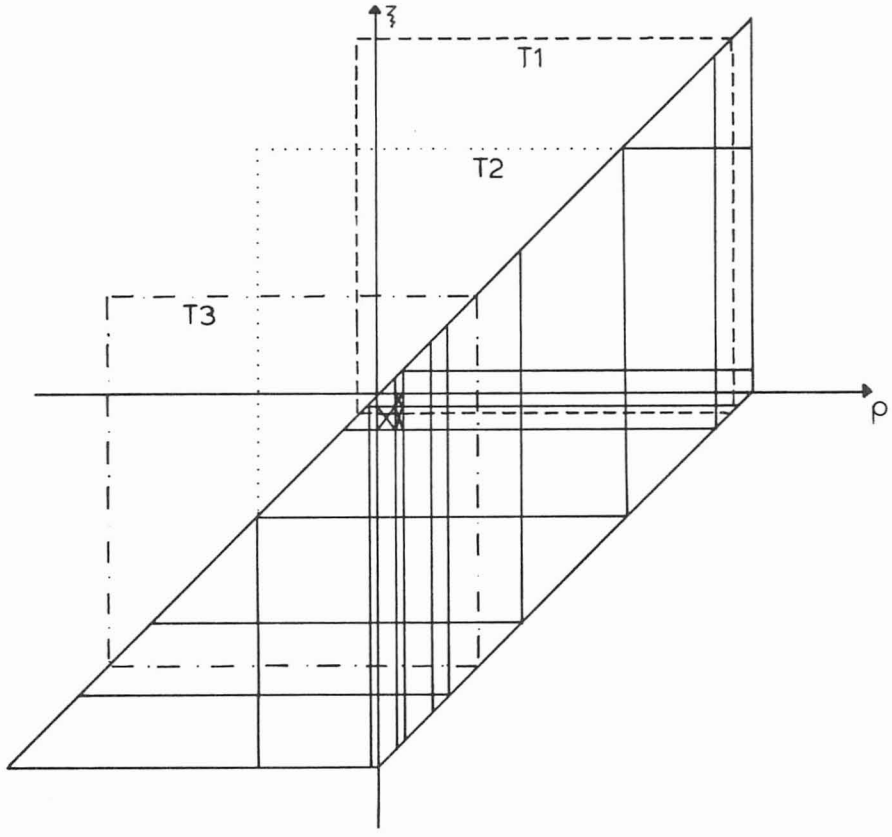

Figure 5.6

Calculation Region for MCS

Using the moving coordinate system as a numerical scheme requires a proper discretization method to be used so that the domain given by Fig. 5.6 can be approximated. The Galerkin finite element can approximate the domain easily whereas it is more difficult with a finite difference technique or other weighted residual methods. Triangular elements are not easily treated with the other techniques. The location of the boundary condition changes as a function of time, and it is therefore also important to choose a method where these are readily applied. In a Galerkin formulation most of the boundaries given by Eq. (5.3) are described by natural boundary conditions (see Section 5.3-2), in which case the final equation is not affected. Less complicated programming is thereby achieved.

As mentioned above the domain over which Eq. (5.11) is to be solved will change in time. Location of the boundaries then also changes in time. For most solutions reported here we simply apply the boundary condition of the node closest to the boundary. This introduces some error, but is usually satisfactory. For one case, the five spot flow when $Pe_1 = 1000$, we moved the nodes on the boundary so that the boundary conditions are evaluated at the correct location. This was necessary to obtain reasonable solutions. Figure 5.7 shows how the computational grid changes as a function of time. At different times a number of elements are taken out of the original grid (Fig. 5.6) to approximate the solution at this time. The discretization is highly nonuniform but as shown in Fig. 5.8 the elements are at any time placed where the front will be.

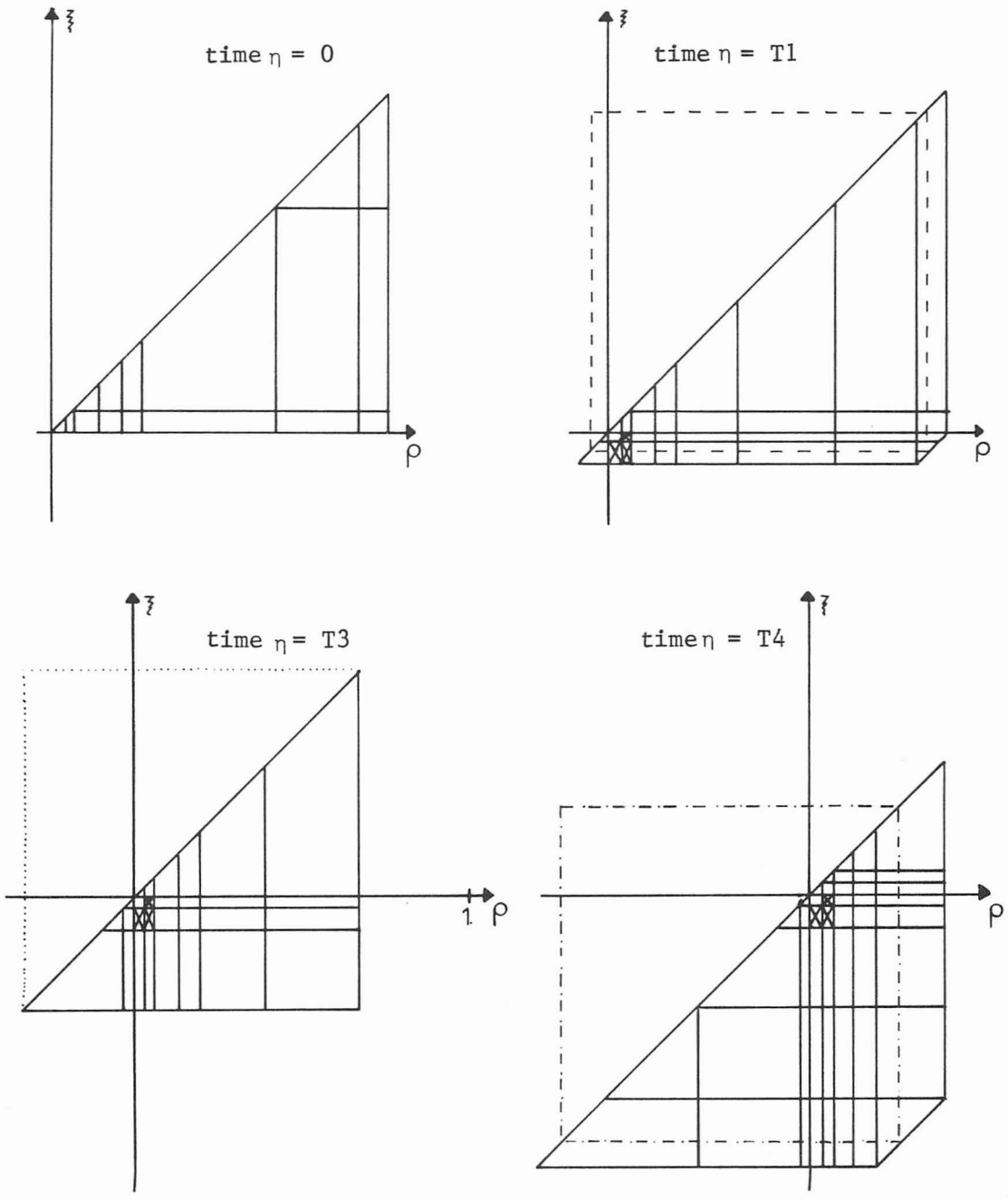

Figure 5.7

Mesh for MCS, Different Times

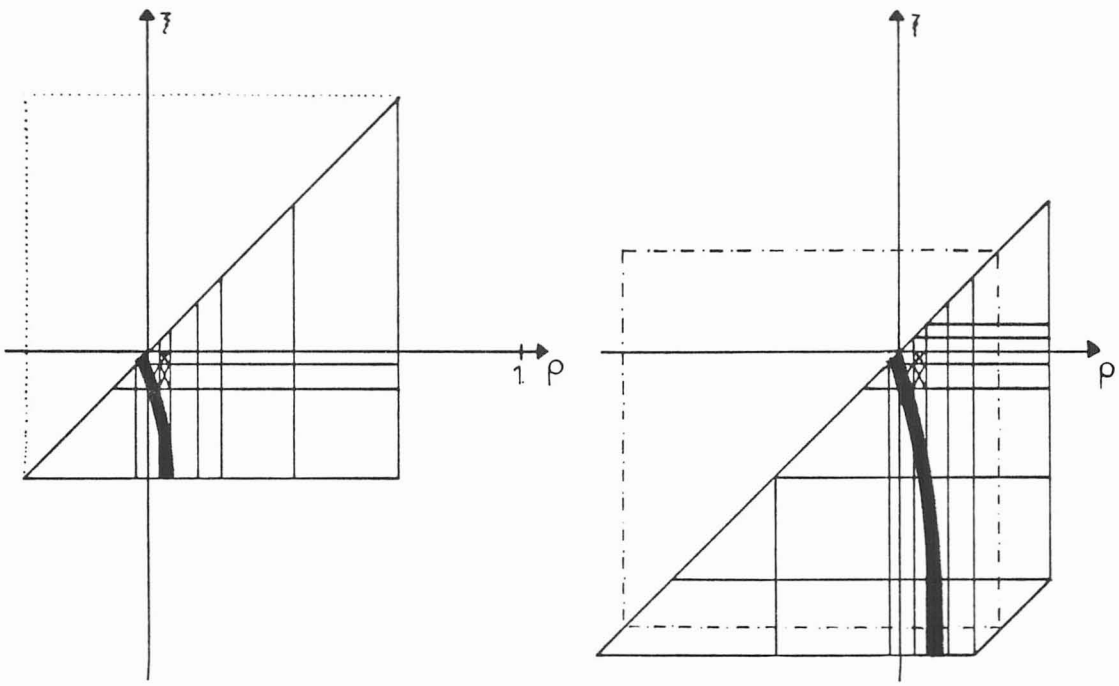

Figure 5.8

Placement in Front in Grid

The details of applying a moving coordinate system are discussed in the following with emphasis on the subjects which are important for MCS.

5.3-2 Galerkin Formulation

The mathematical model given by Eq. (5.7) is solved with a Galerkin finite element method. The Galerkin equation is

$$\int_V \left(\frac{\partial c}{\partial t} \delta c + \delta c \cdot \underline{u} \cdot \nabla c + \nabla \delta c \cdot \underline{\underline{K}} \cdot \nabla c \right) dV$$

$$- \int_S \delta c [q_w (c - c^\circ_w)] dS = 0 \quad .$$

The Euler equation and natural boundary condition can be determined by using

$$\nabla \cdot (\delta c \cdot \underline{\underline{K}} \cdot \nabla c) = \delta c \cdot \nabla \cdot (\underline{\underline{K}} \nabla c) + \underline{\underline{K}} \nabla c \nabla \delta c$$

and Greens theorem.

$$\int_V \nabla \cdot (\delta c \, \underline{\underline{K}} \nabla c) dV = \int_S \vec{n} \cdot (\delta c \, \underline{\underline{K}} \nabla c) dS$$

The Euler equation is then

$$\frac{\partial c}{\partial t} + \underline{u} \nabla c - \nabla \cdot (\underline{\underline{K}} \nabla c) = 0 \tag{5.13}$$

and natural boundary condition becomes

$$\vec{n} \cdot \underline{\underline{K}} \cdot \nabla c - q_w (c - c^\circ_w) = 0 \tag{5.14}$$

At production wells $c = c^\circ_w$ so for all boundary points except at injection wells we have the boundary condition

$$\vec{n} \cdot \underline{\underline{K}} \cdot \nabla c = 0 \qquad \text{or} \qquad \frac{\partial c}{\partial n} = 0 \tag{5.15}$$

At the injection wells an essential boundary condition is used since we want to specify the concentration as a function of time.

Introducing the moving coordinate system does not affect the natural boundary condition, so in the further development of the Galerkin formulation we can use Eq. (5.13). Denoting N_I as the shape function for node I we have

$$c(x,y) = \sum N_I(x,y) \cdot c_I$$

where c_I is the nodal value. The weighting function is denoting N_J. Having

$$\delta c = N_J \quad \text{and} \quad c = \sum N_I \, c_I$$

we get in matrix form

$$\underline{\underline{M}} \frac{dc}{dt} = (\underline{\underline{C}} + \underline{\underline{D}}) \cdot \underline{c} \tag{5.16}$$

The matrix entries are

$$m_{IJ} = \int_A N_I \, N_J \, dA \tag{5.17}$$

$$c_{IJ} = -\int_A N_J \left((u_x - \lambda_x(\eta)) \frac{dN_I}{d\xi} + (u_y - \lambda_y(\eta)) \frac{dN_I}{d\rho} \right) dA \tag{5.18}$$

$$\begin{aligned} d_{IJ} = -\int_A \Bigg(& K_{\xi\xi} \frac{dN_J}{d\xi} \frac{dN_I}{d\xi} + K_{\xi\xi} \frac{dN_J}{d\xi} \frac{dN_I}{d\rho} + K_{\rho\xi} \frac{dN_J}{d\rho} \frac{dN_I}{d\xi} \\ & + K_{\rho\rho} \frac{dN_J}{d\rho} \frac{dN_I}{d\rho} \Bigg) dA \end{aligned} \tag{5.19}$$

Solution of (5.16) is discussed in 5.3-4.

5.3-3 Elements and Integral Approximation

Quadrilateral elements could certainly be used by bending them to approximate the domains shown in Figs. 5.5 through 5.7. If triangles are introduced a nearly regular type grid as shown in the figures can be constructed. It is therefore preferable to combine quadra-

lateral and triangles so that the domain is more easily formed. Element for transitions between fine and coarse mesh has been developed [Gupta, 1979] but are not considered here.

Here are selected quadratic serendipity quadrilaterals and quadratic triangles are selected. Several other studies [Huyakorn et al., 1976; Gray and Van Genuchten, 1978] concluded that the quadratic elements are computational efficient for this type of problem. Recent studies [Young, 1978; Settari, 1976] suggests that cubic C^1-elements may be preferable for low dispersion as found in Chapter II also. The elements chosen are shown in Fig. 5.9.

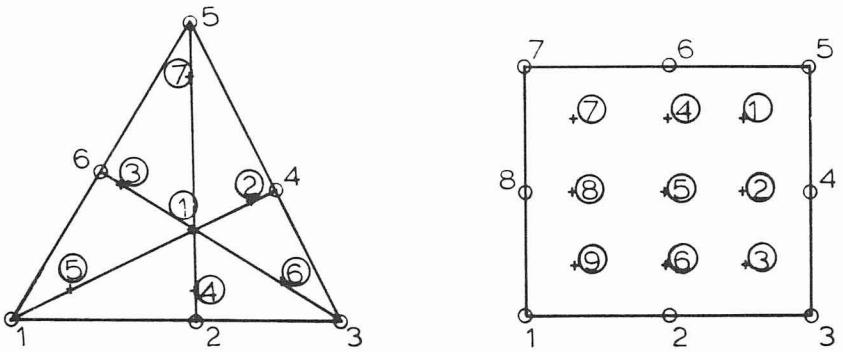

1-n : node values
①-⑨ : quadrature points

Figure 5.9

Elements and Quadrature Points

The integrals given in (5.17) through (5.19) must be evaluated by quadrature. Other studies [Young, 1977; Hillion, 1977; Leone, 1979; Gray and Van Genucten, 1978; Wang and Klein, 1978] indicated that considerable savings can be achieved by choosing formulas where

the qudrature points coincides with the nodal points (e.g., Lobatto quadrature). Here no attempt has been made to choose computational efficient quadrature formulaes. For the quadralaterals a 3 x 3 point Gaussian quadrature was used, so that a polynomial of degree 5 in each direction is integrated exactly [Zienkiewicz, 1971, p. 187]. A seven point formula, which integrates exactly a fifth order polynomial, is used for the triangles.

The gauss points for the quadralaterals are: (here normalized for the domain in one dimension from zero to one)

$$x_g = 1/2 - \sqrt{3/20},\ 1/2,\ 1/2 + \sqrt{3/20} \tag{5.20}$$

and corresponding weights

$$w_g = 5/18,\ \ 4/9,\ \ 5/18 \tag{5.21}$$

For the triangle the points are given in terms of area coordinates.

Point (Fig. 5.9)	Area Coordinate	Weight
1	1/3, 1/3, 1/3	w_1
2	α_1, β_1, β_1	
3	β_1, α_1, β_1	w_2
4	β_1, β_1, α_1	
5	α_2, β_2, β_2	
6	β_2, α_2, β_2	w_3
7	β_2, β_2, α_2	

$$w_1 = 9/40$$

$$\begin{aligned} w_2 &= \frac{155 + \sqrt{15}}{1200} & \alpha_1 &= \frac{9 - 2\sqrt{15}}{21} & \beta_1 &= \frac{6 + \sqrt{15}}{21} \\ w_3 &= \frac{155 - \sqrt{15}}{200} & \alpha_2 &= \frac{9 + 2\sqrt{15}}{21} & \beta_2 &= \frac{6 - \sqrt{15}}{21} \end{aligned} \tag{5.23}$$

5.3-4 Temporal Integration Scheme

It is desirable to find schemes using a variable timestep as discussed in Chapters III and IV, because when applying MCS the time-steps are expected to increase rapidly when the front is well developed. Two predictor-corrector methods were tested solving Eq. (5.16).

For most cases a Crank-Nicholson formulation was used. If

$$\frac{dc}{dt} = f(c)$$

then

$$c^{n+1} = c^n + \frac{\Delta t}{2} [f(c)^{n+1} + f(c)^n] + o(\Delta t^3) \tag{5.24}$$

and for (5.16)

$$[\underline{\underline{M}} + \Delta t/2 \cdot (\underline{\underline{C}} + \underline{\underline{D}})]\underline{c}^{n+1} = [\underline{\underline{M}} - \Delta t/2(\underline{\underline{C}} + \underline{\underline{D}})]\underline{c}^n \tag{5.25}$$

The other scheme is an implicit Euler (backward Euler) or

$$c^{n+1} = c^n + \Delta t \cdot f(c)^{n+1}$$

and for (5.16)

$$[\underline{\underline{M}} + \Delta t(\underline{\underline{C}} + \underline{\underline{D}})]\underline{c}^{n+1} = \underline{\underline{M}} \cdot \underline{c}^{n} \tag{5.26}$$

Both schemes are implicit and it is necessary to decompose the matrix in (5.25) and (5.26) whenever the timestep is changed.

The predictors to the above methods are based on extrapolation from previous timesteps. They are not used in the integration step as seen above, but are used to give an estimate of the truncation error for evaluating a new timestep. For the Crank-Nicholson scheme the predictor is

$$\underline{c}^{p} = \gamma_1 \underline{c}^{n} + \gamma_2 \underline{c}^{n-1} + \gamma_3 \underline{c}^{n-2} \tag{5.27}$$

where

$$\gamma_1 = 1 + \frac{\Delta t_n}{\Delta t_{n-1}} \left(1 + \frac{\Delta t_{n-1} + \Delta t_n}{\Delta t_{n-1} + \Delta t_{n-2}} \right)$$

$$\gamma_2 = - \left(\frac{\Delta t_n}{\Delta t_{n-1}} + \frac{\Delta t_n}{\Delta t_{n-1} \Delta t_{n-2}} (\Delta t_n + \Delta t_{n-1}) \right)$$

$$\gamma_3 = \frac{\Delta t_n \cdot (\Delta t_n + \Delta t_{n-1})}{\Delta t_{n-2} (\Delta t_{n-2} + \Delta t_{n-1})}$$

and for the Euler method

$$\underline{c}^{p} = \gamma_4 \underline{c}^{n} + \gamma_5 \underline{c}^{n-1} \tag{5.28}$$

where

$$\gamma_4 = 1 + \Delta t_n / \Delta t_{n-1}$$

$$\gamma_5 = - \Delta t_n / \Delta t_{n-1}$$

The truncation error is determined after each timestep by the norm

$$||d_{TOTAL}|| = \frac{1}{NT \cdot c_{max}} \sum_{1}^{NP} (dc_i)^2 \qquad (5.29)$$

where NT: number of nodes

c_{max}: Maximum value of c

and

$$dc_i = \frac{c_1}{c_1 + c_2} \left(c_i^{n+1} - c_i^{p} \right)^2 + 0(h^q)$$

where for the second order scheme (q = 4)

$$c_1 = 1/12$$

$$c_2 = 1/6 * \left(1 + \frac{2\Delta t_{n-1} + \Delta t_{n-2}}{\Delta t_n} + \frac{\Delta t_{n-1}^2 + \Delta t_{n-1} \Delta t_{n-2}}{\Delta t_n^2} \right)$$

and for the first order scheme (q = 3)

$$c_1 = 1/2 \qquad c_2 = (1 + \Delta t_{n-1}/\Delta t)/2$$

The new timestep is now calculated by

$$\Delta t_{n+1} = \Delta t_n \cdot (\varepsilon / ||d_{TOTAL}||)^{1/3} \qquad (5.30)$$

ε is a user specified accuracy level (usually 10^{-2} - 10^{-4}), and a restriction of a factor 3 is set for either decreasing or increasing the timestep.

The schemes described here are an analog of those used by Gresho et al. (1978), except they used expressions for the derivative in the predictor. By using extrapolation it is not necessary to invert the mass matrix.

In Eq. (5.26) a matrix must be inverted for each time the time-step changes a frontal solver [Hood, 1976; Irons, 1970] was used, but changed so that only some of the elements (as discussed in 5.3-1) could be chosen to be decomposed. Other studies have used banded matrix solvers [Settari et al., 1976] and iteration schemes [Young, 1978]. Half of the total computation time is spent by the matrix solver depending on how the matrix is set up so it is important that a suitable inversion routine is chosen. The frontal solver and also the banded matrix solver are based on Gaussian elimination in which case the equations are solved to machine accuracy. With an iteration scheme, the equations are never solved exactly, but are solved to within a specified tolerance, although in some cases the iteration scheme itself may not work. Each iteration requires only a small computer time, compared to direct decomposition, but many iterations may be necessary.

5.3-5 Determination of Frontal Velocity

A requirement for applying a moving coordinate system is a determination of the velocity which will keep the front (slug) in a certain area.

For Case I (radial flow) the frontal velocity is known through the exact solution. The position is given by the hyperbolic model (Appendix A)

$$r_{front} = \sqrt{2Pe \cdot t} \tag{5.31}$$

so the radial frontal velocity is

$$\lambda_r(t) = \frac{dr_{front}}{dt} = \frac{Pe}{2t} \tag{5.32}$$

or in cartesian coordinates

$$\lambda_x(t) = \lambda_y(t) = \frac{1}{2} \cdot \frac{Pe}{t} \tag{5.33}$$

The accumulated velocity is

$$\int \lambda_x(t)dt = \int \lambda_y(t)dt = \sqrt{Pe \cdot t} \tag{5.34}$$

For Model I the exact frontal velocity was used but the accumulated velocity, the integral (5.34) was calculated numerically using the trapezoid rule $\left(0(\Delta t^2)\right)$, i.e.,

$$\int_{t+DT} \lambda_x(t)dt \simeq \int_t \lambda_x(t)dt + \frac{\lambda_x(t+DT) + \lambda_x(t)}{2} * DT \tag{5.35}$$

Even though it was not necessary to perform this integration it was desirable to determine how accurate this integration would be. Results showed that the calculated accumulated velocity was within 1% error of the exact value.

Equation (5.25) of (5.26) is used to advance the solution from T to T + DT.

$$[\underline{\underline{M}} + \Delta t/2 \cdot [\underline{\underline{C}}(T) + \underline{\underline{D}}]]^{n+1} \cdot \underline{c}^{n+1} = [\underline{\underline{M}} - \Delta t/2 \cdot [\underline{\underline{C}}(T) + \underline{\underline{D}}]]^{n} \cdot \underline{c}^{n} \tag{5.36}$$

or

$$\underline{\underline{A}}^{1}(T)\ \underline{c}^{n+1} = \underline{\underline{A}}^{2}(T)\ \ \underline{c}^{n}$$

The matrices $\underline{\underline{A}}^{1}$ and $\underline{\underline{A}}^{2}$ both contain the frontal velocity. Different times can be selected to evaluate the frontal velocity and four possibilities were considered here.

1) $\lambda(t)$ evaluated at T for both $\underline{\underline{A}}^{1}$ and $\underline{\underline{A}}^{2}$
2) $\lambda(t)$ evaluated at T + DT/2 for both $\underline{\underline{A}}^{1}$ and $\underline{\underline{A}}^{2}$
3) $\lambda(t)$ evaluated at T + DT for both $\underline{\underline{A}}^{1}$ and $\underline{\underline{A}}^{2}$
4) $\lambda(t)$ evaluated at T for $\underline{\underline{A}}^{2}$ and
   $\lambda(t)$ evaluated at T + DT for $\underline{\underline{A}}^{1}$

With a Peclet number of 50 and the variable timestep adjusted to give very large timesteps the results are shown in Fig. 5.10. Possibility number 4 is not shown but is almost identical with number 2. As seen in the figure, it is most desirable to evaluate the frontal velocity at the end of a timestep rather than in the beginning. The reason for this phenomenon is probably due to the implicit interaction scheme. For a nonlinear problem, the frontal velocity will not be known apriori (e.g., Case II), and it is necessary to determine it numerically. An algorithm to accomplish this and also extrapolate the "old" known velocities to the end of the following timestep is discussed here.

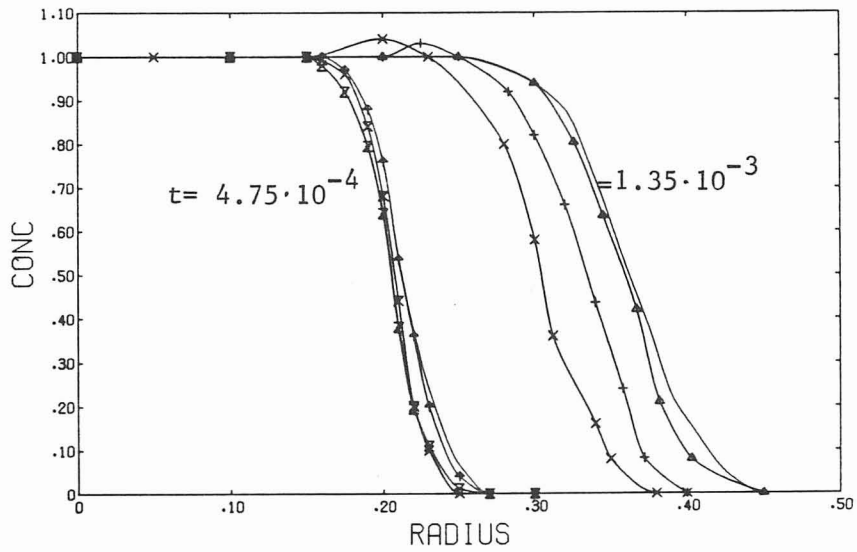

Figure 5.10

Model IM-1, Pe_1 = 50, Effect of Evaluating the Frontal Velocity at Different Times, (Δ) at T+DT, (+) at T+DT/2, ($\times$) at T

The frontal velocity is now defined as

$$\lambda_r(t) = \frac{d(r^* - r_{fr})}{dt} \tag{5.37}$$

where r^* : position on diagonal ($\xi = \rho$) where concentration is 0.5

r_{fr} : reference position on diagonal

In the case of a slug the downstream front is considered until the peak concentration is less than 0.5 after which the location of the peak is considered. Before each timestep the following procedure is done. The velocity after the next timestep (T+DT) is obtained

by using a second order extrapolation of the velocities from previous timesteps. Having performed the timestep the position r^*_{T-DT} is determined. We can now correct the frontal velocity to correspond to what the actual movement was, i.e.,

$$\lambda_r^{\text{corrected}}\ (T+DT) = \lambda_r^{\text{extrapolated}}\ (T+DT) + \frac{r^*_{T+DT} - r^*_T}{DT}$$

If we had been able to stop the movement of the front (slug) completely $r^*_{T+DT} = r^*_T$ and the corrected and extrapolated velocities would be identical. In Fig. 5.11 is shown an example of the extrapolated and corrected velocities. The corrected values are used for the extrapolation step (shown by dotted line), the extrapolated values in the calculation step (5.36) and for the determination of accumulated velocity (5.35).

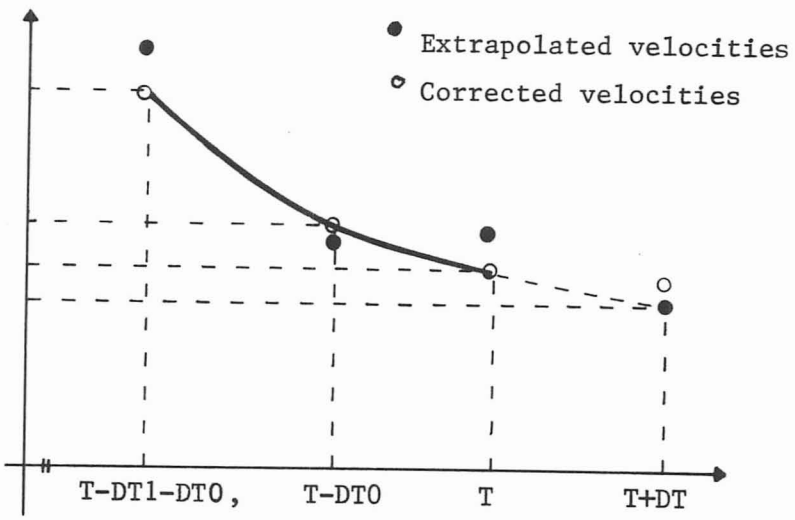

Figure 5.11

Determination of Frontal Velocity

To start this algorithm, a fixed position (r_{fr}) is determined after two timesteps and

$$\lambda_r(T+DT) = \frac{r_T^* - r_{fr}}{DT1}$$

the frontal velocity during the timestep DT1 is used until the extrapolation/correction scheme can be initiated.

After only a few timesteps the corrections were found to be less than 5%. When applying this algorithm to Case I (radial flow) the frontal velocities were found to be within 2% of those predicted by Eq. (5.34). The corrections are smaller the steeper a front is tracked.

5.3-6 Numerical Algorithm for MCS

Section 5.3-1 described the theoretical development of MCS and Figs. 5.6 and 5.7 show how the grid configuration changes throughout the integration. Referring to Figs. 5.7 it is seen that during the time T2 to T3 some elements have been deleted and others added. An algorithm for obtaining the correct elements (out of all the elements as in Fig. 5.6) at a given time and also a scheme to assign values of $\underline{c}^n$ in the newly added elements is described.

Further specifying the location of the boundary conditions exactly is discussed.

At a given time the accumulated velocities

$$ACCX = ACCY = \int_o^t \lambda_x(t')dt' = \frac{1}{\sqrt{2}} \int_o^t \lambda_r(t')dt'$$

are known, so the exact location of the boundary conditions (physical domain) in the MCS is given by the interior quadrant

$$\begin{aligned}
\xi &= -\int_o^t \lambda_x(t')dt' \qquad \text{or} \qquad x = 0 \\
\xi &= 1 - \int_o^t \lambda_x(t')dt'' \qquad \text{or} \qquad x = 1 \\
\rho &= -\int_o^t \lambda_y(t')dt' \qquad \text{or} \qquad y = 0 \\
\rho &= 1 - \int_o^t \lambda_y(t')dt' \qquad \text{or} \qquad y = 1
\end{aligned} \tag{5.38}$$

The lines (or "boxes") shown in Figs. 5.5 through 5.7 and 5.12 are constructed based on (5.38). The four lines in Fig. 5.12b divide the domain into 9 different areas. Taking an element, each node can (using (5.38)) be placed in only one of the nine regions, a number (0-5) (Fig. 5.12c) is assigned to that node. For nodes in region OUT an extra specification (Fig. 5.12c) is made depending on which corner it is closest to. Going through this determination of all nodes in an element we have an array of numbers which now uniquely determine its position. The elimination procedure is then:

A if all nodes in either region W, N, E, S or OUT or a combination but does not have any node in region IN, the element is not assembled , e.g., a triangle with numbers 1,1,1,0,2,2 will not be assembled.

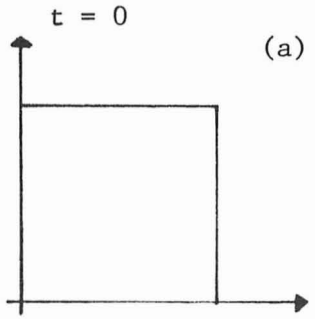

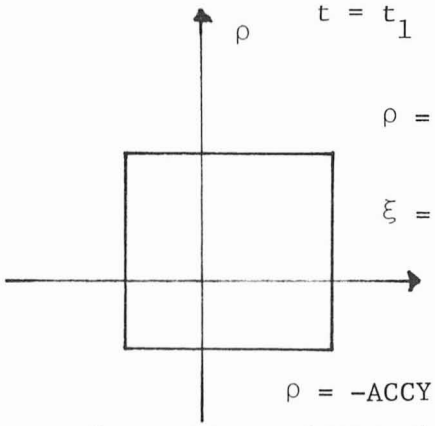

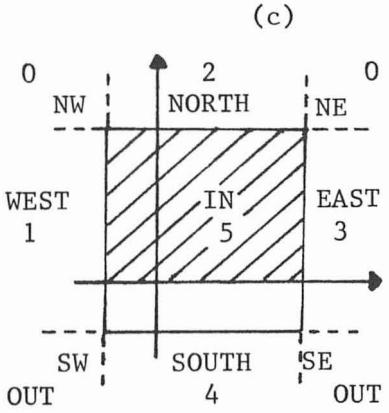

For OUT regions INE = 1 if node in NE-OUT

INE = 0 if node not in NE-OUT

similarly for other corners

Figure 5.12

Numerical Algorithm, MCS

B If all nodes in region IN (5) the element will be assembled, e.g., quadralateral with numbers 5,5,5,5,5,5,5,5.

C If nodes in region IN (5) and either W, N, E, S the element is assembled and boundary condition specified (if any) at closest points to line, e.g., triangle with numbers 5,5,2,2,2,5 is assembled.

D All elements, except those near one of the four corners, are now identified. For a corner element two possibilities exist as the nodes can lie in either 3 or 4 regions.

1) Four regions. In this case the corner is uniquely determined, the boundary condition can be applied and the element assembled, e.g., triangle having nodes in regions IN, W, S and OUT (numbers 0,0,4,5,1,1).

2) Three regions. If the nodes lie in three regions such as S, IN and OUT, the element must be assembled but the corner location could either be SW or SE. As nodes in region OUT are labelled for the closest corner, the corner is uniquely determined.

The above algorithm is performed for each element in the grid and a set of elements is determined for assembling. The boundary conditions are applied when the location of the element is found. As discussed before the location of the boundary condition will not in general be the exact one defined by (5.38).

Any type of boundary condition can be applied, the code is capable of applying the following types

$$c = c_o(t) \qquad \text{(fixed)}$$

$$\int \vec{n} \cdot \underline{\underline{K}} \cdot \nabla c = \int_s q \, dS \qquad \text{(flux)}$$

at any corner or boundary lines. The flux can only be a function of time at well locations.

The assembly of elements described above will result in a set of elements describing the problem between the time T and T+DT since the addition and subtraction of elements will occur in a discontinuous manner, the dependent variables ($\underline{c}^n$ in (5.36)) in newly assembled elements must be assigned values. The situation is shown in Fig. 5.13.

The boundary condition along the boundary where new elements arise is either

$$\frac{\partial c}{\partial n} = 0 \qquad \text{or} \qquad \underline{\underline{K}} \, \frac{\partial c}{\partial n} = 0$$

To assign values in new elements (nodes), interpolation of nodal values closest to the boundary is used, or requiring that the gradient is zero over the boundary

$$\frac{\partial c}{\partial n} = 0$$

The natural boundary condition (5.15) is thereby violated once, but only if $\underline{\underline{K}}$ is not a diagonal tensor.

Referring to Fig. 5.13a, element numbers 1-5 are "old" elements used between T-DT1 and T, and elements 6-10 are "new" elements to be

(a)

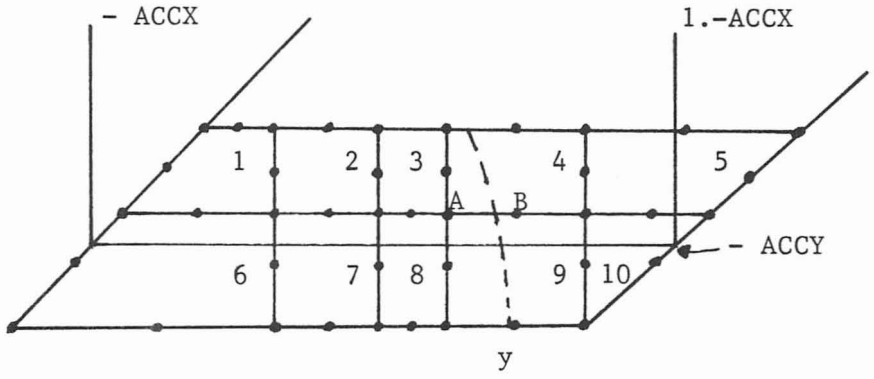

(b)

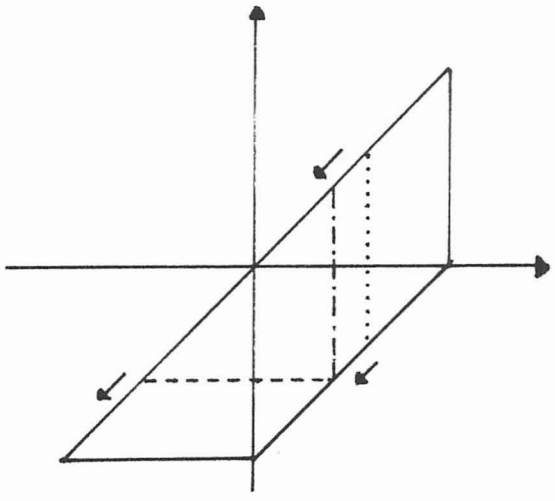

Figure 5.13

Extrapolation of Values in New Elements (a) and specifying the location of the boundary conditions exact (b)

considered between T and T+DT. Elements 1-5 fall in category SOUTH and is stored separately. The nodal value at position y (element 9) is now interpolated linearly between nodes A and B from element 3.

The following procedure was done for specifying the location of the boundary condition exactly for solution of model II D-2, Pe = 1000. Starting from an accumulated velocity of 0.5, the nodes on one vertical (EAST) and one horizontal line (SOUTH) changed location according to Eq. (5.13). When the vertical line (..., Fig. 5.13b) meets the next line (—·—, Fig. 5.13b) in a distance of 0.01, the column of elements between the two elements is deleted and integration continued with the second line (—·— and the horizontal line ———) of nodes changing during the integration. No interpolation was done in the elements affected by changing the EAST boundary.

5.3-7 Material Balance

When solving the Case II model (velocity field as a five spot) no analytical solution is available so the numerical solution can only be compared to experimental data and other numerical calculations. An estimate of the accuracy can however be given by calculating the error from not satisfying the natural boundary condition exactly. Recalling from 5.3-2 Eq. (5.14), the natural boundary condition is

$$\vec{n} \cdot \underline{\underline{K}} \cdot \nabla c - q_w (c - c_w^\circ) = 0 \qquad (5.14)$$

where $\vec{n}$ is the unit normal to a surface, and Eq. (5.14) should be satisfied at any point. The mass flux into or out of the domain at any time t is obtained by integrating (5.14) over the surface.

$$\int_S \vec{n} \cdot \underline{\underline{K}} \cdot \nabla c \, dS - q_w (c - c_w^\circ) = M \tag{5.39}$$

A total mass balance is then given by

$$M_{BC}^{in}(t) - M_{BC}^{out}(t) - M_{prod}(t) + M_{injection}(t) = M_{acc} \tag{5.40}$$

where

$$M_{BC}^{in}(t) = \int_0^t \int_S \vec{n} \cdot \underline{\underline{K}} \cdot \nabla c \, ds \, dt$$ (mass in by violating natural boundary condition)

$$M_{BC}^{out}(t) = \int_0^t \int_S \vec{n} \cdot \underline{\underline{K}} \cdot \nabla c \, ds \, dt$$ (mass out by violating natural boundary condition)

$$M_{prod}(t) = \int_0^t q_w \, c_{well} \, dt$$ (mass taken out at production well (1,1))

$$M_{injec}(t) = \int_0^t q_w \cdot c_{well}^\circ \, dt$$ (mass added at injection well (0,0)

$$M_{acc}(t) = \int_\Omega c(t) d\Omega$$ (accumulated mass in domain)

Equation (5.40) can also be obtained by integrating the sum of Eq. (5.13) and (5.14) over the domain.

When solving Model II the mass flux

$$q_{\Delta t} = \int_s \vec{n} \underline{\underline{K}} \nabla c \, dS$$

is evaluated for each element having a side with a boundary. The fluxes at any time are separated into six categories, one for each of three sides (Fig. 5.14) and depending on whether material flows in or out. These six fluxes are then integrated with a trapezoid rule. A net flux for one side is then obtained by adding the flux in and out of the domain

$$\begin{aligned} M_{BC}(t + \Delta t)_{side,in(out)} &= M_{BC}(t)_{side,in(out)} \\ &= (q_t + q_{t+\Delta t}) * \Delta t/2 \end{aligned} \tag{5.41}$$

In the contours shown in (5.4) a mass flow can be observed by looking at the slope of contour at the surface, Fig. 5.14.

5.4 Results

5.4-1 Symmetry and Integration Order

Initial testing of the program was performed with a Mod model i.e., radial flow and a step change in boundary condit $Pe_1 = 5$ a fixed coordinate system was used. Several different gric were tested and the optimal number of quadrature points for the int approximation was determined. These calculations are discussed

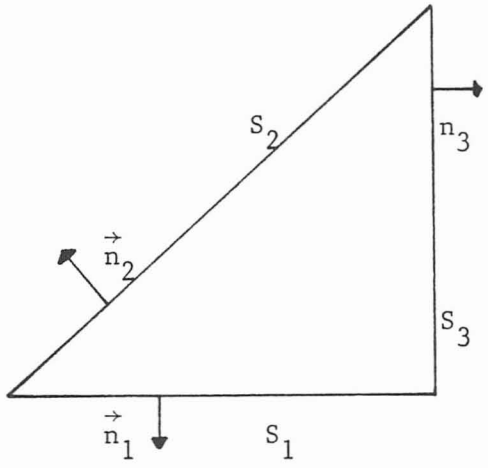

$$\vec{n}_1 = (1,0)$$
$$\vec{n}_2 = \frac{1}{\sqrt{12}}(-1,1)$$
$$\vec{n}_3 = (1,0)$$

Massflux q
- <0 into domain
- $=0$ no flux
- >0 out of domain

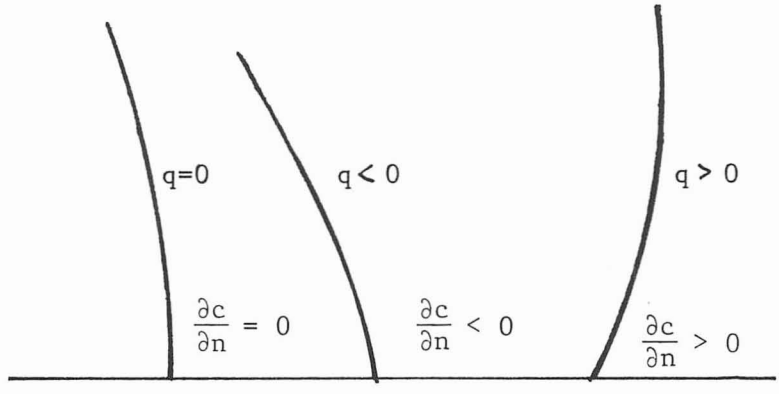

Figure 5.14

Mass Balance in Triangular Domain (longitudinal and transverse diffusivity equal)

The mathematical models considered in this study all have symmetry in the solution. For the radial flow and five spot pattern the symmetry line is between the producer and injector, so the numerical solution must obey this symmetry. Figure 5.15 shows four different element configurations. Mesh I is a 4 x 4 quadralateral, mesh II either 16 triangles to form a triangle or 52 (symmetric distributed) covering the whole area and III is 9 quadralaterals forming a triangle. The integration was performed using 10 fixed timesteps and the solution was compared with an estimate of the error based on

$$||\varepsilon||_{max} = \frac{1}{NT} \quad \{\sum_{1}^{NP} |c_{exact} - c_{node}|^2\}$$

NT being the number of nodes.

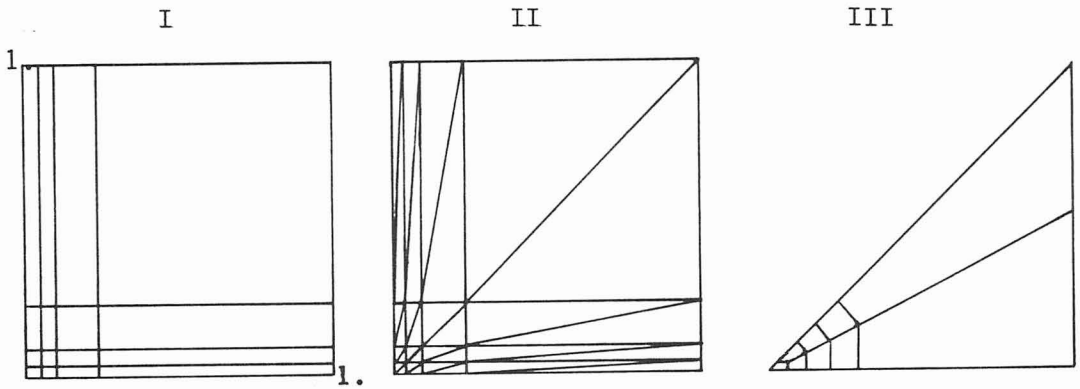

Figure 5.15

Mesh for Symmetry Test

Using the two cases for Mesh II the numerical solution was symmetric about the diagonal as expected. The three cases are compared in accuracy below:

After		I	II	III
5DT	$\|\|\varepsilon\|\| =$	0.34×10^{-3}	0.95×10^{-3}	4.2×10^{-3}
10DT	$\|\|\varepsilon\|\| =$	0.19×10^{-3}	0.43×10^{-3}	0.66×10^{-3}
RSU		161	76	73

(RSU defined in nomenclature)

Even though the error estimate is very simple and crude, some trends can be seen. Shifting from a square domain to the triangular domain, the loss of accuracy is only minor. Comparing mesh II using triangles and mesh III using quadrilaterals the error after 5 DT is much smaller for II than III and after 10 DT the difference is only minor.

The differences in computation time (RSU) reveal that for discretizing the same domain and achieving comparable accuracy two triangles can be used for one quadralateral. The conclusion is that the triangular domain is applicable with minor loss of accuracy, triangles are preferable in areas where the solution must be resolved and quadralaterals can be used other places because they are slightly cheaper.

The number of quadrature points for triangles was varied using Mesh II (fig. 5.15). A seven point formula is capable (section 5.3-2) of integrating exact polynomials up to degree 5 in combined x,y variables. The other formula considered used three quadrature points, so a quadratic function is integrated exactly [Zienkiewicz, 1971]. In this latter case the mass matrix and convective matrix—(5.17) and (5.18)—is not integrated exactly. The results obtained gave oscilla-

tory solutions where as the seven point formula gave stable solutions. It seems important for stability to use the exact mass matrix rather than mass lumping or a low order quadrature for integration. Gresho et al. (1976) observed the same phenomenon and made similar conclusions.

5.4-2 Radial Flow

When the flow field is described by a single well injecting material, the model is one-dimensional but here the numerical solution is obtained over two dimensions. For model IM-1 the corresponding one-dimensional equation is

$$\frac{\partial c}{\partial t} + \frac{Pe}{r}\frac{\partial c}{\partial r} = \frac{1}{r}\frac{\partial}{\partial r}\left(r\frac{\partial c}{\partial r}\right) \tag{5.42}$$

and the analytical solution is given in Appendix A. Compared to the linear flow model in Chapter III the Peclet number will vary spatially as

$$Pe = \frac{Pe_1}{r} \tag{5.43}$$

and close to the well the front will be very steep. For model ID-1 the one-dimensional problem is

$$\frac{\partial c}{\partial t} + \frac{Pe_1}{r}\frac{\partial c}{\partial r} = \frac{1}{r}\frac{\partial^2 c}{\partial r^2} \tag{5.44}$$

Comparing (5.44) to (5.42), the second derivative in (5.44) is multiplied by 1/r where for (5.42) the factor is one. The solution of

(5.42) will therefore have a sharper front than the solution to (5.44).

Numerical solutions of Model IM-1 and ID-1 (or (5.42) and(5.44)) are discussed in the following. The Peclet number (Pe_1) chosen were 50 and 500 and the numerical solutions are discussed individually and then compared. Only solutions with the moving coordinate systems are considered here. Estimates of the number of elements and time-steps needed for computation on fixed grid will be discussed.

The grid used for these calculations are based on the results obtained in Chapter II. In the area containing the front or slug the mesh is constructed based on

$$Pe_1 \Delta x \simeq 2\text{-}5 \tag{5.45}$$

Perpendicular to the front larger increments can be used, such as

$$Pe_1 \Delta x \simeq 5\text{-}10 \tag{5.46}$$

An example of the grid is shown in Fig. 5.16. As the front is steepest for small times the grid is finest close to the origin and the fine mesh is elsewhere spread outward in a radial (circular) manner.

Examining model IM-1 first, the solution for $Pe_1 = 50$ along the diagonal is shown in Figs. 5.10 and 5.17. In Fig. 5.10 the velocity of the MCS (frontal velocity) is evaluated at three different times between T and T + DT and a fixed timestep was used. Evaluating the velocity at T + DT gives the best results. With a variable timestep the "T + DT" solution is shown in Fig. 5.17 and the number of steps as a function of time is shown in Fig. 5.18.

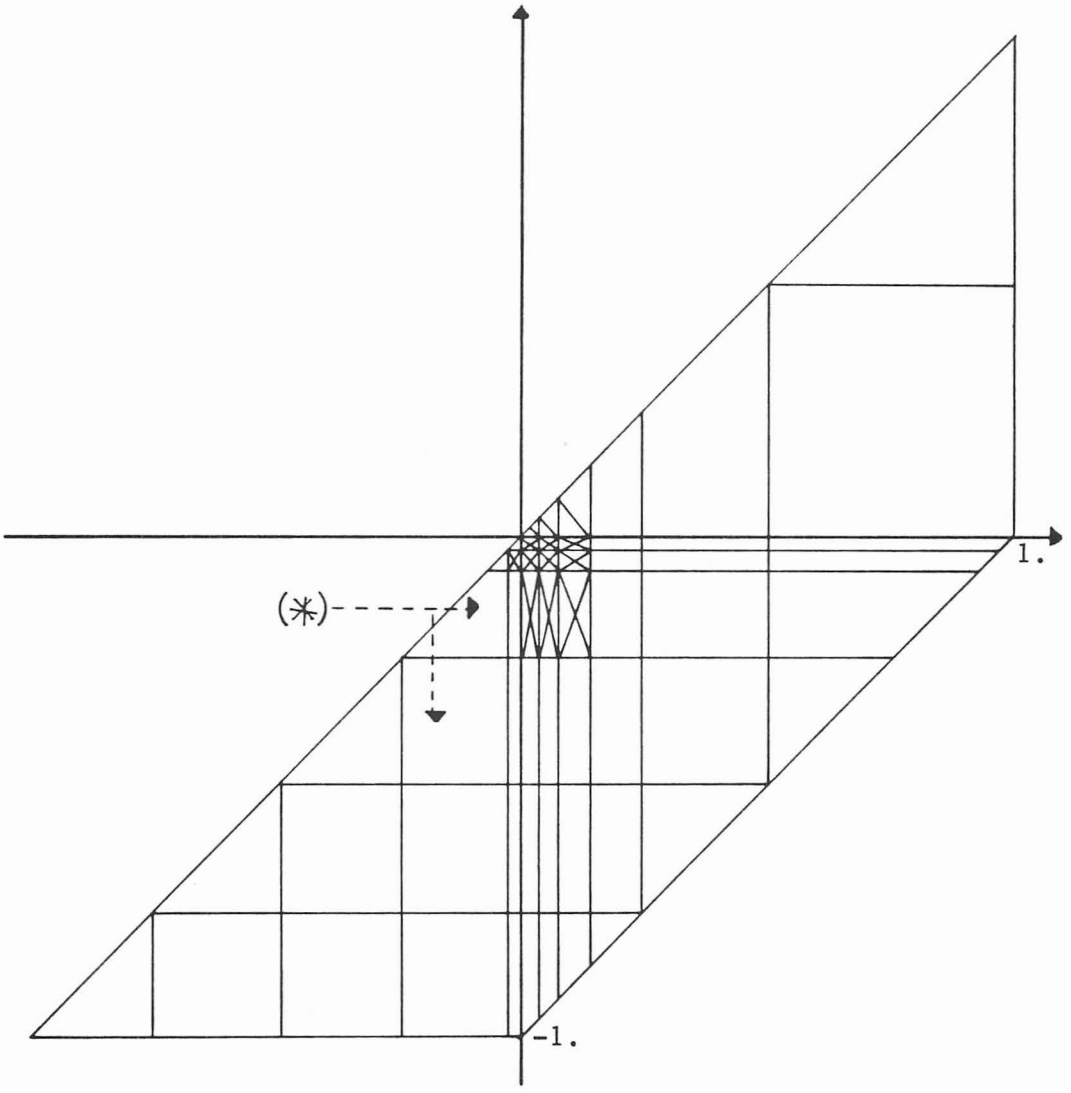

Figure 5.16

Mesh for MCS Calculations

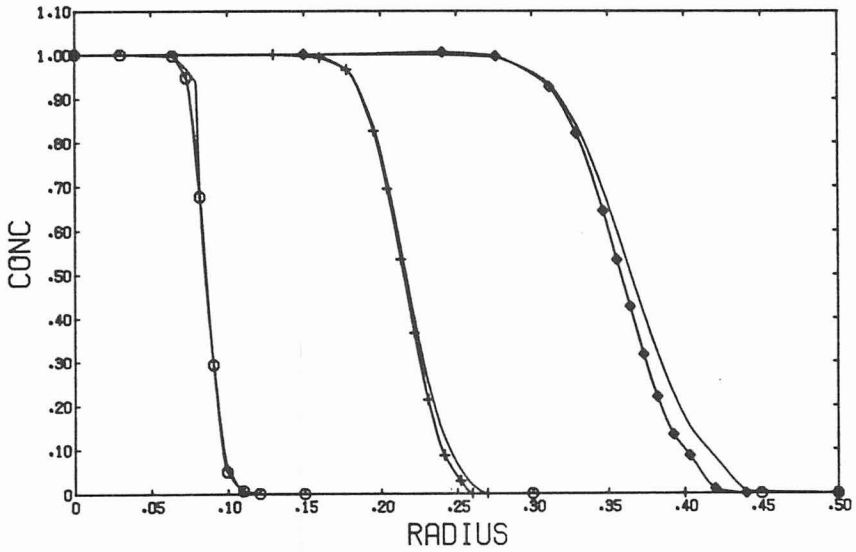

Figure 5.17

Model IM-1, Pe_1 = 50, Solutions at Times 7.5×10^{-5} (O), 4.75×10^{-4} (+), 1.35×10^{-3} (◇)

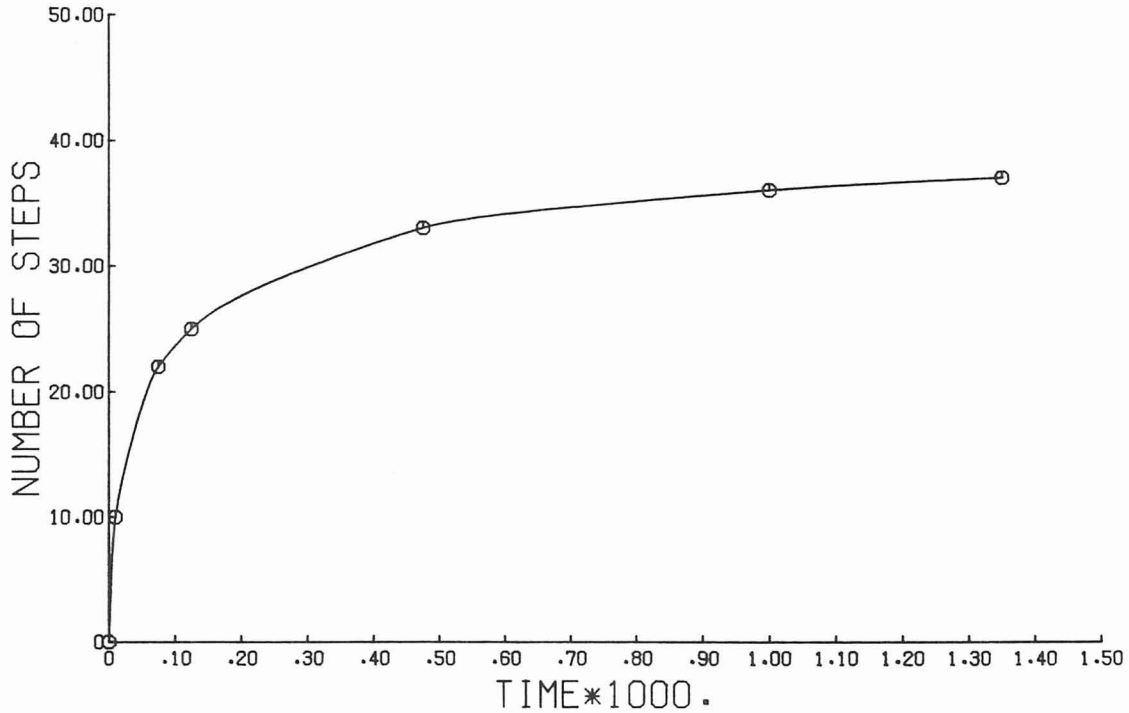

Figure 5.18

Model IM-1, Pe_1 = 50, Number of Steps Function of Time

In the initial period the front is very steep, the numerical solution has some oscillations and many timesteps are therefore needed. At later times the broadening of the front occurs more slowly and the frontal shape and position is relatively unchanged so larger timesteps can be taken. If smaller timesteps were taken for the cases shown in Fig. 5.10 the accuracy would improve, and also more timesteps would be required when the frontal velocity is evaluated at T or T + DT/2. Thirty-four (34) elements and a total of 34 timesteps were used to move the front from the well to a distance of 0.4. This corresponds to injecting $\simeq$ 0.1 pore volume.

For a Peclet number of 500 the solution is shown in Fig. 5.19, both along the diagonal and along y = 0. The solution is symmetric in both directions and very accurate when compared to the exact solution. A total of 71 elements were used and 41 timesteps were necessary to inject 0.05 pore volume. For a higher Peclet number the scheme requires more steps in the beginning.

The same Peclet numbers were used for model ID (dispersion proportional to velocity) as for model IM. The solutions of model ID for high Peclet numbers compares in steepness to solutions of model IM for low Peclet numbers. In Fig. 5.20 is shown a solution for Pe_l = 500 on a grid similar to model IM and Pe_l = 50 . The analytical solution for model IM-1 is drawn too. Comparing this result with Fig. 5.19 (model IM, Pe_l = 50) and a frontal position of radius 0.1, the solutions are very similar as shown in Fig. 5.21. The frontal sharpness depends to a large extent of the dispersion tensor.

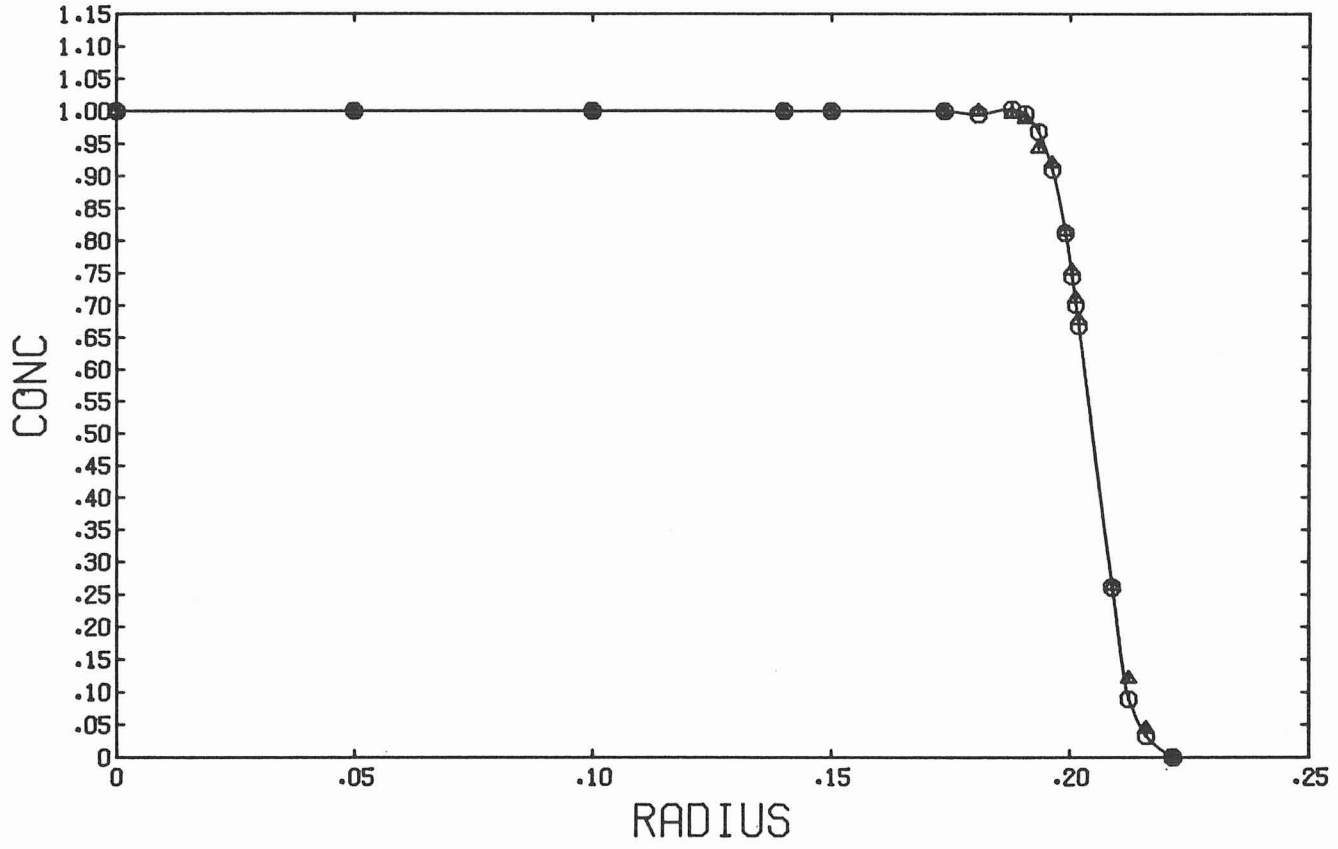

Figure 5.19

Model IM-1, Pe_1 = 500, Solution at t = 4.2 x 10^{-5} (0.04 PV),
—exact solution, (⊕) diagonal, (Δ) y = 0

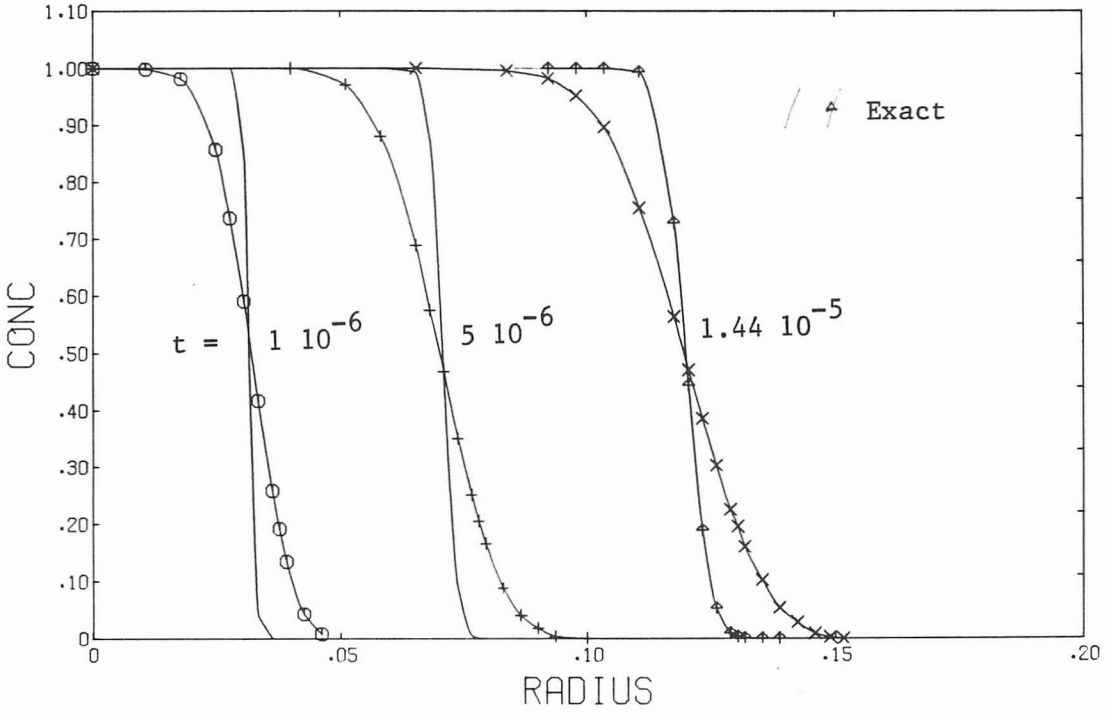

Figure 5.20

Model ID-1, Pe_1 = 500, Solution at Different Times

It is important to model the dispersion tensor correctly for field applications.

As mentioned before no attempt to solve either (5.42) or (5.44) in a fixed coordinate system was done. Estimates of the cost when using a fixed coordinate system to solve model IM-1 are given in Table 5.1 and Table 5.2. In a fixed coordinate system many elements must be used (Chapter II) and the criteria $Pe\Delta x$ reveals if any oscillations can be expected. In Table 5.1 the elements used in the model IM are given with corresponding $Pe\Delta x$-values. For a Pe_1 = 50 only

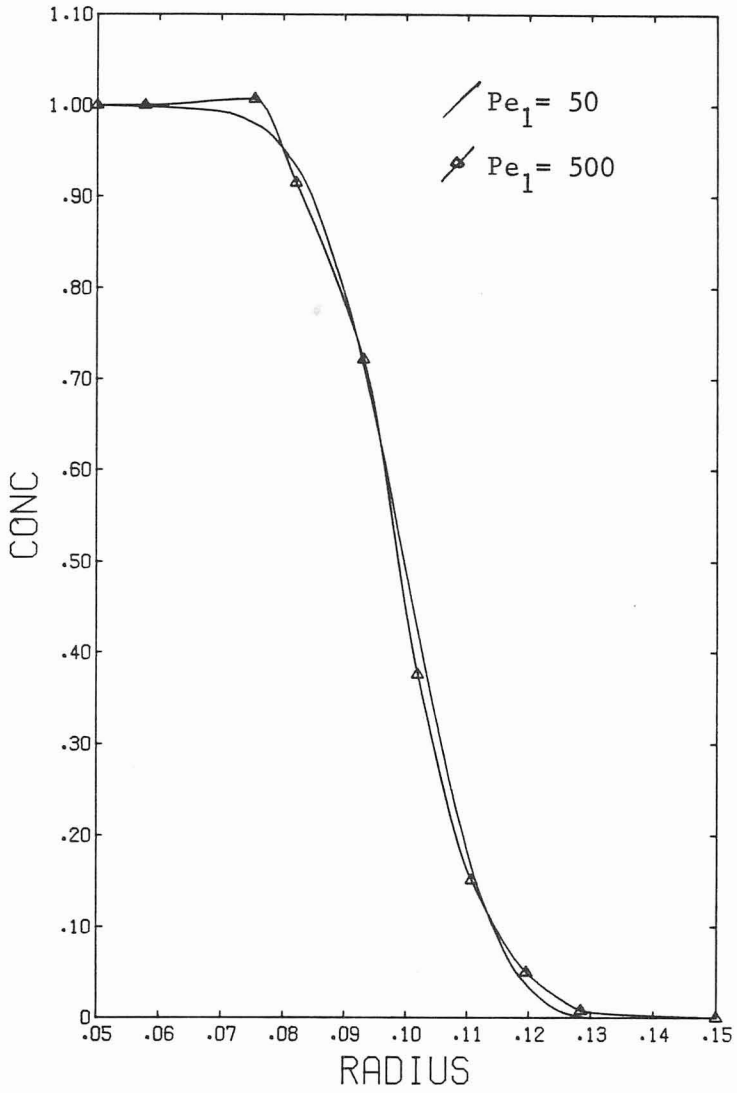

Figure 5.21

Comparison of Model IM-1, Pe = 50 and Model ID-1, Pe_1 = 500 at r_f = 0.1

slight improvement is found but for Pe_1 = 500 with comparable accuracy ($Pe\Delta x \simeq 25$) about 15 times fewer elements are needed. Table 5.2 lists the number of steps used in the calculations together with estimates

Table 5.1

Elements for Fixed and Moving Coordinate System, Model IM-1, Pe_1 = 50, 500

	Pe_1 = 50	Elements	$Pe\Delta x$
MCS	— to r_{front} = 0.37	34	< 1***
	— whole domain	120*	< 1***
Fixed	— whole domain	120**	3.1
		313**	2

	Pe_1 = 500	Elements	$Pe\Delta x$
MCS	— to r_{front} = 0.22	71	< 1***
	— whole domain	160*	< 1***
Fixed	— to r_{front} = 0.22	71	11
	— whole domain	160	38
	— whole domain	31250**	2**
	— whole domain	2500****	25**

* Estimate based on additional number of elements necessary to inject one pore volume in five spot.

** Estimate based on criterias derived in Chapter II, and that the Peclet number is the same everywhere in the domain.

*** Only near the frontal position.

**** Estimate based on Settari et al. (1977) using Galerkin Hermite cubic. Limit based on model ID and insures only minor oscillations. Conversion by a factor 10 used to convert from model ID to IM.

Table 5.2

Timesteps for Fixed and Moving Coordinate System, Model IM, Pe_1 = 50, 500

Pe_1 = 50		Steps to r_f = 0.37	Steps to 1.0 PV injected
MCS	— Variable timesteps	34	100*
Fixed	— Variable timesteps		
	— Lowest Δt	1,080**	10,000
	— Average Δt	34**	340

Pe_1 = 500		Steps to r_f = 0.22	Steps to 1.0 PV injected
MCS	— Lowest t	41	200*
Fixed	— Lowest Δt	1,400**	65,000
	— Average Δt	41**	1,100

* Estimate based on using the last timestep.

** Timesteps from the MCS calculations.

of steps necessary in a fixed coordinate system. For the fixed coordinate system two estimates are given based on the lowest or average timestep used in the MCS. The estimates compare well with other studies [Settari et al., 1976; Young, 1978]. In a fixed coordinate system the timesteps do not change very much during the integration as the stiffness ratio is approximately constant during the integration. The solution changes rapidly at some nodes while other nodes remain nearly constant (Fig. 5.2). In the moving coordinate system the solution will be fairly constant during the whole integration. Roughly a factor 15 fewer timesteps is necessary in the moving coordinate system as compared to a fixed coordinate system

Based on comparing number of elements and timesteps the moving coordinate system is more efficient by a large factor. Differences in setup solution scheme etc. can effect this potential savings in cost and a more detailed comparison based on actual computation time is done in Section 5.4-4.

5.4-3 Five Spot Flow Pattern

The five spot flow pattern is more realistic to reservoir engineering problems, as most on-shore oil fields are developed in this manner. First calculations in both a fixed and moving coordinate system for a Peclet number of 10 are compared. A mass balance is made when injecting a slug. Some results for higher Peclet numbers are given too.

The grid used for $Pe_1 = 10$ in a moving and fixed coordinate system is shown in Fig. 5.22, $Pe\Delta x < 2.5$ for both cases. A model IID is considered with both step change and injection of slug.

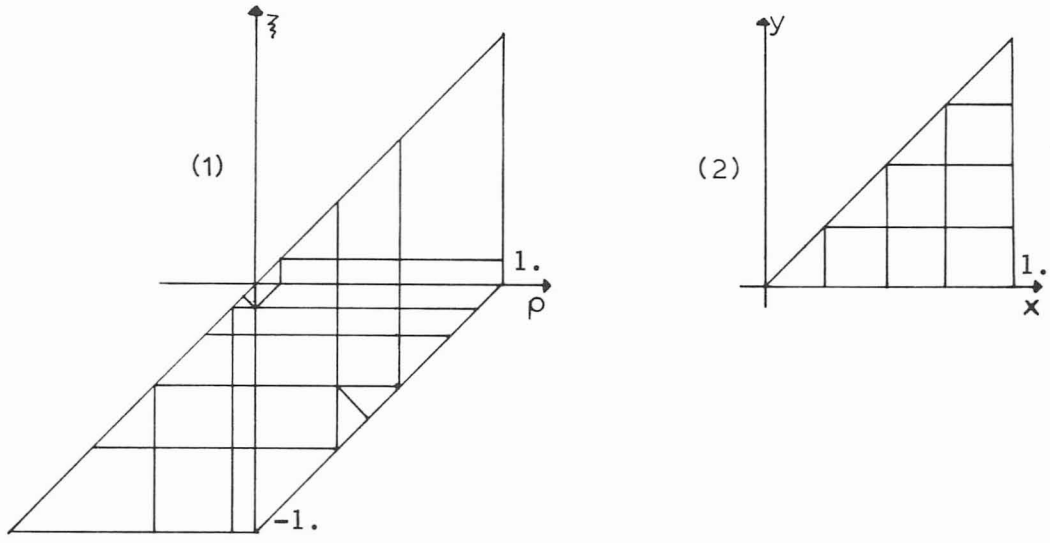

Figure 5.22

Grid for Model IID, Pe = 10

For the step change boundary condition (IID-1) the solution was computed in the fixed coordinate system with a variable timestep scheme and using either Crank-Nicholson or Euler corrector (Section 5.3-4). To measure the temporal truncation error a solution with a small fixed timestep and Crank-Nicholson scheme was obtained. The solutions along the diagonal and along y = 0 are shown in Fig. 5.23. Using a fixed small timestep rather than the variable timestep scheme gave almost identical results except at large pore volumes injected. The fixed timestep solution is only shown for 1.06 PV injected, where the differences can be seen graphically. The Euler corrector tends to smooth the solution for the same number of accumulated steps as seen from the figure. The contours from the fixed timestep solution are shown in Fig. 5.24 at 0.4 and 0.8 pore volumes injected. The curves

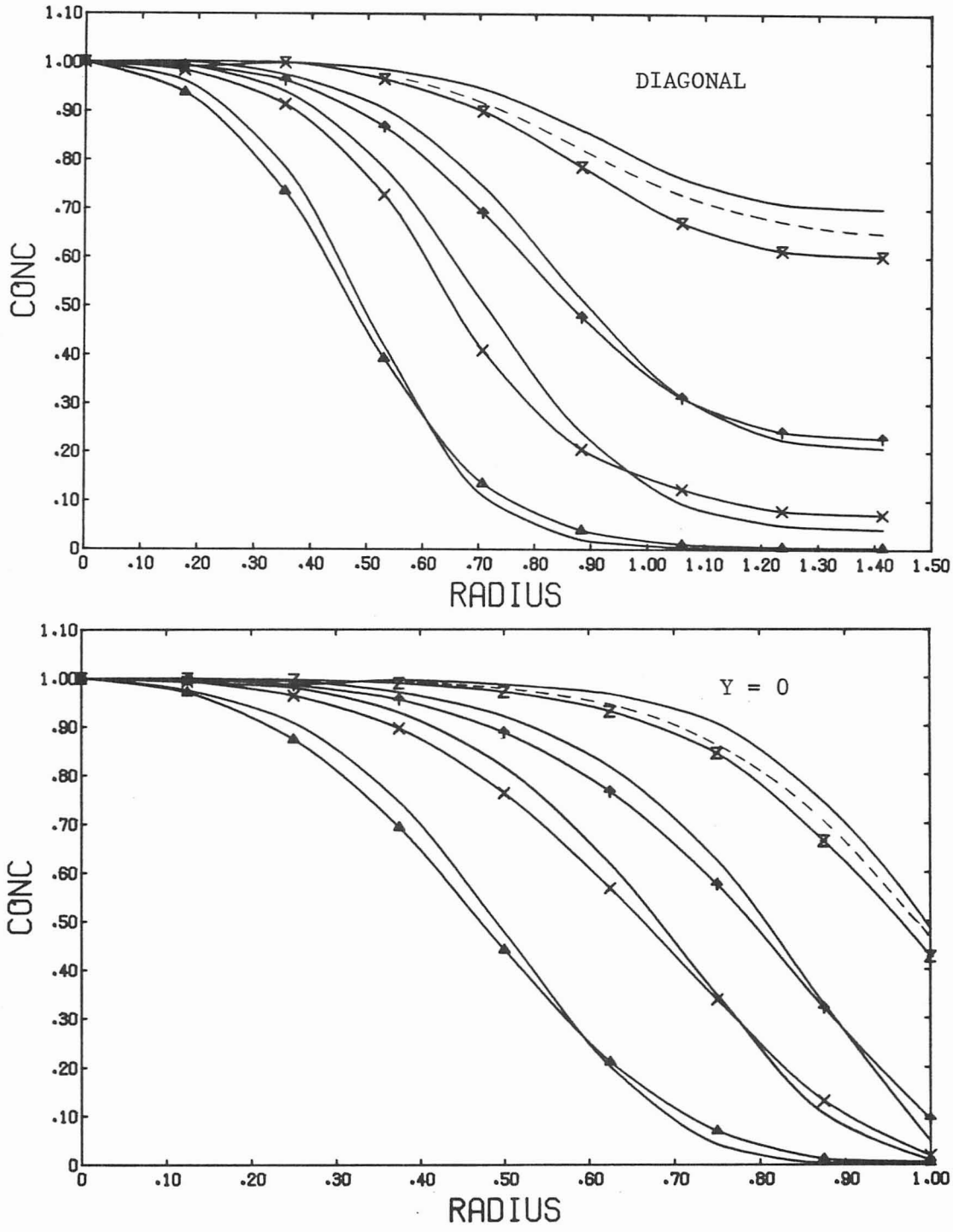

Figure 5.23

Model IID-1, Pe_1 = 10, Diagonal and y = 0, Labelled Euler, Unlabelled: Crank-Nicholson Solutions at Injected PV: 0.2 (Δ), 0.4 (×), 0.6 (♠), 1.06 (⧖)

in Fig. 5.24 are drawn from only a few points and are therefore only approximately correct. The concentration at the stagnation point (x = 1, y = 0) should be zero at all times since the velocity is zero (Fig. 5.2), but as seen in 5.24 the numerical solution gives a nonzero value. If a finer mesh was used in this region a better resolution could be obtained. In Fig. 5.25 is shown the concentration at production well and the stagnation point as a function of the injected pore volumes. The Euler scheme smooths the profile again. The concentration at the stagnation point increases with time and as the gradients are nonzero at this location (Fig. 5.23), the mass balance will be affected. Integrating the concentration at the production well and measuring the mass in the domain (Section 5.4-7), a mass balance can be made as shown in Table 5.3. The error is 2-6%, mainly in the beginning (see discussion, p. 149) and at later times where the concentration at the stagnation point is nonzero. The

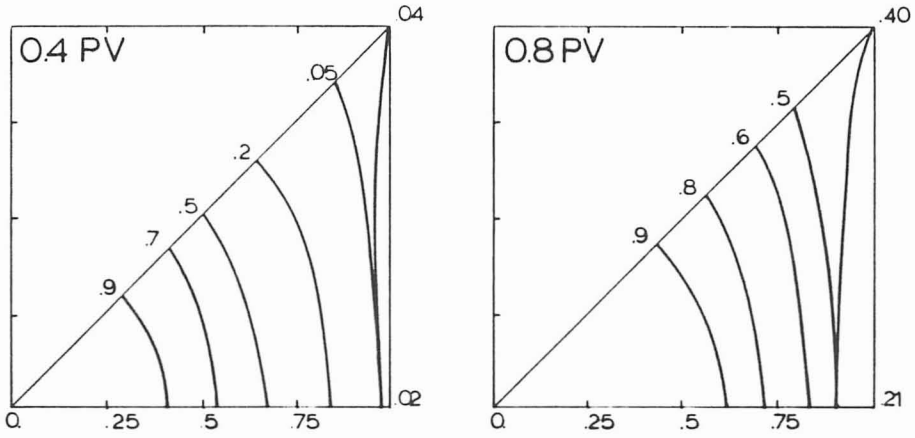

Figure 5.24

Model IID-1, Pe_1 = 10 Contours at 0.4 PV, 0.8 PV

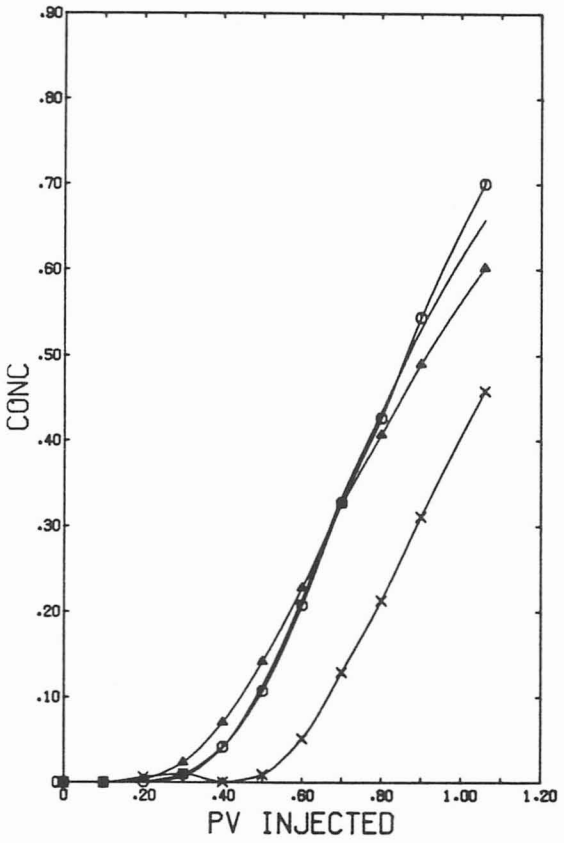

Figure 5.25

Concentration at Production Well: (○) Crank-Nicholsen, (△) Euler, (—) CN, fixed Δt; Stagnation Point (×)

mass balance automatically gives a recovery curve, oil produced versus fluid injected as the mass in the domain

$$\int_A c(t)dA$$

corresponds to the amount of material injected. This is shown in Fig. 5.26 and a result with a higher Peclet number from the study of L. Young (1978) is drawn too. For higher Peclet numbers the breakthrough of the displacing fluid occurslater compared to the low Peclet number.

Table 5.3

Mass Balance

PV	Calc. Mass	Production Well	Total	Exact	Error
0.1	0.54120	0	0.54120	0.050265	7.6%
0.2	0.10544	0	0.10544	0.10053	4.9%
0.3	0.15529	0	0.15529	0.15011	3.5%
0.4	0.20482	0.00153	0.20635	0.20027	3.0%
0.5	0.25081	0.005605	0.25642	0.24975	2.6%
0.6	0.29298	0.01539	0.30837	0.2999	2.8%
0.7	0.33194	0.0322	0.36414	0.3534	3.0%
0.8	0.36059	0.05615	0.41674	0.39976	4.2%
0.9	0.38665	0.08622	0.47244	0.45003	5.0%
1.06	0.41838	0.1473	0.56568	0.52857	7.0%

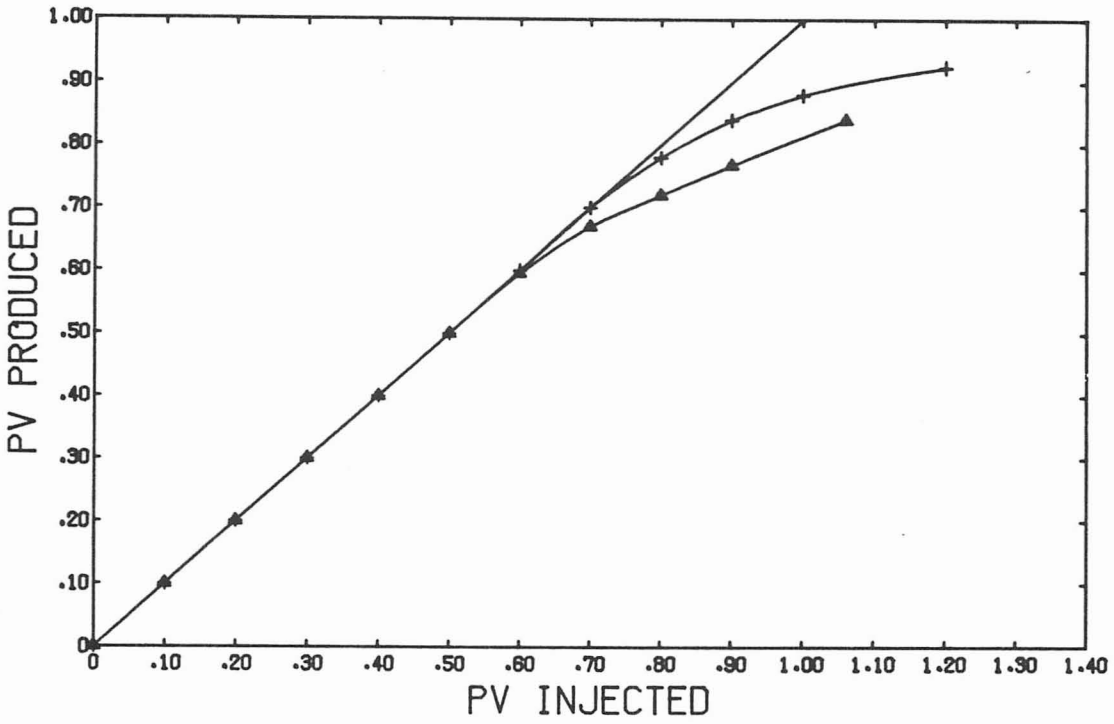

Figure 5.26

Recovery Curve, Model IID-1, ☆ Pe_1 = 10, ✶ Pe_1 = 72.5

When the moving coordinate system was used rather than the fixed, the solution was almost the same. Figure 5.27 shows the solution along the diagonal and along y = 0 at different times, the more accurate fixed timestep solution from Fig. 5.23 is drawn too for comparison. Only close to the boundary can a discrepancy be detected, which is caused by not locating the boundary conditions exactly. This is shown in Fig. 5.28 at 0.7 pore volumes injected. The boundary condition using MCS is located at a radius of 1.72 instead of at $\sqrt{2}$ = 1.414 but the slope at the false boundary is approximately zero so the boundary condition is satisfied, but improperly placed. A

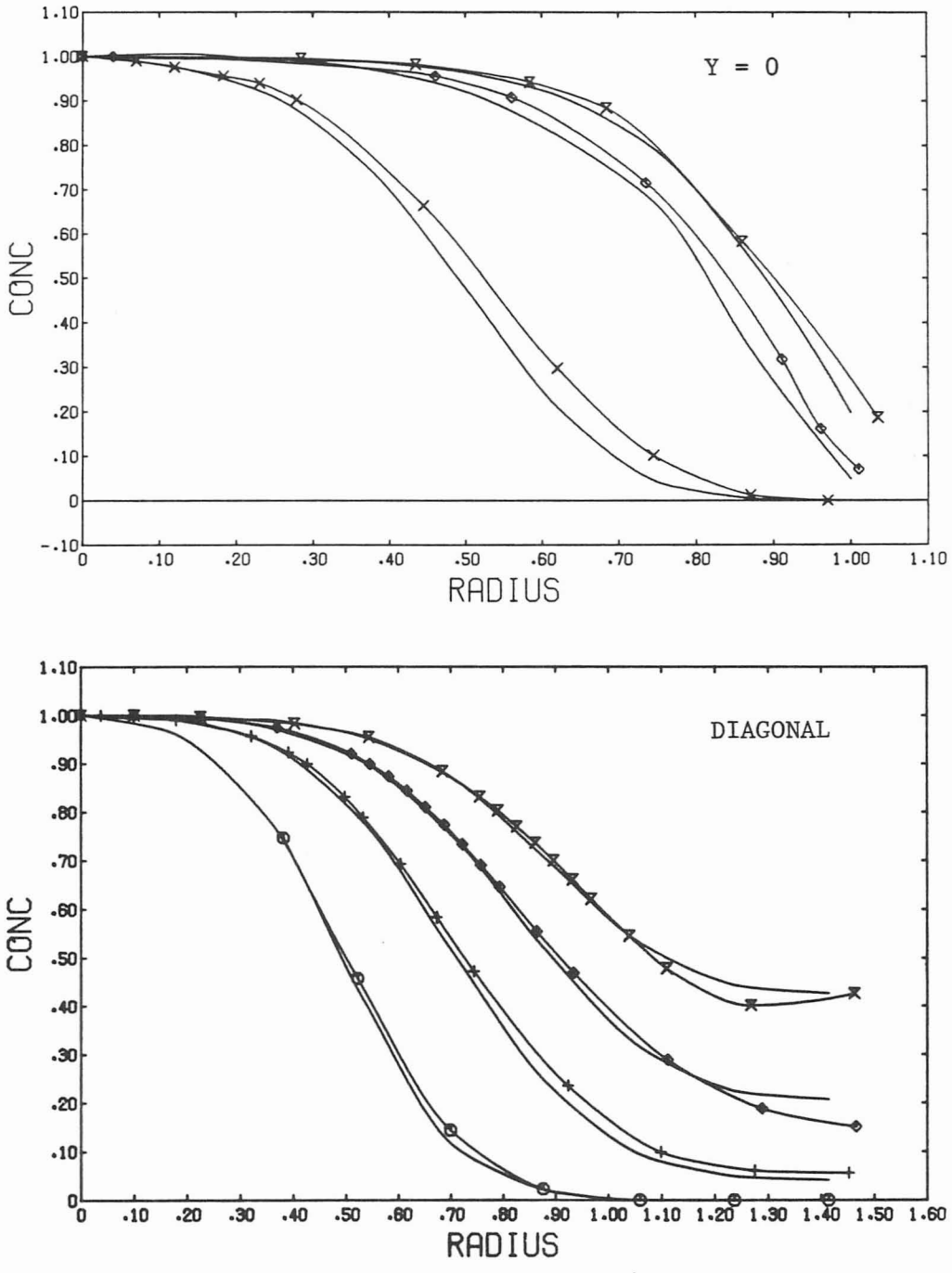

Figure 5.27

Model IID-1, Pe_1 = 10, Diagonal and y = 0, Solutions at Injected PV: 0.2(× ○), 0.4 (+), 0.6 (◇), 0.8 (⧖), — FCS as Figure 5.23

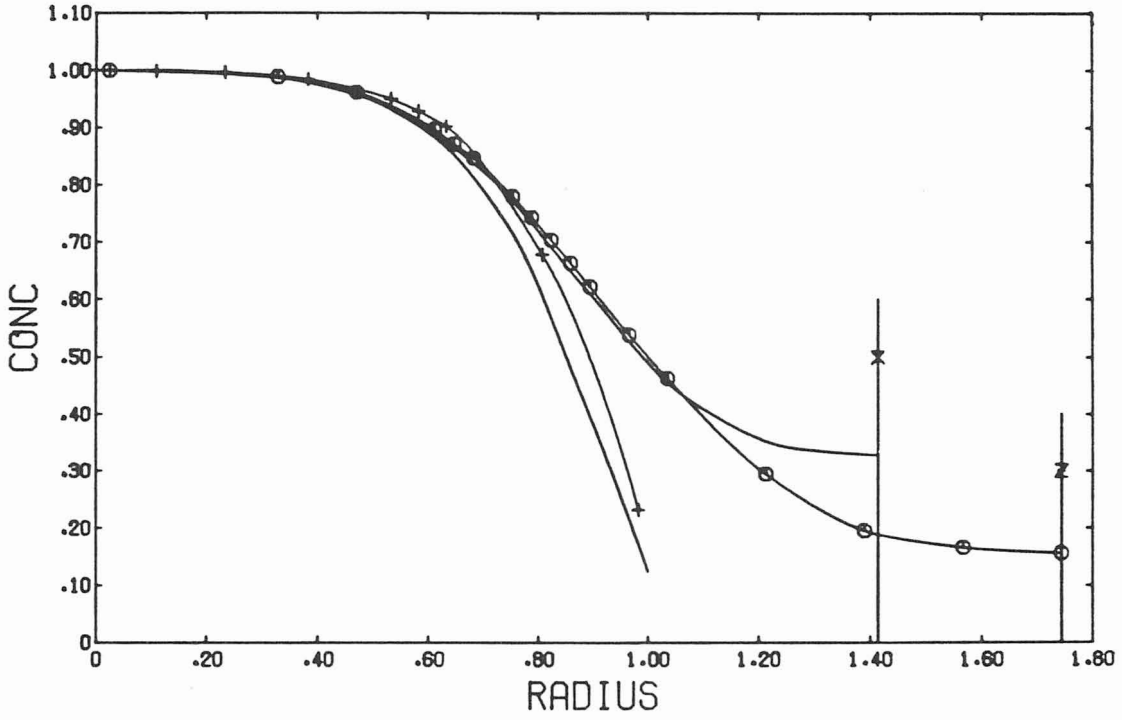

Figure 5.28

Model IID-1, Pe_l = 10, Solution at 0.7 PV (o) Diagonal MCS,(+) y = 0, MCS, ⅄ MCS boundary — Fixed CS

correction based on the area difference could be made so that the concentration at the production well (Figure 5.29 would not show the nondesirable jumps.

The number of timesteps used both for a fixed grid and MCS with Pe = 10 is shown in Fig. 5.30. The advantages described previously with MCS does not hold for small Peclet numbers as the solution changes much more than for higher Peclet numbers. About twice the number of steps used with the fixed coordinate system must be used for the MCS (same EPS used in both cases).

With model IID-2 (slug injection) and a fixed coordinate system, Crank-Nicholson corrected and variable timesteps a solution was ob-

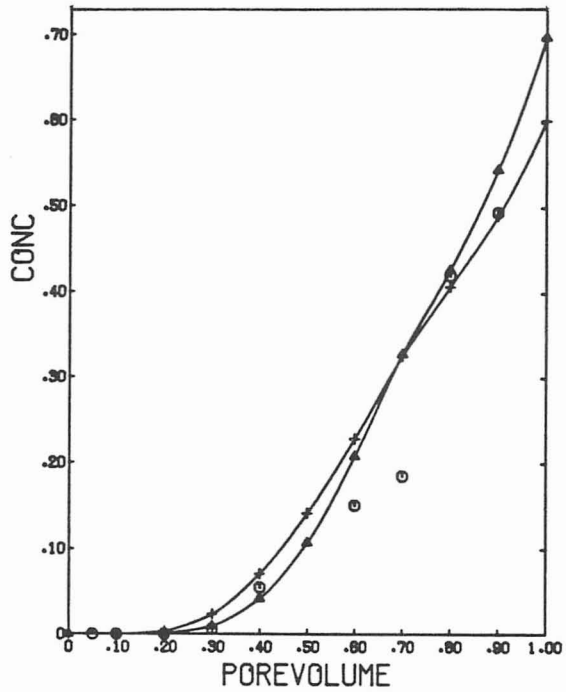

Figure 5.29

Concentration at Production Well, Model IID-1, Pe_1 = 10, (Δ) Crank-Nicholsen, (+) Euler, (Ø) MCS, Crank-Nicholsen

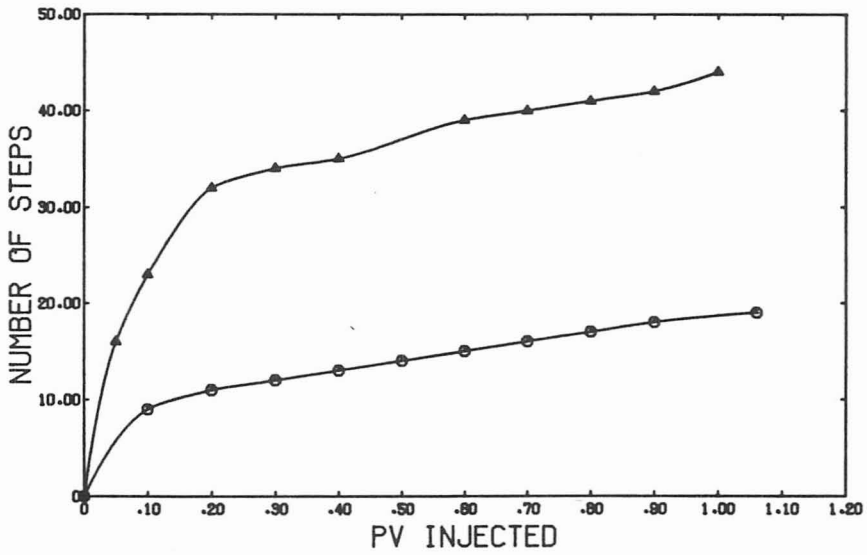

Figure 5.30

Number of Timesteps, Model IID-2, Pe_1 = 10, (Ø) FCS, (Δ) MCS

tained, and a detailed mass balance performed. A Peclet number of 10 and the mesh (2) shown in Fig. 5.22 were used. The solution obtained along the diagonal and along y = 0 is shown in Fig. 5.31. The approximate contours are shown in Fig. 5.32.

The solution shows the trends of what can be expected to happen physically; a peak (bank) of material being pushed toward the producing well much faster than towards the stagnation point. Again the concentration at the stagnation point is nonzero because of poor discretization.

A mass balance as described in Section 5.4-7 was performed for this example. In Fig. 5.33 is shown the accumulated mass diffused in and out of the three boundary lines. The net mass in and out is given in Fig. 5.33 too. At initial times (c = 1) a net flux in through the south and diagonal boundary line occurs, but when the injection stops (c = 0) mass flows out with approximately the same rate as it flows in, so the net flux is nearly zero.

The mass balance found in Table 5.3 is therefore also caused by flow in at initial times. A total mass balance is shown in Fig. 5.33 too, where the accumulated mass flow out by the production well is calculated from Fig. 5.34. The exact mass injected was 0.065 but a total of 0.083 can be accounted for. The difference can be attributed to the net flux in at initial times through the south and diagonal boundary lines. The mass balance error in this example is therefore up to 30% which must be attributed to mainly a poor discretization (initial times).

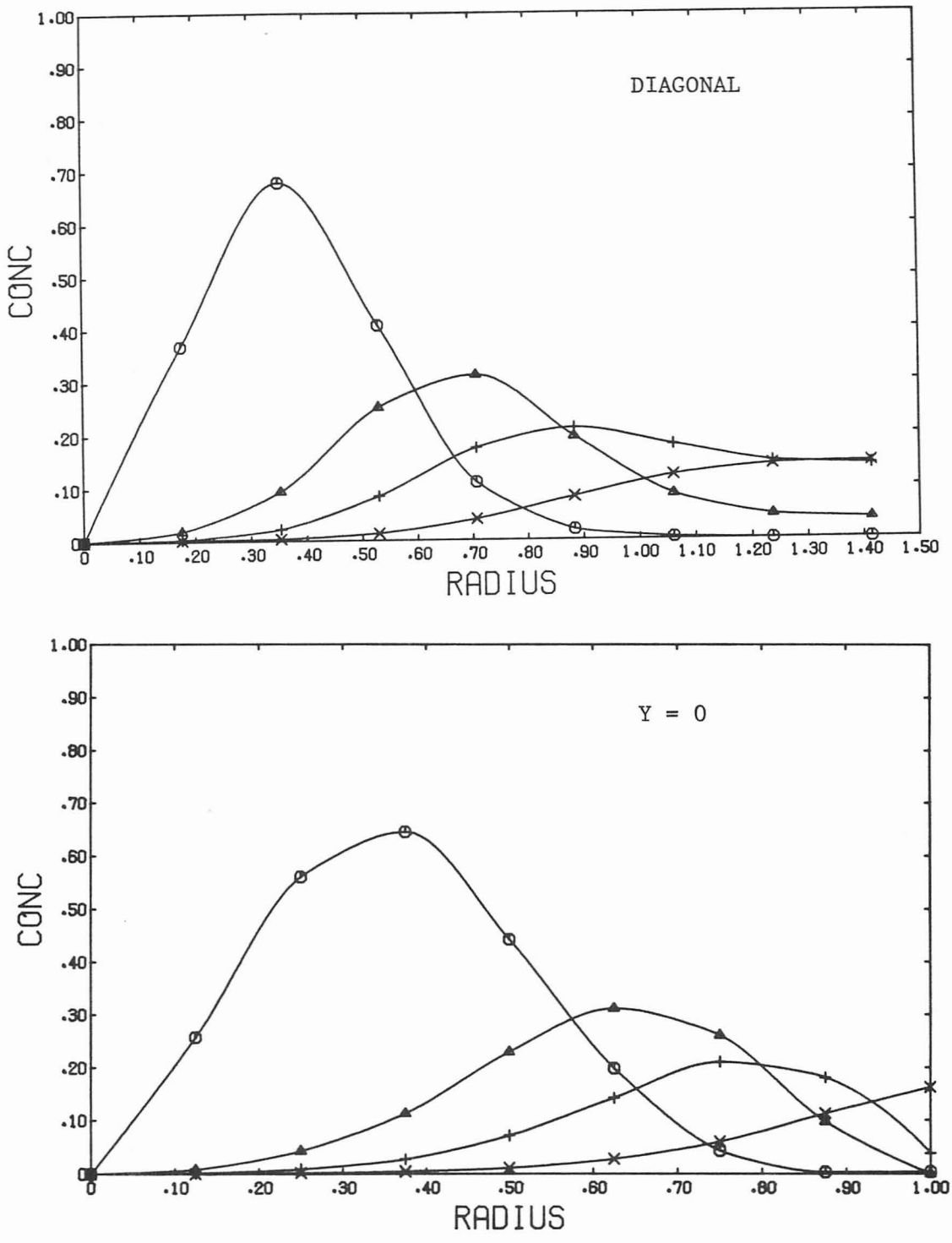

Figure 5.31

Model IID-2, Pe_1 = 10, Diagonal and y = 0, Solutions at Injected Pore Volumes: 0.2 (○), 0.4 (Δ), 0.6 (+), 1 (x)

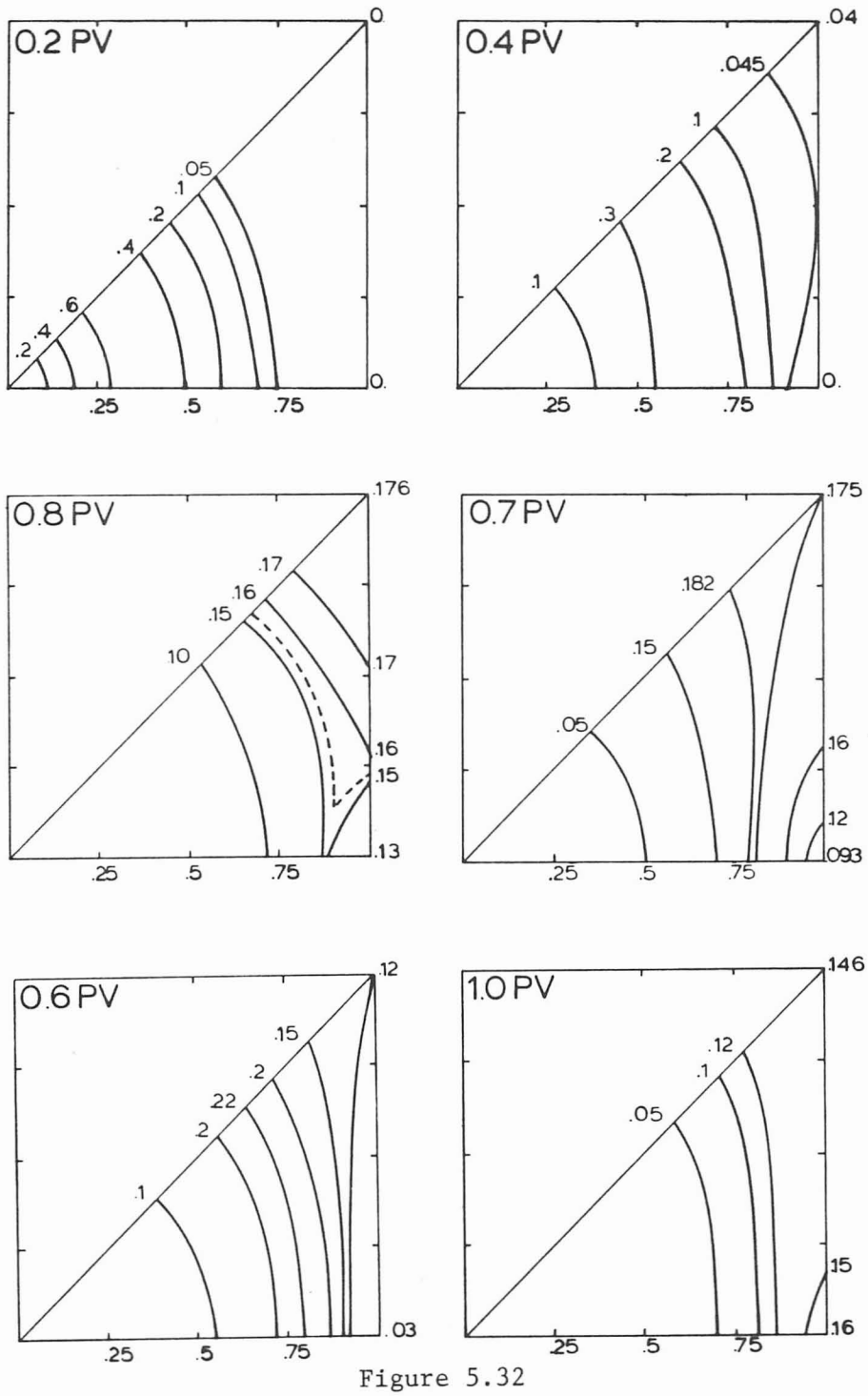

Figure 5.32

Model IID-2, Pe_1 = 10, Contours

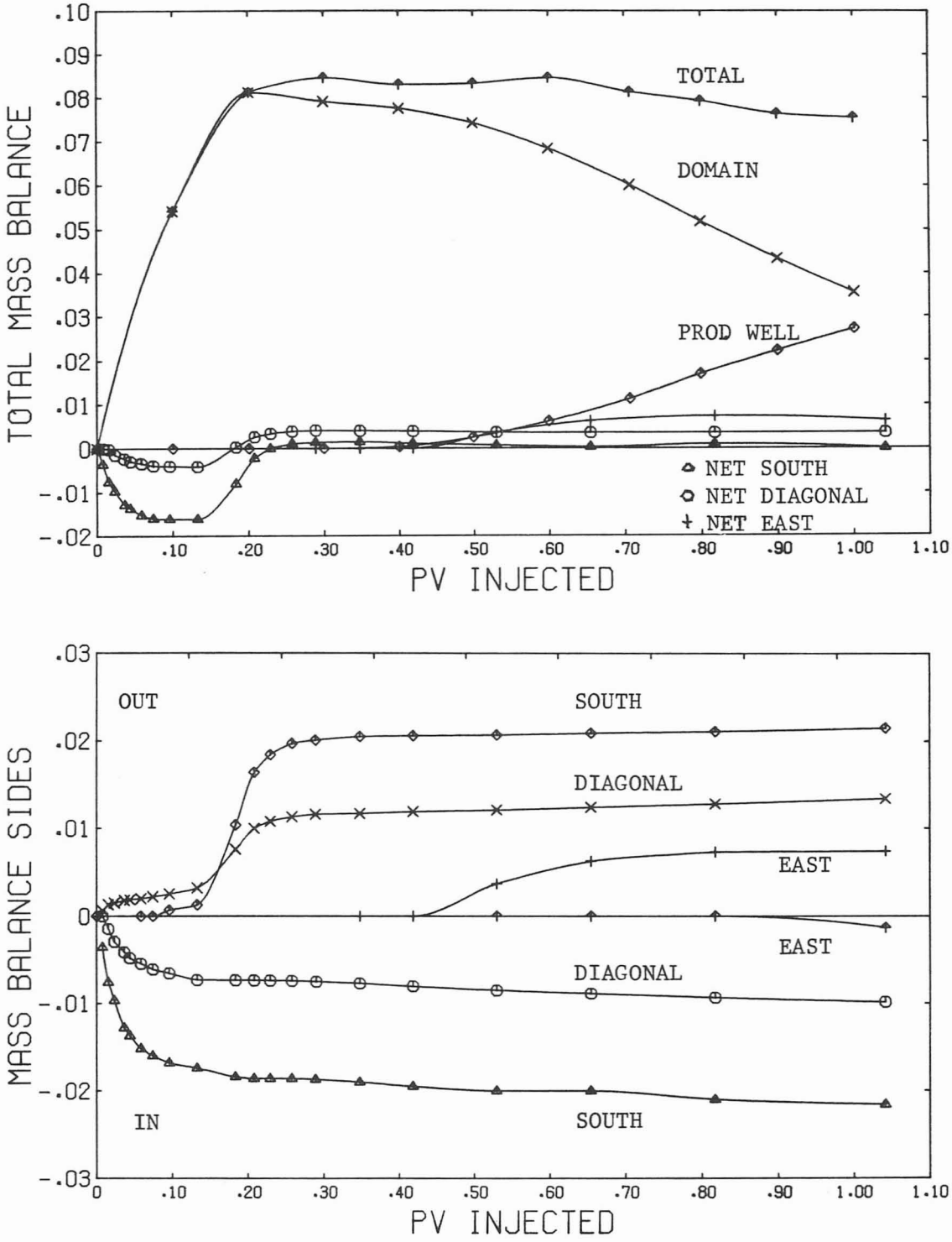

Figure 5.33

Model IID-2, Pe_1 = 10, Mass Balance

Even though $Pe\Delta x$ is small the discretization must be even finer to give an accurate solution especially near the wells and stagnation point. Mass balance calculations are an effective tool to check the accuracy of the solution.

In Fig. 5.34 is shown the concentration at the production well together with the results of another study [L. Young, 1978]. The profile is steeper for larger Peclet numbers and the placement of the peak is a function of the amount injected. Injecting large quantities the peak is shifted to larger injected pore volumes. The peak for this case is misplaced as the mass balance error by the stagnation point will lower and change the position of the peak to earlier times.

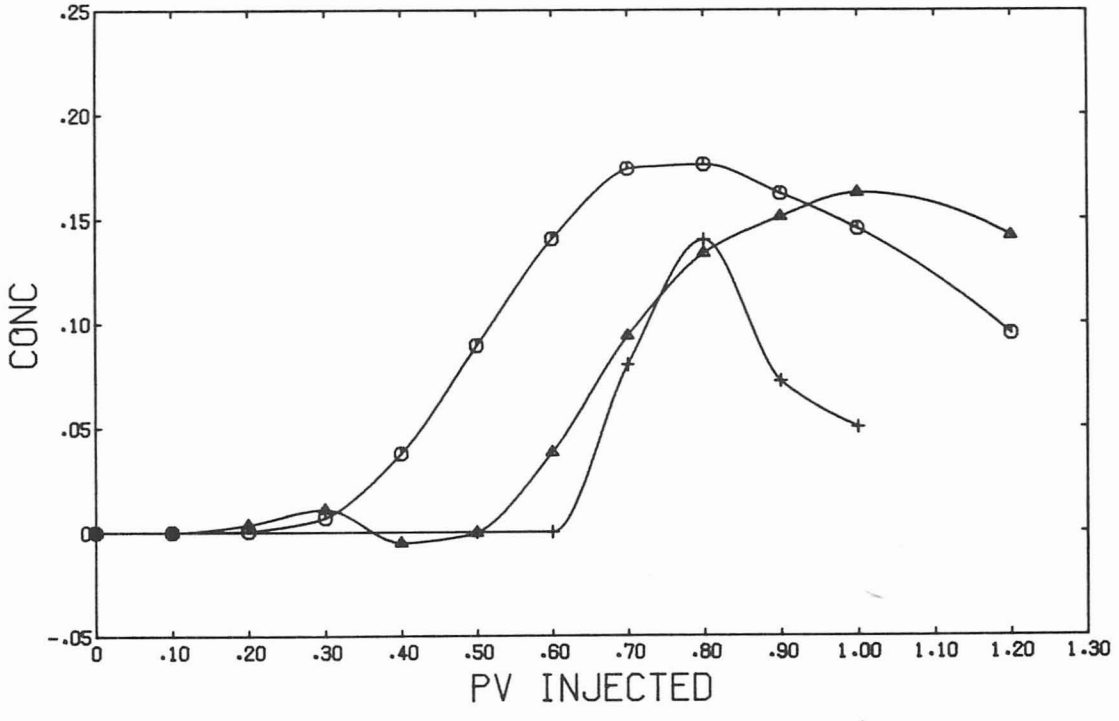

Figure 5.34

Model IID-2, Pe_1 = 10, o production well, Δ stagnation point; Pe_1 = 300, + production well

Using model IIM-1 and a Peclet number of 50 solutions were obtained to a total of 0.44 pore volume injected. The mesh with a total of 80 elements is shown in Fig. 5.35.

The solution along the diagonal and y = 0 is shown in Fig. 5.35. The exact solution with radial flow (5.42) is shown in the figures too. A "bump" is observed at later times which was not observed for Pe_1 = 10. This is probably caused by time truncation error. The contours at 0.44 PV are shown in Fig. 5.36 together with the used mesh and it is seen that the elements are correctly placed by having many nodes where the steep profile is and elsewhere only a few. A total of 80 elements and 60 timesteps were used to inject 0.44 PV. Further integration was performed but the results showed large oscillations. It was found later with a more difficult problem that if the location of boundary conditions is specified exactly, these instabilities disappear.

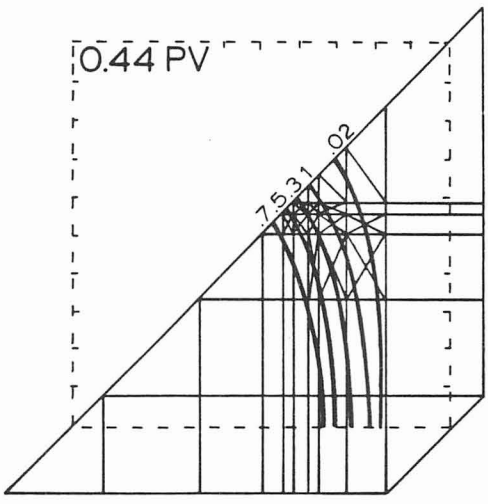

Figure 5.35

Model IIM-1, Pe_1 = 50, Contours at 0.44 PV

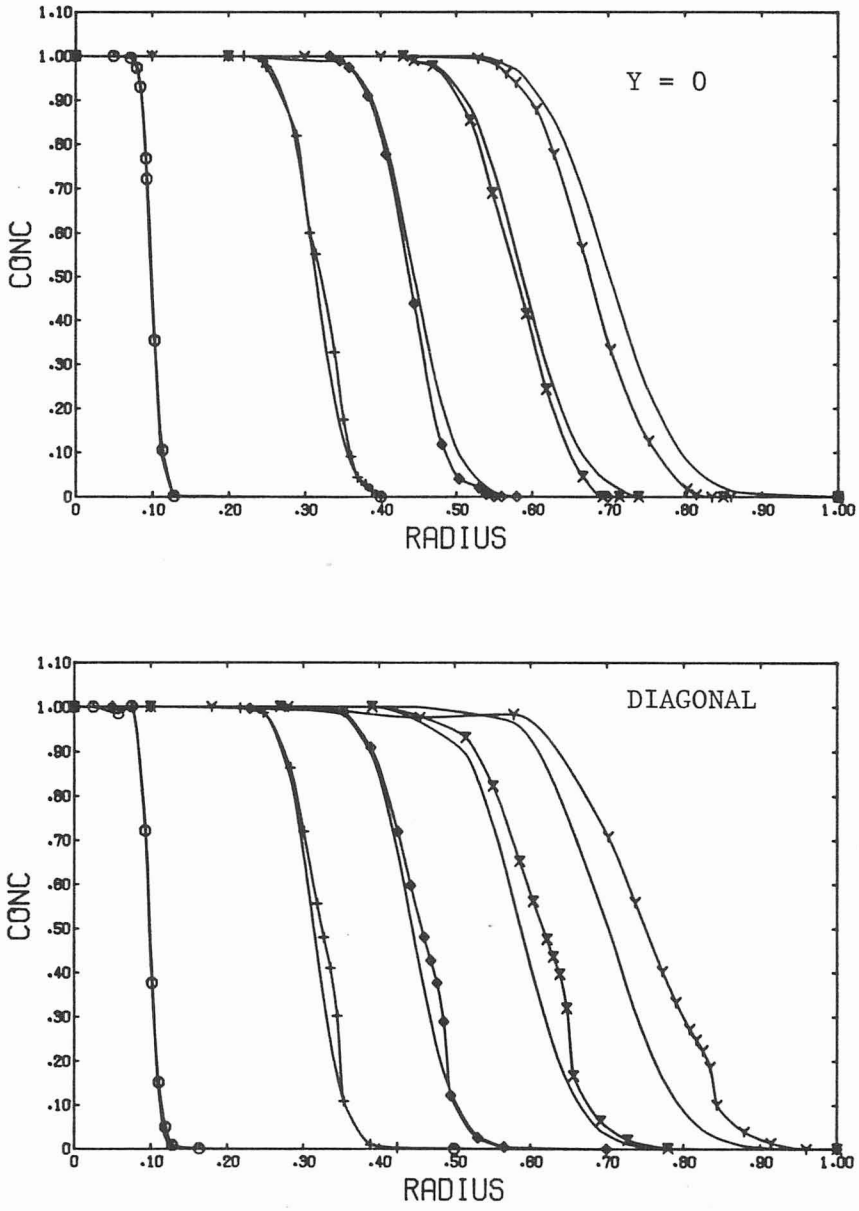

Figure 5.36

Model IIM-1, Pe_1 = 50, along diagonal and y = 0, solutions at 1×10^{-4} (o), 1×10^{-3} (+), 2×10^{-3} (◇), 3.5×10^{-3} (x), 5×10^{-3} (Y)

5.4-4 Five Spot Flow With High Peclet Number

The preceeding two sections showed that the moving coordinate system is applicable to two-dimensional problems. The number of elements and timesteps were considerably smaller than if a fixed coordinate system was used. In this section the result of solving a model IID-2, injecting a 0.05 pore volume (PV) slug with a Peclet number of 1000 is discussed. In contrast to the other examples considered in this chapter comparisons to the other studies can be made for this example.

Young (1978) and Settari et al. (1976) solved the same model with a Galerkin formulation using respectively Lagrange and Hermite cubic elements. Both used a 10 x 10 element grid and 1100 timesteps to inject one pore volume. Second order implicit integration routines were considered.

Solving the model with MCS the locations of the boundary conditions are specified exactly with the algorithm described in 5.3-6. A total of 105 elements and 113 timesteps were used to inject 0.5 pore volume. The grid used is shown in Fig. 5.16 with the area denoted by (*) in Fig. 5.16 shown in Fig. 5.37. When the injection of slug material stops (at 0.05 PV), two fronts (if considering line between wells) develop. The upstream front (closest to injector) will move towards the downstream front (closest to producer) at later times (see Fig. 5.38). In the area where the upstream front is moving more elements are needed. These additional elements are shown in Fig. 5.37;

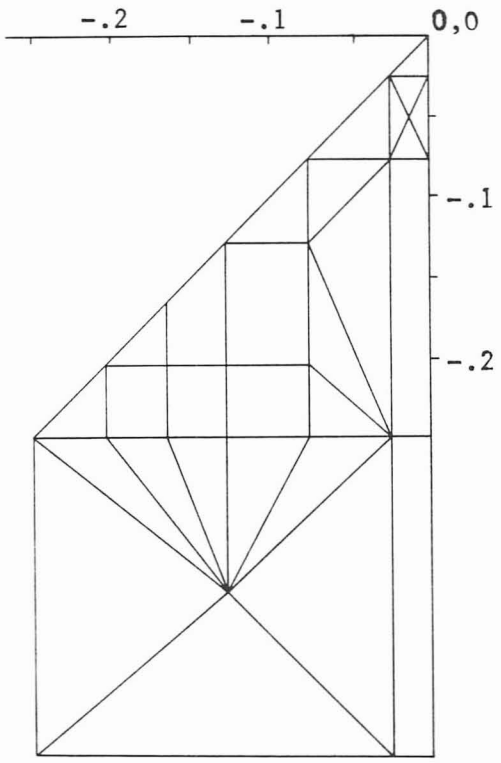

Figure 5.37

Part of Grid for Model IID-2, Pe = 1000.
(The rest is shown in fig. 5.16)

if a continuous slug (model IID-1) was considered these elments would not have been needed.

Figure 5.38 shows the solution along the diagnoal and y = 0 at different times. The front is steepest at early times but the MCS enables accurate solutions because the elements are concentrated in the frontal region. At 0.5 PV the solution is compared to the results of Young (1978) and Settari et al. (1976) in Fig. 5.39. The oscillations especially behind the slug is nearly eliminated with MCS and the slug is better approximated as evident from Fig. 5.40 where

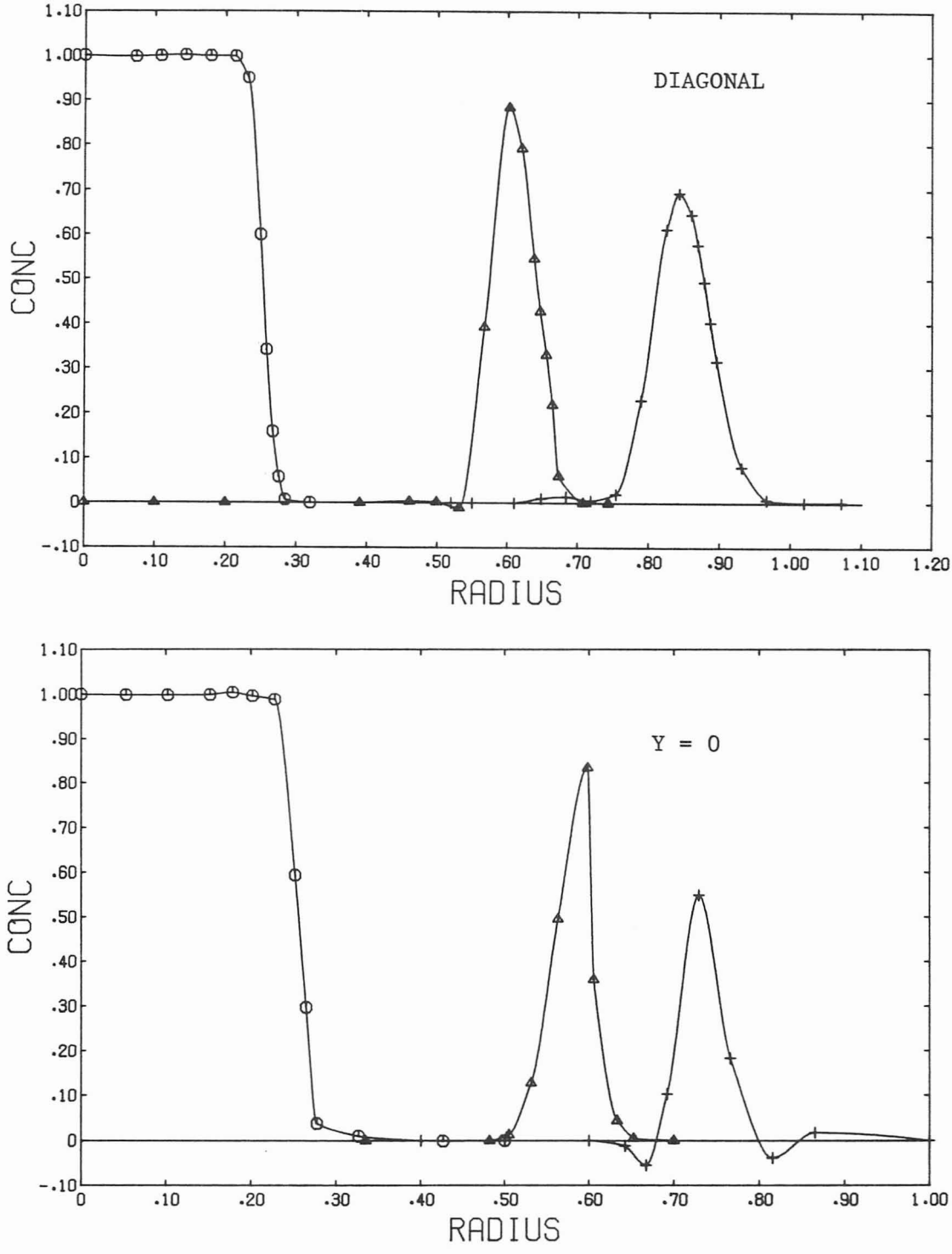

Figure 5.38

Model IID-2, Pe = 1000, Solution Along the Diagonal and y = 0 at 0.05, 0.3 and 0.5 PV Injected

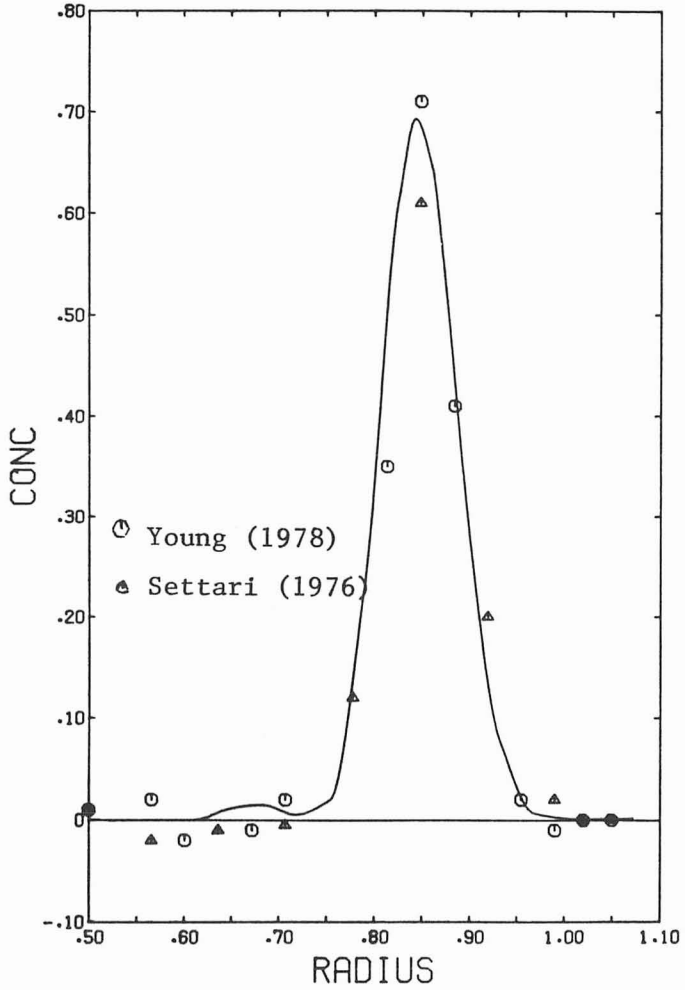

Figure 5.39

Model IID-2, Pe = 1000, Solution at 0.5 PV
Comparisons to Young (1978) and Settari *et al.* (1977)

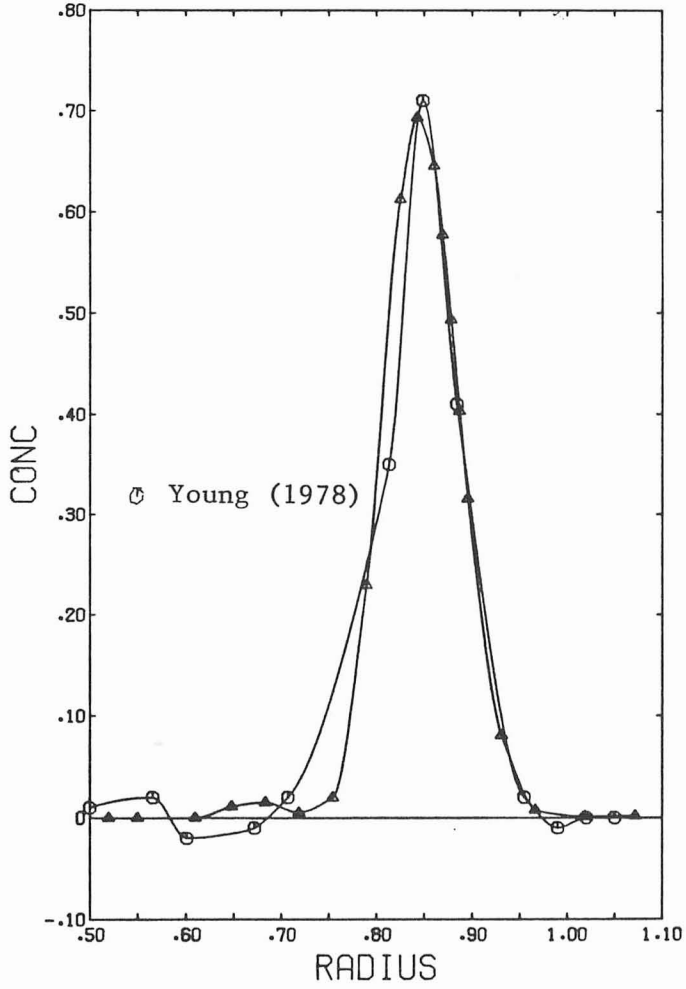

Figure 5.40

Model IID-2, Pe = 1000, at 0.5 PV
Comparison to Young (1978)

the solution by Young (1978) is drawn too. The contours at different pore volumes are shown in Fig. 5.41. Note that the slug length thins more at the boundaries of the pattern than along the diagonal, which is an effect of the divergent flow pattern. This results also in a higher peak concentration being maintained along the diagonal. This phenomenon is important in the design of chemical flooding processes which must maintain a critical maximum of concentration to give high area sweep efficiency.

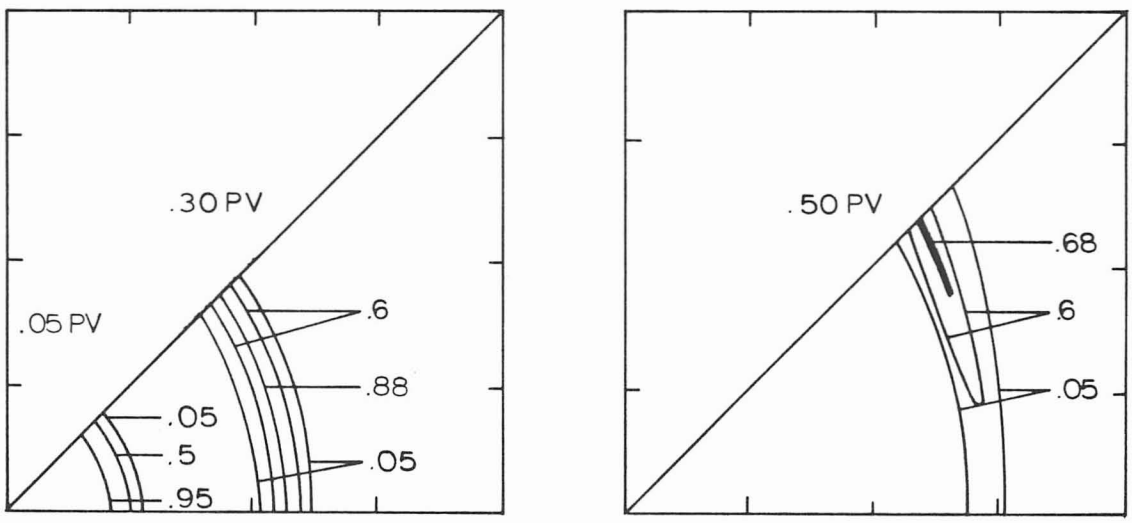

Figure 5.41

Model IID-2, Pe = 1000, 0.05 PV Slug, Contours

The solution was only computed to 0.5 PV because the variable timestep scheme described in 5.3-4 did not decrease the timesteps adequately. The flow pattern is divergent towards the production well and the frontal velocity will increase as the slug moves towards

this well. Reductions in the timesteps are therefore necessary as the solutions will change more rapidly compared to the initial period. The timestep algorithm works well when the Δt is being increased, but it does not work well when Δt is being decreased.

5.4.5 Computational Efficiency

In the preceeding sections, results of using the developed program were presented. In the following section the efficiency of the program and comparisons to other methods are discussed.

In Table 5.4 is listed the distribution of computation time among different parts of the program. The main portion of time is spent on calculating matrix-entries by quadrature and solution of algebraic equations. Using a renumbering scheme during the integration and a sparse matrix solver would achieve savings compared to the frontal solver. The total execution time is mostly dependent on the number of nodes and timesteps used. CONDIF uses per timestep

$$\text{CPU-time} = 4.0\ (\text{NT})^{1.4}\ \text{msecs/timestep, CDC 6400} \qquad (5.47)$$

where NT is the total number of nodes.

We compare the efficiency of the developed program to two studies: Settari et al. (1976) and Young (1978) using a fixed coordinate system (FCS). Both of these studies consider mathematical models where the velocities are either known (only parabolic equation, linear problem) or calculated as part of the problem (elliptic and parabolic equation, nonlinear problem). The latter case arises when the velo-

Table 5.4

Distribution of Computation Time

	% of Total CPU-Time
Data input tape writing, input from tape	4
Calculation of matrix entries	43
Tape reading	4
Inversion of matrix	45
Miscellaneous	4
	100%

cities depend on the concentration and is discussed in detail in Chapter VI. For the linear problem it is only necessary to evaluate the coefficients once in FCS; for the nonlinear problem this must be done in each timestep. Using MCS the savings for the linear problem can not be achieved because the velocities must be recomputed at different locations in each timestep. This means that if the same number of elements and timesteps are used in FCS and MCS, MCS would take more computer time by a factor of about 2 (Table 5.4). MCS depends on using fewer elements and fewer timesteps to achieve its improvement (for this linear problem with a known velocity).

The basis for the comparison is solving a model IID-2 injecting 0.05 PV slug with a Peclet number of 1000 and injecting a total of

1.0 pore volume. We compare in the two cases mentioned above:

I : Velocities known (Formula 5.8). Only parabolic equation solved.

II : Miscible displacement model (Chapter VI), where an elliptic equation is solved to obtain the velocities together with the parabolic equation.

The data available is listed in Table 5.5. We develop comparisons based on reasonable extrapolations of these data. Young (1978) compares the cost of using his scheme to the method of Settari et al. on the same computer and to get the best comparison we therefore use the data from Young for the method of Settari et al. The execution time used on the University of Washington computer CDC 6400 is approximately 5 times slower than the computer IBM 370/168.

We assume for both case I and II that using a 10×10 grid with cubic elements and 1100 timesteps in FCS give same accuracy as a MCS solution using an average of 80 quadratic (linear) elements and 226 timesteps. The accuracy of the three methods is compared at 0.5 PV for case I in Section 5.4-4. The solution obtained with MCS was computed only to 0.5 PV so we estimate conservatively that the double number of timesteps is necessary to 1.0 PV. For case II Young uses the same number of elements and timesteps as for case I, to obtain solutions (i.e., same difficulty in solving Case II as Case I), so we assume that MCS uses the same number of elements and timesteps for case II as used for Case I. Additional assumptions and extrapola-

Table 5.5

Data for the Comparison, Different Studies

	Young	Settari *et al.*	MCS
Galerkin formulation	10 x 10 element grid Lagrange, cubic	10 x 10 element grid Hermite,cubic	average 80 elements Serendipity, quadratic
Quadrature	Lobatto	Gaussian	Gaussian
Solution method	Time split scheme (iterative)	Direct solution	Direct solution (frontal solver)
Integration scheme	2nd order Runge-Kutta	2nd order Runge-Kutta	Crank-Nicholson
Number of timesteps to	1100 steps to 1.0 PV	1100 steps to 1.0 PV	113 to 0.5 PV
Case I CPU secs/node/Δt	0.07 msecs		35 msecs (formula 5.47)
Case II CPU secs/node/Δt	1 msecs	21.0 msecs	
Total exec. time Case I Case II	70 secs 1100 secs		805 secs
Computer	IBM 370/168	IBM 370/168	CDC 6400

tions necessary for the comparison are given in the following under each comparison.

Table 5.6 compares the execution time per node and timestep at the number of nodes given in Table 5.5; the details for the estimates are given in the figure. The iterative solution technique is about 100 times faster for case I and about 10 times for case II. In the latter case the matrix is recomputed in each timestep and more iterations are necessary, because it is a nonlinear problem. Settari et al. and CONDIF both use a direct solution technique so approximately the same execution time is expected. As seen in Table 5.6 they compare closely despite possible differences in programming efficiency. This indicates also that a reasonable conversion factor is used.

The number of elements and timesteps used in FCS and MCS are very different so comparing the total execution time is more appropriate. Tables 5.7 and 5.8 list the execution time for the two cases.

Taking case I first, two estimates are given. Using CONDIF an estimate of the total execution time is given for solving in FCS with a direct solution technique assuming the same number of elements and timesteps as Young (1978). By combining MCS and iterative solution technique we assume the same number of elements and timesteps as MCS-direct solve, but use the execution time per node and timestep given by Young. The FCS-iterative scheme is comparable with MCS using a direct solver. Both schemes are over a factor 60 faster

Table 5.6

Computation Time Per Node and Timestep, Different Methods
(CPU-time on IBM 370/168, msecs/node/timestep)

Scheme	Case I: Parabolic Eqn.	Case II: Elliptic/Parabolic Eqn.
Direct Solution		
Settari et al.		21
this study	7* (12)*	10** (19)
Iterative solution		
Young, L.	0.07	1.0

* CONDIF uses 36 msecs/Δt/node for 80 elements or 255 nodes (formula 5.45) on CDC 6400. Converting between CDC 6400 and IBM 370/168 gives 7 msecs. In brackets same estimate but with 931 nodes and subtracting 30% for unnecessary setup costs.

** CONDIF uses 36 msecs/Δt/nodes (at 255 nodes, MCS). Solving for velocities take $\sim$50% CPU-time more per timestep. Same conversion factor used. In brackets the same estimate but with C°-cubic, 10 x 10 grid (961 nodes). CONDIF uses 62 msecs/Δt/nodes so (62 + 31)/5 = 19 msecs/Δt/node.

Table 5.7

Comparison of Total Execution Time to 1.0 PV Injected,
Case I (CPU-times on IBM 370/168)

Scheme	Fixed Coordinate System	Moving Coordinate System
(secs)	10 x 10 grid, 921 unknown and 1100 timesteps	Average 80 elements, 255 nodes, 230 timesteps
Direct Solution		
this study C° quadratic	-----	310*
this study C° cubic	12,300**	-----
Iterative Solution		
L. Young	70	2***

* Actual CPU-time used were 810 to 0.5 PV. Assuming the double number of timestep is necessary gives 1620 secs, and converting to IBM 370/168 gives 310 secs.

** Estimated from Table 5.6. 12 msecs×961×1100 = 12300 secs.

*** Estimated using L. Young's execution time. 0.07 msecs×200×150 = 2 secs.

Table 5.8

Comparison of Total Execution Time to 1.0 PV Injected,
Case II (CPU-times on IBM 370/168)

Scheme	Fixed Coordinate System	Moving Coordinate System
(secs)	10 x 10 grid 1100 timesteps	200 nodes average 150 timesteps
Direct Solution		
Settari et al. (C'-cubic)	21800*	-----
This study MCS C° quadrature	-----	470**
Iterative Solution		
L. Young	880.0	30***

* From Table 5.5. We have 21 msecs×948×1100 = 21800 secs.

** Extrapolated time (Table 5.7) was 320 secs. Adding 50% for solving for velocities give 470 secs.

*** Estimate based on Young's CPU-time per node and timestep. We have 1 msecs×200 x 150 = 30 secs.

than FCS-direct solver. The estimate for MCS-iterative scheme indicates that a major reduction can be achieved by such a combination.

With case II where the velocities are unknown the comparison is more correct, because all the methods must recompute the coefficient matrix in each timestep. Solving case II with MCS requires about 50% more computation time than case I as found in Chapter VI. An estimate of using MCS-iterative solver is given again based on the execution time used by Young (Table 5.6). MCS-direct solver is again comparable in cost to FCS-iterative solver with MCS being slightly faster. Comparing to FCS-direct solver both schemes are over 40 times faster.

For higher Peclet numbers the developed program is much more efficient than any FCS-scheme. For a Peclet number 10 times higher, the costs are estimated when the velocity is determined by the program. For MCS we estimate conservatively upward and for FCS downward (see Table 5.9). For MCS an additional 100 elements (on the average) is assumed to cover the sharp front region and also a doubling of the number of timesteps. Only at start and at breakthrough more timesteps are needed as the front otherwise will have a fairly fixed position in MCS. For FCS the number of elements are estimated from Settari et al. so that in this case 10,000 elements are needed. Also a linear dependence of execution time per node is assumed (exponent 1 in Eq. 5.47). For injecting one pore volume the execution times required are listed in Table 5.9. Over a factor 10 is gained by using MCS-

Table 5.9

Estimates of Computation Times For Pe = 10,000

Scheme	Fixed Coordinate System	Moving Coordinate System
	100 x 100 grid* 1100 timesteps	400 nodes (average) 300 timesteps
Direct solver	∿20,000,000 secs**	8,000 secs***
Iterative solver	90,000 secs**	120 secs ****

* Following Settari et al. a 100 x 100 grid gives "acceptable" accuracy for this Peclet number.

** Entry in Table 5.7, multiplied by 100.

*** Using formula 5.47 gives 18 secs/timesteps, adding 50% for velocity solution and with 300 timestep a total of 8,000 secs is obtained.

**** From Table 5.5: 1 msecs×400×300 = 120 secs.

direct solver rather than FCS-iterative solver. Combining MCS with iterative solver the reduction is even larger.

5.5 Conclusions

Application of a moving coordinate system to two-dimensional parabolic equations is feasible. Sharp fronts with unknown velocity can be tracked. For high Peclet numbers the location of the boundary conditions must be specified exactly, otherwise unstable solutions result. The variable timestep scheme increased the timesteps by a factor 500 during the integration and thus gave a major reduction in

the number of timesteps. The timesteps could not be adequately decreased with the variable timestep scheme for high Peclet numbers. Triangles are preferable where the solutions must be carefully resolved while quadrilaterals are preferable elsewhere.

With radial flow from one well, the solutions were comparable with an exact solution. The sharpness in the solutions is affected by the form of the dispersion tensor. With a molecular diffusion dyadic and a certain Peclet number the sharpness in the solution compares with solutions using a dispersion dyadic proportional to the velocity and a Peclet number ten times higher. A substantial reduction in the number of elements and timesteps is achieved compared to schemes using a fixed coordinate system.

For a five spot flow pattern the solutions can be analyzed in accuracy with an integrated mass balance. Near the stagnation point, more elements are necessary to get accurate solutions than the criteria in Chapter II dictates. For a test problem with a Peclet number of 1000 the MCS is 50 times faster than schemes with a fixed coordinate system (FCS) if both schemes use a direct solution technique. MCS is comparable in cost to FCS with an iterative solution technique. If both MCS and FCS schemes use an iterative solution technique, MCS would be 10-20 times faster than FCS. For more difficult problems, MCS would achieve even larger reductions in the computation time.

The goal set in Chapter I of achieving reduction in the computation time by at least one order of magnitude compared to current industry standard (Settari et al., 1976) is reached with the moving

coordinate system. The cost comparison was based on projections and the moving coordinate system is 50 times faster than the oil industry's program and comparable with the study by Young (1978). For very high Peclet numbers and/or more cost efficient matrix setup and solver the projected reductions for using the moving coordinate system is even larger.

Chapter VI

MISCIBLE DISPLACEMENT

6.1 Introduction

For all the enhanced oil recovery processes the flow of several components in often more than two phases must be modelled accurately. The mathematical models consist of several coupled nonlinear parabolic and elliptic equations. It is therefore important to show that the moving coordinate system can be applied to such a coupled system of equations.

The mathematical model discussed in this chapter describes the flow of two miscible components in a porous media. Miscible displacement and migration of non-ionic tracers can be calculated assuming equal density of both components. The viscosity of the components can be different and small adsorption rates can be accounted for. As the flow field depends on the viscosity, the pressure field must be calculated in combination with the component mass balance. The model consists of one elliptic equation (for the determination of pressure) and one parabolic equation (for the determination of component concentration).

When a fluid displaces an in-situ fluid with a higher viscosity, hydrodynamic instability (fingering) can occur. Laboratory experiments [Haberman, 1962; Mahaffey, 1966; Claridge, 1972] have analyzed the influence of fingering on recovery efficiency, but the results are very scattered. Several statistical theories [Scheidegger, 1970]

have been made to quantify theoretically the fingering. Deterministic models can only be used when fingering already has been initiated. Dispersion stabilizes the hydrodynamic instability. The fingering occurs as a function of the ratio between the viscosity of the displacing and the in-situ fluid and the dispersion level. Numerical simulation of the process can determine for which parameters fingering occur.

Peacemann (1962), Settari (1976) and Young (1978) solved the same mathematical model as is discussed here. For cases where fingering can occur these studies do not agree. For general treatment of fingering a stochastic approach must be used as the phenomenon is random.

The mathematical formulation of a two component system in a porous medium is described in Section 6.2 together with the necessary assumptions. Typical values for the physical parameters are given. The solution method for the moving coordinate system applied to both elliptic and parabolic equations is discussed in Section 6.3. Comparison of analytical and calculated pressure fields is shown in Section 6.4 and some preliminary results of calculating miscible displacement given.

6.2 Mathematical Model

6.2-1 Continuity Equation

For a two component system where both fluids are miscible only one phase exists, so that the conservation of total mass is [Pinder et al., 1978]

$$\phi h(x,y) \frac{\partial \rho}{\partial t} + \nabla \cdot (h \rho \vec{u}) = 0 \qquad (6.1)$$

where ϕ is the porosity (L^3/L^3)

$h(x,y)$ formation thickness (L)

ρ the density, in general is a function of the concentration of component (M/L^3)

$\vec{u}$ linear velocity (L/T)

The Navie-Stoke's equation can not be used to describe the flow field in a porous media because of the complicated geometry. The semi-imperical Darcy's law [Darcy, 1856] is used, which is supported by experimental evidence [Scheidegger, 1960]

$$\vec{u} = -\frac{k}{\mu} (\nabla p - \rho g \nabla Z) \qquad (6.2)$$

where

k is the permeability (resistence to flow)

μ is the viscosity, in general a function of the component concentration

Z the formation depth relative to surface (+Z direction upward)

Darcy's law represents a linear relationship between the velocity $\vec{u}$ (L/T) and the gradient of the pressure (or head). Experiments suggest [Ergun, 1952] that the relation is only linear for small velocities $|\vec{u}|$ and quadratic for larger $|\vec{u}|$ or

$$|\nabla p| = K_1 \cdot |\vec{u}| + K_2 |\vec{u}|^2 \qquad (6.3)$$

Equation (6.3) has been used successfully in calculation of pressure drop in chemical reactor design; for two-dimensional flow patterns Eq. (6.3) may not be valid [Scheidegger, 1962].

In the following Darcy's law will be used, since the linear velocities are small and Eq. (6.2) is valid [Scheidegger, 1960].

Combining (6.1) and (6.2) gives

$$\phi h \cdot \frac{\partial \rho}{\partial t} + \nabla \cdot \left(\frac{k \rho h}{\mu} \cdot (\nabla p - \rho g \nabla Z) \right) = 0 \tag{6.4}$$

or by using

$$\frac{d\rho}{dt} = \frac{d\rho}{dp} \frac{dp}{dt} \tag{6.5}$$

we obtain

$$\phi h \frac{d\rho}{dp} \cdot \frac{dp}{dt} + \nabla \cdot \left(\frac{k \rho h}{\mu} \cdot (\nabla p - pg \nabla Z) \right) = 0 \quad .$$

For miscible displacement when gas flow is not considered

$$\frac{d\rho}{dp} \simeq 0$$

the final equation is

$$\nabla \cdot (\rho h \vec{u}) = 0 \quad \text{or} \quad \nabla \cdot \left((kh) \frac{\rho}{\mu} (\nabla p - \rho g \nabla Z) \right) = 0 \tag{6.6}$$

In (6.6) k, ρ is constant, h, Z can be a function over the area and the viscosity is a function of the component concentration. The viscosity function is discussed in 6.2-3 and typical numbers are given in 6.2-4.

The boundary condition associated with (6.6) is for the five spot flow pattern (Fig. 5.1) as described in Chapter V.

$$\vec{u} \cdot \vec{n} = 0 \qquad \text{(no flow across the boundary)} \tag{6.7}$$

and at well locations

$$-2\pi r_w \cdot [\vec{n} \cdot (\rho u)] = q_w \cdot \rho^* \tag{6.8}$$

where

r_w : well radius

ρ^* : density of injected or produced fluid at surface conditions

q_w : volumetric flow rate measured at surface conditions. (q positive if injection and negative if production)

Equation (6.8) specifies the amount of material injected or produced.

6.2-2 Component Equations

Both for miscible displacement of oil with an alcohol or slug injection of polymer, two components are encountered. In the following a two component system is therefore discussed.

Mass conservation of the components can either be given by mass fractions or densities

$$\begin{aligned} w_1 + w_2 &= 1 \\ \rho_1 + \rho_2 &= \rho \end{aligned} \tag{6.9}$$

Mass densities are

$$\rho_i = w_i \rho \tag{6.10}$$

and the mass flux of component i

$$\vec{n}_i = \rho_i \vec{u}_i \qquad \text{and} \qquad \vec{n}_1 + \vec{n}_2 = \rho \vec{u} \tag{6.11}$$

so the mass average velocity is given by

$$\vec{u} = w_1 \vec{u}_1 + w_2 \vec{u}_2 \tag{6.12}$$

The diffusion (or dispersion) is modelled as a result of the difference between the mass average velocity and the component velocity

$$\vec{j}_i = \rho_i (\vec{u}_i - \vec{u}) = -\rho \cdot \underline{\underline{K}} \cdot \nabla u_i \tag{6.13}$$

where $\underline{\underline{K}}$ is the diffusion tensor (detailed discussion in 6.3-3).

The conversation of each of the components

$$\begin{aligned} \phi h \frac{\partial \rho_1}{\partial t} + \nabla \cdot (h \cdot \vec{n}_1) &= r_1 \\ \phi h \frac{\partial \rho_2}{\partial t} + \nabla \cdot (h \cdot \vec{n}_2) &= r_2 \end{aligned} \tag{6.14}$$

where r_1, r_2 is the production rate (or adsorption rate). The total mass balance is obtained by adding the two component balances in (6.14); Eq. (6.9) or (6.6) is obtained with the requirement that

$$r_1 + r_2 = 0 \tag{6.15}$$

We assume that both the adsorption and desorption rates are significant small so the overall mass balance is not affected ($r_1 \approx 0$, $r_2 \approx 0$).

The adsorption is modelled by

$$r_i = -h(1 - \phi)\rho_r \frac{\partial \Theta_1}{\partial t} \tag{6.16}$$

Further discussion of how r_1 is approximated is done in Section 6.2-3. Only one component mass balance is needed along with the total mass balance (6.9); the second component can be obtained by difference. Reducing (6.14) by (6.11) and (6.13) we have

$$\phi h \frac{\partial \rho_1}{\partial t} + \nabla \cdot h \rho_1 \vec{u} = \nabla \cdot (h \rho \underline{\underline{K}} \nabla w_1) + r_1 \tag{6.17}$$

As we assume the density of both components is the same, the density in (6.17) can be divided out and the form of (6.17) is then in volume fractions

$$\phi h \frac{\partial c}{\partial t} + \nabla \cdot (h \vec{u} c) = \nabla \cdot (h \underline{\underline{K}} \nabla c) + r_1 \tag{6.18}$$

The convective term can be reduced by (6.6)

$$\nabla \cdot (h \vec{u} c) = c \cdot \nabla \cdot (h \vec{u}) + \vec{u} h \cdot \nabla c$$

so (6.18) becomes

$$\phi h \frac{\partial c}{\partial t} + \vec{u} h \cdot \nabla c = \nabla \cdot (h \underline{\underline{K}} \nabla c) + r_1 \tag{6.19}$$

Along all sides of the triangle (shown in Fig. 5.1) the overall mass balance satisfies (6.7) ($\vec{u} \cdot \vec{n} = 0$) or that no material flows across the boundary. This must also be satisfied for each of the components so the boundary condition for Eq. (6.19) is

$$\vec{n} \cdot \underline{\underline{K}} \cdot \nabla c = 0 \qquad \text{(no dispersive flux across boundary)} \tag{6.20}$$

At a well location we have

$$-2\pi r_w \cdot [h \vec{n} \cdot \underline{\underline{K}} \cdot \nabla c] = q\ (c^{\circ}_{well} - c_{well}) \tag{6.21}$$

This equation says that the convective and dispersive flux must equal the injected (produced) amount. At producing wells $c^{\circ}_{well} = c_{well}$ and (6.21) simplifies to (6.20).

6.2-3 Functional Relations

In this section various topics from 6.2-1 and 6.2-2 are discussed.

A diffusion tensor is usually associated with the intrinsic motion of fluid molecules due to their thermal agitation [Bird et al., 1960]. Dispersion is a mechanical effect due to the interconnections of the flow channels in a porous medium. So even though they show up phenomenologically in a similar fashion, they are due to entirely different physical causes. The dispersion depends therefore on the direction and magnitude of the fluid velocity

$$K_{ij} = D_M + \alpha\ |\vec{u}|^{\beta}$$

The longitudinal and transverse dispersion coefficient can be measured experimentally [Scheidegger, 1960]

$$\begin{aligned} K_{long} &= D_M + \alpha_L \frac{|\vec{u}|}{\phi} \\ K_{trans} &= D_M + \alpha_T \frac{|\vec{u}|}{\phi} \end{aligned} \tag{6.22}$$

and α_L, α_T determined. An example of dispersion coefficients is given in Fig. 6.1. In two dimensions the dyadic product

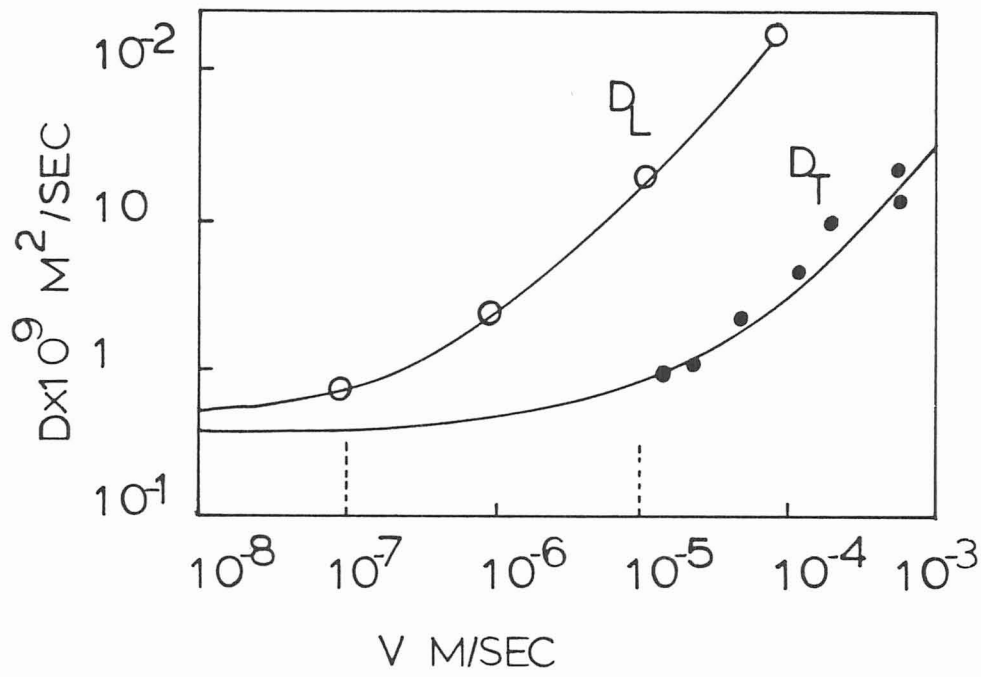

Figure 6.1

Dispersion as a Function of the Velocity
(taken from Scheidegger (1960) p. 305 [Berea sandstone])

$$\underline{\underline{K}}(\vec{u}) = \delta_i \, \delta_j \, D_M + \frac{\alpha_L}{\phi}\left(\frac{\vec{u}}{|\vec{u}|}\,\vec{u}\right) + \frac{\alpha_T}{\phi}\left(\frac{\hat{u}}{|\vec{u}|}\,\hat{u}\right) \tag{6.23}$$

will form a tensor $\underline{\underline{K}}$. Equation (6.23) is given in a coordinate system following the flow field, we need to transform (6.23) into the cartesian coordinate system. Referring to Fig. 6.2

$$\vec{u} = u_x\vec{i} + u_y\vec{j}\,, \quad \hat{u} = u_y\vec{i} - u_x\vec{j}$$

and

$$\underline{\underline{K}}(\vec{u}) = \delta_i \, \delta_j \, D_M + \frac{\alpha_L}{\phi}\,(\vec{u}\,\vec{I}) + \frac{\alpha_T}{\phi}\,(\hat{u}\,\vec{t})$$

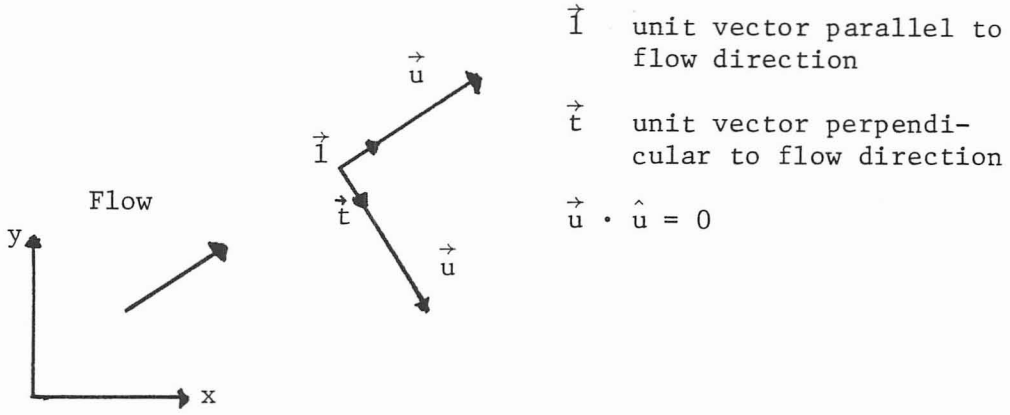

Figure 6.2

Dispersion Tensor

we get

$$(\vec{u}\,\vec{l}) = \frac{1}{|\vec{u}|}\begin{pmatrix} u_x^2 & u_x u_y \\ u_x u_y & u_y^2 \end{pmatrix}$$

$$(\hat{u}\,\vec{t}) = \frac{1}{|\vec{u}|}\begin{pmatrix} u_y^2 & -u_x u_y \\ -u_x u_y & u_x^2 \end{pmatrix}$$

and substituting into (6.23) the dispersion tensor in cartesian coordinates becomes

$$\underline{\underline{K}} = \delta_i \, \delta_j \, D_M + \frac{1}{\phi} \begin{bmatrix} \alpha_L \frac{u_x^2}{|u|} + \alpha_T \frac{u_y^2}{|u|} & (\alpha_L - \alpha_T) \frac{u_x u_y}{|u|} \\ (\alpha_L - \alpha_T) \frac{u_x u_y}{|u|} & \alpha_T \frac{u_x^2}{|u|} + \alpha_L \frac{u_y^2}{|u|} \end{bmatrix} \tag{6.24}$$

Scheidegger (1960) and Peaceman (1966) obtain (6.24) too, but in a more formal mathematical way. Typical values of α_L, α_T and D_M are given in Table 6.1.

The adsorption rate as defined by (6.16) is difficult to measure during a displacement process, but the amount of material adsorbed can more readily be obtained. Experiments [Lake, et al., 1977] have shown that for most components the adsorption rate is much faster than the mass flow. By assuming a Langmuir kinetic model (monomolecular adsorption)

$$\frac{\partial \Theta_1}{\partial t} = K_1 \left[1 - \frac{\Theta_1}{\Theta^*} \right] - K_2 \frac{\Theta_1}{\Theta_1^*} \tag{6.25}$$

and that the adsorption rate is so fast that equilibrium prevails, Eq. (6.25) can be solved to give the instantaneous concentration on the rock surface

$$\Theta_1 = \frac{ac}{1 + bc} \tag{6.26}$$

where

$$a = (K_1/K_2)\Theta_1^* \quad , \qquad b = K_1/K_2 \tag{6.27}$$

Table 6.1

Typical Values, Flooding Technique

Parameter	Typical Value	Reference
Density of oil	$\sim$900 kg/ m^3	Haynes, 1976
Viscosity oil in place	1-200 cP	---
Viscosity fluid displacing	1-2000 cP	---
Viscosity function (a)	4	Settari, 1976; Young, 1978
Five spot area*	2-910 x 10^4 m^2	Haynes
Permeability	20-2500 md	---
Porosity	0.15-0.40	Scheidegger, 1974
Rock type (preferable)	sandstone	Haynes
Mixing length ($\alpha_L \sim 8\alpha_T$)	0.03-0.15 m 0.002 m	Settari et al. Perkins and Johnston 1963, sandstone
Molecular diffusion coefficient	$\sim 7.10^{-10}$ m^2/sec	Perkin et al., 1963
Injection rates	<320 m^3/day	Haynes, 1976
Well diameter	0.15 m	Settari, Young
Formation depth	200-1800 m	Haynes, 1976

Table 6.1 (Continued)

Parameter	Typical Value	Reference
Fluid velocity**	10^{-7} - 10^{-5} m/s	Scheidegger, Fig. 54
Peclet number		
$= \langle \frac{u \cdot L}{K} \rangle$	6×10^{4} - 6×10^{6}	
$= \langle \frac{L}{\alpha} \rangle$	26 - 1.3×10^{4}	Settari, et al.
	2×10^{5}	Perkins and Johnston

* Pattern size $3 \cdot 10^{5}$ m^2 production well recommended for enhanced oil recovery processes by Haynes (1976), L = 390 m along diagonal between production and injection wells

** Measured in middle of five spot.

Other adsorption isotherms [Smith, 1970] could be studied but are not considered in this work. The effect of adsorption on the frontal steepness is to increase the steepness as material is drawn away from the flowing fluid.

The alcohol or polymer which is displacing the oil well for most cases have a different viscosity than the in-situ oil. As the phases are soluble the viscosity for any concentration level must be known. Bird et al. (1960) discuss various mixing formulations here the empirical correlation

$$\mu(c) = \frac{\mu_1 \mu_2}{\left[\left((1-c)\mu_1\right)^{1/a} + \left(c\mu_2\right)^{1/a}\right]^a} \tag{6.28}$$

found in the petroleum literature [Settari, Young] is used. Typical numbers for μ_1, μ_2 and a are given in Table 6.1.

If the displacing fluid has a lower viscosity than the in-situ oil a flow instability is present, which will cause fingering of the displacing fluid into the oil rich part of the domain [Scheidegger, 1960; Settari, 1976]. The mobility ratio is defined as

$$Mo = \frac{\mu_{\text{in-situ fluid}}}{\mu_{\text{displacing fluid}}} \tag{6.29}$$

and instabilities (fingering) occur depending on the mobility ratio ($Mo > 1$) and the level of dispersion [Scheidegger, 1960].

For a mobility ratio of one and no adsorption the model is identical with the model treated in Chapter V.

6.2-4 Summary

The mathematical model consists of two coupled equations. An elliptic equation determines the pressure field

$$\rho \cdot \nabla \cdot (h \vec{u}) = 0 \quad \text{or} \quad k\rho \cdot \nabla \cdot \left[\frac{h}{\mu} (\nabla p - \rho g \nabla Z)\right] = 0 \tag{6.6}$$

where

ρ,k is constant

h,Z can be a function of the spatial coordinates

μ the viscosity function given by (6.28)

For the five spot flow pattern the boundary condition over all sides is

$$\vec{u} \cdot \vec{n} = 0 \tag{6.7}$$

and at well locations

$$-2\pi r_w \cdot [h (\vec{n} \rho \vec{u})] = \rho^* \cdot q \tag{6.8}$$

The parabolic equation for determination of the component concentration (when (6.26) is substituted into (6.19)), is

$$h\left[\phi \frac{\partial c}{\partial t} + \frac{(1-\phi)\rho_r}{\rho} \cdot \frac{\partial \Theta_1}{\partial c} \frac{\partial c}{\partial t}\right] + \vec{u}\, h \nabla c = \nabla \cdot (h \underline{\underline{K}} \nabla c). \tag{6.30}$$

$\underline{\underline{K}}$ is defined in (6.24).

The boundary condition on all sides is

$$\vec{n} \cdot \underline{\underline{K}} \cdot \nabla c = 0 \qquad \text{(no dispersive flux out)}$$

and at the injection well

$$-2\pi r_w \ (h \ \vec{n} \underline{\underline{K}} \nabla c) = q \ (c^{\circ}_{well} - c_{well}) \quad .$$

In Table 6.1 is given a list of typical physical parameters for an oil reservoir, which could be treated by a flooding technique.

The equations must be solved for very large Peclet numbers as seen from Table 6.1. The case of Pe = 1000 is therefore only a minimum of what can be expected in an actual field study.

The assumptions used for the described model are:

1) Darcy's law
2) Liquid two component system density same for both fluids)
3) Anisotropic dispersion tensor ($K_{ij} = K_{ji}$)
4) Amount of adsorpt material negligible compared to total mass in system
5) Adsorption rate so fast that instantaneous equilibrium prevails.

6.3 Solution Method

The solution scheme for the component equation given in 6.2-4 is very similar to that described in 5.3. Both the parabolic and elliptic problem are solved in MCS. Emphasis is here given on solution of the elliptic problem (6.6). A sequential method, where the two equations are solved in a step by step manner, is used in contrast to a simultaneous scheme, where the two equations are solved at the same time.

6.3-1 Galerkin Formulation and Integral Approximation

The equations are solved with a Galerkin finite element method. The Galerkin formulation is

$$\int_A \left(\frac{kh}{\mu} \nabla\delta p \cdot (\nabla p - \rho g \nabla Z)\right) dA - \int_S \delta p[q_1] dS = 0 \qquad (6.31)$$

where δ_p is the weighting function. To obtain the Euler equation we integrate by parts

$$\nabla \cdot \left(\delta p \frac{kh}{\mu} \nabla p\right) = \delta p \cdot \nabla \cdot \left(\frac{kh}{\mu} \nabla p\right) + \frac{kh}{\mu} \nabla\delta p \nabla p$$

and apply the divergence theorem:

$$\int_V \nabla \cdot \left(\delta p \frac{kh}{\mu} \nabla p\right) dV = \int_S \vec{n} \left(\delta p \cdot \frac{kh}{\mu} \nabla p\right) dS$$

Equation (6.31) can now be written as

$$\int_A \delta p \left[\nabla \cdot \left(\frac{kh}{\mu} (\nabla p - \rho g \nabla Z)\right)\right] dA$$

$$+ \int_S \delta p \left(\vec{n} \frac{kh}{\mu} (\nabla p - \rho g \nabla Z) - q_1\right) dS = 0$$

As this is true for arbitrary δp, the Euler equation is

$$\nabla \cdot \left(\frac{kh}{\mu} (\nabla p - \rho g \nabla Z)\right) = 0 \qquad (6.32)$$

and the natural boundary condition becomes

$$\vec{n} \cdot \left(\frac{kh}{\mu} (\nabla p - \rho g \nabla Z)\right) = \vec{n} \cdot \vec{u} = q_1$$

$$\left(q_1 = \frac{q_w}{2\pi r_w}\right) . \qquad (6.33)$$

where q_1 is the specified flux on the boundary. If we do not specify any boundary condition the natural boundary condition is

$$\vec{n} \cdot \vec{u} = 0$$

Introducing the moving coordinate system does not effect any of the above equations as the pressure field is calculated instantaneously. The coordinate x,y however transforms to ξ, ρ as in Section 5.3-1.

The pressure is approximated by a linear trial function (denoted by * to distinguish from quadratic)

$$\delta p = N_j^* \qquad p = \sum N_I^* \, p_I \quad . \tag{6.34}$$

In matrix form the Eq. (6.31) is now

$$\underline{\underline{A}} \, \underline{p} = \underline{b}^1 + \underline{b}^2 \tag{6.35}$$

where

$$a_{IJ} = \int_A \left(\frac{kh}{\mu}\right) \cdot \left(\frac{dN_J^*}{d\xi} \frac{dN_I^*}{d\xi} + \frac{dN_I^*}{d\rho} \frac{dN_I^*}{d\rho}\right) dA \tag{6.36}$$

$$b_J^{\,1} = \int_S \mathbf{N_J^*} \cdot q_1 \, dS \tag{6.37}$$

$$b_J^{\,2} = -\int_A \left(\frac{kh}{\mu}\right) \cdot \left(\frac{dN_I^*}{d\xi} \left(-\rho g \frac{dZ}{d\xi}\right) + \frac{dN_J^*}{d\rho} \cdot \left(-\rho g \frac{dZ}{d\rho}\right)\right) dA \tag{6.38}$$

In 6.3-2 a modified Galerkin formulation of the pressure equation is presented.

Approximation of the integrals in (6.36) through (6.38) is examined on page 193.

For the component equation (6.30) the Galerkin formulation is

$$\int_V \left[\phi h g(c) \frac{\partial c}{\partial t} \delta c + h \, \delta c \, \vec{u} \cdot \nabla c + h \, \nabla \delta c \cdot \underline{\underline{K}} \cdot \nabla c \right] dV -$$

$$\int_S \delta c [q_w (c - c^\circ_{well})] dS = 0 \qquad (6.39)$$

Verification of Euler and natural boundary conditions is similar to Section 5.3-2. The adsorption term (the function g(c)) makes no difference in the derivations. The Euler equation is

$$\phi h g(c) \frac{\partial c}{\partial t} + \underline{u} \cdot \nabla c - \nabla \cdot (\underline{\underline{K}} \nabla c) = 0 \qquad (6.40)$$

and the natural boundary condition becomes

$$\vec{n} \, \underline{\underline{K}} \, \nabla c - q_w (c - c^\circ_{well}) = 0 \qquad (5.14)$$

We apply the moving coordinate in a similar fashion as done for Eq. (5.10). Equation (6.30) becomes

$$\phi h g(c) \frac{\partial c}{\partial \eta} + \left[u_x h - \phi h g(c) \lambda_x(\eta) \right] \frac{\partial c}{\partial \xi} +$$

$$\left[u_y h - \phi h g(c) \lambda_y(\eta) \right] \frac{\partial c}{\partial \rho} = \frac{\partial}{\partial \xi} \left[h \, K_{\xi\xi} \frac{\partial c}{\partial \xi} \right] +$$

$$\frac{\partial}{\partial \xi} \left[h \, K_{\xi\rho} \frac{\partial c}{\partial \rho} \right] \div \frac{\partial}{\partial \rho} \left[h \, K_{\rho\xi} \frac{\partial c}{\partial \xi} \right] + \frac{\partial}{\partial \rho} \left[h \, K_{\rho\rho} \frac{\partial c}{\partial \rho} \right] \qquad (6.41)$$

The concentration is approximated by the same quadratic elements as in Chapter V.

$$c = \sum N_I \, c_I \qquad \delta c = N_J \quad . \tag{6.42}$$

Equation (6.39) is then in matrix form

$$\underline{\underline{M}} \frac{d\underline{c}}{dt} = (\underline{\underline{C}} + \underline{\underline{D}}) + \underline{b}^c \tag{6.43}$$

The coefficients in (6.43) are

$$m_{IJ} = \int_A \phi h \, g(c) \, N_I \, N_J \, dA \tag{6.44}$$

$$c_{IJ} = \int_A \left(\left(u_x h - \phi h g(c) \lambda_x(\eta) \right) N_J \frac{dN_I}{d\xi} + \left(u_y h - \phi h g(c) \lambda_x(\eta) \right) N_J \frac{dN_I}{d\xi} \right) dA \tag{6.45}$$

$$d_{IJ} = \int_A \left((hK_{\xi\xi}) \frac{dN_J}{d\xi} \frac{dN_I}{d\xi} + (hK_{\xi\rho}) \frac{dN_J}{d\xi} \frac{dN_I}{d\rho} + (hK_{\rho\xi}) \frac{dN_J}{d\rho} \frac{dN_I}{d\xi} + (hK_{\rho\rho}) \frac{dN_J}{d\rho} \frac{dN_I}{d\rho} \right) dA + \int_{\text{wells}} N_J \cdot (q_w \, N_I)/(2\pi r_w) dS \tag{6.46}$$

$$b_J^c = \int_{\text{wells}} N_J \, (q_w \, c^\circ_{\text{well}})/(2\pi r_w) dS \tag{6.47}$$

Only essential type boundary conditions are applied at the wells (concentration as function of time).

When the nonlinear effects are included the integrals in (6.36) through (6.38) and (6.44) through (6.46) are computed by quadrature similar to Section 5.3-3. For example (6.44) is calculated by

$$\int_A \phi h g(c) N_I \, dA \simeq \phi \sum_{IG=1}^{N_{gauss}} h^{IG}(\xi_{GP}, \rho_{GP}) \cdot g^{IG}(c_{GP}) \cdot N_I^{IG}(\xi_{GP}, \rho_{GP}) \cdot N_J^{IG}(\xi_{GP}, \rho_{GP}) \cdot w_i \cdot da_i \qquad (6.48)$$

GP : Gauss point

and

$$c_{GP} \simeq \sum_{IG=1}^{N_{gauss}} N_I^{IG}(\xi_{GP}, \rho_{GP}) \cdot c_I$$

If we had used

$$[g(c)]^{GP} = \sum_{IG=1}^{N_{gauss}} g^{IG}(c_I) \cdot N_I^{IG}(\xi_{GP}, \rho_{GP})$$

artificial dispersion is introduced, as described by Finlayson and Nelson (1977).

6.3-2 Modifications to Pressure Approximation

The conventional method for solving the elliptic problem (6.6) is described in 6.3-1. The well is approximated by a source or sink

because the ratio of the well radius to the element sides is less than 10^{-3}. The numerical solutions close to the well are, however, not very good (see Section 6.4-1), since the singularity at the well location can not be satisfactorily approximated. Peaceman (1978) Spivak et al. (1976), Chappelear (1979) describe methods for correcting the pressures near the wells. They propose to use the analytical solution in the vicinity of the wells either by specifying the analytical solution there, or by adding a correction to the numerical determined pressure.

When applying MCS the domain changes in which the pressure distribution is solved for (5.3-1). The wells are therefore not always located at nodes, since the grid is not kept fixed. Two methods are examined in this study for approximating the pressures accurately in MCS.

The first approach is similar to the method by Chappelear (1979) and Peaceman (1978). In the well element the pressures are specified with

$$p = \frac{q\mu}{2\pi r_w kh} \ln \left[(x - x_w)^2 + (y - y_w)^2 \right] \qquad (6.49)$$

which is the exact solution for radial flow given in (5.2) also. For a nonlinear problem (6.49) is only exact in the vicinity of the well. The Neuman boundary condition is thereby changed to an essential boundary condition.

In the second approach we incorporate an analytical function into the trial function

$$p = f(\xi, p) + \sum N_I^* P_I \quad . \tag{6.50}$$

The function f is the analytical solution to the linear problem in a five spot as given in Eq. (5.3). We are then solving for the difference (corrections) between this function and the solution to (6.6) and are not concerned with the unbounded behavior near the well. For a mobility ratio of one the corrections should in fact be zero. Hayes et al. (1977) used the same idea as described above except they only applied the analytical function in the well element. Using the function over the whole domain rather than only in the vicinity of the well should be better for a mobility ratio of one, because the function is the exact solution everywhere in the domain. For a mobility ratio different from one the difference between the two approaches might not be very large.

By introducing f in (6.50) the final matrix equations change. Substituting (6.50) into (6.31) with the same weighting function we get in the matrix form

$$\underline{\underline{A}}\ \underline{p} = \underline{b}^1 + \underline{b}^2 + \underline{\underline{b}}^3 \tag{6.51}$$

where a_{IJ}, b_J^1, b_J^2 are defined by (6.36) through (6.38). The extra term is

$$b_J^3 = -\int_A \left(\frac{kh}{\mu} \frac{dN_I^*}{d\xi} \frac{df}{d\xi} + \frac{dN_J^*}{d\rho} \frac{df}{d\rho} \right) dA \qquad (6.52)$$

which only effects the right hand side.

The boundary conditions are not affected by this alteration. As the function f gives the correct injection rate and is exact only at the well locations we can choose to specify the pressure zero there, which says that the correction is zero at that point. If the Neumann boundary condition is used at the wells the pressure must be specified zero elsewhere at one node. In MCS we can specify the corrections to be zero in the well elements to avoid specifying the flux boundary condition. The choices of how to specify the boundary condition is not trivial, and the various possibilities will affect the result. Further discussion is done in 6.4-1. Hayes et al. (1977) applied Neumann boundary conditions only and refined mesh close to the well was necessary for obtaining accurate pressures.

6.3-3 Temporal Integration Scheme

The same schemes as described in 5.3-4 will be used again, except that the corrector must be modified to account for the nonlinear terms. Referring to (6.43)

$$\underline{\underline{M}}^{n+1/2,s} \frac{\underline{c}^{n+1,s+1} - \underline{c}^{n,s}}{\Delta t} = \frac{1}{2} \left(\underline{\underline{C}}^n \underline{c}^n + \underline{\underline{D}}^n \underline{c}^n \right)$$

$$+ \frac{1}{2} \left(\underline{\underline{C}}^{n+1,s} + \underline{\underline{D}}^{n+1,s} \right) \underline{c}^{n+1,s+1} + \underline{b}^c \qquad (6.53)$$

is a second order corrector, if iterations are performed to proper convergence (see below). Three forms of (6.49) are examined.

1) $\underline{\underline{M}}^{n+1/2} \rightarrow \underline{\underline{M}}^{n}$, $\underline{\underline{C}}^{n+1} \rightarrow \underline{\underline{C}}^{n}$, $\underline{\underline{D}}^{n+1} \rightarrow \underline{\underline{D}}^{n}$

1 iteration

2) $\underline{\underline{M}}^{n+1/2} \rightarrow \underline{\underline{M}}^{p}$, $\underline{\underline{C}}^{n+1} \rightarrow \underline{\underline{C}}^{p}$, $\underline{\underline{D}}^{n+1} \rightarrow \underline{\underline{D}}^{p}$

the predictor (subscripted p) from Eq. (5.27) used as initial guess at t^{n+1}. Only one iteration performed.

3) Same as 2) but iteration done to convergence.

Only alternative 3) is a second order method. Equation (6.53) represents a successive substitution iteration procedure; by using a Newton-Raphson faster convergence can be achieved.

Proof of (6.53) being a second order method is given below. Starting from

$$g(c)\,\frac{dc}{dt} = f(c)$$

and applying the integration scheme

$$g^{n+1/2}(c)\,\frac{c^{n+1} - c^{n}}{\Delta t} = \frac{1}{2}\left[f^{n+1}(c) + f^{n}(c)\right] + O(\Delta t^{2}) \qquad (6.50)$$

Expanding the functions in (6.50) at t^{n}

$$c^{n+1} = c + c^{1}\,\Delta t + c^{11}\,\Delta t^{2}/2$$

$$f^{n+1} = f + f^{1}\,\Delta t + f^{11}\,\Delta t^{2}/2 \qquad (6.51)$$

$$g^{n+1/2} = g + g^{1}\,\Delta t/2 + g^{11}\,\Delta t^{2}/8$$

and substituting into Eq. (6.50) we get

$$[g + g^{1}\,\Delta t/2 + g^{11}\,\Delta t^{2}/8][c^{1} + c^{11}\,\Delta t/2] =$$

$$f + f^{1}\,\Delta t/2 + f^{11}\,\Delta t^{2}/4$$

Reducing we get

$$(gc^{1} - f) + \Delta t/2 \cdot \frac{d}{dt}(gc^{1} - f)$$

$$+ \Delta t^{2}/4[c^{1}\,g^{11}/2 + c^{11}\,g^{1} + c^{111}\,g - f^{11}]$$

$$+ \text{higher order terms} = 0$$

or that

$$g\,\frac{dc}{dt} = f + \Delta t^{2}/4\,[g^{1}\,c^{11}/2 + c^{11}\,g^{1} + c^{111}\,g - f^{11}]$$

$$= f + 0(\Delta t^{2})$$

so (6.49) is a second integration scheme.

6.4 Results

6.4-1 Pressure Equation—One Well

Solution of the pressure equation (6.35) are examined for flow from one well. The formulation described in 6.3-1 is used. Four different mesh configurations were used and are shown in Fig. 6.3. For simplicity all physical parameters are set to unity

$$k = h = \phi = \mu = q_1 = 1 \quad .$$

One essential type boundary condition is necessary for solving the elliptic equation with a Neuman boundary condition. The location of the essential boundary condition (reference pressure) affects the numerical results. In Fig. 6.4 is shown the pressures and velocity components by specifying the reference pressure in different locations (A, B in Fig. 6.4 refers to Fig. 6.3). Since the trial functions vary linearly the velocities are piecewise constant as illustrated in Fig. 6.4b. Even though the mesh is very coarse, the velocities in the middle of the domain are close to the exact values. In the region where the pressure is specified to zero the solution is not physical (increasing velocity). Using mesh C and corner C to specify the reference pressure gives the best solution except near corner C. The pressure specification must be done at infinity to obtain good solutions. If only a small part of the physical domain is considered, errors are introduced.

Solving for the flow from one well must be done in a sufficient large domain, which renders the effect of truncating on infinite domain. By insulating the location of reference pressure specification

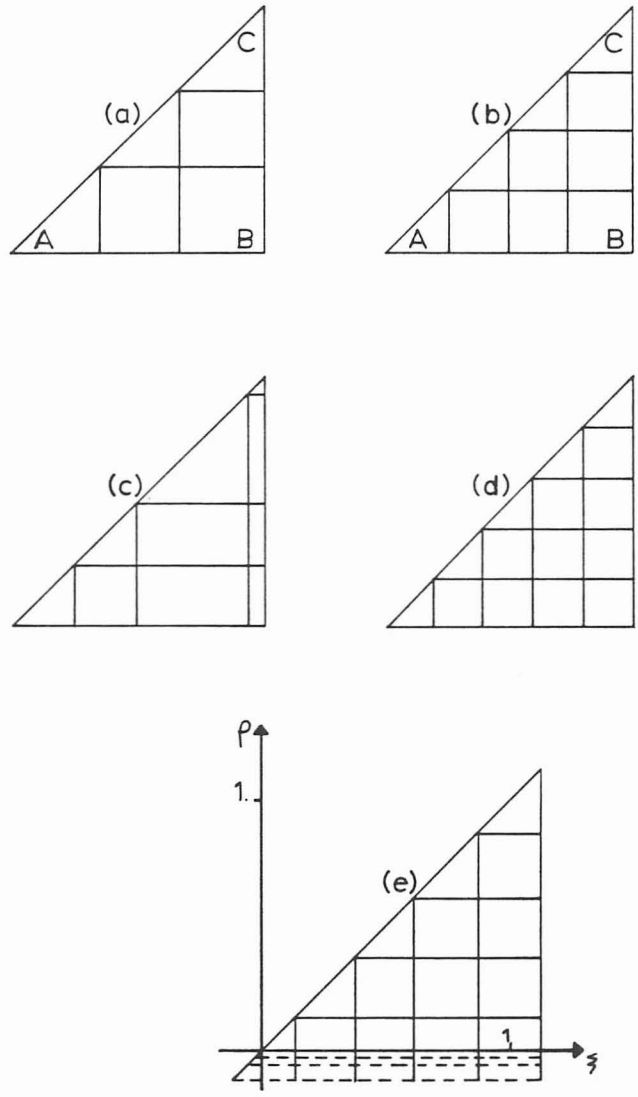

Figure 6.3

Mesh for Pressure Solutions

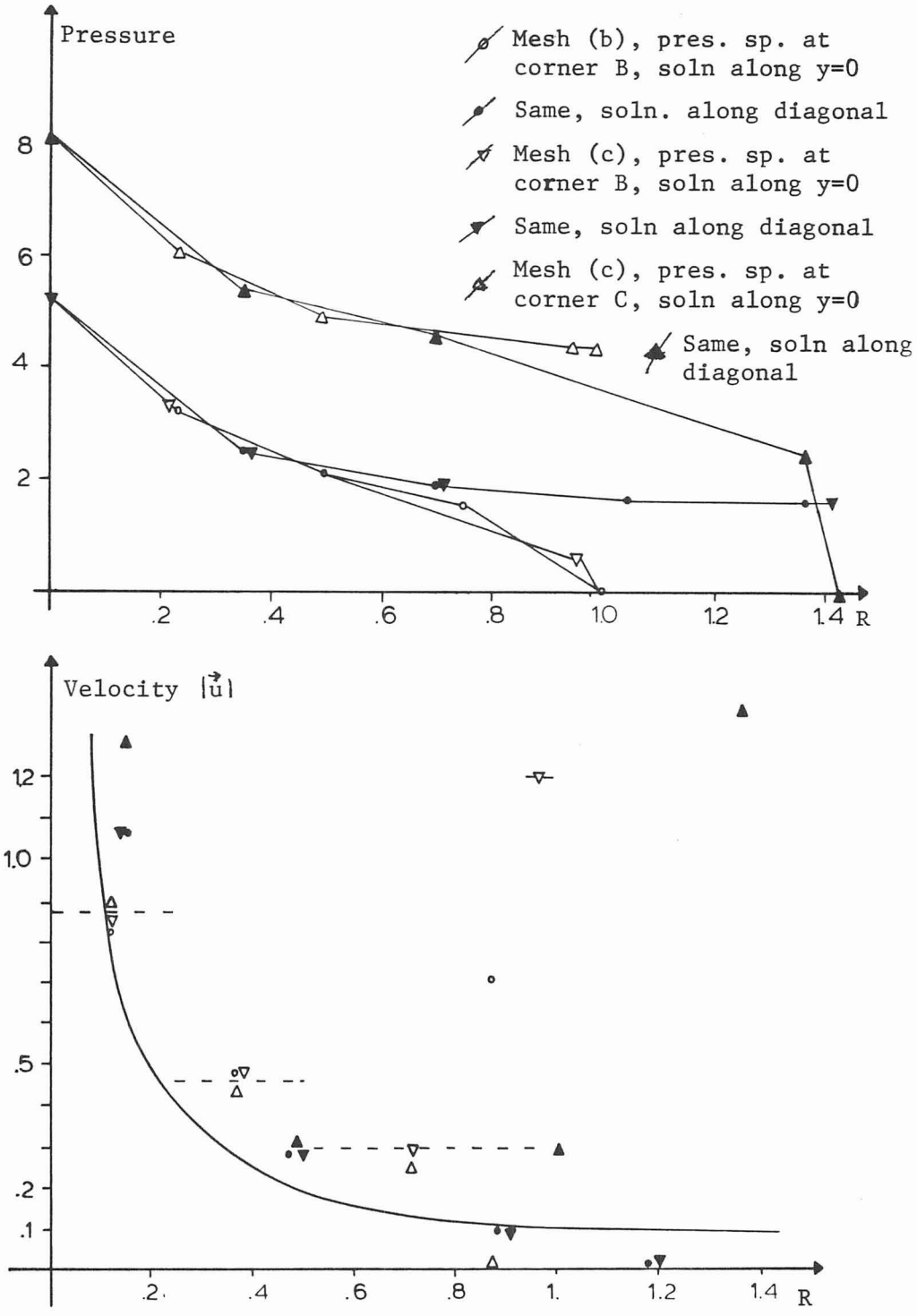

Figure 6.4

Solution to Elliptic Equation, Radial Flow,
Pressures and Velocities

furthest away from the well, the best results are obtained. For a five spot flow pattern this problem does not occur because the flow field is contained within an area.

6.4-2 Pressure Equation — Five Spot

Results of using various numerical approaches to solve the pressure equation are examined. The exact solution for five spot flow is given in Section 5.2. The following possibilities are examined:

I: Flux boundary condition (standard formulation as described in 6.3-1). Source and sink are placed at node locations and the reference pressure specified at the stagnation point.

II: Fixed boundary condition near well using the analytical solution for radial flow (formulation described in 6.3-2).

III: Incorporating analytical solution into the trial function (formulation described in 6.3-2).

We use the meshes from Fig. 6.3 again and for simplicity all the physical parameters are set to unity as in 6.4-1.

The first approach (I) is applicable for solutions in the fixed coordinate system. The pressure solution is shown in Fig. 6.5. The pressure at the well should achieve an infinite value and close to the well the solution is not very good. The velocity components are shown in Fig. 6.6 and in the center of the domain they are reasonable close to the exact solution. In the moving coordinate system the well changes location so using this approach would give

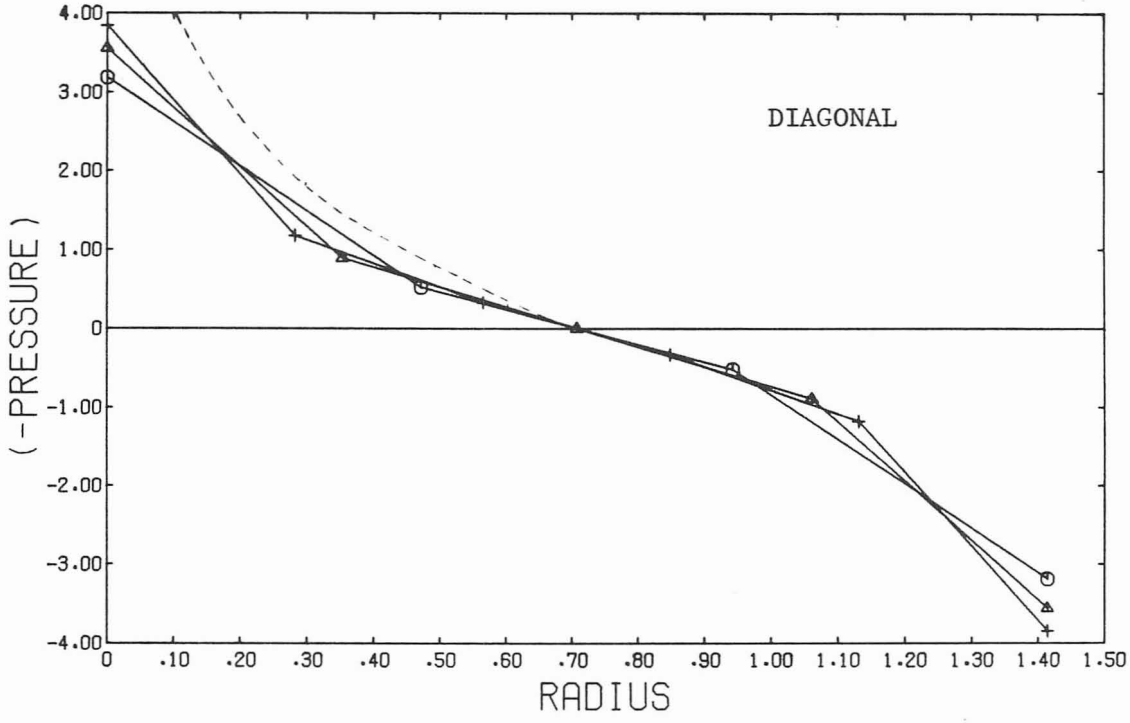

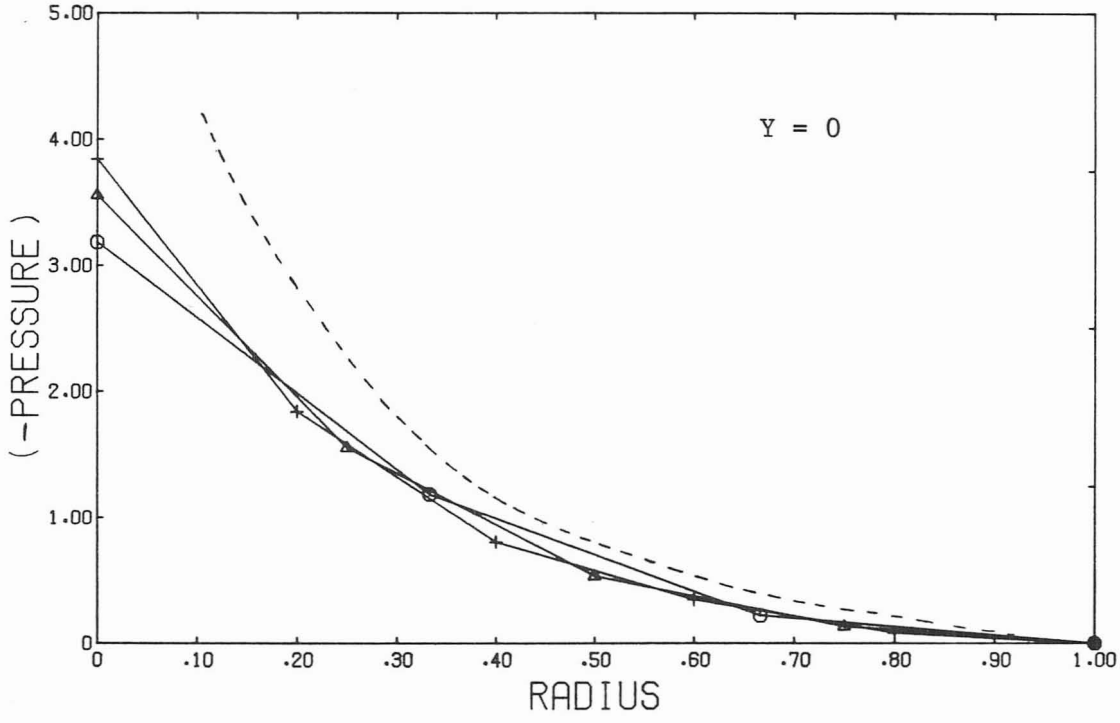

Figure 6.5

Solution to Pressure Equation, Five Spot Well, Pattern, Diagonal
(+ mesh (a), Δ mesh (b), ⭘ mesh (a), --- exact)

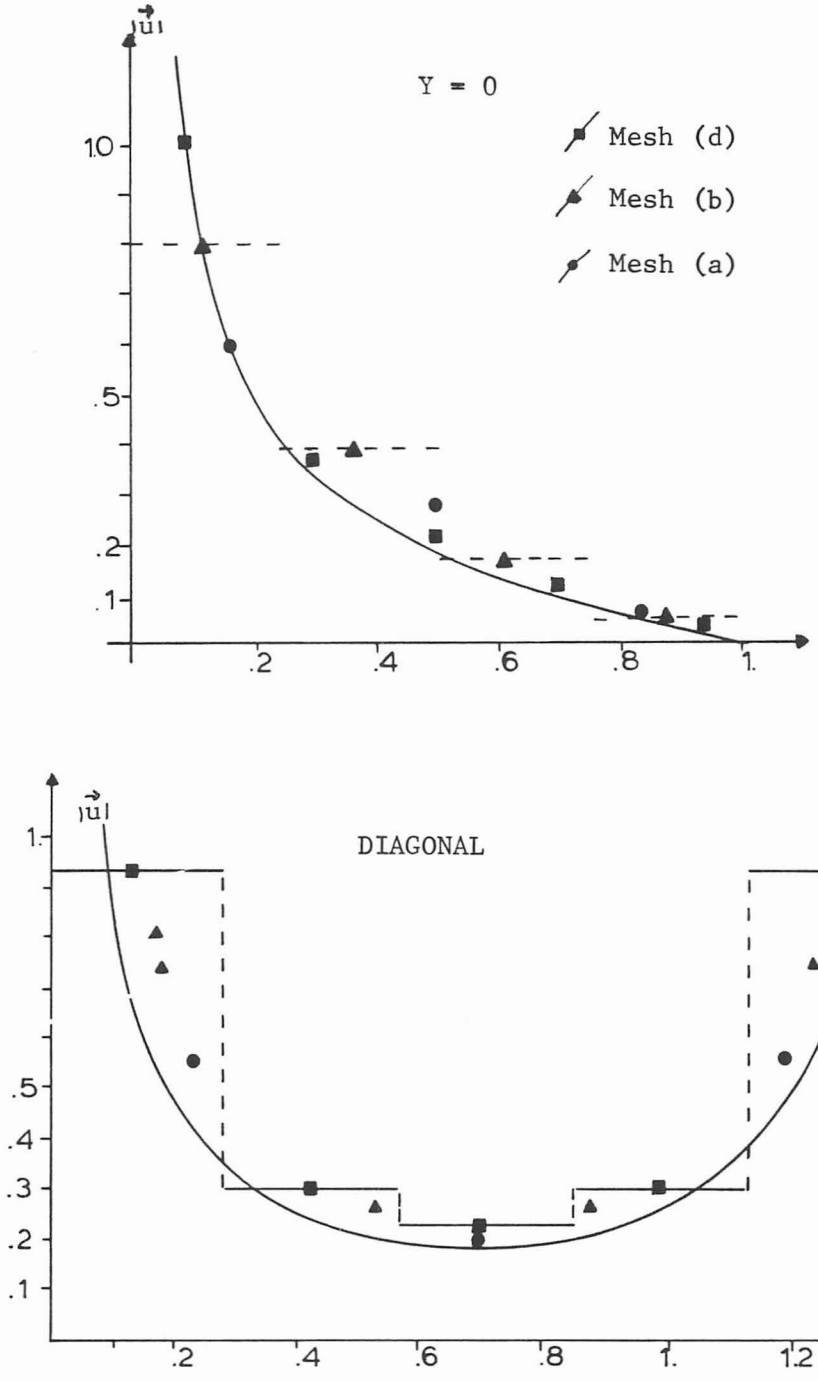

Figure 6.6

Velocities Along y = 0 and Diagonal in Five Spot

very shifting velocities because the well would have to move in jumps between nodes.

With the second approach (II) the pressures at nodes in the element where the well is located has the exact value. Solutions are examined with mesh (e), Fig. 6.3 and varying the south boundary. The pressure solution is shown in Fig. 6.7. In the middle of the domain the slope of the solution is reasonably close to the others obtained (Fig. 6.6) but near the wells, the velocity will vary from zero to a high value depending on the location of the south boundary. If more elements were considered the same phenomenon would also happen near the well. The conclusion is that approach II can not be used for MCS-calculations, because of the variations near the well.

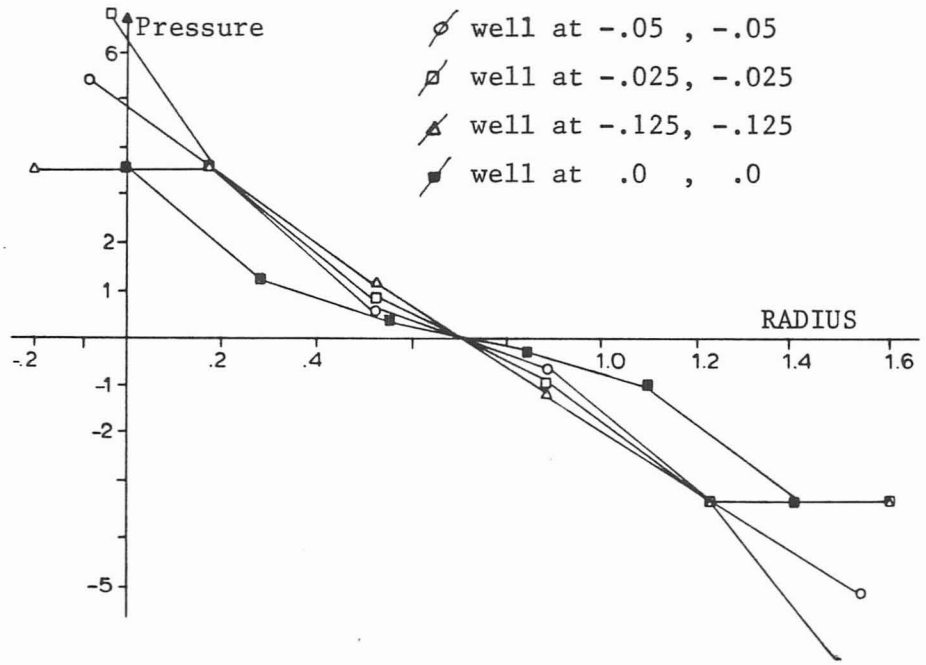

Figure 6.7

Solution to Pressure Equation, Five Spot, Along Diagonal

Incorporating the exact solution (III) in the trial function gave much better results. The results are given as the difference between the exact solution and numerically obtained, so we define the correction pressure by

$$P_{correction} = P_{numerical} - P_{exact}$$

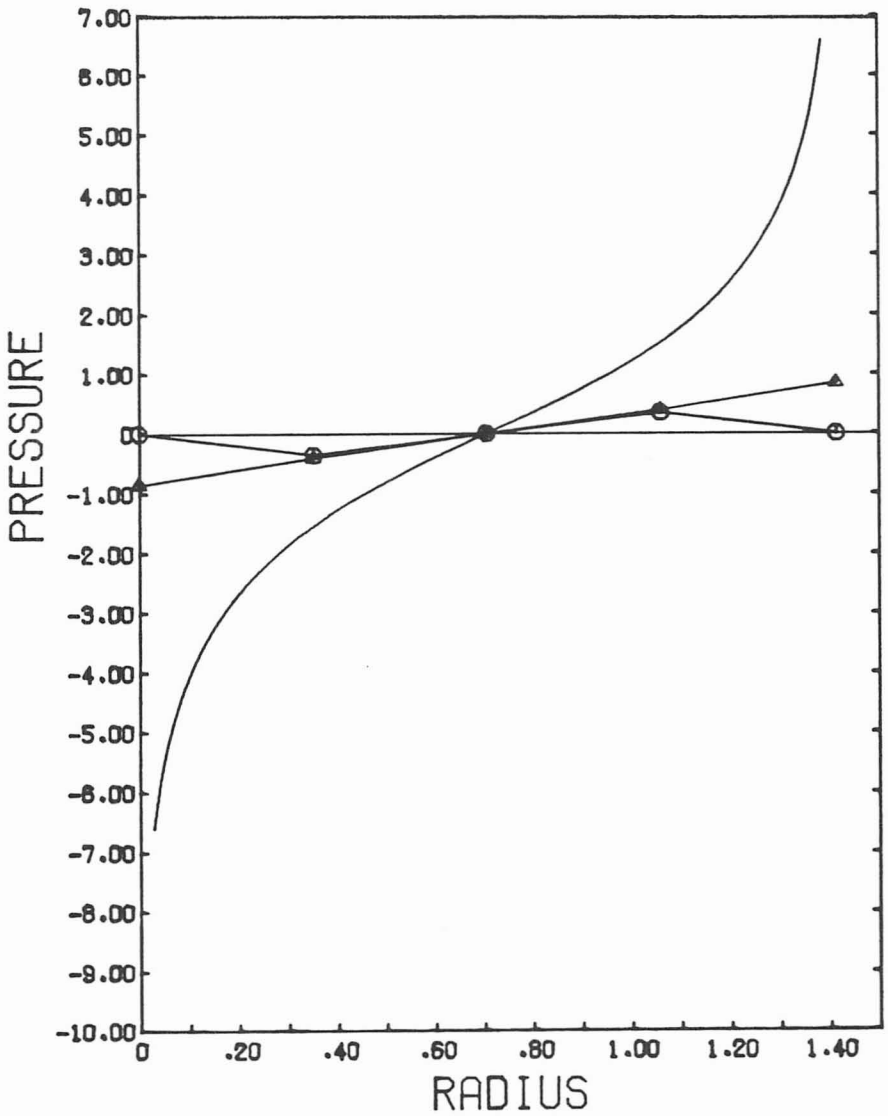

Figure 6.8

Solution to Pressure Equation, -- exact,
△ Correction (A), ○ Correction (B)

Mesh (b) in Fig. 6.3 is used in these calculations. In Fig. 6.8 is shown the correction pressure for two possibilities of specifying the boundary conditions. Using the Neuman boundary condition at the well and setting the reference pressure to zero at the stagnation point (possibility A) much larger corrections are seen than by specifying the correction pressure to zero at the wells (possibility B). The velocities are also more accurate as seen in Fig. 6.12 by specifying zero correction pressure. In both cases however only small corrections are seen.

As mentioned earlier in Section 6.3-2 the corrections should be zero in both cases because we substitute in the analytical solution. If the integrals in (6.52) were calculated exactly instead of by a quadrature the corrections would indeed be zero. Especially near the well error is introduced because the integrals in this region are not well determined as the derivative of the function goes to an infinite value. This problem is nearly avoided by specifying the correction pressure to zero at the well (or close to in MCS), as we then do not have to compute integrals near the well. As seen in Fig. 6.9 the velocities for possibility B are within a few percent of the exact value. Comparing these results to the solution of Hayes et al. (1977) the corrections obtained by incorporating the analytical function everywhere in the domain is smaller than by only using the analytical behavior in the well element. Hayes et al. used the Neuman boundary condition at the well which affects the accuracy as discussed above.

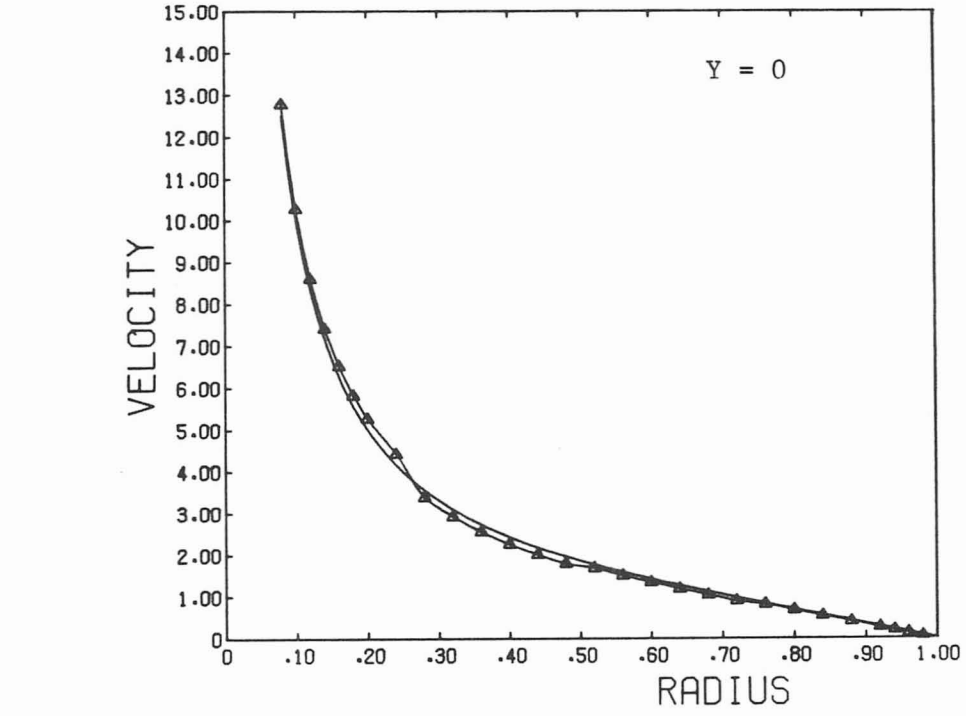

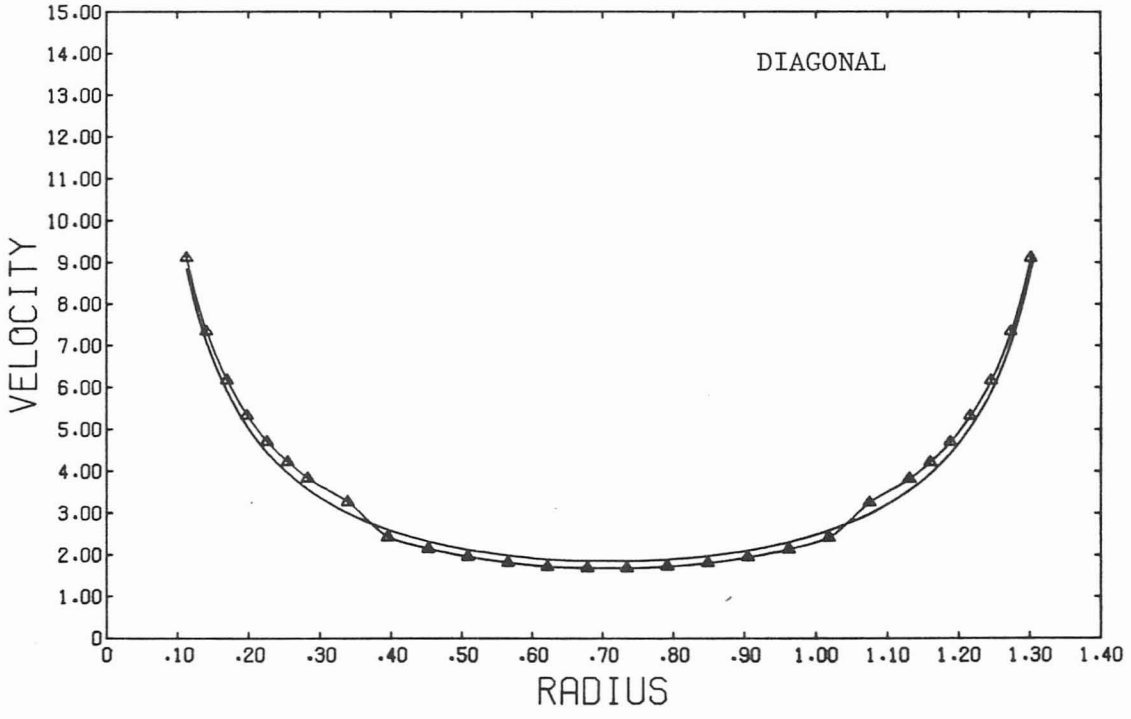

Figure 6.9

Velocity Along Diagonal and y = 0 Incorporating Analytical Solutions -- exact, ∆ numerical determined (possibility B)

With the third possibility (III) of solving the pressure equation accurate pressure and velocity solutions can be obtained even with linear trial functions. For the miscible displacement model where the viscosity varies MCS enables us to have the most elements where the viscosity changes rapidly. The same advantage as was achieved for parabolic equation is therefore also obtained for the elliptic equation.

6.4-3 Adverse Mobility Ratio

For a mobility ratio of one the miscible displacement model discussed in this chapter is identical with the model considered in Chapter V. When the mobility ratio is different from one the elliptic and parabolic equation is coupled as the visosity depends on the concentration. In this section a solution with an adverse mobility ratio (i.e., the viscosity of the in situ fluid is higher than the injected fluid) is examined.

For a mobility ratio of ten (Eq. 6.29) and a Peclet number of 72.5 a solution was obtained using a fixed coordinate system. The pressure equation was solved with the approach described in Section 6.3-2 (Possibility IIIB, Section 6.4-2) where the viscosity of the injected fluid is used in the analytical function (6.49) at all places in the domain. The integration scheme number 2) (Section 6.3-3) was used together with the variable timestep scheme. The physical parameters used are given in Table 6.3 and for simplicity most of the

Table 6.2

Physical Parameter for Solution of M = 10, Pe = 72.5

$k = 1\ m^2$ $\quad \phi = 1$ $\quad r_w = 1\ m$ $\quad Z = h = 1\ m$
$\rho = 10^3 kg/m^3$
$L = 1\ m$
$Q_w = 455.32\ m^3/s = Q_{injected} = -Q_{produced}$
$D_M = 0$ $\quad \alpha_L = \alpha_T = 0.01379$
$\mu_{in\ situ} = 10\ cp$ $\}$ $M = 10$
$\mu_{injected} = 1\ cp$
$a = 4$ (formula 6.28)
$Pe_1 = \frac{L}{\alpha} = 72.5$
$M = 10$

values are set equal to one. Twenty-one (21) elements in the triangular domain (Fig. 5.1) were used and a total of 27 timesteps were necessary for injecting 1.2 pore volume.

The concentration contours of the injected fluid are shown in Fig. 6.10 and the velocities are different injected pore volumes in Fig. 6.11. A decrease in the velocity is observed downstream of the frontal position because the fluid here has a higher viscosity. The velocity of the fluid increases towards the production well in order to conserve mass (i.e., the same production as injection rate). The

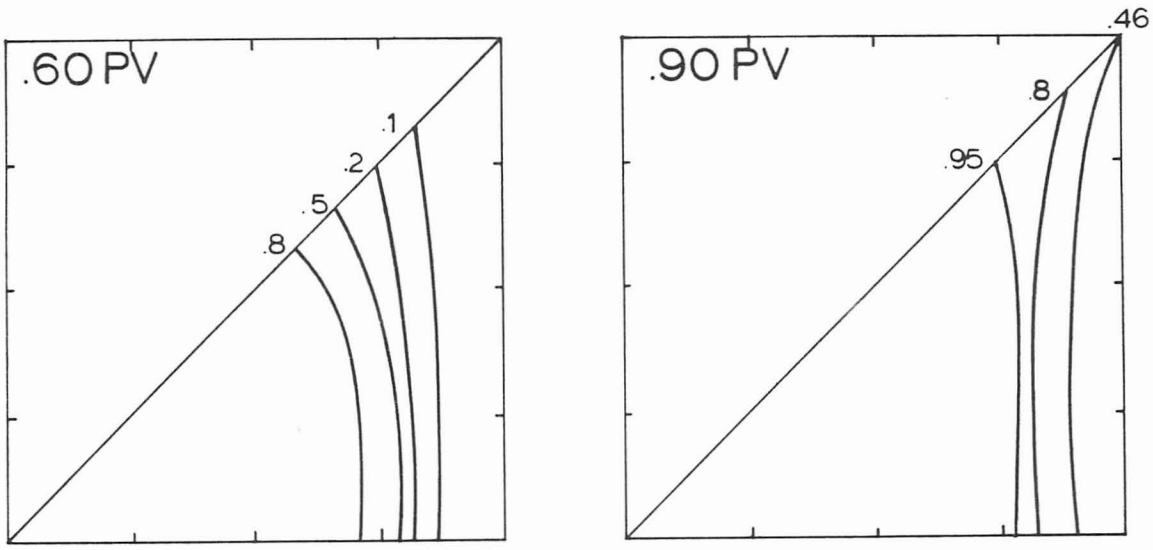

Figure 6.10

Contours at 0.6 PV and 0.9 PV

effect of adverse mobility is best shown by comparing to a solution with a mobility ratio of one for the same Peclet number. The fractional recovery of amount of in situ fluid produced at different injected pore volumes is a convenient way of comparing the solutions for different mobility ratios. The recovery or amount of material produced can be determined by either calculating the amount of material in the domain

$$\int_A c dA$$

or by integrating the concentration at the producing well over time

$$Pe \int_o^t c dt \qquad \text{(production well)}$$

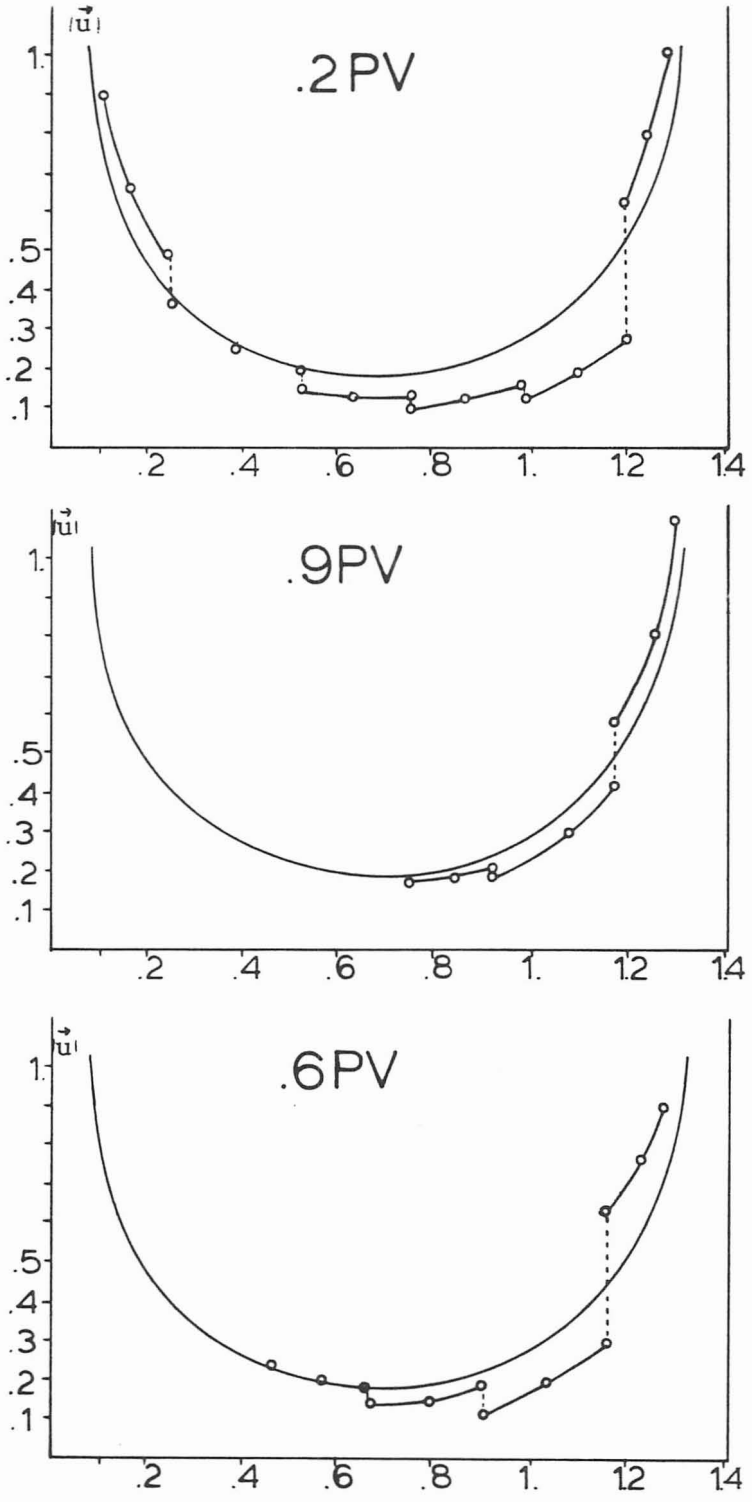

Figure 6.11

Velocities for M = 10, Pe = 72.5 at 0.2, 0.6, 0.9 PV Injected

The recovery obtained by using either method was found to be identical for this example. The fractional recovery is shown in Fig. 6.12 together with the results obtained by Young (1978) using the same model and physical parameters for mobility ratios of one and ten. A decrease in the recovery is observed relative to a mobility ratio of one but the decrease was not as pronounced as seen by Young (1978). The decrease is expected because the more divergent flow pattern for higher mobility ratios causes a lower sweep efficiency. The calculations by Young (1978) were examined for effects of mesh spacing error whereas the result obtained in this study was not. Even though the pressure

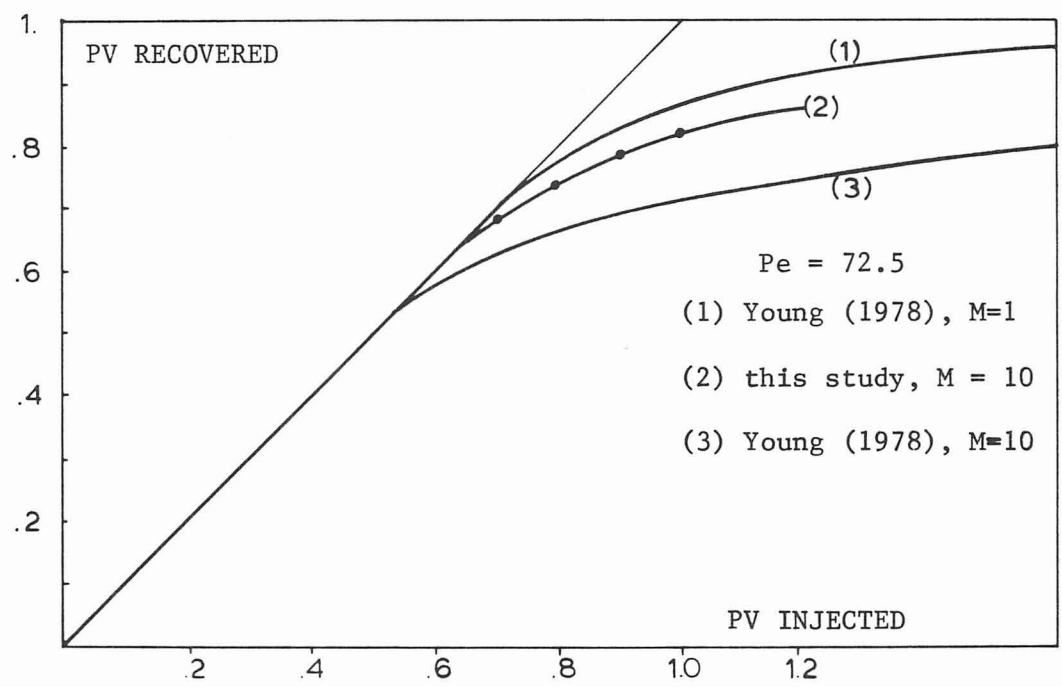

Figure 6.12

Recovery Curve, Adverse Mobility

singularity is removed by the analytical function, the velocity corrections (difference between solution and analytical function) are constant over each element and as seen in Fig. 6.12 the velocities vary in jumps between elements. A finer mesh is needed to obtain a more accurate description of the velocities. With higher order trial functions for the pressure these jumps in the velocities can be avoided. An analytical function with viscosities varying according to the concentration at the nearest well instead of a constant value would give a better pressure solution.

The computation time used for this example was approximately 50% higher than that for solving the model in Chapter V. The component equation used nearly the same CPU-time as estimated by formula 5.45 and solution time of the pressure equation was 50% of the time given by formula 5.45.

6.5 Conclusions

The moving coordinate system is applicable to mathematical models where a parabolic equation is coupled to an elliptic equation. The advantage for a parabolic problem of having the elements in the region where sharp changes in the solution occur is achieved for elliptic problems also.

The pressure singularity at the well is not stationary when MCS is applied and the best solutions are achieved by incorporating the exact analytical solution near the well in the trial function.

Preliminary results for an adverse mobility ratio show the trend observed by other studies.

Chapter VII

CONCLUSIONS AND RECOMMENDATIONS

From the analysis and comparison of the numerical methods for solving convective diffusive equations with dominating convection the following conclusions are made:

1) An extensive number of nodes/elements is needed for accurate simulation of even simple processes. The computation time required is impractical for very large Peclet numbers and two-dimensional problems.

2) Low order methods are preferable when poor accuracy (oscillations) can be allowed, whereas higher order methods are preferable when highly accurate (no oscillations) solutions are required.

A new solution technique, Moving Coordinate System is developed to solve these problems. From the study we conclude:

3) The moving coordinate system (MCS) is applicable to nonlinear one- and two-dimensional coupled elliptic-parabolic problems.

4) The location of the boundary conditions must be specified exactly in the MCS for two-dimensional problems and nonlinear one-dimensional problems.

5) Single nonlinear one-dimensional equations can be solved with cost savings of a factor 20-40.

6) The miscible displacement model in two dimensions can be solved with a cost savings of a factor of 50 compared to schemes with a fixed coordinate system, when both use a direct solution tech-

nique. The MCS code developed in this study is comparable in cost to an optimized finite element code using a time-split procedure.

7) Elliptic equations combined with parabolic equations can be solved with the same cost savings as obtained for parabolic equations alone.

8) Elliptic equations with singularities can be solved efficiently by incorporating analytic expressions in the trial functions. With the moving coordinate system the capability of solving sharp front problems is extended.

We recommend the following considerations to be taken into account when applying MCS to a set of parabolic-elliptic equations:

1) Using a time-split scheme to solve the equations rather than a direct solution technique can increase the efficiency by a large factor. For nonlinear problems convergence of a time-split scheme is not always insured.

2) Half the cost of solving the equations with a Galerkin finite element method is used to calcualte matrix entries. Substantial reductions in the computation time can be achieved by using efficient quadrature schemes, especially for linear problems.

3) For general application to two-dimensional problems automatic mesh generation and better algorithms for changing the mesh are desirable.

4) A variable timestep scheme, which enables better control of accuracy and selection of new timesteps is desirable.

BIBLIOGRAPHY

Abromowitz, M., I.A. Stegun, Handbook of Mathematical Functions, National Bureau of Standards, Applied Mathematical Series, 55, 1972.

Albright, N., P. Concus, and W. Proshurowski, "Numerical Simulation of the Multidimensional Buckley-Leverett Equation by a Sampling Method," SPE 7681, Proc. of Symposium on Reservoir Simulation, Soc. Pet. Eng., Denver, January 1979.

Aktas, Z. and H.J. Stetter, "A Classification and Survey of Numerical Methods for Boundary Value Problems in Ordinary Differential Equations," Int. J. Num. Meth. Engng. 11, pp. 771-796 (1977).

Aris, R., "On the Dispersion of a Solute in a Fluid Flowing Through a Tube," Proc. Roy. Soc., London, A235, 67, 1956.

Bailey, H.R. and B.K. Larkin, "Conduction-convection in Underground Combustion," Soc. Pet. Eng. Trans., AIME, Vol. 219, pp. 320-331 (1960).

Baker, A.J., M.O. Soliman, and D.W. Pepper, "A Timesplit Finite Element Algorithm for Environmental Release Prediction," Proc. of Finite Elements in Water Resources, London, July 1978, p. 453.

Baldwin, E., "Prediction of Tracer Performance in a Five Spot Pattern," J. Pet. Tech., pp. 513-517 (April 1966).

Barett, K.F. and G. Demunski, "Nonself Adjoint Problems and Essential Boundary Conditions," Int. J. Num. Meth. Engng. 14, pp. 507-513 (1979).

Bird, R.B., W.E. Stewart and E.N. Lightfoot, Transport Phenomena, J. Wiley, New York, 1960.

Blöttner, F.G., "Variable Grid Scheme Applied to Turbulent Boundary Layers," Computer Methods in Applied Mechanics and Engineering 4, pp. 179-194 (1974).

Brenner, H., "The Diffusion Model of Longitudinal Mixing in Beds of Finite Length, Numerical Values," Chem. Eng. Sci. 17, pp. 229-243 (1962).

Brigham, E. O., The Fast Fourier Transform, Prentice-Hall, Inc., New Jersey, 1974.

Buckley, S.E. and M.C. Leverett, "Mechanism of Displacement in Sands," Trans., AIME, Vol. 195, p. 91 (1952).

Carey, C.F. and B.A. Finlayson, "Orthogonal Collocation on Finite Elements," Chem. Eng. Sci. 30, pp. 587-596 (1975).

Carrier, G.F. and C.E. Pearson, Partial Differential Equations, Academic Press, New York, 1976.

Carslaw, H.S. and J.C. Jaeger, Conduction of Heat in Solids, Oxford University Press, 1959.

Chan, R.K.C., "A Balanced Expansion Technique for Constructing Accurate Finite Difference Advection Schemes," Int. J. Num. Meth. Engng. 12, pp. 1131-1150 (1978)

Chappelar, J.E. and A.S. Williamson, "Representing Wells in Numerical Reservoir Simulation-Theory and Implementation," SPE 7697, Proc. from Symposium on Reservoir Simulation, Soc. Pet. Eng., Denver, January 1979.

Chaudhari, N.M., "An Improved Numerical Technique for Solving Multi-dimensional Miscible Displacement," Soc. Pet. Eng. J. 11, pp. 277-284 (1971).

Chase, C.A., "Variational Simulation with Numerical Decoupling and Local Mesh Refinement," SPE 7689, Proc. from Symposium on Reservoir Simulation, Soc. Pet. Eng., Denver, January 1979.

Chien, T.C., "A General Finite Difference Formulation for Navier-Stoke's Equation," Computer and Fluids, 5, pp. 15-31 (1977).

Christie, I. and A.R. Mitchell, "Upwinding of High Order Galerkin Methods in Conduction-convection Problems," Int. J. Num. Meth. Engng. 12, pp. 1764-1771 (1978).

Christie, I., D.F. Griffiths, A.R. Mitchell and O.C. Zienkiewicz, "Finite Element Methods for Second Order Differential Equations with Significant First Derivative," Int. J. for Num. Meth. Engng. 10, pp. 1389-1396 (1976).

Claridge, E.L., "Prediction of Recovery in Unstable Miscible Flooding," Soc. Pet. Eng. J., pp. 143-155 (April 1972).

Concus, P. and W. Proskurowski, "Numerical Simulation of a Nonlinear Hyperbolic Equation by the Random Choice Method," submitted to J. Com. Physics, 1979.

Courant, R., W. Friedrichs and H. Lewy, "Über die Partiellen Differenzen-gleichungen des Mathematischen Physic," Math. Annalen 100.

Courant, R. and D. Hilbert, Methods of Mathematical Physics, Interscience, 1962.

Crowl, D. A. and R.A. Piccirelli, "Application of Computer Models to the Retorting of Oilshale," Proc. of Advances in Computer Methods for Partial Differential Equations, Bethelehem, 1979.

Douglas, J. Jr, H.H. Rachford and T. Dupont, Jr., "The Application of Various Methods to Waterflooding Problems," J. Can. Pet. Tech. 8, pp. 79-85 (1969).

Douglas, J. Jr, B.L. Darlow, M. Wheeler, and R.P. Kendall, "Selfadaptive Galerkin Methods for One-Dimensional, Two-Phase Immiscible Flow," SPE 7679, Proc. from Symposium on Reservoir Simulation, Soc. Pet. Eng., Denver, January 1979.

Downing, L.A. and W.K. Morrison, "Convection and Dispersion in a Porous Medium," Computers and Fluids 4, pp. 65-75, 1976.

Eigenburger, G. and J.B. Butts, "A Modified Crank-Nicholsen Technique with Non-equidistant Spacesteps," Chem. Eng. Sci. 31, pp. 681-691, 1976.

Ergun, S., "Fluid Fluid Through Packed Columns," Chem. Eng. Progr. 48, 89 (1952).

Finlayson, B. A., Nonlinear Analysis in Chemical Engineering, McGraw-Hill, 1979.

Finlayson, B. A., The Method of Weighted Residuals and Variational Principles, Academic Press, New York, 1972.

Finlayson, B.A., "Water Movement in Desiccated Soils," Proc. of 1st Int. Conf. on Finite Elements in Water Resources, Princeton University, July 1976, W.G. Gray, G.F. Pinder and C.A. Brebbia (Eds.), pp. 3.91-3.106.

Finlayson, B.A. and R.W. Nelson, "A Preliminary Investigation into the Theory and Techniques of Modelling the Natural Moisture Movement in Unsaturated Sediments," Report BCSR-40, Boeing Computer Services, Richland, WA, (September 1977).

Finlayson, B.A., "OCFE-progress and Potential," Proc. from Advances in Computer Methods for Partial Differential Equations, Bethelehem, 1979.

Foster, W.R., "A Low-Tension Waterflooding Process," J. Pet. Tech. 25, pp. 205-210, 1973.

Fritts, M.J., "Numerical Approximation on Distorted Lagragian Grids," Proc. from Advances in Computer Methods for Partial Differential Equations, Bethelehem, June 1979.

Garder, A.O., Jr., D.W. Peaceman and A.L. Pozzi, Jr., "Numerical Calculation of Multi-Dimensional Miscible Displacement by Method of Charactersitics," Soc. Pet. Eng. J. 4, pp. 26-36 (1964).

Gill, W.N. and R. Sankarasubramanin, "Exact Analysis of Unsteady Diffusion," Proc. Roy. Soc., London, A316-350, 1970.

Gray, W.G. and G.F. Pinder, "An Analysis of the Numerical Solution of the Transport Equations," Water Resources Research, 12, p. 547 (1976).

Gray, W.G. and M.T. Van Genuchten, "Economical Alternatives to Gaussian Quadrature Over Isoparametric Quadralaterals," Int. J. Num. Meth. Engng. 12, pp. 1478-1484, 1978.

Gresho, P.M. and R.L. Lee, "Don't Suppress the Wiggles — They Are Telling You Something!" Proc. from Conf. Finite Elements Methods for Convection Dominated Flows, A.I.Ch.E., New York, December 1979.

Gresho, P.M., R.L. Lee and R.L. Sani, "Advection-dominated Flows, with Emphasis on the Consequences of Mass Lumping," Proc. of the Second Int. Symp. on Finite Element Methods in Flow Problems, Italy, pp. 743-756, June 1976.

Gresho, P.M., R.L. Lee, R.L. Sani and T.W. Stullich, "On the Time Dependent FEM Solution of the Incompressible Navier-Stokes Equations in Two- and Three-Dimensions," Proc. from Finite Elements in Fluid Mechanics, London, July 1978.

Gupta, A.K., "A Finite Element for Transition from Fine Coarse Mesh," Int. J. Num. Meth. Engng. 12, 1979.

Haberman, B., "The Efficiency of Miscible Displacement as a Function of Mobility Ratio," Trans. AIME, 219, pp. 264-272, 1960.

Haynes, H.J., L.W. Trasher, M.L. Katz, and T.R. Eck, "An Analysis of the Potential for Enhanced Oil Recovery from Known Field in the United States—1976-2000," National Petroleum Council, December 1976.

Hayes, L.J., R.P. Kendall and M.F. Wheeler, "The Treatment of Sources and Sinks in Steady State Reservoir Engineering Simulations," Proc. from Advances in Computer Methods for Partial Differential Equations II, Bethelehem, 1977.

Heinrich, J.C. and O.C. Zienkiewicz, "Quadratic Finite Element Schemes for Two-Dimensional Convective Transport Equations," Int. J. Num. Meth. Engng. 11, pp. 1831-1844 (1977).

Hillion, P., "Numerical Integration Over Triangle," Int. J. Num. Meth. Engng. 11, pp. 797-815, 1977.

Hindemarch, A.C., Report UCID30130, Lawrence Livermore Laboratory, February 1976.

Hood, P., "Frontal Solution Program for Unsymmetric Matrices," Int. J. Num. Meth. Engng. 110, pp. 379-389, 1976.

Hopkins, T.R. and R. Wait, "A Comparison of Galerkin, Collocation and the Method of Lines for PDE," Int. J. Num. Meth. Engng. 12, pp. 108-1108, 1978.

Hughes, T.J.R., "A Simple Scheme for Developing Upwind Finite Elements," Int. J. Num. Meth. Engng. 12, pp. 1359-1366, 1978.

Huyakorn, P.S. and K. Nilkua, "Solution of Transient Transport Equation Using an Upstream Finite Element Method," submitted to Journal of Applied Mathematical Modelling.

Huyakorn, P.S. and C. Taylor, "Finite Element Models for Coupled Ground Water Flow and Convective Dispersion," Proc. from Finite Elements in Water Resources, Princeton University, pp. 1.131-1.151, July 1976.

Huyakorn, P.S., G.F. Pinder, C.R. Faust and J.W. Mercer, "A Finite Element Simulation of Two Phase Flow in Porous Media," Proc. from the Symposium on Computational Techniques for Boundary Value Problems in Applied Mechanics, New York, 1978.

Ikegawa, M., "A New Finite Element Technique for the Analysis of Steady Viscous Flow Problems," Int. J. Num. Meth. Engng. 14, pp. 103-714 (1979).

Irons, B.M., "A Frontal Solution Program for Finite Element Analysis," Int. J. Num. Meth. Engng. 2, pp. 5-32 (1970).

Javandel, I. and P.A. Witherspoon, "Application of the Finite Element Method to Transient Flow in Porous Media," Soc. Pet. Eng. J., pp. 241-252, September 1968.

Jensen, O.K. and B.A. Finlayson, "Oscillation Limits for Weighted Residual Methods," submitted to Int. J. Num. Meth. in Engng.

Jensen, O.K. and B.A. Finlayson, "Solution of the Transport Equations Using a Moving Coordinate System," accepted for publication in Advances in Water Resources.

Jenson, V.G. and G.V. Jeffrey, Mathematical Methods in Chemical Engineering, Academic Press, London, 1963.

Lake, L.W. and F.G. Helfferich, "The Effect of Dispersion, Cation Exchange and Polymer/Surfactant Adsorption on Chemical Flood Environment," SPE 6769, Proc. from Annual Conf. of Soc. Pet. Eng., Denver, October 1-3, 1977.

Lantz, R.B., "Quantitative Evaluation of Numerical Diffusion," Soc. Pet. Eng. J., 11, pp. 315-320 (1971).

Lapidus, L. and J.H. Seinfeld, Numerical Solution of Ordinary Differential Equations, Academic Press, New York, 1971.

Laumbach, D.D., "A High Accuracy Finite-Difference Technique for Treating the Convection-Diffusion Equation," Soc. Pet. Eng. J. 15, pp. 517-531 (1975).

Le Blanc, J.L. and B.H. Caudle, "A Streamline Model for Secondary Recovery," Soc. Pet. Eng. J., pp. 7-12, March 1971.

Lee, H. L. and E. N. Lightfoot, "Preliminary Report on Ultrafiltration-induced Polarization Chromatography—An Analog of Field-Flow Interaction," Separation Science, 11, pp. 417-440 (1976).

Leonard, B.P., "The Quick Finite Difference Method for the Convection Diffusion Equation," Proc. from Symposium on Reservoir Simulation, Soc. Pet. Eng., Denver, January 1979.

Leone, J.M., P.M. Gresho, S.T. Chan and R.L. Lee, "A Note on the Accuracy of Gauss-Legendre Quadrature in the Finite Element Method," Int. J. Num. Meth. Engng. 14, pp. 769-773 (1979).

Mahaffey, J.L., W.M. Rutherford and C.S. Matthews, "Sweep Efficiency by Miscible Displacement in a Five Spot," Soc. Pet. Eng. J., pp. 73-80, March 1966.

Marietta, M.G. and G.W. Swan, "Particle Diffusion in Electrostatic Precipitations," Chem. Eng. Sci. 31, pp. 795-801 (1976).

Marino, M.A., "Numerical and Analytical Solutions of Dispersion in Finite Adsorbing Porous Medium," Water Res. Bull. 10, pp. 81-90 (1974).

Masliyah, J.H. and D. Kumar, Proc. from "Application of OCFE to a Miscible Displacement Problem," Advances in Computer Methods for Partial Differential Equations, Bethelehem, June 1979.

McDonald, B.E. and S.T. Zalesak, "Flow Correction Algorithms for Multidimensional Transport," Proc. from Advances in Computer Methods for Partial Differential Equations, Bethelehem, June 1979.

McMichaels, C.L., and G.W. Thomas, "Reservoir Simulation by Galerkin Method," Soc. Pet. Eng. J., pp. 125-138, June 1973.

Mercer, J.W. and C.R. Faust, "The Application of Finite Element Methods to Immiscible Flow in Porous Media," Proc. from Conference on Finite Elements in Water Resources, Princeton, July 1976.

Morel-Seytoux, H.J., "Unit Mobility Ratio Displacement Calculations for Pattern Floods in Homogeneous Medium," Soc. Pet. Eng. J., 9, pp. 217-227 (1966).

Morel-Seytoux, H.J., "Analytical Methods in Waterflooding Predictions," Soc. Pet. Eng. J., 9, pp. 247-258 (1965).

Moult, A., D. Burley and H. Rawson, "The Numerical Solution of Two-Dimensional Steady Flow Problems by the Finite Element Methods," Int. J. Num. Meth. Engrg. 14, pp. 11-36 (1979).

Peaceman, D.W., "Improved Treatment of Dispersion in Numerical Calculation of Multidimensional Miscible Diplacement," Soc. Pet. Eng. J., pp. 213-216, September 1966.

Peaceman, D.W., "A Nonlinear Stability Analysis of Difference Equations Using Semi-implicit Mobility," SPE 5735, Proc. from Conference on Finite Elements in Water Resources, Princeton, July 1976.

Peaceman, D.W. and H.H. Rachford, "Numerical Calculation of Multidimensional Miscible Displacement," Soc. Pet. Eng. J. 2, pp. 327-339 (1962).

Peaceman, D.W., Fundamentals of Numerical Reservoir Simulation, Elsevier, Amsterdam, 1978.

Perkin, T.K. and O.C. Johnston, "A Review of Diffusion and Dispersion in Porous Media," Soc. Pet. Eng. J., pp. 70-84, March 1963.

Pinder, G.F. and H.H. Cooper, "A Numerical Technique for Calculating the Transient Position of the Saltwater Front," Water Res. Research, 6, pp. 681-703 (1971).

Pinder, G.F. and E.O. Frind, "A Collocation Finite Element Approach for Potential Problems in Irregular Domains," Int. J. Num. Meth. Engng. 14, pp. 681-703 (1979).

Prakash, A., "Finite Element Solution of the Nonself Adjoint Convective Dispersion Equation," Int. J. Num. Meth. Engng. 11, pp. 269-288 (1977).

Prenter, P.M., Splines and Variational Methods, J. Wiley, New York, 1975.

Price, H.S., R.S. Varga and J.E. Warren, "Application of Oscillation Matrices to Diffusion-convection Equations," J. Math. Physics 45, pp. 301-311 (1966).

Price, H.S., J.C. Cavendish and R.S. Varga, "Numerical Methods of Higher-Order Accuracy for Diffusion-Convection Equation," Soc. Pet. Eng. J., 8, pp. 293-303 (1968).

Rachford, H.H., "Numerical Calculation of Immiscible Displacement by a Moving Reference Point Method," Soc. Pet. Eng. J., 6, pp. 87-101 (1966).

Rapoport, L.A. and W.J. Leas, "Properties of Linear Waterflood," Trans. AIME, 196, pp. 139-148 (1953).

Rhee, H., B.F. Bidin and N.R. Amundson, "A Study of the Shock Layer in Equilibrium Exchange Systems," Chem. Eng. Sci. 26, pp. 1571-1580 (1971).

Roache, P.J., Computational Fluid Dynamics, Hermosa Publications, Albequerque, 1972.

Roberts, G.E. and H.H. Kaufmann, Tables of Laplace Transformation, Philadelphia, Saunders, 1966.

Runchal, A.K., "Comparative Criteria for Finite-Difference Formulations for Problems of Fluid Flow," Int. J. Num. Meth. Engng. 11, pp. 1667-1679 (1977).

Runchal, A.K., "Convergence and Accuracy of Three Finite Difference Scheme for a Two-dimensional Conduction and Convection Problem," Int. J. Num. Meth. Engng. 4, pp. 541-550 (1977).

Russell, R.D. and J. Christiansen, "Adaptive Mesh Selection Strategies for Solving Boundary Value Problems," Siam. J. Num. Anal. 7, pp. 59-80 (1978).

Saitoh, T., "A Numerical Method for Two-dimensional Navie-Stokes Equation by Multipoint Finite Difference," Int. J. Num. Meth. Engng. 11, pp. 1439-1454 (1977).

Scheidegger, A.E., The Physics of Flow Through Porous Media, University of Toronto Press, 1974.

Settari, A., H.S. Price and T. Dupont, "Development and Application of Variational Methods for Simulation of Miscible Displacement in Porous Media," SPE 5721, Proc. from Symposium on Reservoir Simulation, Soc. Pet. Eng., Los Angeles, February 1976.

Sincovec, R.F., "Generalized Collocation Methods for Time-Dependent Nonlinear Boundary Value Problems," Symposium on Numerical Simulation of Reservoir Performance, Los Angeles, February 1976.

Smith, I.M., "Integration in Time of Diffusion and Diffusion-Convection Equations," Proc. from 1st Int. Conf. on Finite Elements in Water Resources, Princeton University, July 1976, pp. 1.3-1.20.

Smith, I.M., R.V. Faraday and B.A. Connors, "Rayleigh-Ritz and Galerkin Finite Element Methods for Diffusion and Convection Problems," Water Resources Res., 9, pp. 593-606, 1973.

Smith, J.M., Chemical Engineering Kinetics, McGraw Hill, Kogakusha, 1970.

Spalding, D.B., "A Novel Finite Difference Formulation for Differential Expressions Involving First and Second Derivatives," Int. J. Num. Meth. Engng. 4, pp. 551-559 (1970).

Spivak, A., H.S. Price and A. Satter, "Solution of the Equations for Multi-dimensional Immiscible Flow by Various Methods," SPEJ 5723, Conf. on Finite Elements in Water Resources, Princeton, July 1976.

Stegemeier, G.L., D.D. Laumbach and C.W. Volek, "Representing Steam Processes with Vacuum Models," SPE 6787, Proc. from Annual Conf. of Soc. Pet. Eng., Denver, October 1977.

Stone, H.L. and P.L.T. Brian, "Numerical Solution of Convective Transport Problems," A.I.Ch.E. J., 9, p. 681 (1963).

Thomas, R.L. and J.D. Martinez, "Domal Salt Plumes in Ground Water," Proc. from Finite Elements in Water Resources, Princeton, 1976.

Todd, M.R. and C.A. Chase, "A Numerical Simulator for Predicting Chemical Flood Performance," SPE 7689, Proc. from Symposium on Reservoir Simulation, Soc. Pet. Eng., Denver, January 1979.

Todd, M.R., P.M. O'Dell, and G.J. Hirasahi, "Methods for Increased Accuracy in Numerical Reservoir Simulators," Soc. Pet. Eng. J., pp. 515-530, December 1972.

Van Genuchten, M.T., F.G. Pinder and E.G. Frind, "Simulation of Two-dimensional Contaminant Transport with Isoparametric Hermitian Finite Elements," Water Resources Res., 13, pp. 451-458 (1977).

Van Genuchten, M.T., "On the Accuracy and Efficiency of Several Numerical Schemes for Solving Convective-dispersive Equation," Proc. from 1st Int. Conf. on Finite Elements in Water Resources, Princeton University, July 1976.

Varoglu, E. and W.D.L. Finn, "A Finite Element Method for the Diffusion-convection Equation," Proc. from Finite Elements in Water Resources, London, July 1978, p. 4.3.

Villadsen, J. and M. Michelsen, Solution of Differential Equations by Polynomial Approximation, Prentice-Hall, 1977.

Wang, A.H. and R.L. Klein, "A Numerical Method to Obtain Optimal Quadrature Formulars," Int. J. Num. Meth. Engrg. 12, pp. 487-504 (1978).

Warren, J.E., R.L. Reed and H.S. Price, "Theoretical Considerations of Reverse Combustion in Tarsand," Trans. AIME, 219, pp. 109-123 (1960).

Weeks, G.E. and T.L. Cost, "An Algorithm for Automatically Tracking Ablating Boundaries," Int. J. Num. Meth. Engng. 14, pp. 441-450 (1979).

Wheatley, M.J., "A Version of Two Point Upstream for Use in Implicit Numerical Reservoir Simulators," SPE 7677, Proc. from Symposium on Reservoir Simulation, Soc. Pet. Eng., Denver, January 1979.

Wilkinson, J.H., The Algebraic Eigenvalue Problem, Oxford, Charendon Press, 1965.

Yanosik, J.L. and T.A. Macrachen, "A Nine Point Finite Difference Reservoir Simulator for Realistic Prediction of Unfavorable Mobility Ratio Displacement," Symposium on Numerical Simulation of Reservoir Performance, Los Angeles, February 1976.

Young, L.C., "An Efficient Finite Element Method for Reservoir Simulation," SPE 7413, Proc. from 53rd Annual Conference of Soc. Pet. Eng., AIME, Houston, October 1978.

Young, L.C., "A Preliminary Comparison of Finite Element Methods for Reservoir Simulation," Proc. from Advances in Computer Methods for Partial Differential Equations II, IMACS (AICA), pp. 307-320 (1977).

Ziewieniuch, J.L., and L. Gladwell, "Analysis of Explicit Difference Methods for a Diffusion-convection Equation," Int. J. Num. Meth. Engng. 12, pp. 899-916 (1978).

Zienkiewicz, O.C., The Finite Element Method in Engineering Science, McGraw-Hill, London, 1971

Appendix A

ANALYTICAL SOLUTIONS TO TRANSPORT EQUATIONS

Exact solutions to transport equations are presented. Some are used for comparisons to numerical solutions, others given for general review.

A.1 Constant Velocity

The linear convective-diffusive (C-D) equation

$$\frac{\partial c}{\partial t} + Pe \frac{\partial c}{\partial x} = \frac{\partial^2 c}{\partial x^2} \tag{A.1}$$

with

$$\begin{aligned} a_1 c + b_1 \frac{\partial c}{\partial x} &= c_1 \quad , \quad x = 0 \quad t > 0 \\ a_2 c + b_2 \frac{\partial c}{\partial x} &= c_2 \quad , \quad x = 1 \quad t > 0 \\ c &= c_3 \quad , \quad x > 0 \quad t = 0 \end{aligned} \tag{A.2}$$

has been solved in a number of different ways. The Peclet number is here defined as

$$Pe = \frac{uL}{D}$$

where u is the linear velocity, L the length of domain and D the diffusion coefficient.

A.1-1 Series Solution

Exact solution can be obtained for some cases of the boundary condition (A.2). For $a_2 = b_1 = c_2 = c_3 = 0$ we have

$$\left.\begin{aligned} c &= 1 && \text{at} \quad x = 0 \\ \frac{\partial c}{\partial x} &= 0 \quad \text{or} \quad c = 0 && \text{at} \quad x = 1 \end{aligned}\right\} \quad t > 0$$

$$c = 0 \qquad x > 0 \qquad t = 0$$

To solve (A.1) by series solution we must construct homogeneous boundary conditions. For the B.C. $c(1,t) = 0$ we use

$$u(x,t) = c(x,t) + f(x)$$

where

$$f(x) = \frac{e^{Pe} - e^{Pex}}{1 - e^{Pe}}$$

so

$$\frac{\partial u}{\partial t} + Pe \frac{\partial u}{\partial x} = \frac{\partial^2 u}{\partial x^2}$$

and

$$\begin{aligned} \text{B.C.} \quad & u(0,\ t > 0) = 0 \\ & u(1,\ t > 0) = 0 \\ & u(x > 0,\ t = 0) = \frac{e^{Pe} - e^{Pex}}{1 - e^{Pe}} \end{aligned} \qquad \text{(A.3)}$$

For B.C. $\frac{\partial c}{\partial x}(1,t) = 0$ we use $f(x) = -1$ and we recover (A.3) with change in right B.C. to $\frac{\partial u}{\partial t}(1,t) = 0$ and $u(x > 0,\ t = 0) = -1$.

Applying the separation of variables technique, the solution can be determined. For the B.C. $c(1,t) = 0$, the solution is

$$c(x,t) = \frac{e^{Pe} - e^{Pex}}{e^{Pe} - 1} - 4\, e^{\frac{Pe}{2}x - \frac{Pe^2}{4}\cdot t} \times$$

$$\sum \frac{n\pi}{Pe^2/4+(n\pi)^2}\, e^{-n^2\pi^2 t} \sin n\pi x \qquad (A.4)$$

and the eigenvalues are

$$\mu_i = -\, Pe^2/4 - n^2\pi^2 \quad , \quad n = 1,2,\ldots\infty$$

For the B.C. $\frac{\partial c}{\partial x}(1,t) = 0$ the eigenvalues can only be determined through the transcendental equation

$$\tan y = -\frac{2}{Pe}\, y$$

and

$$\lambda_i = -\frac{Pe^2}{4} - y^2 \qquad (A.5)$$

The series solutions are not useful for computational purposes for large Peclet numbers since the term

$$\frac{n\pi}{(n\pi)^2 + Pe^2/4}$$

decreases very slowly as n increases. For high Peclet numbers ($>10^3$) n must be large (over 10^6) to compute a solution.

A.1-2 Laplace Transformations

For convective-diffusion with reaction

$$\frac{\partial c}{\partial t} + u \frac{\partial c}{\partial x} + K_1 c = D \frac{\partial^2 c}{\partial x^2} \tag{A.6}$$

and the boundary conditions

$$\left.\begin{aligned} c &= c_o \qquad x = 0 \\ \frac{\partial c}{\partial x} &= 0 \qquad x = 1 \end{aligned}\right\} \quad t > 0$$

$$c = 0 \qquad x > 0 \qquad t = 0$$

Marino (1974) gives a number of different analytical solutions. Most of them are not computationally useful. For $k_1 = 0$ and a semi-infinite domain the solution to (A.6) is

$$c = c_o/2(\text{erfc } [x - ut]/2\sqrt{Dt}) +$$

$$c_o/2\ e^{ux/D} \cdot (\text{erfc } [x + ut]/2\sqrt{Dt}) \tag{A.7}$$

which can be used provided $c(1,t) < 10^{-16}$. With alternative boundary conditions (form A.1)

$$\left.\begin{aligned} Pec - \frac{dc}{dx} &= Pe \qquad x = 0 \\ \frac{dc}{dx} &= 0 \qquad x = 1 \end{aligned}\right\} \quad t > 0$$

$$c = 0 \qquad x > 0 \qquad t = 0$$

Brenner (1962) provides a solution which can be used computationally, too.

A.1-3 Other Solutions

Analytical solution to related convection-diffusion problems including adsorption effects, diffusion in pipeflow, etc. can be found in the literature. Lee et al. (1976), Rhee (1971), Aris (1955), Gill et al. (1970) and Marietta (1976) are good starting points.

A.2 Radial Velocity

A.2-1 Parabolic Equation

The convective-diffusion equation in radial coordinates is

$$\frac{\partial c}{\partial t} + \frac{Pe}{r}\frac{\partial c}{\partial r} = \frac{1}{r}\frac{\partial}{\partial r}\left(r\frac{\partial c}{\partial r}\right) \qquad (A.10)$$

The Peclet number is here defined by

$$Pe = \frac{Q}{D} \quad .$$

where Q is the volumetric flow per radia and D the diffusion coefficient. We seek the analytical solution with the boundary condition

$$\begin{array}{llll} c = 0 & r > 0 & t = 0 & (a) \\ c = 1 & r = 0 & t > 0 & (b) \\ c = 0 & r \to \infty & t > 0 & (c) \end{array} \qquad (A.11)$$

To solve (A.10) and (A.11) we apply a Laplace transformation

$$\bar{c} \cdot s + \frac{1}{r}(Pe - 1)\frac{d\bar{c}}{dr} - \frac{d^2\bar{c}}{dr^2} = 0 \qquad (A.12)$$

and

$$\bar{c} = 1/s \qquad \text{at} \qquad x = 0$$

(A.12) is a Bessel equation, transforming $\bar{c}$ by

$$\bar{c} = c^* \cdot r^{\lambda/2}, \qquad \lambda = Pe$$

we have

$$\frac{d\bar{c}}{dr} = \frac{dc^*}{dr} \cdot r^{\lambda/2} + \lambda/2 \cdot r^{\lambda/2-1} \cdot c^*$$

$$\frac{d^2\bar{c}}{dr^2} = \frac{d^2c^*}{dr^2} \cdot r^{\lambda/2} + \lambda r^{\lambda/2-1} \cdot c^* + \lambda/2(\lambda/2 - 1)r^{\lambda/2-2} \cdot c^*$$

and substituted into (A.12) we obtain

$$c^* \cdot s \cdot r^{\lambda/2} - r^{\lambda/2-1} \cdot \frac{dc^*}{dr} + r^{\lambda/2-2} \cdot c^* \cdot \lambda^2/4 -$$

$$\frac{d^2c^*}{dr^2} \cdot r^{\lambda/2} = 0$$

or

$$\frac{d^2c^*}{dr^2} + \frac{1}{r}\frac{dc^*}{dr} - \left[(\sqrt{s})^2 + \frac{(\lambda/2)^2}{r^2}\right] \cdot c^* = 0 \qquad (A.13)$$

(A.13) is "the second form of the modified Bessel Equation," which has the general solution

$$c^* = A \cdot I_{\lambda/2} \cdot (\sqrt{s} \cdot r) + B \cdot K_{\lambda/2} \quad (\sqrt{s}\, r)$$

$I_{\lambda/2}$ is monotic increasing so we must require A = 0, because c^* is finite for $r \to \infty$ (A.11c). We get

$$\bar{c} = c^* \cdot r^{\lambda/2} = B \cdot r^{\lambda/2} \cdot K_{\lambda/2} (\sqrt{s} \cdot r) \qquad (A.14)$$

To evaluate the constant B in (A.14), the boundary condition (A.11b) must be applied. $K_{\lambda/2}(r) \to \infty$ for $r \to 0$, but as $r^{\lambda/2} K_{\lambda/2}(r)$ is finite [Abromowitz et al., 1972], we have

$$r^{\lambda/2} \cdot K_{\lambda/2} (\sqrt{s} \cdot r) \simeq \frac{1}{2} \cdot \Gamma(\lambda/2) \cdot 2^{\lambda/2} \left(\frac{1}{\sqrt{s}}\right)^{\lambda/2} \text{ as } r \to 0$$

B can now be evaluated with (A.11b)

$$\frac{1}{s} = B \cdot r^{\lambda/2} \cdot \left(1/2 \cdot \Gamma(\lambda/2) \cdot 2^{\lambda/2} \quad \frac{1}{s^{\lambda/4}} \cdot \frac{1}{r^{\lambda/2}}\right) \text{ as } r \to 0$$

giving

$$\bar{c} = 2^{1-\lambda/2} \cdot r^{\lambda/2} \cdot \frac{1}{\Gamma(\lambda/2)} \cdot s^{\lambda/4-1} \cdot K_{\lambda/2} (\sqrt{s} \cdot r). \qquad (A.15)$$

(A.15) is inverted to Robert et al. (1966)

$$c(r,t) = \frac{\Gamma(\lambda/2,\ r^2/4t)}{\Gamma(\lambda/2)} = \frac{\Gamma(Pe/2,\ r^2/4t)}{\Gamma(Pe/2)} \qquad (A.16)$$

where $\Gamma(a,b)$ is the incomplete gamma function

$$\Gamma(\lambda/2,\ r^2/4t) = \int_{r^2/4t}^{\infty} e^{-u} \cdot u^{\lambda/2-1}\, du$$

$$\Gamma(\lambda/2) = \int_{0}^{\infty} e^{-u} \cdot u^{\lambda/2-1}\, du \quad . \qquad (A.17)$$

In statistical theory (A.17) is the χ^2-distribution function and values are therefore easily obtained from either tables or existing computer packages.

Carslaw and Jaeger (1959) obtain a solution if (A.11b) is changed to

$$c = 1 \qquad \text{at} \qquad r = r_o \neq 0$$

and the solution is

$$c(r,t) = 1 + \frac{2}{\pi}\left(\frac{r}{r_o}\right)^{\lambda/2} \int_o^\infty e^{-u^2 t} \cdot \frac{[J_{\lambda/2}(ur)Y_{\lambda/2}(ur_o) - Y_{\lambda/2}(ur)Y_{\lambda/2}(ur_o)]}{u \cdot [J^2_{\lambda/2}(ur_o) + Y^2_{\lambda/2}(ur_o)]}\, du \qquad \text{(A.18)}$$

A.2-2 Hyperbolic Equation

For very high Peclet numbers (A.10) is very similar to

$$\frac{\partial c}{\partial \tau} + \frac{Pe}{r}\frac{\partial c}{\partial r} = 0 \qquad \text{(A.19)}$$

Using boundary condition (A.11a,b) and the Laplace transformation

$$\bar{c}s + \frac{Pe}{r}\frac{d\bar{c}}{dr} = 0$$

or with (A.11b)

$$\bar{c} = \frac{1}{s} e^{-Pe/2\, r^2 s} \quad .$$

which has the solution

$$c = c(r - \sqrt{2Pet}) = \text{constant} \qquad \text{(A.20)}$$

(A.20) is useful to calculate the amount of injected material in two-dimensional problems (Chapters V and VI).

A.2-3 Other Solutions

Several analytical solutions involving radial flow with different initial conditions are given in Bailey *et al.* (1960) and Warren *et al.* (1960).

Appendix B

OSCILLATION LIMITS FOR WEIGHTED RESIDUAL METHODS

In Section 2.3-2 an analysis is given of a weighted residual method using the model problem

$$Pe \frac{dc}{dx} = \frac{d^2c}{dx^2} \tag{2.6}$$

The solution to (2.6) satisfies

$$\frac{dc}{dx} < 0 \quad \text{for all } x \in [0,1] \tag{2.13}$$

and we require that the numerical methods must satisfy (2.13) at any point in the domain. The "grid Peclet number" $Pe\Delta x$ or oscillation limit determines where (2.13) is satisfied. It is found that if

$$Pe\Delta x < A$$

where A varies for different methods, the numerical solution will be monotone. In this appendix the constant A is determined for Galerkin, orthogonal collocation and moments finite element methods.

The following notation is used in this appendix. The interval zero to one is divided into NE equal elements and the corner nodes are then

$$x_i = i \cdot \Delta x, \quad i = 0,1,\ldots,NE$$

For interior collocation points or midside nodes (Galerkin), a fraction is added to the integer index i. For NCOL interior collocation points

(or NCOL midside nodes [Galerkin]) the notation is

$$x_i + k, \quad k = \frac{NC}{NCOL + 1}, \quad NC = 1,2,\ldots,NCOL$$

The collocation points are given in text. The value of c at a node (corner, midside, collocation point) is denoted by an index corresponding to the nodal numbering.

The discretized equations form a matrix $\underline{M}$, the structure is shown for different methods too. The coefficients in $\underline{M}$ are taken from Villadsen and Michelsen (1977) and Finlayson (1979).

B.1 OCFE — Legendre-quadratic

Applying OCFE with one interior collocation point to the model problem gives the following structure of matrix $\underline{M}$

$$\begin{pmatrix}
1 & 0 & 0 & & & & & \\
x & x & x & & & & & \\
x & x & x & x & x & & & \} i \\
 & & x & x & x & & & \\
 & & x & x & x & x & x & \} i+1 \\
 & & & & x & x & x & \\
 & & & & & \cdot & \cdot & \cdot \\
 & & & & & & \cdot & \cdot \\
 & & & & & & x & x & x \\
 & & & & & & 0 & 0 & 1
\end{pmatrix}$$

The equation at the collocation point is ($u = 0.5$, $c_{i+1/2}$)

$$[4 + Pe\Delta x]c_{i-1} - 8c_{i-1/2} + [4 - Pe\Delta x]c_i = 0 \qquad (B.1)$$

and at corner nodes (c_i); the continuity of slope gives

$$c_{i-1} - 4\, c_{i-1/2} + 6\, c_i - 4\, c_{i+1/2} + c_{i+1} = 0 \qquad (B.2)$$

When (B.1) is substituted in (B.2) the $c_{i+1/2}$ - values can be eliminated

$$[2 + Pe\Delta x]c_{i-1} - 2\, c_i + [2 - Pe\Delta x]c_{i+1} = 0 \qquad (B.3)$$

Equation (B.3) is a difference equation with the solution

$$c_i = A + B\psi^i \qquad (B.4)$$

where ψ now is

$$\psi = \frac{1 + Pe\Delta x/2}{1 - Pe\Delta x/2} \qquad (B.5)$$

The values of A and B are determined by the boundary conditions. Expression for $c_{i+1/2}$ can now be obtained by substituting (B.4) into (B.1)

$$c_{i+1/2} = A + B\psi^i \quad \frac{1 - Pe^2\Delta x^2/8}{1 - Pe\Delta x/2}$$

As c varies quadratically over the element

$$c(u) = a_o + a_1 u + a_2 u^2$$

and

$$c(o) = c_i$$

$$c(1/2) = c_{i+1/2}$$

$$c(1) = c_{i+1}$$

we obtain

$$a_o = c_i$$

$$a_1 = -3c_i + 4c_{i+1/2} - c_{i+1} \qquad \text{(B.6)}$$

$$a_2 = 2c_i - 4c_{i+1/2} + 2c_{i+1}$$

The criterion can now be evaluated,

$$\frac{dc}{du} = a_1 + 2a_2 u < 0 \quad \text{for all } u\varepsilon[0,1].$$

By substituting (B.4) and (B.5) into (B.6) we obtained

$$\frac{dc}{du} = A(u - u_1)$$

and

$$u_1 = \frac{1}{2} - \frac{1}{Pe\Delta x} \quad .$$

Thus for

$$Pe\Delta x > 2 \rightarrow \text{slope } \frac{dc}{du} > 0$$

$$Pe\Delta x < 2 \rightarrow \text{slope } \frac{dc}{du} < 0$$

The oscillationlimit is therefore $Pe\Delta x < 2$. If we look at monotonicity for the nodal values $(c_i, c_{i+1/2})$ the same limit is obtained.

B.2 OCFE — Legendre-cubic

The matrix structure of $\underline{M}$ is now

$$
\begin{pmatrix}
1 & 0 & 0 & 0 & & & & & & & & \\
x & x & x & x & & & & & & & & \\
x & x & x & x & & & & & & & & \\
x & x & x & x & x & x & x & & & & & \} \ i \\
 & & & x & x & x & x & & & & & \\
 & & & x & x & x & x & & & & & \\
 & & & x & x & x & x & x & x & x & & \\
 & & & & & & x & x & x & x & & \} \ i+1 \\
 & & & & & & x & x & x & x & & \\
 & & & & & & \cdot & \cdot & \cdot & \cdot & & \\
 & & & & & & & & & \cdot & \cdot & \cdot \\
 & & & & & & & & & x & x & x & x \\
 & & & & & & & & & 0 & 0 & 0 & 1
\end{pmatrix}
$$

The equation at the first collocation points $c_{i-2/3}$ ($u = 0.2113$) is

$$
\begin{aligned}
&[16.3912 + 2.7311\ Pe\Delta x]c_{i-1} + [-24. - 1.7311\ Pe\Delta x]c_{i-2/3} + \\
&\qquad [12. - 1.7311\ Pe\Delta x]c_{i-1/3} + \\
&\qquad [-4.3912 + 0.7311\ Pe\Delta x]c_{i} = 0
\end{aligned}
\tag{B.7}
$$

and at the second collocation points $c_{i-1/3}$ $9u + 0.7887)$

$$
\begin{aligned}
&[-4.3912 - 0.7311\ Pe\Delta x]c_{i-1} + [12 + 1.7311\ Pe\Delta x]c_{i-2/3} + \\
&\qquad [-24 + 1.7311\ Pe\Delta x]c_{i-1/3} + \\
&\qquad [16.3912 - 2.7311\ Pe\Delta x] = 0
\end{aligned}
\tag{B.8}
$$

The continuity requirement at the corner nodes c_i is

$$-c_{i-1} + 2.1962\ c_{i-2/3} - 8.1962\ c_{i-1/3} + 14c_i - 8.1962\ c_{i+1/3} + 2.1962c_{i+2/3} - c_{i+1} = 0 \qquad (B.9)$$

With the difference equations for element i+1, see figure above, the equations are combined to eliminate the variables $c_{i-1/3}$, $c_{i-2/3}$, $c_{i+1/3}$, $c_{i+2/3}$, and we obtain

$$[1 + Pe\Delta x/2 + Pe^2\Delta x^2/12]c_{i-1} + [-2 - Pe^2\Delta x^2/6]c_i + [1 - Pe\Delta x/2 + Pe^2\Delta x^2/12]c_{i+1} = 0 \qquad (B.10)$$

(B.10) has the solution (B.4) where ψ is

$$\psi = \frac{1 + Pe\Delta x/2 + Pe^2\Delta x^2/12}{1 - Pe\Delta x/2 + Pe^2\Delta x^2/12} \qquad (B.11)$$

Expressions for $c_{i+1/3}$ and $c_{i+2/3}$ can now be obtained

$$c_{i+1/3} = A + B\psi^i \frac{1 - 0.2887\ Pe\Delta x + 0.008015\ Pe^3\Delta x^3}{1 - Pe\Delta x/2 + Pe^2\Delta x^2/12} \qquad (B.12)$$

$$c_{i+2/3} = A + B\psi^i \frac{1 + 0.2887\ Pe\Delta x + 0.008015\ Pe^3\Delta x^3}{1 - Pe\Delta x/2 + Pe^2\Delta x^2/12} \qquad (B.13)$$

The solution by OCFE-Hermite cubic and OCFE-Legendre cubic is the same at all points as shown in Section B.4. The criterion is therefore also identical. Oscillations in the solution do not occur

provided

$$Pe\Delta x < \sqrt{12} = 3.464 \quad .$$

If monotonicity only between nodal values is considered the criterion is $Pe\Delta x < 4.3912$.

B.3 OCFE — Legendre-quartic

The matrix structure of $\underline{M}$ is

$$\begin{pmatrix}
1 & 0 & 0 & 0 & 0 & & & & & & & & & & \\
x & x & x & x & x & & & & & & & & & & \\
x & x & x & x & x & & & & & & & & & & \\
x & x & x & x & x & & & & & & & & & & \\
x & x & x & x & x & x & x & x & x & & & & & & \\
 & & & & x & x & x & x & x & & & & & & \\
 & & & & x & x & x & x & x & & & & & & \\
 & & & & x & x & x & x & x & & & & & & \\
 & & & & x & x & x & x & x & x & x & x & x & & \\
 & & & & & & & & \cdot & \cdot & \cdot & \cdot & \cdot & \cdot & & \\
 & & & & & & & & & & & & \cdot & \cdot & & \\
 & & & & & & & & & & & & 0 & 0 & 0 & 0 & 1
\end{pmatrix}$$

At the first collocation point ($u = 0.1127$, $c_{i-3/4}$) the equation is

$$[53.238 + 5.323\ Pe\Delta x]c_{i-1} + [-73.33 - 3.873\ Pe\Delta x]c_{i-3/4} +$$

$$[26.666 - 2.0656\ Pe\Delta x]c_{i-1/2} +$$

$$[-13.33 + 1.291\ Pe\Delta x]c_{i-1/4} +$$

$$[6.7621 - 0.6721\ Pe\Delta x]c_{i} = 0 \qquad \text{(B.14)}$$

and at the second collocation point ($u = 0.5$, $c_{i-1/2}$) we have

$$[-6 - 1.5\ Pe\Delta x]c_{i-1} + [16.66 + 3.2275\ Pe\Delta x]c_{i-3/4} +$$

$$[-21.333]c_{i-1/2} + [16.66 - 3.2275\ Pe\Delta x]c_{i-1/4} +$$

$$[-6 - 1.5\ Pe\Delta x]c_{i+1} = 0 \qquad \text{(B.15)}$$

At the third collocation point ($u = 0.7873$, $c_{i-1/4}$) we have

$$[6.7621 + 0.6721\ Pe\Delta x]c_{i-1} + [-13.33 - 1.291\ Pe\Delta x]c_{i-3/4} +$$

$$[26.666 + 2.0656\ Pe\Delta x]c_{i-1/2} +$$

$$[-73.33 + 3.873\ Pe\Delta x]c_{i-1/4} +$$

$$[53.238 - 5.323\ Pe\Delta x]c_{i} = 0 \qquad \text{(B.16)}$$

and the continuity equation at the corner node c_i

$$c_{i-1} - 1.8724\ c_{i-3/4} + 2.666\ c_{i-1/2} - 14.788\ c_{i-1/4} +$$

$$26\ c_i - 14.788\ c_{i+1/4} + 2.666\ c_{i+1/2} -$$

$$1.8784\ c_{i+3/4} + c_{i+1} = 0 \qquad \text{(B.17)}$$

By proper addition of (B.14) through (B.16) to (B.17) (element i and i+1) the nodal values $c_{j+1/4}$, $c_{j+1/2}$ and $c_{j+3/4}$, $j = i, i - 1$ can be eliminated. The reduced equation is

$$[1 + Pe\Delta x/2 + Pe^2\Delta x^2/10 + Pe^3\Delta x^3/120]c_{i-1} +$$

$$[-2 - Pe^2\Delta x^2/5]c_i +$$

$$[1 - Pe\Delta x/2 + Pe^2\Delta x^2/10 - Pe^3\Delta x^3/120]c_{i+1} = 0 \qquad (B.18)$$

The solution to (B.18) is again (B.4), the function ψ is

$$\psi = \frac{1 + Pe\Delta x/2 + Pe^2\Delta x^2/10 + Pe^3\Delta x^3/120}{1 - Pe\Delta x/2 + Pe^2\Delta x^2/10 - Pe^3\Delta x^3/120} \qquad (B.19)$$

Expression for the $c_{i+1/4}$, $c_{i+1/2}$ and $c_{i+3/4}$ can now be obtained with (B.14) through (B.16) and (B.4) and (B.18).

$$c_{i+1/4} = A + B\psi^i \frac{1 - 0.3873\ Pe\Delta x + Pe^2\Delta x^2/20 - Pe^4\Delta x^4/2400}{1 - Pe\Delta x/2 + Pe^2\Delta x^2/10 - Pe^3\Delta x^3/120} \qquad (B.20)$$

$$c_{i+1/2} = A + B\psi^i \frac{1 - Pe^2\Delta x^2/40 - Pe^4\Delta x^4/1920}{1 - Pe\Delta x/2 + Pe^2\Delta x^2/10 - Pe^3\Delta x^3/120} \qquad (B.21)$$

$$c_{i+3/4} = A + B\psi^i \frac{1 + 0.3873\ Pe\Delta x + Pe^2\Delta x^2/20 - Pe^4\Delta x^4/2400}{1 - Pe\Delta x/2 + Pe^2\Delta x^2/10 - Pe^3\Delta x^3/120} \qquad (B.22)$$

To get the criterion we now have

$$c(u) = a_o + a_1 u + a_2 u^2 + a_3 u^3 + a_4 u^4$$

and

$$c(o) = c_i$$

$$c(u_1) = c_{i+1/4} \qquad (u_1 = 0.112701665)$$

$$c(u_2) = c_{i+1/2} \qquad (u_2 = 0.5)$$

$$c(u_3) = c_{i+3/4} \qquad (u_3 = 1 - u_1)$$

$$c(1) = c_{i+1}$$

and the constants are evaluated to

$$a_o = c_i$$

$$a_1 = -13c_i + 14.788c_{i+1/4} - 2.666c_{i+1/2} + 1.878c_{i+3/4} - c_{i+1}$$

$$a_2 = 42c_i - 61.03158\, c_{i+1/4} + 29.333c_{i+1/2} - \qquad \text{(B.23)}$$

$$22.308c_{i+3/4} + 12c_{i+1}$$

$$a_3 = -50c_i + 79.57661c_{i+1/4} - 53.333c_{i+1/2} +$$

$$53.757c_{i+3/4} - 30c_{i+1}$$

The criterion can now be evaluated by using (B.20) through (B.23), and we find

$$\frac{dc}{du} = a_1 + 2a_2u + 3a_3u^2 + 4a_3u^3$$

$$= \text{Const}\ \psi^i \Big[(1 - Pe\Delta x/2 + Pe^2\Delta x^2/10 + Pe^3\Delta x^3/120)$$

$$+ Pe\Delta x\ (1 - Pe\Delta x/2 + Pe^2\Delta x^2/10) \cdot u$$

$$+ Pe^2\Delta x^2\ (1 - Pe\Delta x/2) \cdot u^2/2$$

$$+ Pe^3\Delta x^3 \cdot u^3/6\Big]$$

$$= \text{Const}\ \psi^i \cdot P_n(u) \qquad \text{(B.24)}$$

and $P_n(u) > 0$ for all $Pe\Delta x > 0$. The functional ψ given by (B.19) can be rewritten to

$$\psi = \frac{(Pe\Delta x + 4.6444)(Pe^2\Delta x^2 + 7.3556\ Pe\Delta x + 25.8376)}{(Pe\Delta x - 4.6444)(Pe^2\Delta x^2 - 7.3556\ Pe\Delta x - 25.8376)} \qquad (B.25)$$

and for

$$\psi > 0 \quad \text{for} \quad Pe\Delta x < 4.6444$$

$$\psi < 0 \quad \text{for} \quad Pe\Delta x > 4.6444 \quad .$$

For $Pe\Delta x > 4.66$, ψ^i (and therefore also the slope) changes sign from element to element. Oscillations in the solution provided

$$Pe\Delta x < 4.6444 \qquad (B.26)$$

If we compare nodal values c_i, $c_{i+1/4}$, $c_{i+1/2}$, $c_{i+3/4}$ and c_{i+1} for monotonicity the same criterion arises.

B.4 OCFE — Hermite-cubic

The structure of matrix $\underline{\underline{M}}$ is

$$\begin{pmatrix}
x & x & x & & & & & \\
x & x & x & & & & & \\
 & x & x & x & x & & & \\
 & x & x & x & x & & & \\
 & & & x & x & x & x & \\
 & & & x & x & x & x & \\
 & & & \cdot & \cdot & \cdot & \cdot & \cdot \\
 & & & & & & x & x & x
\end{pmatrix}
\begin{matrix} \\ \\ \\ \} \ i \\ \\ \} \ i+1 \\ \\ \\ \end{matrix}$$

The equation at the first collocation point (u = 0.2113) in element i

$$[-3.4641 + Pe\Delta x]c_i + [-2.7321 - 0.2887\ Pe\Delta x\ ]c_i^1 +$$

$$[3.4641 - Pe\Delta x]c_{i+1} +$$

$$[-0.7321 + 0.2887\ Pe\Delta x]c_{i+1}^1 = 0 \qquad (B.27)$$

where c_i^1 is the derivative of c at x_i, notation otherwise similar. At the second collocation point (u = 0.7887)

$$[3.4641 + Pe\Delta x]c_i + [0.7321 + 0.2887\ Pe\Delta x]c_i^1$$

$$[-3.4641 - Pe\Delta x]c_{i+1} +$$

$$[2.7321 - 0.2887\ Pe\Delta x]c_{i+1}^1 = 0 \qquad (B.28)$$

Taking the difference equations for element i-1 too, we can eliminate for slopes c_{i-1}^1, c_i^1 and obtain

$$[1 + Pe\Delta x/2 + Pe^2\Delta x^2/12]c_{i-1} + [-2 - Pe^2\Delta x^2/6]c_i +$$

$$[1 - Pe\Delta x/2 + Pe^2\Delta x^2/12]c_{i+1} = 0$$

which is similar to Eq. (B.10). The solution is then also (B.4) with the function ψ given in (B.11). The slope at the corner nodes is obtained by combining (B.4), (B.11) with (B.27) and we find

$$c_i^1 = B \cdot Pe\Delta x \cdot \psi^i$$

To evaluate the criterion, we use

$$c(u) = a_o + a_1 u + a_2 u^2 + a_3 u^3$$

$$c(o) = c_i \qquad \frac{dc}{du}(o) = c_i^1 \tag{B.29}$$

$$c(1) = c_{i+1} \qquad \frac{dc}{du}(1) = c_{i+1}^1$$

which gives the constants

$$\begin{aligned} a_o &= c_i \\ a_1 &= c_i^1 \\ a_2 &= -3c_i - 2c_i^1 + 3c_{i+1} - c_{i+1}^1 \\ a_3 &= 2c_i + c_i^1 - 2c_{i+1} + c_{i+1}^1 \end{aligned} \tag{B.30}$$

Evaluating the constants a_i and substituting them into (B.29) gives an expression for c over the whole element $u\varepsilon[0.1]$. By setting $u = 0.2113$ or $u = 0.7889$ (collocation points) we recover the expressions for $c_{i+1/3}$ and $c_{i+2/3}$ from (B.12) and (B.13). The two cubic methods (OCFE-Hermite and OCFE-Legendre) give therefore identical solutions and the criterion must be the same. We obtain

$$\begin{aligned} \frac{dc}{du} &= a_1 + 2a_2 u + 2a_3 u^2 \\ &= \text{Const}\ (u - u_1)(u - u_2) \end{aligned}$$

where

$$u_{1,2} = 1/2 - 1/Pe\Delta x \pm \sqrt{\frac{1}{12} - \frac{1}{Pe^2 \Delta x^2}} \tag{B.31}$$

so for

$$Pe\Delta x > \sqrt{12} \quad \frac{dc}{du} > 0 \quad \text{and} \quad \frac{dc}{du} < 0 \quad \text{for } u\varepsilon[0.1]$$

$$Pe\Delta x < \sqrt{12} \quad \frac{dc}{du} < 0 \quad \text{and} \quad \text{all } u\varepsilon[0.1]$$

The solution does not oscillate provided

$$Pe\Delta x < \sqrt{12}$$

The nodal values are always monotonic and the slope at the nodes is always negative, so based on the nodal values no criterion exists.

B.5 OCFE — Hermite-quartic

Structure of matrix $\underline{M}$ is

$$\begin{pmatrix}
x & x & x & x & & & & & & & & \\
x & x & x & x & & & & & & & & \\
x & x & x & x & & & & & & & & \\
 & & x & x & x & x & x & & & & & \\
 & & x & x & x & x & x & & & & & \\
 & & x & x & x & x & x & & & & & \\
 & & & & & x & x & x & x & x & & \\
 & & & & & x & x & x & x & x & & \\
 & & & & & x & x & x & x & x & & \\
 & & & & & & & & & & x & x & x & x \\
 & & & & & & & & & & x & x & x & x \\
 & & & & & & & & & & x & x & x & x
\end{pmatrix}$$

The equation at the first collocation point ($u_1 = 0.1127$) for element i-1 is

$$[-4.64 + 0.6\ Pe\Delta x]c_{i-1} + [-3.32 - 0.587\ Pe\Delta x]c^1_{i-1} + [0.8 - 0.155\ Pe\Delta x]c^*_{i-1} + [4.64 - 0.6\ Pe\Delta x]c_i + [-1.323 + 0.187\ Pe\Delta x]c_i^1 = 0 \qquad (B.32)$$

and at the second collocation point ($u_2 = 0.5$)

$$3/2\ Pe\Delta x\ c_{i-1} + [-1 + Pe\Delta x/4]c^1_{i-1} - c^*_{i-1} - 3/2\ Pe\Delta x\ c_i + [1 + Pe\Delta x/4]c_i^1 = 0 \qquad (B.33)$$

and at the third collocation point ($u_3 = 1 - u_1$)

$$[4.64 + 0.6\ Pe\Delta x]c_{i-1} + [1.323 + 0.187\ Pe\Delta x]c^1_{i-1} + [0.8 + 0.1549\ Pe\Delta x]c^*_{i-1} + [-4.64 - 0.6\ Pe\Delta x]c_i + [3.323 - 0.587\ Pe\Delta x]c_i^1 = 0 \qquad (B.34)$$

Repeating the equations for element i, we can eliminate the variables c^1_{j-1}, c^*_{j-1}, j=i, i+1, i+2 and Eq. (B.18) is obtained. The solution is then (B.4) and (B.19) again. The slope can be found by substituting (B.4) and (B.19) into (B.32) through (B.34) and we find

$$c_i^1 = B \cdot Pe\Delta x \cdot \psi^i$$

and also

$$c_i^* = B\,\psi^i \frac{Pe^4\Delta x^4/24}{1 - Pe\Delta x/2 + Pe^2\Delta x^2/10 - Pe^3\Delta x^3/120}$$

Evaluating the constants in

$$c(u) = a_o + a_1 u + a_2 u^2 + a_3 u^3 + a_4 u^4$$

c can now be calculated over the whole element. For u equal to the collocation points (0.1127, 0.5, 0.8873) expressions (B.20) through (B.22) are recovered, so OCFE-Legendre and OCFE-Hermite with quartic polynomials give identical solutions. The criterion is given in (B.26). Comparing nodal values for monotonicity and the sign of the slopes the same criterion (B.26) is obtained.

B.6 Galerkin — Lagrange-cubic

The structure of the matrix $\underline{M}$ is similar to OCFE-Legendre with quadratic polynomials.

The equation for the midside node $c_{i-2/3}$ (u = 1/3) in element i-1 is

$$[-378 + 57\ Pe\Delta x]c_{i-1} + 864\ c_{i-2/3} + [-594 - 81\ Pe\Delta x]c_{i-1/3} + [108 + 24\ Pe\Delta x]c_i = 0 \qquad (B.35)$$

and at node $c_{i-1/3}$ (u = 2/3) we have

$$[108 - 24\ Pe\Delta x]c_{i-1} + [-594 + 81\ Pe\Delta x]c_{i-2/3} + 864\ c_{i-1/3} + [-378 - 57\ Pe\Delta x]c_i = 0 \qquad (B.36)$$

For the corner node, we find

$$[-26 + 7\ Pe\Delta x]c_{i-1} + [108 - 24\ Pe\Delta x]c_{i-2/3} +$$

$$[-378 + 57\ Pe\Delta x]c_{i-1/3} + 592\ c_i +$$

$$[-378 - 57\ Pe\Delta x]c_{i+1/3} + [108 + 24\ Pe\Delta x]c_{i+2/3} +$$

$$[-26 - 7\ Pe\Delta x]c_{i+1} = 0 \qquad \text{(B.37)}$$

Taking the equations for element i too, we can combine the equation to eliminate $c_{i-2/3}$, $c_{i-1/3}$, $c_{i+1/3}$ and $c_{i+2/3}$ and find

$$[1 + Pe\Delta x/2 + Pe^2\Delta x^2/10 + Pe^3\Delta x^3/120]c_{i-1} +$$

$$[-2 - Pe^2\Delta x^2/5]c_i +$$

$$[1 - Pe\Delta x/2 + Pe^2\Delta x^2/10 - Pe^3\Delta x^3/120]c_{i+1} = 0$$

which is identical to Eq. (B.18). The solution is therefore also given by Eqs. (B.4) and (B.18). Expression for the other nodes are now with (B.35) through (B.37).

$$c_{i+1/3} = A + B\psi^i \frac{1 - Pe\Delta x/6 + 19\ Pe^2\Delta x^2/90 + 11\ Pe^3\Delta x^3/3240}{1 - Pe\Delta x/2 + Pe^2\Delta x^2/10 - Pe^3\Delta x^3/120} \qquad \text{(B.38)}$$

$$c_{i+2/3} = A + B\psi^i \frac{1 + Pe\Delta x/6 + 19\ Pe^2\Delta x^2/90 - 11\ Pe^3\Delta x^3/3240}{1 - Pe\Delta x/2 + Pe^2\Delta x^2/10 - Pe^3\Delta x^3/120} \qquad \text{(B.39)}$$

To evaluate the constants we have

$$c(u) = a_o + a_1 u + a_2 u^2 + a_3 u^3$$

$$c(o) = c_i \qquad c(1/3) = c_{i+1/3}$$

$$c(2/3) = c_{i+2/3} \qquad c(1) = c_{i+1}$$

and find

$$a_o = c_i$$

$$a_1 = \frac{1}{2}\left[-11c_i + 18c_{i+1/3} - 9c_{i+2/3} + 2c_{i+1}\right]$$

$$a_2 = \frac{9}{2}\left[2c_i - 5c_{i+1/3} + 4c_{i+2/3} - c_{i+1}\right] \qquad \text{(B.40)}$$

$$a_3 = \frac{9}{2}\left[-c_i + 3c_{i+1/3} - 3c_{i+2/3} + c_{i+1}\right]$$

The criterion can now be evaluated by

$$\frac{dc}{du} = a_1 + 2a_2 + 3a_3 u^2 < 0$$

$$= \psi^i (u - u_1)(u - u_2)$$

where

$$u_{1,2} = \frac{1}{2} + \frac{1}{Pe\Delta x} \pm \frac{1}{Pe\Delta x}\sqrt{\frac{1}{20}(Pe\Delta x - A_1)(Pe\Delta x - A_2)} \qquad \text{(B.41)}$$

and

$$A_1 = 5 + \sqrt{45} \simeq 11.7$$

$$A_2 = 5 - \sqrt{45} \simeq -1.7$$

Here $(u - u_1)(u - u_2)$ does not change sign but the factor ψ^i does as described in (B.3). For

$$Pe\Delta x < 4.6444 \qquad \psi > 0 \qquad \frac{\partial c}{\partial x} < 0$$

$$Pe\Delta x > 4.6444 \qquad \psi < 0 \qquad \frac{\partial c}{\partial x} < 0 \quad \text{or} \quad \frac{\partial c}{\partial x} > 0$$

the solution will not oscillate provided

$$Pe\Delta x < 4.6444$$

By examining the nodal values for monotonicity the same criterion is obtained.

B.7 Galerkin — Quardratic-Upstream

A Galerkin formulation with "upstream" quardratic shape function (or quadratic shape function and asymmetric weighting function) was derived by Heinrich and Zienkiewicz (1977). Hughes (1978) developed a similar scheme that achieves upwinding too. The method is here examined for the oscillation limit. Two parameters (α, β) determine the upstream character. The equations are taken from Heinrich and Zienkiewicz (1977).

Matrix structure is the same as for ordinary Galerkin formulation. The equation at the midside node (u = 1/2) and element i-1 is

$$[1 + (1 + \beta)\ Pe\Delta x/4]c_{i-1} + [-2 - \beta\ Pe\Delta x/2]c_{i-1/2} +$$

$$[1 - (1 - \beta)\ Pe\Delta x/4]c_i = 0 \qquad \text{(B.42)}$$

and at corner nodes (u = 1)

$$[1 + (1 + \alpha)\ Pe\Delta x/2]c_{i-1} + [-8 - (2 + \alpha)\ Pe\Delta x 2c_{i-1/2} +$$

$$[14 + Pe\Delta x\ \alpha]c_i + [-8 + (2 + \alpha)\ Pe\Delta x]c_{i+1/2} +$$

$$[1 - (1 - \alpha)\ Pe\Delta x/2]c_{i+1} = 0 \qquad \text{(B.43)}$$

Repeatedly the difference equations in element i, the variables $c_{i-1/2}$ and $c_{i+1/2}$ can be eliminated. We find

$$\left(3 - Pe\Delta x/2 - \frac{2\ Pe\Delta x + (\alpha - 2)\ Pe^2\Delta x^2/4}{2 + \beta\ Pe\Delta x/2}\right)c_{i-1} +$$

$$\left(-6 + \frac{Pe^2\Delta x^2}{2 + \beta\ Pe\Delta x/2}\right)c_i +$$

$$\left(3 + Pe\Delta x/2 + \frac{2\ Pe\Delta x + (\alpha + 2)\ Pe^2\Delta x^2/4}{2 + \beta\ Pe\Delta x/2}\right)c_{i+1} = 0$$

and the solution is

$$c = A + B\ \psi^i$$

and

$$\psi = \frac{6 + 3(P/2 + 1)\ Pe\Delta x + (2 + \alpha + \beta)\ Pe^2\Delta x^2/4}{6 + 3(P/2 - 1)\ Pe\Delta x + (2 - \alpha - \beta)\ Pe^3\Delta x^3/4} \qquad \text{(B.44)}$$

Substituting (B.43) and (B.44) into Eq. (B.42) the solution at the midside node is

$$c_{i+1/2} = A + B\psi^i \cdot \frac{12 + 6\ \beta\ Pe\Delta x + (3/4\ \beta^2 - 1)Pe^2\Delta x^2 + (\alpha - \beta)Pe^3\Delta x^3/8}{[6 + 3(P/2-1)Pe\Delta x + (2-\alpha-\beta)Pe^2\Delta x^2/4][2 + Pe\Delta x \cdot \beta/2]} \qquad \text{(B.45)}$$

The weighting function is here cubic but the variation of c is still quadratic. We have therefore

$$c(u) = a_o + a_1 u + a_2 u^2$$

and the expressions (2.45) can be used to calculate the constants a_j. The criterion is then

$$\frac{dc}{du} = a_1 + 2a_2 u$$

and

$$u_1 = -a_1/2a_2$$

Using (2.45) and (B.44) and (B.45) we find

$$u_1 = \frac{1}{Pe\Delta x} \cdot \left\{ -1 + (1/2 - \alpha/6 - \beta/12)Pe\Delta x + \frac{\alpha(\alpha + \beta)Pe^2\Delta x^2/6}{12 + (3\beta - \alpha)Pe\Delta x} \right. \tag{B.46}$$

For $\alpha = \beta = 0$ we recover (2.46). Heinrich and Zienkiewicz (1977), gives optimal parameter choice of α, β so the exact solution is obtained at the nodes. The parameters are

$$\beta_{opt} = \coth (Pe\Delta x/4) - 4/Pe\Delta x \tag{B.47}$$

$$\alpha_{opt} = 2 \operatorname{tgh}\left(\frac{Pe\Delta x}{2}\right)[1 + \beta_{opt}/Pe\Delta x + 12/Pe^2\Delta x^2] - 12/Pe\Delta x - \beta_{opt}$$

and for

$$Pe\Delta x \to \infty \qquad \rightarrow \qquad \alpha_{opt} = \beta_{opt} \to 1 \quad .$$

Using (B.46) for $Pe\Delta x \to \infty$ and $\alpha = \beta = 1$ we have $u_1 \to 1/4$ so oscillations will occur even though full upstream weighting is used. The extreme point u_1 (B.46) is calculated for a number of $Pe\Delta x$ using the optimal parameters α, β

$Pe\Delta x$	α_o	β_o	u_1
2	0.164	0.054	-0.02
2.1	0.172	0.060	-10^{-4}
2.15	0.175	0.064	0.01
∞	1	1	0.25

The solution does not oscillate provided

$$Pe\Delta x < 2.1$$

Examining the nodal values c_i, $c_{i+1/2}$, c_{i+1} for monotonicity, we find that these will be monotone. If we therefore only look at nodal values there will be no oscillationlimit.

B.8 Moments-cubic

The structure of $\underline{\underline{M}}$ is similar to OCFE-Hermite with cubic polynomials. The equations are

$$[1.732 - Pe\Delta x/2]c_i + [1.366 + 1.443\ Pe\Delta x]c_i^1 +$$

$$[-1.732 + Pe\Delta x/2]c_{i+1} +$$

$$[0.366 - 0.1443\ Pe\Delta x]c_{i+1}^1 = 0 \qquad (B.48)$$

and

$$[-1.732 - Pe\Delta x/2]c_i + [-0.3666 - 0.1443\ Pe\Delta x]c_i^1 +$$

$$[1.732 + Pe\Delta x/2]c_{i+1} +$$

$$[-1.366 + 0.1443\ Pe\Delta x]c_{i+1}^1 = 0 \qquad (B.49)$$

Taking (B.48) and (B.49) for a neighboring element too, we can again eliminate the variables c_j, c_{j+1}^1, $j=i-1$, i to get

$$[1 + Pe\Delta x/2 + Pe^2\Delta x^2/12]c_{i-1} + [-2 - Pe^2\Delta x^2]6c_i +$$

$$[1 - Pe\Delta x/2 + Pe^2\Delta x^2/12]c_{i+1} = 0$$

giving (B.4) and ψ as (B.11). The slopes become $c_i^1 = B \cdot Pe\Delta x\ \psi^i$.

The variation in c is therefore identical with that of OCFE-Hermite-cubic and the two methods give identical results. The criterion is also identical (B.31).

$$Pe\Delta x < \sqrt{12} \quad .$$

The solution with OCFE-Hermit is therefore identical with the moments method. The criterion is thus also identical

$$Pe\Delta x < \sqrt{12}$$

Appendix C

Input Instructions to CONDIF Program

This appendix contains the input instructions for the CONDIF program, examples of data and control cards. The program solves all models discussed in Chapters V and VI.

C.1 Input Instructions

The input data cards are organized into 6 groups:

A : Model and solution method

B : Physical parameters

C : Mesh specification

D : Initial and boundary conditions

E : Integration parameters

F : Miscellaneous

For starting a simulation all groups must be specified. If restarting group A, E, F needs only be considered.

C.1-1 Group A: Model and Solution Method

The mathematical model, the solution method (MCS or not) and type of input and output is selected.

Card 1: MARK,IMOVE,NVERS (3I5)

MARK specifies the equation to be solved

MARK = 1 Parabolic equation and velocity constant

= 2 Parabolic equation (model I/II, Section 5.2)

= 3 Elliptic equation (6.3) alone

= 4 Elliptic and parabolic equation (sequence 1)

IMOVE specifies in which coordinate system the equations are solved

IMOVE = 0 Fixed coordinate system

= 1 Moving coordinate system and using closest nodes as boundary condition

= 2 Moving coordinate system and changing node location (not general for full run, See 5.3-6)

NVERS specifies which flow field is used for MARK = 2

NVERS = 1 Radial flow

= 2 Five spot flow

for MARK = 4 (see Section 6.3-3)

NVERS = 1 Nonlinear treated explicitly ($\underline{c}^n$)

= 2 Nonlinearities treated extrapolated ($\underline{c}^p$)

= 3 Nonlinearities treated implicit (iterations)

Card 2: LTIM,MTRD,MTRIT (3I5)

Maximum execution time, type of input and output are selected

LTIM = n Maximum CPU time allowed in solution

MTRD = 0 Input from cards/intercomp

= 1 Input from tape

MTRIT = 0 Output on line printer only

= 1 Output on tape also.

C.1-2 Group B: Physical Parameters

The physical parameters to the equation(s) are specified. The input depends on the choice of MARK. For

MARK = 1 or 2

Card 1: PEX,PEY (2F10.5)

Peclet number in x and y direction (use PEX=PEY)

Card 2: DIFM, ALFAL,ALFAT (3F10.5)

Dispersion tensor with

DIFM molecular diffusion coefficient

ALFAL mixing length longitudinal direction

ALFAT mixing length transverse direction } (6.24)

Length normalized to 1 automatically. Use DIFM = 1, ALFAL = ALFAT = 0 for model I/IIM and DIFM = 0, ALFAT = ALFAL = 1 for model I/IID.

MARK = 3 or 4

Card 1: ALX,ALY (2F10.5)

Length of domain in x and y direction (use ALX=ALY)

Card 2: PHI,PERMEA(1)

PHI : porosity

PERMEA(1) : total permeability

Card 3: DIFM,ALFAL,ALFAT

Dispersion tensor defined under MARK = 2/3 above, can use any value here.

Card 4: HEI(I),I=1,10 (8F10.5, two cards)

HEI(1) thickness of domain

HEI(I),I=2,10 defines function h(x,y)

$H=HEI(1) + HEI(2)X + HEI(3)X^2 + HEI(4)X^3 + HEI(5)Y + HEI(6)Y^2 + HEI(7)Y^3 + HEI(8)XY + HEI(9)XY^2 + HEI(10)X^2Y$

Card 5: ZEI(I),I=1,10 (8F10.5, two cards)

ZEI(1) depth of domain

ZEI(I),I=2,10 defines function Z(x,y)

similar expression as function h(x,y) above

Card 6 : DENSI(1)

Density of phase (both components)

Card 7: VISCO(I),I=1,3 (3F10.5)

VISCO(1) : Solvent (injecting) fluid viscosity

VISCO(2) : Oil (in place) fluid viscosity

VISCO(3) : Exponent l in mixing formula (6.28)

Card 8: ADSORB(I),I=1,3 (3F10.5)

ADSORB(1) : Rock density (capacity)

ADSORB(2) : Constant b formula (6.26)

ADSORB(3) : Constant a formula (6.26)

Card 9: WELLR (F10.5)

Well radius (in meters)

C.1-3 Group C: Mesh Specification

The elements layout is specified, the main parameter card No. 1 indicates type of input, see explanation below.

Card 1: NCORD (I5)

NCORD = 1 Automatical generation of mesh

= 2 Same as above but specify coordinate

= 3 All coordinates and node numbering provided by the user

Card 2: NH

Total number of nodes

For NCORD=1,2 a rectangular mesh as shown below is made.

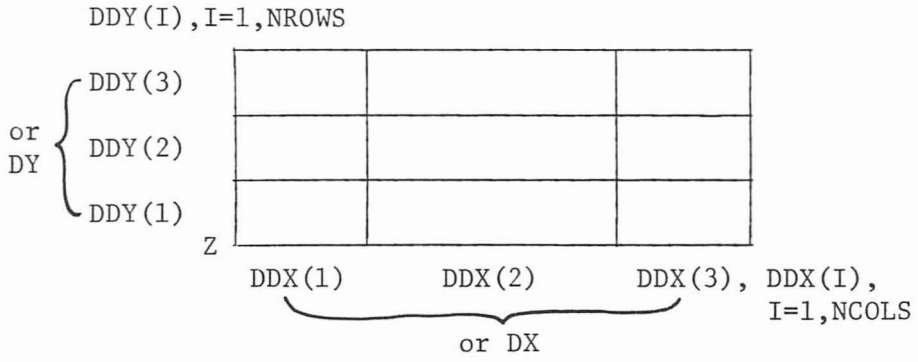

For the construction, we define:

NROWS : number of elements in y-direction

NCOLS : number of elements in x-direction

DDY(I): The y-increment between successive elements

DDX(I): The x-increment between successive elements

Z : Position of lower left corner in coordinate system

For NCORD = 1 the increments in x- and y-direction between successive elements (DDX,DDY) are fixed to DX, DY. Z is fixed to 0., 0. The user specifies:

Card 3: NROWS,NCOLS (2I5)

Card 4: DX,DY (2F10.5)

For NCORD = 2 more options are available; the user specifies

Card 3: NROWS,NCOLS (2I5)

Card 4: DDX(I),I=1,NCOLS (6F10.5)

Card 5: DDY(I),I=1,NROWS (6F10.5)

Card 6: XZ,YZ (2F10.5)

Position of lower left corner Z.

For NCORD=3 the user must specify each corner and midside node (not necessary if corner nodes connected with straight lines) on a separate card.

Card 3-N+3: CORD(N,1), CORD(N,2) [N cards of 2F10.5]

Node locations.

Card N+4: 0 (zero) (I5)

This terminates reading of coordinates. The number of elements, node numbering, and type of element: quadratic, serendipity and triangular, is specified.

Card N+5: NE (I5)

Number of elements

N+5 - N+NE+5: NBN,NODE(I,J),J=1,NBN [NE cards of 9I5]

NBN = 6 triangular element

= 8 serendipity element

The global node numbering must be started from lower left corner, if not done part of program does not work properly.

Examples of proper specification

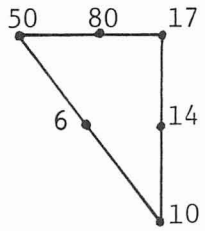

NODE(I,J)= 10 14 17 80 50 6

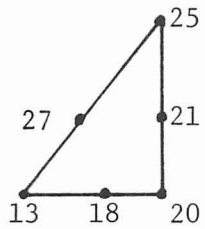

NODE(I,J)= 13 18 20 21 25 27

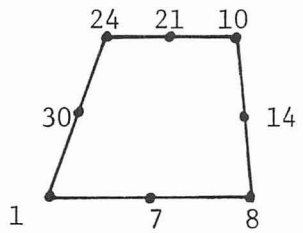

NODE(I,J)= 1 7 8 14 10 21 24 30

C.1-4 Group D: Initial and Boundary Conditions

Rectnagular and triangular domains can be treated with this program. For input and programming purposes, following notation is used

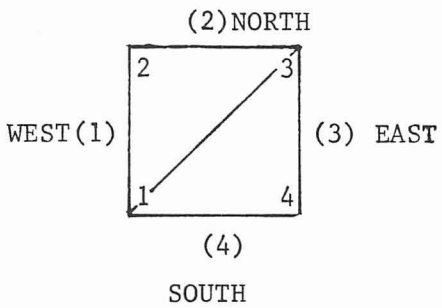

The sides are numbered 1-4, where side 1 is West, side 2 North etc. The corners are numbered 1-4 starting from South-West (1).

Initial condition is specified first and then boundary conditions. The user must specify boundary conditions at all 4 sides and 4 corners in the domain.

Card 1: IINT (I5)

IINT=0 One initial concentration over the whole domain

=n Initial concentration at n nodes differs from CINT (see below).

Card 2: CINT (F10.5)

Initial concentration over the whole domain

Card 3: J,CNEW(J),IINT Cards (I5,F10.5)

Initial concentration CNEW(J) differ from CINT at node J.

If IINT=0 omit this card.

Card 4: Boundary condition for each corner (4 total). For each corner specify card 4a (and 4b) sequentially.

Card 4a: ICCORN(J),Corner J (I5)

ICCORN(J)=0 natural boundary condition essential boundary condition

If ICCORN(J)=0 omit 4b

Card 4b: CCORN(J,III),TCCORN(J,III),III=1,5 [5 cards of 2F10.5]

The concentration at corner J at times TCCORN(J,III) is specified. In between the times TCCORN, the concentration is linearly interpolated.

Continue with card 8 if all corners are specified otherwise return to card 4a.

If MARK=3/4 the pressure specification is done in a similar form as the concentration specification. If MARK=1,2 skip to card 15.

For pressure we have

Card 8: IINT (I5)

Card 9: PINT (F10.5)

Card 10: J,PNEW(J) (I5,F10.5)

Initial pressure PNEW(J) at node J differs from PINT.

If IINT=0 omit this card.

Card 11: Boundary condition for each corner (4 total). For each corner specify card 11a (and 11b) sequentially.

Card 11a: IPCORN(J), corner J (I5)

IPCORN(J)=Ø natural boundary conditions

=1 essential boundary condition

=2 flux (source/sink) boundary condition

If IPCORN(J)=Ø omit 11b

Card 11b: PCORN(J,III),TPCORN(J,III),III=1,5 [5 cards of 2F10.5]

The pressure or fluc at times TPCORN(J,III) is specified. In between the times TPCORN the value is linearly interpolated.

Continue with card 15 if all corners are specified otherwise return to card 11a.

The boundary conditions for concentration along the sides are specified by 4 cards:

Card 15: NSID,IBCC(NSID),BDD(NSID,1) (4 cards of 2I5,F10.5)

NSID : side number as referred to above figure

ICBB(NSID)=0 natural boundary condition

=1 essential boundary condition

BCC(NSID,1)=0 if IBCC(NSID)=0

= concentration at boundary NSID at all times

If MARK=1/2 skip to Group E

The boundary conditions for pressure along the sides are specified similarly by 4 cards:

Card 19: NSID,IBCP(NSID),BCP(NSID,1) (4 cards of 2Is,F10.5)

NSID side number

IBCP(NSID)=0 natural boundary condition (no integration on boundary elements performed)

=1 essential boundary condition

=2 flux boundary condition

BCP(NSID,1)=0 if IBCP(NSID)=0

= pressure at boundary NSID at all times (IBCP(NSID)=1)

= flux in x direction

BCP(NSID,2)= flux in y direction } (IBCP(NSID)=2)

C.1-5: Group E: Integration Parameters

In this group parameters for output and integration routine are specified. If input is not read from tape (restarted) skip to card 2.

Card 1: ITAPE (I5)

ITAPE specifies which beginning time to read from (see below, card 3)

Card 2: MAX (I5)

Number of times ($\leq$ 14) printout is wanted

Card 3: TPRINT(III),III=1,MAX (7F10.5)

Printout of concentration/pressure at times TPRINT(III). Each time a printout (line printer) is made at a certain time the same information is stored on TAPE8 (if MTRIT=1)

Card 4: DT (E10.3)

Beginning timestep or fixed timestep depending on choice of EPS (card 5)

Card 5: EPS (E10.3)

EPS < 1. (usually 10^{-3} - 10^{-5}), variable timestep scheme, starting with DT (card 4)

EPS = 1. fixed timestep DT during whole integration

EPS = 2. fixed timestep DT in intervals TPRINT(I) to TPRINT(I+1); starts with card 4, and as last cards MAX number of cards specifying DT in the next time interval

For MARK=4 and NVERS=3 read in

Card 6: ITMAX (I5)

Maximum number of iterations on solution of the parabolic equation

Card 7: EPS(1) (E10.3)

Level of accuracy for iterations. Error defined by

$$EP = \frac{\sum (\underline{c}^{n+1,s+1} - \underline{c}^{n+1,s})^2}{NT}$$

where NT: number of nodes in grid (may be different from NH)

C.1-6 Group F: Miscellaneous

Card 1: IANY(I),I=1,3 (3I5)

IANY(1) = 1 printout of velocities at gauss points for every TPRINT(I). Use only for MARK=4 if desired

= 0 no printout

IANY(2) Not used

IANY(3) = 1 Mass balance over sides done, printout every timestep

= 0 No mass balance

Card 2: blank

For IMOVE≠2 skip to card 9

CONDIF can change the location of two vertical and one horizontal line of nodes. Corresponding element numbers and nodes must be specified.

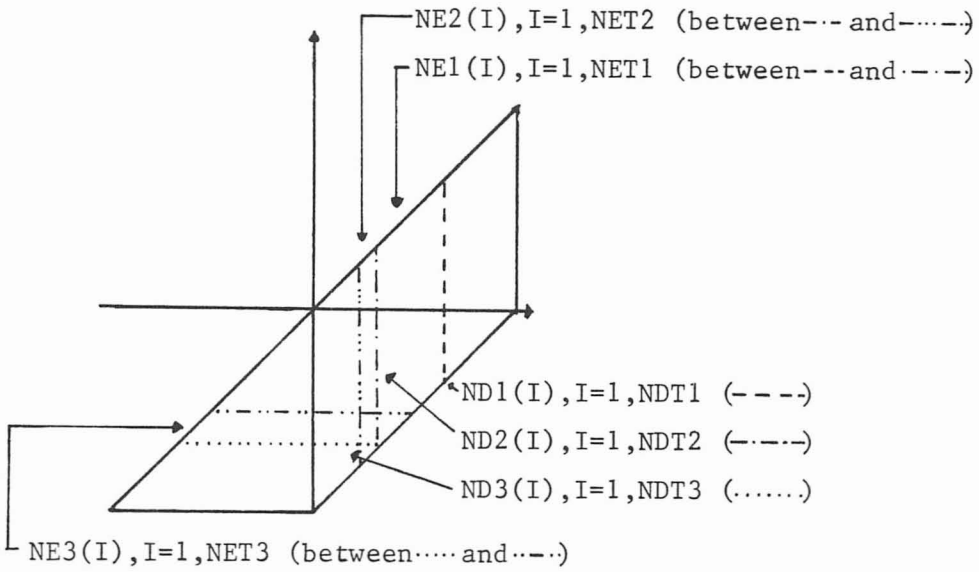

Only the elements closest to the line pointed into the physical domain is affected. The nodes and elements are specified by

NET1,NET2,NET3 : number of elements in columns or rows defined in figure above

NE1(I),NE2(I),NE3(I): element numbers in columns or row (see figure)

ND1(I),ND2(I),ND3(I) : node numbers along the lines defined by figure above

Card 3 : NET1,(NE1(I),I=1,NET1) (10I5)

4 : NDT1,(ND1(I),I=1,NDT1) (10I5)

5 : NET2,(NE2(I)I=1,NET2) (10I5)

6 : NDT2,(ND2(I),I=1,NDT2) (10I5)

7 : NET3,(NE3(i),I=1,NET3) (10I5)

8 : NDT3,(ND3(I),I=1,NDT3) (10I5)

If EPS = 2 is selected MAX-1 cards of DT for following intervals is specified

9 : DT (MAX-1 cards) (E10.3)

C-2 Examples of Data

On the following pages two examples of data set are given. Example 1 is the calculation of Model IID-2, Pe_1 = 1000 case from Chapter V. Example 2 is a restart of the same simulation.

```
  2        1          0
490        0          1         0
  1        0          0
  1.                  1.
   .001                .001
  1.                  1.
  3
288
  1        1.                    .0
  2        1.                    .5
  3        1.                   1.
  4         .5                   .5
  5         .5                   .0
  6         .25                  .0
  7         .25                  .25
  8         .15                  .0
  9         .15                  .15
 10         .075                 .075
 11         .075                 .0
 12         .025                 .025
 13         .025                 .0
 14         .0125                .0125
 15         .0                   .0
 40         .975                -.025
 41         .5                  -.025
 42         .25                 -.025
 43         .15                 -.025
 44         .075                -.025
 45         .025                -.025
 46         .0                  -.025
 47        -.025                -.025
 55         .1                  -.0125
 56         .05                 -.0125
 57         .0125               -.0125
 77         .925                -.075
 78         .5                  -.075
 79         .25                 -.075
 80         .15                 -.075
 81         .075                -.075
 82         .025                -.075
 83         .0                  -.075
 84        -.025                -.075
 85        -.075                -.075
 93         .1                  -.05
 94         .05                 -.05
 95         .0125               -.05
 96        -.0125               -.05
122         .75                 -.25
123         .5                  -.25
124         .25                 -.25
125         .15                 -.25
```

126	.075	-.25
127	.025	-.25
128	.0	-.25
129	-.025	-.25
130	-.25	-.25
138	.1	-.15
139	.05	-.15
140	.0125	-.15
162	.5	-.5
163	.25	-.5
164	.15	-.5
165	.075	-.5
166	.025	-.5
167	.0	-.5
168	-.025	-.5
169	-.25	-.5
170	-.5	-.5
189	.25	-.75
190	.15	-.75
191	.075	-.75
192	.025	-.75
193	.0	-.75
194	-.025	-.75
195	-.25	-.75
196	-.5	-.75
197	-.75	-.75
216	.15	-.85
217	.075	-.925
218	.025	-.975
219	.0	-1.
220	-.025	-1.
221	-.25	-1.
222	-.5	-1.
223	-.75	-1.
224	-1.	-1.
246	-.075	-.125
247	-.125	-.125
248	-.075	-.2
249	-.075	-.25
250	-.125	-.25
251	-.125	-.2
252	-.175	-.175
253	-.175	-.2
254	-.175	-.25
255	-.225	-.225
256	-.225	-.25
257	-.125	-.375
0		
105		

6	4	19	2	17	3	18		
8	5	20	1	16	2	19	4	21
8	6	27	5	21	4	22	7	23
8	8	26	6	23	7	24	9	25
6	8	25	9	28	10	29		
6	11	30	8	29	10	31		
6	11	31	10	32	12	33		
6	13	34	11	33	12	35		
6	13	35	12	36	14	37		
6	15	38	13	37	14	39		
8	41	49	40	48	1	20	5	50
8	42	51	41	50	5	27	6	52
8	43	53	42	52	6	26	8	54
6	44	59	43	60	55	63		
6	43	54	8	61	55	60		
6	55	61	8	30	11	62		
6	44	63	55	62	11	64		
6	44	64	11	66	56	65		
6	56	66	11	34	13	68		
6	45	67	56	68	13	69		
6	45	71	44	65	56	67		
6	45	69	13	245	57	70		
6	57	245	13	38	15	73		
6	46	72	57	73	15	75		
6	46	74	45	70	57	72		
6	47	76	46	75	15	58		
8	78	87	77	86	40	49	41	88
8	79	89	78	88	41	51	42	90
8	80	91	79	90	42	53	43	92
6	80	92	43	97	93	98		
6	93	97	43	59	44	99		
6	81	100	93	99	44	102		
6	81	101	80	98	93	100		
6	81	102	44	103	94	104		
6	94	103	44	71	45	107		
6	82	106	94	107	45	108		
6	82	105	81	104	94	106		
6	82	108	45	109	95	110		
6	95	109	45	74	46	111		
6	83	112	95	111	46	242		
6	83	113	82	110	95	112		
8	84	116	83	242	46	76	47	119
6	85	121	84	119	47	120		
8	123	133	122	131	77	87	78	132
8	124	134	123	132	78	89	79	135
8	125	136	124	135	79	91	80	137
6	125	137	80	141	138	142		
6	138	141	80	101	81	145		
6	126	144	138	145	81	243		
6	126	143	125	142	138	144		
6	126	243	81	147	139	146		
6	139	147	81	105	82	148		

6	127	149	139	148	82	150		
6	127	151	126	146	139	149		
6	127	150	82	153	140	152		
6	140	153	82	113	83	154		
6	128	155	140	154	83	156		
6	128	160	127	152	140	155		
8	129	161	128	156	83	116	84	157
6	246	158	84	121	85	159		
6	247	260	246	159	85	261		
6	129	157	84	158	246	268		
6	129	268	246	258	248	267		
8	251	264	248	258	246	260	247	263
8	253	270	251	263	247	271	252	272
6	255	274	253	272	252	273		
6	249	266	129	267	248	259		
8	250	265	249	259	248	264	251	269
8	254	279	250	269	251	270	253	280
8	256	275	254	280	253	274	255	276
6	130	278	256	276	255	277		
6	162	171	122	133	123	172		
8	163	173	162	172	123	134	124	174
8	164	175	163	174	124	136	125	176
8	165	177	164	176	125	143	126	178
8	166	179	165	178	126	151	127	180
8	167	181	166	180	127	160	128	182
8	168	183	167	182	128	161	129	184
6	257	286	129	266	249	285		
6	257	285	249	265	250	284		
6	257	284	250	279	254	283		
6	257	283	254	275	256	282		
6	257	282	256	278	130	281		
6	168	184	129	286	257	287		
6	169	288	257	281	130	186		
6	169	185	168	287	257	288		
6	170	187	169	186	130	188		
6	189	198	162	173	163	199		
8	190	200	189	199	163	175	164	201
8	191	202	190	201	164	177	165	203
8	192	205	191	203	165	179	166	204
8	193	206	192	204	166	181	167	208
8	194	207	193	208	167	183	168	209
8	195	210	194	209	168	185	169	211
8	196	212	195	211	169	187	170	213
6	197	215	196	213	170	214		
6	216	225	189	200	190	229		
8	217	226	216	229	190	202	191	230
8	218	227	217	230	191	205	192	231
8	219	228	218	231	192	206	193	232
8	220	244	219	232	193	207	194	233
8	221	234	220	233	194	210	195	235
8	222	236	221	235	195	212	196	237
8	223	238	222	237	196	215	197	239
6	224	240	223	239	197	241		

```
   0
  .0
   1
1.              0.00E-0
1.            3.1831E-5
0.              3.20E-5
0.              3.00E 1
0.              4.00E 1
   0
   0
   0
   1       0     0.0
   2       0     0.0
   3       0     0.0
   4       0     0.0
.0
   6
1.5915E-5 3.1831E-5 6.3662E-5 1.9099E-4 2.5465E-4 3.1831E-4
   0.20E-7
    .6E-3
0.
.33333333



   2       1       0
  91       1       1       0
   4
   2
 2.7002E-4 2.8647E-4 2.2280E-4  2.5465E-4  2.8647E-4
  7.250E-6
  1.


 6       3      12      28      45      73      88
11     162     172     123     132      78      88     41     50      5
21       4
 7       4      13      29      46      74      89     97
13     189     199     163     174     124     135     79     90     42
52       6      23       7
```

C.3 Control Cards

Control cards for execution of CONDIF at the University of Washington Academic Computer CDC 6400 are given. It is assumed that the program is compiled with FTN and stored in an EDITLIB library. To run, use:

```
Name,CM140000,Txxx,IOYYY,PØ,BAT                    (*)
Account card
ATTACH(COMPIL,ID=_____)
ATTACH(TAPE2,RESULTS,ID=____)                      (**)
PUBLIC(IMSLFTN)
LDSET(LIB=COMPIL/IMSLFTN,PRESET=ZERO)
CONDIF,PL=15000.                                   (***)
EXIT,P.
REWIND(TAPE8)
                                                   (****)
CATALOG(TAPE8,RESULTS,ID=_____)
*EOR       (or 7/8/9  in column 1)
DATA
*EOF       (or 6/7/8/9 in column 1)
```

where

(*) IO secs as 1.5 * CPU secs (YYY = 1.5 xxxx)

(**) Omit if no restart.

(***) PL is maximum number of lines to print (Default is 5000)

(****) Omit of no saving of tape output